Université de Montréal

The Nature and Origin of Spatial and Temporal Variations in the Gravity Fields of Telica and Masaya Volcanoes, Nicaragua

par

Alexandre Beaulieu
Département de géologie
Faculté des arts et des sciences

Mémoire présenté à la Faculté des études Supérieurs
en vue de l'obtention du grade de
Maître ès sciences (M. Sc.)

Janvier 1999

Université de Montréal
Faculté de études supérieures

Ce mémoire intitulé

Gravity and Microgravity Experiments at Telica and Masaya Volcanoes, Nicaragua

Présenté par:

Alexandre Beaulieu

A été évalué par un jury composé des personnes suivantes:

Président-rapporteur: Dr. Michel Chouteau

Membre du Jury: Dr. Walter E. Trzcienski

Membre du Jury: Dr. Hazel Rymer

Membre du Jury: Dr. John Stix

Mémoire accepté le: 99.01.25

Frontispiece

Telica

Masaya

Abstract

Knowledge of the internal structures and dynamics of volcanoes is an important element in understanding and being able to forecast volcanic activity. developments in the field of gravity studies during the last decade have permitted better definition of the principal structures in volcanic environments and the processes governing the internal dynamics of volcanoes. This study is a presentation of different applications of gravity at two Nicaraguan volcanoes, Telica and Masaya. A static gravity survey was carried out at Telica to identify Bouguer gravity anomalies. The presence of a positive anomaly centered on the active crater defines a large, shallow intrusion in the Telica complex. It is oriented north-northwest-south-southeast, with dimensions of 2 km × 2 km × 6 km, and located at an approximate depthto top of 1 km. North-trending faults and the alignment of cones in the complex have a similar orientation to this intrusion. Microgravity measurements were made at Masaya. Modelling of the gravity changes at Masaya showed that the gravity changes are produced by fluctuations of the density, caused in turn by variations in the degree of vesiculation in the magma. A possible correlation of these fluctuations with solar and lunar tides was observed. A model for density changes in magma in terms of their exsolved and dissolved volatile contents was developed. This model shows that observable changes in gravity at the surface are produced by density variations caused by fluctuations in dissolved or exsolved volatile contents for shallow to relatively deep magma chambers (1-6 km). The volatile element that produces the largest density changes is H_2O.

Resumen

Un conocimiento de la estructura y la dinámica de los volcanes constituye un aspecto importante para poder comprender y pronosticar su comportamiento geológico. Los desarrollos científicos dentro del campo de estudios de la gravedad durante la última década nos han permitido una mejor definición de las estructuras principales que caracterizan el ambiente volcánico, y también de los procesos que controlan la dinámica interna de los volcanes. Este artículo presenta las varias aplicaciones técnicas de la gravedad en el estudio de dos volcanes nicaraguenses: Telica y Masaya. Una investigación de la gravedad estática fué realizada en Telica con el objeto de identificar anomalías de gravedad Bouguer. La presência de una anomalía positiva con su centro colocado sobre el cráter activo indica la existencia de un gran cuerpo intrusivo de poca profundidad dentro del complejo de Telica. La intrusión tiene una orientación de norte noroeste (NNW) hacia el sur sudeste (SSE), y sus dimensiones son 2 km por 2 km por 6 km. La superficie del cuerpo se encuentra a una profundidad de aproximadamente 1 km. Fallas con orientación norte - sur, y el arreglo linear de los conos volcanicos del complejo demuestran una orientación paralela a esta intrusión. Medidas microgravimétricas fueron coleccionadas en Masaya. Un modelo de los cambios de la gravedad en Masaya fue desarrollado, y este muestra que las variaciones en el campo de gravedad son debidas a la fluctuación de la densidad, debido, a su vez, a variaciones en el nivel de vesicularisación dentro del magma. Fué notada una posible relación entre estas fluctuaciones y las mareas lunares. Además, el modelo explica bien las variaciones de densidad dentro del magma como resultado del contenido de componentes volátiles disueltos. Este

modelo nos enseña que las variaciones de la gravedad notadas en la superficie son debidas a las variaciones en la densidad producidas por fluctuaciones en el contenido de elementos volatiles disueltos o exdisueltos en cámaras magmáticas a profundidades entre 1 y 6 km. H_2O es el componente volátil que produce la mayor variación en densidad.

Résumé

Dans le cadre de ce mémoire, deux volcans nicaraguayens ont été étudiés. Tous deux sont situés dans la chaîne volcanique d'Amérique Centrale, dans la partie ouest du Nicaragua, proche de l'Océan Pacifique. Telica est un stratovolcan situé à 12.603° N and 86.845° W dans le sud-ouest du Nicaragua. Il fait partie d'un complexe volcanique composé de plusieurs édifices (Santa Clara, Cerro Aguero et San Jacinto) situés dans la chaîne des Marabios. Le cône volcanique est pentu et contient un cratère de 700 m de diamètre et d'environs 120 m de profondeur. Les roches du complexe volcanique de Telica consistent en un chevauchement de coulées de lave, de tephras, de dépôts alluvionnaires et de lahars. L'activité volcanique à Telica depuis la conquête espagnole consiste en des périodes allongées d'émission de soufre et de nombreuses petites éruptions stromboliennes et phréatiques. Une augmentation de l'activité sismique est présentement en cours depuis 1996, le nombre d'événements étant passé de 100/jour à 220/jour entre le mois de décembre 1996 et le mois de juin 1997. Le dégazage du volcan reste très faible pendant cette période.

Le volcan Masaya est situé à 11.984° N et 86.161° W, 25 km au sud-ouest de Managua, capital du Nicaragua. Il fait partie de la caldeira de Masaya qui a des dimensions de 11.5 km par 6 km allongée selon une direction nord-ouest et sud-est, parallèlement à la chaîne volcanique. Dans la caldeira, une série d'évents en forme semi-circulaire se sont développés après la formation de la caldeira; ce sont les cônes de Masaya, de Nindirí, de Comalito, de Cerro Montosa et d'Arenal. Des cratères d'effondrement se sont formés dans les deux cônes principaux (Masaya et Nindirí): Santiago, Masaya, Nindirí et San Pedro. Santiago est présentement en phase de

dégazage intense depuis 1993, il rejette dans l'atmosphère plusieurs centaines à quelques milliers de tonnes de SO_2 par jour. Durant les 150 dernières années, Masaya a connu plusieurs épisodes de dégazage semblable de façon cyclique. Deux coulées de lave se sont produites dans la caldeira: en 1670, d'un débordement du lac de lave de Nindirí au nord, et en 1772, d'une fissure sur le flanc nord-est du cône de Masaya.

Les objectifs principaux de ce mémoire sont d'expérimenter deux façons d'utiliser les méthodes gravimétriques sur les volcans et de démontrer leur utilité en ce qui a trait à l'accroissement de la connaissance sur la structure et le dynamisme interne des volcans. Premièrement, une carte des anomalies de Bouguer du volcan Telica est construite et des modélisations sont effectuées sur ces anomalies. Deuxièmement, des études microgravimétriques temporelles à différentes échelles de temps (annuelle, mensuelle, hebdomadaire et quotidienne) sont effectuées à Masaya. Troisièmement, un modèle théorique sur la variation de la densité des magmas en relation avec leur contenu en volatiles est échafaudé. Et quatrièmement, le modèle précédent est utilisé pour discuter des causes des variations temporelles de gravité à Masaya. Afin de combler ces objectifs, deux saisons de terrain furent conduites pendant lesquelles un total de 245 mesures de gravité et de GPS ont été prises dans la région du complexe volcanique de Telica et plusieurs mesures de microgravité ont été prises de façon répétitive à des échelles de temps différentes à Masaya.

L'étude de gravité statique à Telica a permis d'ébaucher une carte des anomalies gravimétriques du complexe volcanique. Des modélisations faites à partir de profils sur la carte des anomalies ont démontré la présence d'une intrusion à faible profondeur sous le complexe. Ce corps aurait une taille approximative de 2 × 2 × 6 km, allongé selon une direction nord-nord-ouest et sud-sud-est, à une profondeur de 1 km. Le contraste de densité entre ce corps et les roches encaissantes serait entre 400-600 kg m^{-3}. Les structures régionales concorderaient avec la présence d'une telle intrusion. Cette intrusion pourrait vraisemblablement être le réservoir magmatique ayant nourri les volcans du complexe de Telica.

Les études temporelles de microgravité à Masaya ont permis d'observer un lien entre les marées lunaire et solaire et les variations gravimétriques. Effectivement, il est démontré que les variations de gravité observées à Masaya sont causées par des changements de densité du magma sous le cratère de Santiago. Ces changements de densité seraient eux-mêmes causés par des fluctuations dans la quantité de bulles dans le magma. Un lien mécanique entre ce processus et les marées est une possibilité. Le dégazage important de Masaya montre peut-être aussi une relation avec les variations de gravité, mais il est difficile de trouver une relation directe puisque les mesures de SO_2 sont plus éparses que celles de gravité. De toute façon, si les variations de gravité sont causées par des changements dans la quantité de gaz dans le magma, il est sûr qu'il y a un lien entre le dégazage et les variations de gravité.

La modélisation théorique des changements de densité des magmas à des pressions différentes avec les volatiles montre qu'il est possible d'observer des changements de gravité pour des chambres magmatiques, des dômes ou des conduits magmatiques d'une certaine taille. L'exsolution de volatiles dans un magma provoque un changement de densité important facile à repérer pour des corps magmatiques importants et de faible profondeur (1-6 km). Des variations du contenu en volatile en milieu sous-saturé sont aussi possible à observer, même si elles produisent des changements de densité de moindres importances. Il est aussi démontré qu'à de faible profondeur, le volatile le plus efficace pour faire varier la densité est H_2O, le CO_2 étant à des concentrations trop faibles à ces profondeurs.

Ce travail à permis de démontrer la présence d'un réservoir magmatique à Telica. La surveillance de l'activité volcanique peut être focalisée au-dessus de ce corps afin de mieux cerner tout renouvellement de magma ou d'augmentation de pression à l'aide de microgravité ou de méthodes sismiques. Une meilleure connaissance du système volcanique interne de Masaya peut aider à mieux prévenir les futures périodes de dégazage et de possibles éruptions.

L'utilisation des techniques gravimétriques en milieu volcanique augmente les connaissances des processus magmatiques et de la structure interne sous les volcans. En intégrant ces données avec d'autres méthodes géologiques, géochimiques et géophysiques, notre connaissance des systèmes volcaniques s'accroît. Cela permet de mieux prévoir les comportements volcaniques qui peuvent poser des dangers pour les populations vivant aux alentours des volcans actifs.

Acknowledgements

First, many great thanks to John Stix, my supervisor, who helped me with the science, and especially my bad English. To Hazel Rymer also, without whom it would not have been possible because of the instruments she loaned me and her knowledge on the subject. Special thanks to all the people who helped me in the field: Glyn Williams-Jones and Isabelle Lépine, to whom I'm sorry for the «calor» in Nicaragua, Sandy Achibald, Katie St-Amand, Mike Burton, Lisa Boardman and Dora Knez. The help and collaboration of the peoples of INETER was greatly appreciated, especilly from Martha Navarro and Wilfried Strauch for the science and the bureaucratic stuff, Don Orlando, Alejandro Acosta and his brother Luis for driving us and Oscar Péres for entertainment. Loads of thanks to all the guards of Masaya National Park and the director Mrs Guttieres who gave us unlimited access at all times. The hospitality of the Hotel Regis and the family Gómes des Castillo will never be forgotten; this is a great place to stay, and a great breakfast also. Thanks to all the people of the Département de Géologie de l'Université de Montréal for supporting me all along. Also thanks to the students with whom I made a fiesta a couple of times (which releases some magmatic pressure from my brain). Finally, but not least, I'm very grateful to my girfriend Véronique, who supported me and endured the fact that I was not always with her but far away in a foreign country.

Table Of Contents

List of Figures

List of Tables

General introduction

Introduction

Gravity surveys of volcanic areas provide an excellent means to define and understand the subsurface structures of volcanoes. With the technological improvements in the past few years in the field of the Global Positioning System (GPS), new approaches in the field of gravity are now possible. These techniques give us a way to study mass movement and accumulation or loss of gas beneath volcanoes, which in turn help us understand their activity and forecast eruptions. Gravity variations observed in the past have been difficult to interpret because of a lack of good elevation control (Eggers et al., 1976; Eggers and Chavez, 1979; Eggers, 1983; Vieira et al., 1986). Microgravity measurements with precision to better than 10 μGal and levelling with precision to better than 2 cm can now be acquired rapidly on volcanoes (Rymer, 1989; Brown et al., 1991). With accumulation of data and experience, interpretation of *time-varying* gravity features on volcanoes becomes more reliable and meaningful (Rymer, 1994; Rymer and Locke, 1995).

In the present study, two volcanoes were surveyed using two different methods of gravity monitoring. At Telica volcano, Nicaragua, a conventional static gravity survey was conducted to make a map of the Bouguer anomalies of the crater area. At Masaya volcano, microgravity monitoring was conducted to observe temporal variations at different scales (yearly, monthly and daily variations).

Telica is an active volcano in northwestern Nicaragua that is part of the chain of Quaternary volcanoes along the western margin of Central America. The Santa Clara, Cerro de Aguero and San Jacinto edifices coalesce with Telica to form a group of volcanic centers that is part of the Marrabios range. Historic activity at Telica for the last 500 years consists of extended periods of solfataric activity and numerous small explosive eruptions (Lefebure, 1986). Masaya volcano is part of Masaya caldera, situated in the same Quaternary volcanic chain as Telica. Historic activity at Masaya includes lava lake formation, pit crater formation and two lava flows which were erupted in 1670 from an overflow of the lava lake of Nindirí to the north and in 1772 from a fissure on the northeast flank of the Masaya cone (Rymer et al., 1998). Geological evidence also shows episodes of pyroclastic cone-building eruptions. Plinian airfalls are also known to have occurred from Masaya caldera (Williams, 1983). During the past 150 years, episodes of strong degassing have occurred, showing a cyclic interval of about 25 years. These degassing crises, five in total since 1852, represent the degassing of approximately 10 km^3 of basaltic magma (Stoiber et al., 1986). Rymer et al. (1998) monitored the volcano from 1993 to 1997 using microgravity techniques, levelling instruments, GPS and COSPEC measurements. Masaya caldera also has been investigated using other geophysical techniques (Bouguer gravity, seismology and magnetotellurics) (Metaxian, 1994; Metaxian and Lesage, 1997). Presently, Masaya is monitored on a continuous basis with one seismic station by INETER (Instituto Nicaragüense de Estudios Territoriales).

Objectives

The main goals of this thesis are to (1) map and model the gravity anomalies of Telica volcano, (2) monitor microgravity variations on different timescales (yearly, monthly, weekly and daily) at Masaya volcano, (3) build a model for gravity changes related to variations in the dissolved and exsolved volatile content in the magma under volcanic edifices, and (4) discuss possible causes of gravity variations with time at Masaya and, using the previous theoretical model, explain the changes observed. To achieve these goals, two seasons of fieldwork were conducted where gravity and microgravity data were acquired at Telica and Masaya volcanoes. At Telica, 245 gravity and GPS measurements were taken around the crater area. Microgravity measurements at Masaya volcano were taken repeatedly each day and week during the two field seasons to obtain adequate data with which to observe temporal variations at different timescales. Leica GPS 200 dual-frequency differential receivers were used for positioning of the gravity stations at Telica and for monitoring altitude variations at Masaya. LaCoste and Romberg meter G-513 and Scintrex meter were use for the gravity work.

Locations

Masaya Volcano

Masaya volcano is a large basaltic shield volcano situated at 11.984° N and 86.161° W, 25 km southeast of Managua, which is the capital of Nicaragua (Fig. I-1). The summit of Masaya volcano is situated at 624 m above sea level. Masaya caldera is 11.5 km by 6 km, elongated in the northwest-southeast direction, and parallel to the volcanic chain. An 8 km^2 lake at 135 m altitude is situated in the southeastern part of the caldera. Inside the caldera, a semi-circular set of vents have developed from post-caldera eruptions; they include Masaya, Nindirí, Comalito, Cerro Montosa and Arenal cones (Fig. I-2). Four pit craters have been formed in the two main cones (Masaya and Nindirí), including the Masaya, Santiago, Nindirí and San Pedro pit craters (Fig. I-3) (Rymer et al., 1998). Santiago is the active crater at the present time.

FIGURE I-1

Location of Telica and Masaya volcanoes in the Central American Front. Shaded strips are proposed segment boundaries of Soitber and Carr (1973).

0 50 100 km
0 50 100 mi
N
HONDURAS
Golfo de Fonseca
Caribbean Sea
Telica volcano
Nicaragua
Lago de Managua
MANAGUA
Islas del Maiz
Masaya volcano
Lago de Nicaragua
Pacific Ocean
COSTA RICA

FIGURE I-2

Locations of volcanic centers in the Masaya caldera (From Maciejewski, 1995).

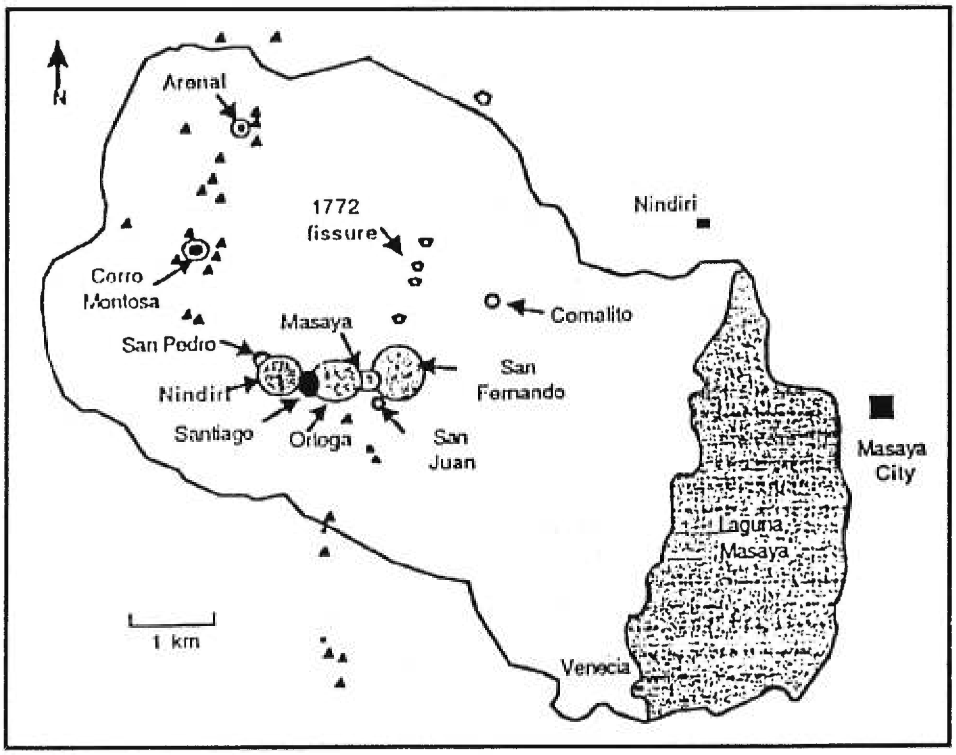
N
Arenal
1772
fissure
Nindiri
Cerro
Montosa
Comalito
Masaya
San Pedro
San
Fernando
Nindiri
Santiago
Ortega
San
Juan
Masaya
City
Laguna
Masaya
1 km
Venecia

FIGURE I-3

Aerial photo of Masaya caldera showing the different pit crater (From McClelland et al., 1989).

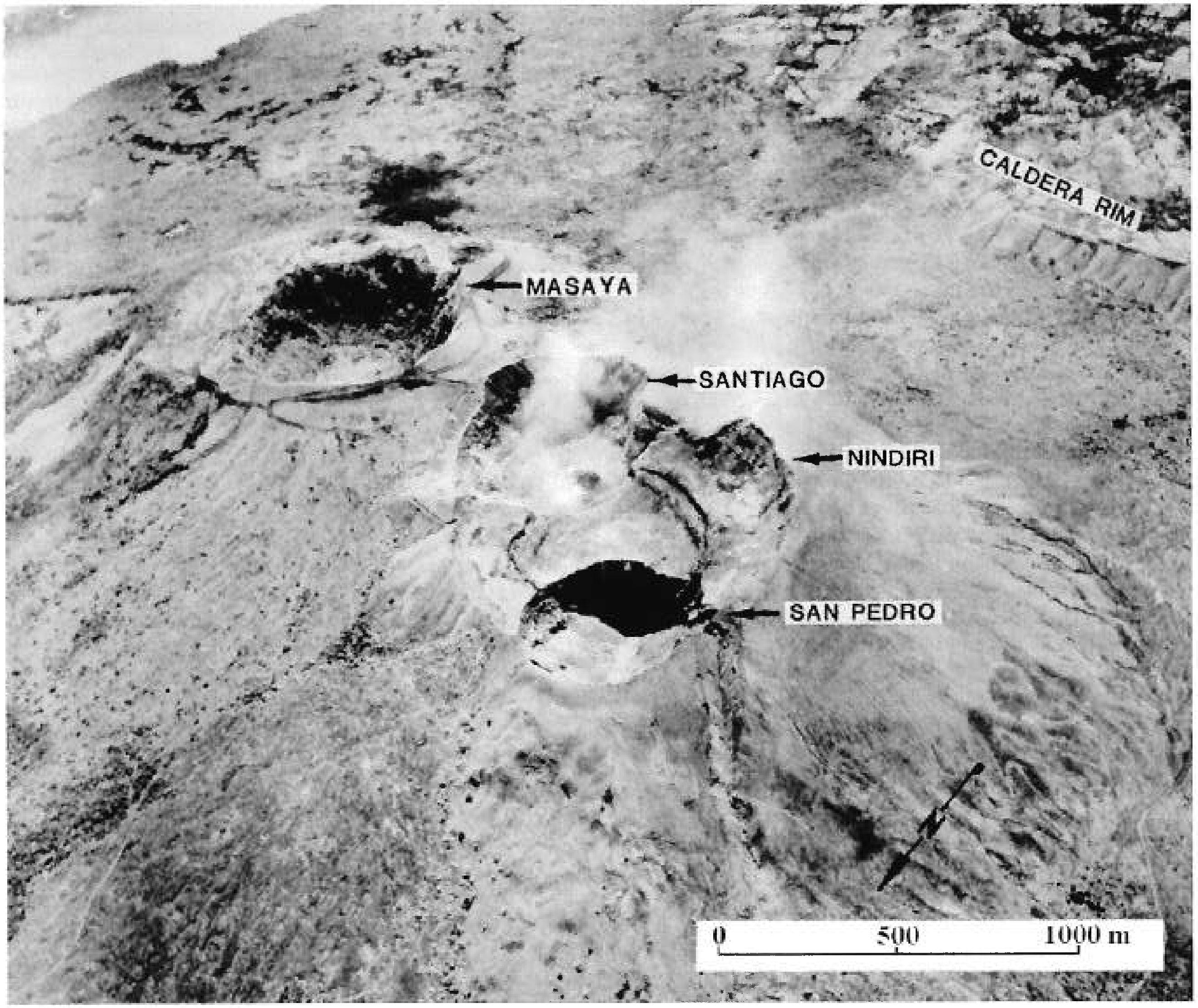
CALDERA RIM
MASAYA
SANTIAGO
NINDIRI
SAN PEDRO
0
500
1000 m

Telica Volcano

Telica volcano is a composite volcano located at 12.603° N and 86.845° W, 19 km north of León, Nicaragua's second largest city, at the northwestern edge of a large volcanic complex (Fig. I-1). The summit of Telica is 1040 m above sea level. The Telica volcanic complex is situated in the central part of the Marabios Range (Fig. I-4). Telica has a very steep sided cone with a double crater measuring 700 m in diameter (Fig. I-5). The southern crater, which is presently active, is at least 120 m in depth. None of the other cones in the volcanic complex which comprise the large ridge of El Liston are active.

Geological Setting

Regional Geology

Telica and Masaya volcanoes are situated in the Nicaraguan Quaternary volcanic chain located near the southern end of the active Central American volcanic front. This front is part of the Meridional Structural Domain which includes Costa Rica, Panama and southwestern Nicaragua. The volcanic front is the result of plate convergence between the Cocos and Caribbean plates (Malfait and Dinkelman, 1972; Carr, 1984) (Fig. I-6). The Central American volcanic chain, consisting of 38 active volcanoes, has been divided into 7 linear segments along the Pacific margin of Central America (Stoiber and Carr, 1973) (Fig. I-7). In Nicaragua, two tectonic segments divide the volcanic chain. Masaya caldera is located in the eastern Nicaraguan segment, about 25 km southeast of the boundary between the two segments, and Telica is found in the western Nicaraguan segment (Fig. I-1). The

FIGURE I-4

Volcanoes of the Marabios Range. Volcano El Viejo and San Jacinto are now called San Cristobal and Santa Clara, respectively (From Lefebure, 1986).

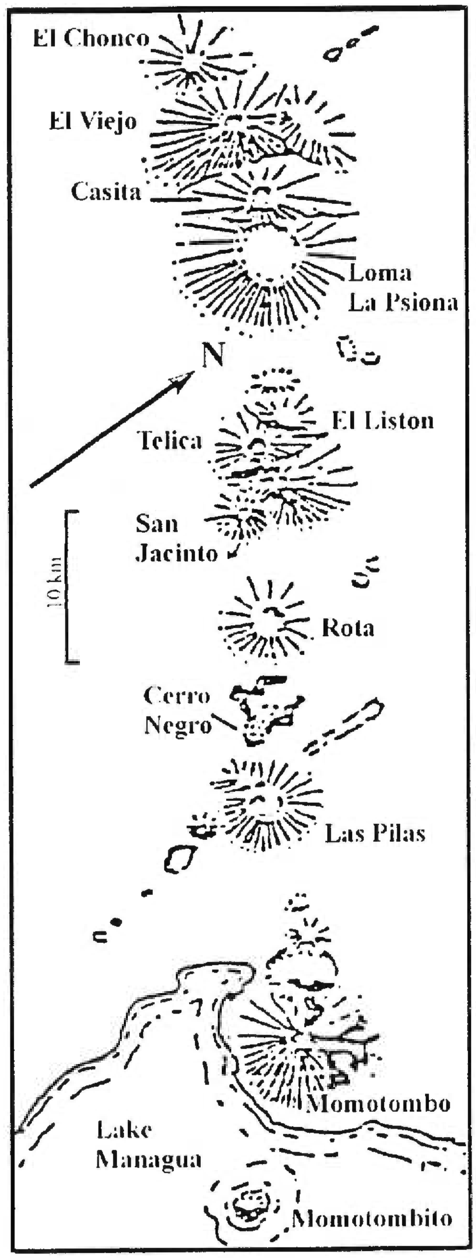
El Chonco
El Viejo
Casita
Loma
La Psiona
N
El Liston
Telica
San
Jacinto
10 km
Rota
Cerro
Negro
Las Pilas
Momotombo
Lake
Managua
Momotombito

FIGURE I-5

A view of Telica crater from the east side.

FIGURE I-6

Plate tectonic setting of the Middle American island arc (From Lefebure, 1986).

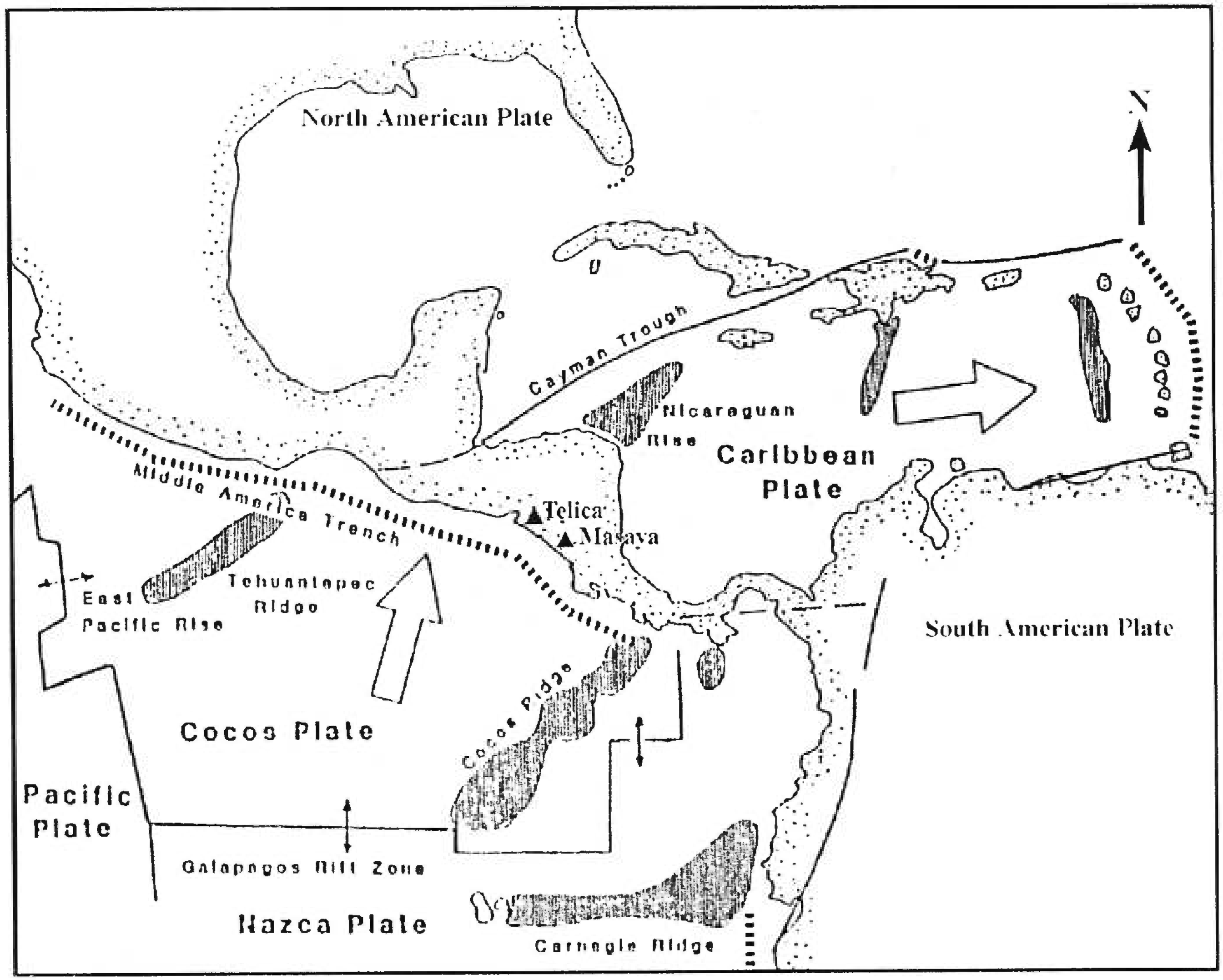
North American Plate
N
Cayman Trough
Nicaraguan
Rise
Caribbean
Plate
Middle America Trench
Telica
Masaya
East
Pacific Rise
Tehuantepec
Ridge
Cocos Plate
Cocos Ridge
Pacific
Plate
Galapagos Rift Zone
Nazca Plate
Carnegie Ridge
South American Plate

FIGURE I-7

Map of the Quaternary volcanoes of Central America (From Weyl, 1980).

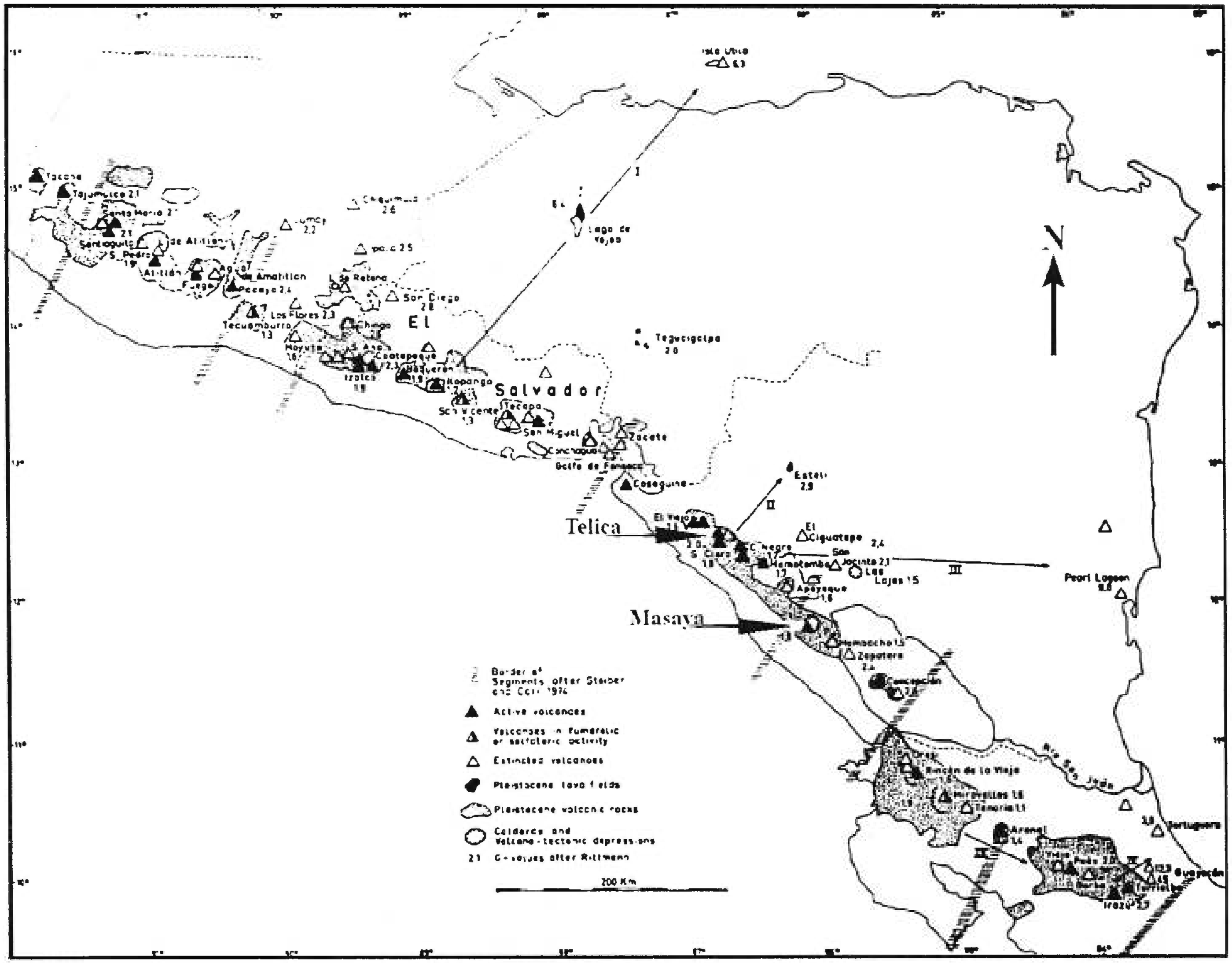

N
Telica
Masaya
El
Salvador
Tegucigalpa 2.0
Pearl Lagoon
Golfo de Fonseca
Coseguina
Rio San Juan
Active volcanoes
Extincted volcanoes
Pleistocene lava fields
Pleistocene volcanic rocks
200 Km

northern part of this volcanic chain where the Telica complex is found, the Marabios chain, is mainly dominated by volcanic complexes, individual stratocones, cinder and spatter cones. In the central part of the volcanic chain lie the main ignimbrite centers: the Malpaisillo caldera at the north and the Managua-Las Sierras-Masaya Complex at the south (Metaxian, 1994; Viramonte et al., 1997; Lefebure, 1986).

Central America is divided by Weyl (1980) into two units: the northern part which is underlain by a basement of continental crust (Paleozoic) and the southern part which consists of oceanic crust overlain by younger sediments and volcanics (Tertiary). The contact between the two units is thought to underlie the Managua Graben in the area of the Nejapa Alignment in Managua (Bice, 1990, from Maciejewski, 1995). Nine structural provinces, corresponding to the distribution of formations of different age, were identified in Nicaragua (Garayar, 1977, from Weyl, 1980). This scheme is reflected in the general geological map of the country (Fig. I-8). McBirney and Williams (1965) proposed the following as the most important physiographic units in Nicaragua: the Atlantic Coastal Plain, the Interior Highland, the Nicaraguan Depression and the Pacific Coastal Plain. This structural scheme is shown in a northeast-southwest geological cross-section (Fig. I-9).

The basement rocks of Central America extend from Guatemala southward to northern Nicaragua. They form a sequence of schists, phyllites, marbles and quartzites called the Nueva Segovia Formation of Paleozoic age that was intruded by Cretaceous plutonic rocks (Lefebure, 1986). The Bocay basin, in the northwestern frontier region of Nicaragua near Honduras, is oriented northeast-southwest and is mainly composed of terrestrial and marine sediments (Bracchi and Giudice, 1958;

FIGURE I-8

Geologic map of Nicaragua (From Weyl, 1980).

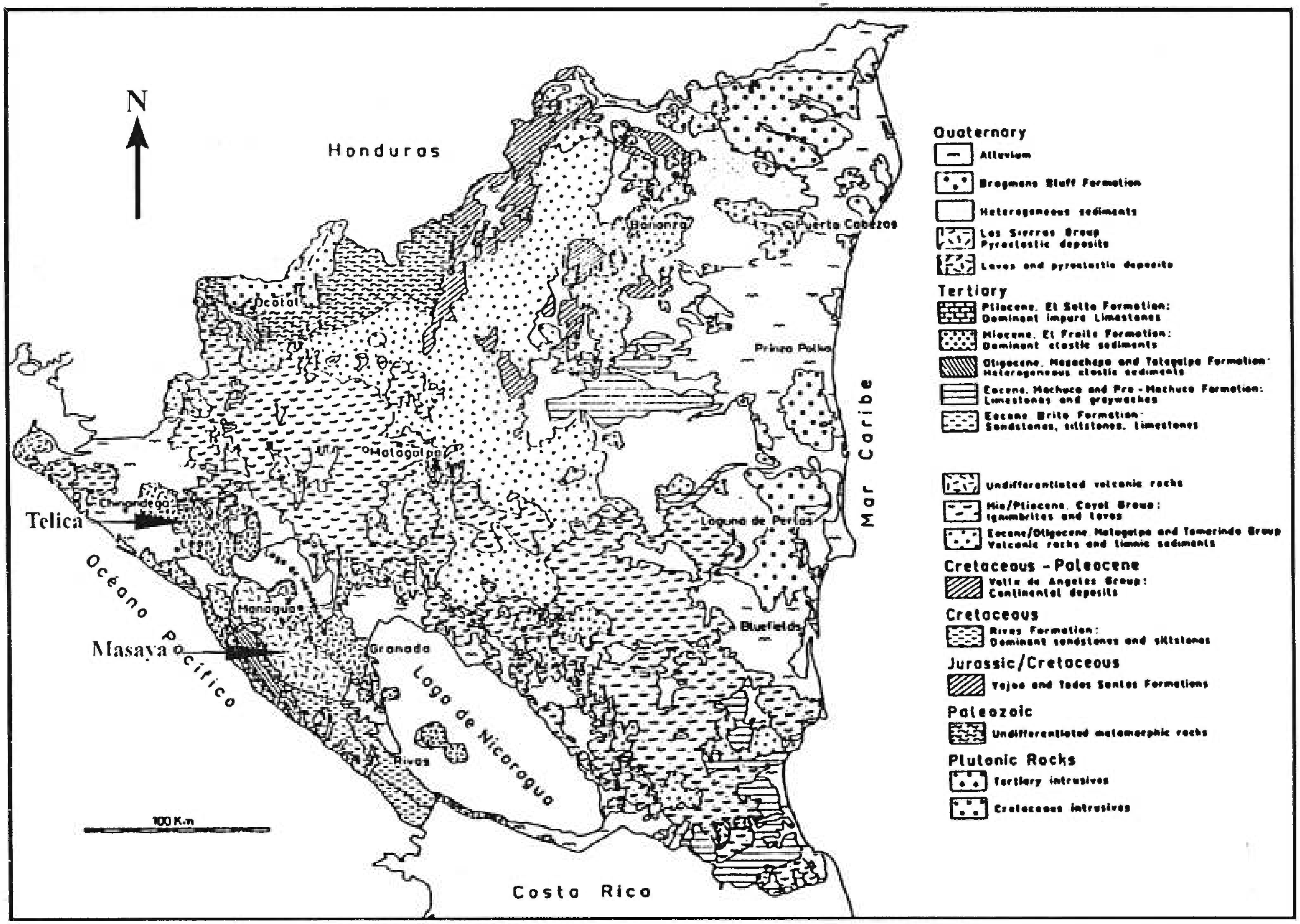
N
Honduras
Mar Caribe
Costa Rica
Océano Pacífico
Lago de Nicaragua
Telica
Masaya
Ocotal
Bonanza
Puerto Cabezas
Prinza Polka
Matagalpa
Chinandega
León
Managua
Granada
Rivas
Laguna de Perlas
Bluefields
100 Km
Quaternary
Alluvium
Bragmans Bluff Formation
Heterogeneous sediments
Las Sierras Group
Pyroclastic deposits
Lavas and pyroclastic deposits
Tertiary
Pliocene, El Salto Formation:
Dominant impure Limestones
Miocene, El Fraile Formation:
Dominant clastic sediments
Oligocene, Masachapa and Totogalpa Formation:
Heterogeneous clastic sediments
Eocene, Machuca and Pre-Machuca Formation:
Limestones and greywackes
Eocene Brito Formation:
Sandstones, siltstones, limestones
Undifferentiated volcanic rocks
Mio/Pliocene, Coyol Group:
Ignimbrites and lavas
Eocene/Oligocene, Matagalpa and Tamarindo Group
Volcanic rocks and limnic sediments
Cretaceous - Paleocene
Valle de Angeles Group:
Continental deposits
Cretaceous
Rivas Formation:
Dominant sandstones and siltstones
Jurassic/Cretaceous
Yojoa and Todos Santos Formations
Paleozoic
Undifferentiated metamorphic rocks
Plutonic Rocks
Tertiary intrusives
Cretaceous intrusives

FIGURE I-9

Generalized geological section through southwestern Nicaragua (From Weyl, 1980).

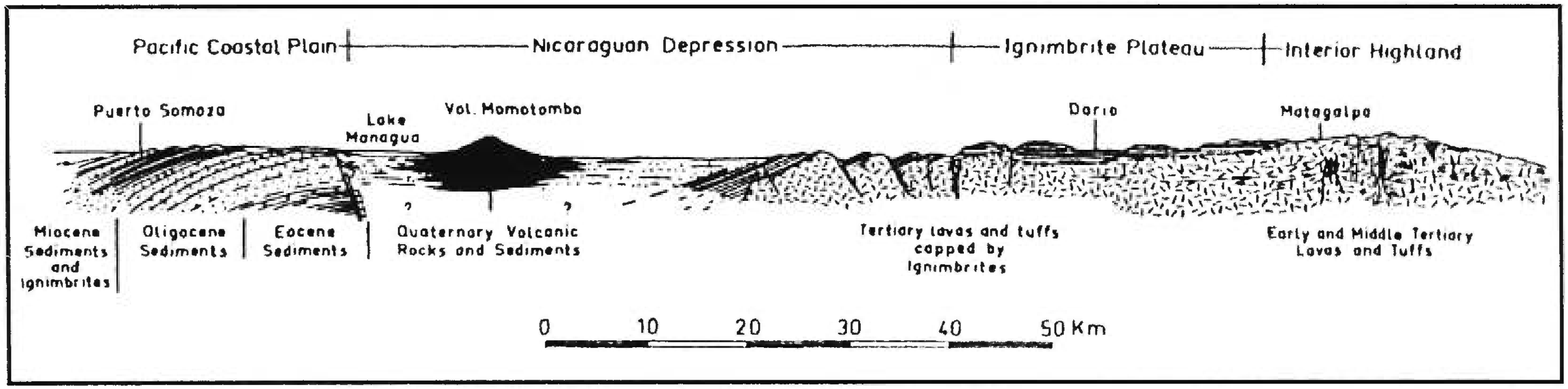
Pacific Coastal Plain
Nicaraguan Depression
Ignimbrite Plateau
Interior Highland
Puerto Somoza
Lake Managua
Vol. Momotombo
Dario
Matagalpa
Miocene Sediments and Ignimbrites
Oligocene Sediments
Eocene Sediments
Quaternary Volcanic Rocks and Sediments
Tertiary lavas and tuffs capped by Ignimbrites
Early and Middle Tertiary Lavas and Tuffs
0
10
20
30
40
50 Km

Rivera, 1962, from Weyl, 1980). The Mosquitia basin, which is the northeastern continuation of the Bocay Basin, is one of the largest Mesozoic-Tertiary sedimentary basins in Central America (Karim et al., 1966; Mills et al., 1967; Mills and Hugh, 1974; Arden, 1969 and 1975, from Weyl, 1980). The Interior Highlands are mainly composed of Tertiary volcanic sequences that are divided into the Matagalpa, Lower and Upper Coyol Groups. They are composed of accumulations of pyroclastic flows, lava flows, tuffs and epiclastic breccias with minor associated sediments (Lefebure, 1986). The Nicaraguan Depression, a broad shallow graben, is the dominant structural feature in Nicaragua and is probably late Miocene in age (McBirney and Williams, 1965). It is filled in part with pyroclastic material coming form the Las Sierras group into the central part of the depression (Metaxian, 1994). The sedimentary formations in Nicaragua consist of the Rivas, Brito, Masachapa, El Fraile and El Salto Formations (Lefebure, 1986) (Table I-1).

Geology of Masaya Volcano

The origin of Masaya caldera is controversial. McBirney (1956) believed that the caldera was formed after a series of collapses due to a migration of the magma chamber. For Williams (1983) and Bice (1985), the formation of the caldera results from a series of collapses due to strong magmatic eruptions, all of basaltic composition, including plinian and ignimbrite eruptions. Kieffer and Creusot-Eon (1982) suggested that the caldera was the result of an enormous phreatomagmatic eruption which produced a huge depression of "maar" type. Masaya caldera is itself situated within another caldera, the Las Sierras caldera formed 20 000-30 000 years ago, which resulted in the formation of the Masaya Lapilli Bed (van Wyk de Vries,

Table I-1
Statigraphic correlation chart of southwestern Nicaragua (From Viramonte et al., 1997)

Period	Epoch	Time (Ma)	Nicaraguan Depression: South	Central	North	Interior highlands
Quaternary	Holocene		Marrabios volcanoes	Las Sierras formation	Marrabios volcanoes	Back arc volcanics
	Pleistocene	1	(El Salto formation)			
Tertiary	Pliocene	13	erosional gap	Tamarindo formation	Tamarindo formation	El Coyol formation
	Miocene	25	El Fraile formation	El Fraile formation		El Coyol formation
	Oligocene	36	Masachapa formation	Masachapa formation	Masachapa formation	Matagalpa formation
	Eocene	58	El Brito formation	El Brito formation	El Brito formation	Matagalpa formation
	Paleocene	63	Rivas formation	Rivas formation	Rivas formation	Pre-Matagalpa
Cretaceous		135	Pre-Rivas	Pre-Rivas	Pre-Rivas	
Pre-Cretaceous			Nicoya complex ophiolite?	Nicoya complex ophiolite?	Nicoya complex ophiolite?	Metamorphic basement

1993). Masaya caldera was formed during the eruption that deposited the Masaya Tuff between between 6000 and 2000 years ago (Walker et al., 1993).

Masaya caldera is different from the other volcanoes in the volcanic chain. Not only does it have large-volume explosive basaltic activity, the pre-caldera activity resulted in the construction of a low shield volcano with a form that does not match the composite volcanoes which dominate the Nicaraguan volcanic front (Walker et al., 1993, Metaxian, 1994). Poorly vegetated lavas cover the floor of the caldera. Since the sixteenth century, only two lava flows have been known to erupt. The first lava flow was the result of an overflow in 1670 from the Nindirí pit which contained a 1 km wide lava lake at the time (Rymer et al., 1998). The second lava flow was erupted from a fissure on the flank of the Masaya cone in 1772 (Fig. I-10). The only other historic lava is found in Santiago crater which is still active at present, and in Nindirí crater in 1852 (Rymer et al., 1998).

Santiago crater is the main site of activity since it formed in 1858-1859. A lava lake covered the floor of Santiago in 1948 and 1965; the solidified lava is now broken by concentric faults (McBirney, 1956). The active vent of Santiago is now situated in an inner crater 150 m deeper than the main crater which is itself 150 m deep (Fig. I-11). Incandescence is often visible at the bottom of the crater. The volcanic rocks from Masaya are all basalts or basaltic andesites showing very little compositional variation compared to other Central American volcanoes. They also have a low content in Al_2O_3 and a high concentration in FeO, showing a tholeiitic differentiation trend. These compositional variations and the evolution of the caldera is the result of open-system magmatic differentiation in a large, shallow magma chamber (Walker et al., 1993). A gravity anomaly was first reported by Connor and Williams (1990) and

FIGURE I-10

Masaya caldera and the 1670 and 1772 lava flows (From Kieffer and Creusot-Eon, 1992).

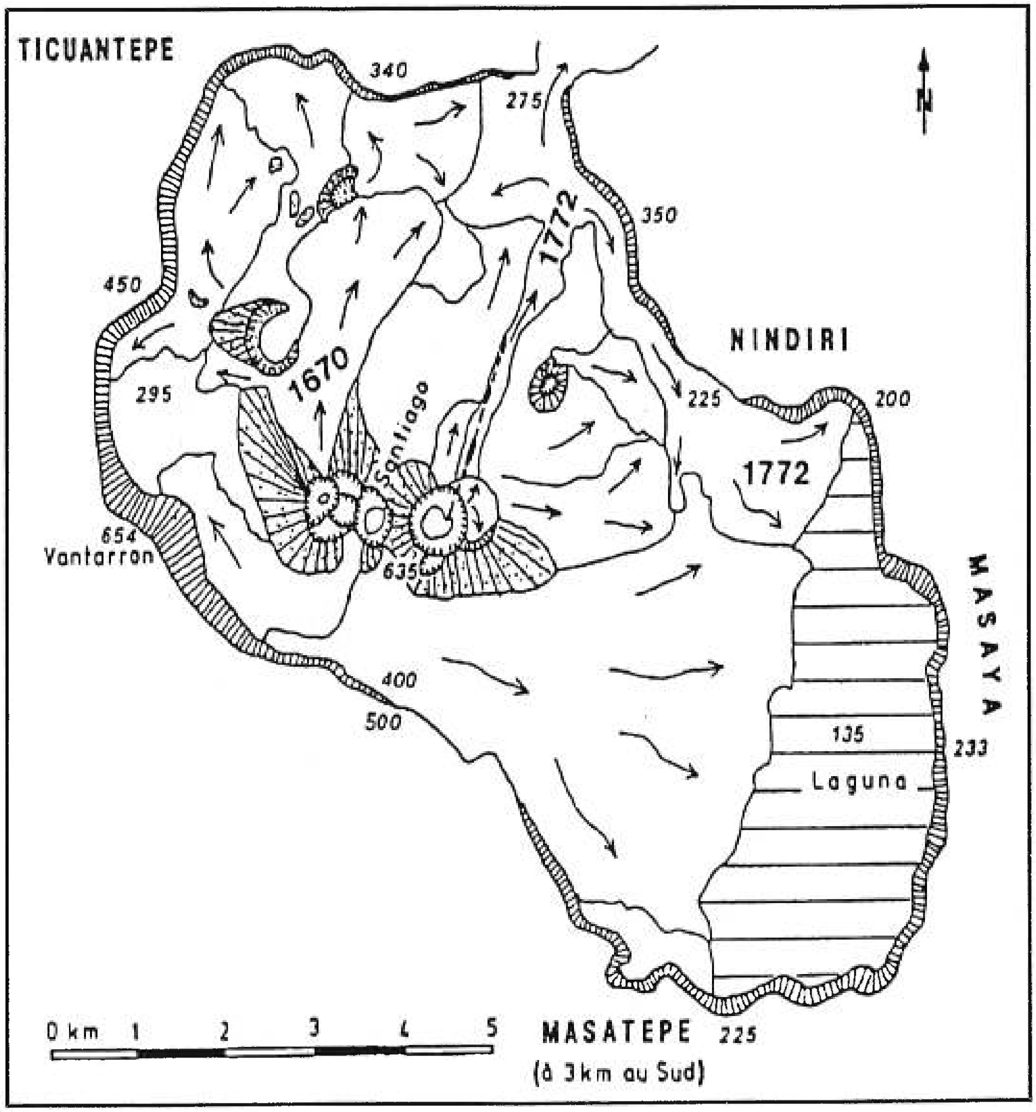

TICUANTEPE
340
275
N
350
1772
450
NINDIRI
1670
295
Santiago
225
200
1772
654
Vantarron
635
MASAYA
400
500
135
233
Laguna
0 km 1 2 3 4 5
MASATEPE
225
(à 3km au Sud)

FIGURE I-11

A view of the active vent at the bottom of Santiago crater.

FIGURE I-12

Geologic map of Masaya caldera showing the different geologic units (From Walker et al., 1993).

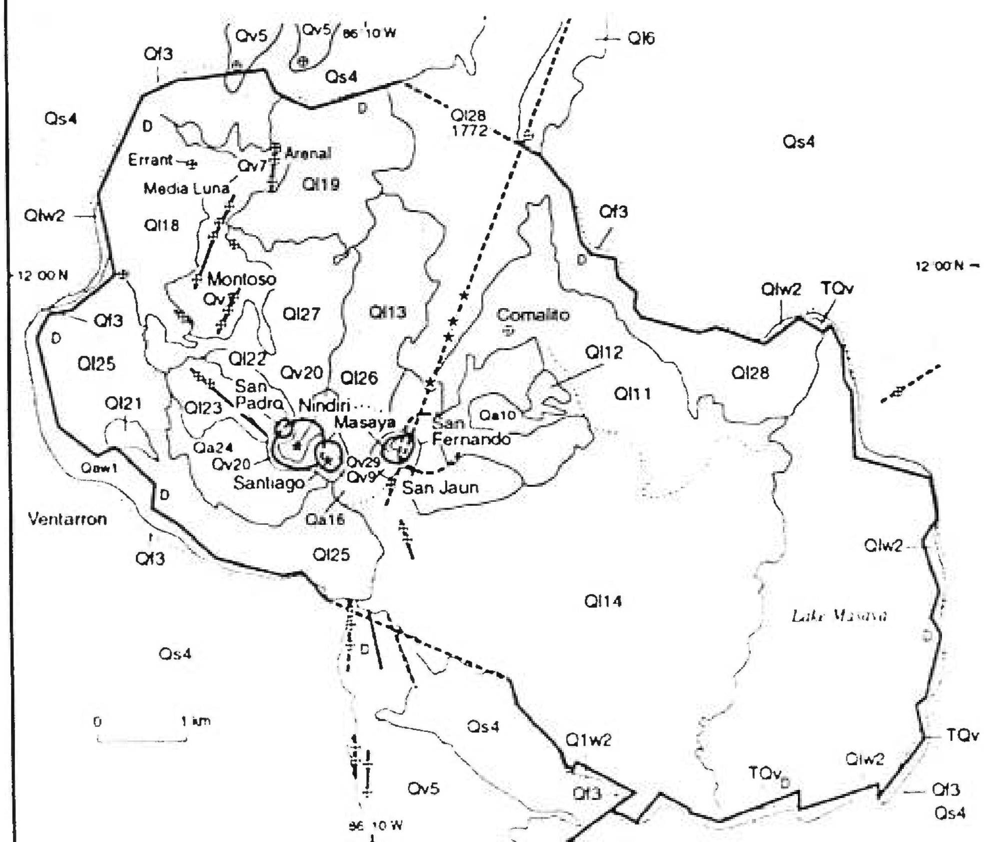

Masaya Caldera Complex, Nicaragua

age	unit	description	event
QUATERNARY	Ql 29	lava lake of 1965	
			Santiago Crater collapse 1953
	Ql 28	aa lava flow and associated fissure-erupted ash and scoria of 1772	
	Ql 27	aa lava flow and lava lake of 1670	
			Nindiri Crater Collapse pre-1524
	Ql 26	pahoehoe lava flow of Oviedo	
	Ql 25	pahoehoe lava flow with abundent lava tubes	
	Qa 24	scoria and ash (probably from site of Nindiri crater)	
	Ql 23	blocky lava and spatter erupted from fissure on NW flank of San Pedro crater	
	Ql 22	lava probably erupted from San Pedro crater	
	Ql 21	lava flow exposed below Ventarron	
	Qv 20	Nindiri complex-cinder cones, lava flows and lava lakes	
	Ql 19	aa lava flow with possible compound nature	
	Ql 18	aa lava flow probably from fissure N of Montoso	
			Masaya Crater collapse
	Ql 17	blocky lava flow and lava lake	
	Qa 16	scoria and ash, locally agglutinated	
	Ql 14	aa lava flow with abundent vesicles, overlain at head by scoria and ash, locally agglutinated	
	Ql 13	pahoehoe lava flow	
	Ql 12	Casa Vieja lava flow	
	Ql 11	Comalito aa lava flow and associated fissure-erupted scoria and ash (widely agglutinated)	
	Qa 10	ash and scoria	
	Qv 9	Masaya Crater Complex-cinder cones, lava flows, and lava lakes; Santiago Crater Complex-cinder cones and lava flows	
			San Fernando Crater collapse
	Qv 7	Lava and scoria and ash deposits (oldest of caldera flow, correlation and exact stratigraphic position uncertain)	
	Ql 6	Railroad flow-massive lava erupted from N caldera margin	
	Qv 5	lavas and scoria and ash deposits erupted after caldera collapse from caldera-bounding faults or on flanks	
			Caldera collapse 2,250-6,500 y.b.p.
	Qs 4	pyroclastic surge deposits	Masaya Tuff (Bice, 1985)
	Qf 3	pyroclastic flow deposits	Masaya Tuff (Bice, 1985)
	Qlw 2	lavas of caldera wall (includes minor ashfall and pyroclastic flow deposits)	
	Qaw 1	scoria and ashfall deposits of caldera wall (includes Masaya Triple Layer and Masaya Lapilli plinian deposits (Williams, 1983 and Bice, 1985)	
PLIO-PLEISTOCENE	TQv	Las Sierras Formation-pyroclastic flow or mudflow deposits exposed in area of Lake Masaya	
	★	historically active volcanic vent	
	÷	vent	
	- - -	fault or eruptive fissure; concealed	
	·····	contact; location approximate	

refined by Metaxian (1994). From a Bouguer survey of the caldera area, Metaxian (1994) postulated the presence of a dense body 500 kg m^{-3} higher than the surrounding rocks and centered at 6 km depth, of 6 km thickness, with the roof at a depth of 2-3 km. There is also a magnetic anomaly which has been modlled in terms of the same structure (Metaxian, 1994).

The basement of the caldera comprises the Las Sierras Formation (Williams, 1983). In the west, the caldera walls are made up only of basaltic ignimbrites, a 73 m thick sequence that formed the Fontana Lapilli, which is a major regional stratigraphic marker (Williams, 1983). Pyroclastic eruptions have produced extensive Strombolian deposits on the caldera floor and on the slopes of the volcano (Williams, 1983). Voluminous and widespread surge deposits are found around the caldera, and overlain by pyroclastic flow and fallout deposits which are believed by Williams (1983) to be associated with caldera collapse. Detailed mapping of the geologic units in the vicinity of the caldera was done by Williams (1983) (Fig I-12).

Geology of Telica Volcano

The Telica Volcanic Complex covers approximately 80 km^2 and extends from the town of Telica in the south to Las Marias in the north. Also near the complex, the city of San Jacinto lies to the east and Colonia Agricola Cristo Rey to the west (Fig. I-13). Telica volcano is a stratovolcano of basaltic to andesitic composition. The volume of the Telica complex is estimated at 30 km^3 of volcanic material (Stoiber and Carr, 1973). The following description of the Telica complex comes mainly from Lefebure (1986).

The Telica complex can be divided geomorphologically into elevated areas which are Cerro Los Portillo and San Jacinto, a lava "apron" and the volcanic cones

FIGURE I-13

Map of the Telica volcanic complex and surrounding towns (From Lefebure, 1896).

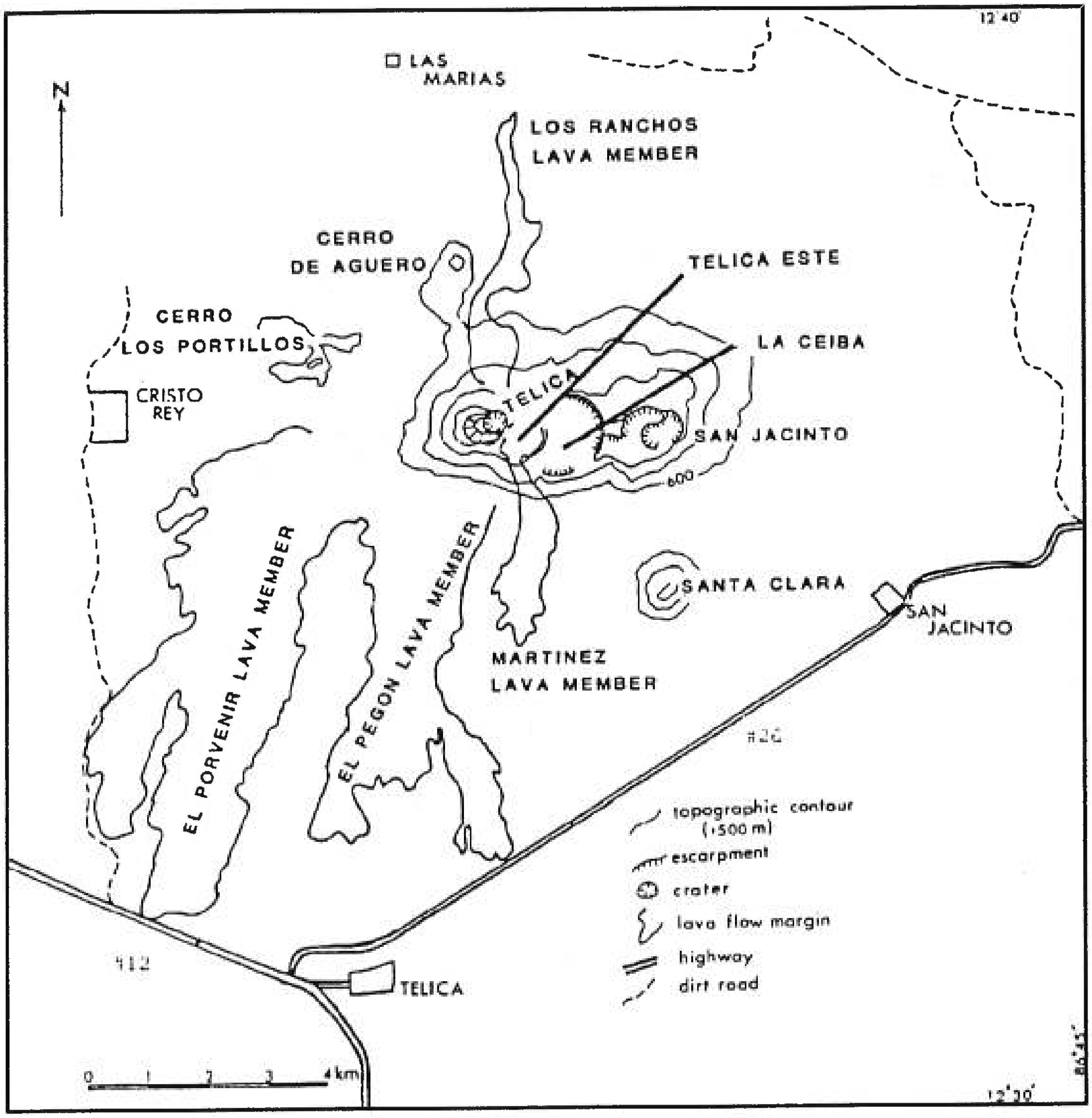

12°40'
LAS MARIAS
N
LOS RANCHOS LAVA MEMBER
CERRO DE AGUERO
TELICA ESTE
CERRO LOS PORTILLOS
LA CEIBA
CRISTO REY
TELICA
SAN JACINTO
600
EL PORVENIR LAVA MEMBER
EL PEGON LAVA MEMBER
SANTA CLARA
SAN JACINTO
MARTINEZ LAVA MEMBER
#26
topographic contour (>500 m)
escarpment
crater
lava flow margin
highway
dirt road
#12
TELICA
0 1 2 3 4 km
12°30'
86°45'

Table 1-2

Formations of the Telica volcanic complex (Adapted from Lefebure, 1986)

Period	Epoch	Formation	Lithology	Unit
Quaternary	Recent	Telica	alluvium and Colluivium	9
			basalt lava and tephra	8
	Recent or Pleistocene	San Jacinto	andesite lava	7
			altered basalt lapillistone and tuff	6
		Santa Clara	basalt lava and tephra	5
		Cerro de Aguero	basalt lava and tephra	4
		El Najo	basalt lava	3
		La Ceiba	andesite lava	2
Tertiary or Quaternary	Pliocene or Pleistocene	Cerros Los Portillos	basalt lava	1

of Telica, Santa Clara and Cerro de Aguero. The Telica complex consist of lavas, tephra, alluvium, lahars and intrusive rocks (Table I-2). The most abundant rock types are lava flows and tephra of basaltic and andesitic composition. Epiclastic rocks can be found in valleys on the flanks of the volcanic centers and in the surrounding plains. Outcrops of hypabyssal intrusive rocks are visible on the older volcanic centers. Telica, the only active cone in the complex at present, is also the youngest cone and rests on the other volcanic centers of the complex. McBirney and Williams (1965) believed the volcanoes of the Marrabios Range, including the Telica Complex, to be of Quaternary age. Lefebure (1986) separated the Telica Complex into eight different volcanic units (Table I-3) and identified 14 lava flows. Fumarolic activity occurs in the crater of Telica volcano, which is most intense during and immediately after the rainy season from April to July. North-south-oriented faults are common on the volcano (van Wyk de Vries, 1993). Hot springs are also present at 8 localities in the central, eastern and northern parts of the volcanic complex. The shape of the Telica edifice represents the construction and destruction of at least three successive edifices (Lefebure, 1986).

Volcanic Activity

Volcanic Activity of Masaya

Masaya volcano has been persistently active since the beginning of the sixteenth century. The activity is characterised by episodes of lava lake formation associated with strong gas emissions since the formation of Santiago crater in 1858-1859 (Stoiber et al., 1986). Plinian and ignimbrite eruptions also occurred in the

Table I-3

Description of the volcanic units of the Telica complex (From Lefebure, 1986)

Formation	Unit	Name	Phenocrysts	Groundmass
Telica	8c	Black pyroxene basalt porphyry tephra deposits	plag (An_{70-65}) augite olivine (Fo_{75})	labradorice and clinopyroxene microlites, opaques and sideromelane
	8b	Gray pyroxene basalt porphyry flows	plag (An_{50-65}) augite olivine (Fo_{85-80}) orthopyroxene opaques	labradorite, clinopyroxene and olivine microlices, opaques, +/- sideromelane
	8a	Gray pyroxene basalt porphyry lapilli and ash	plag (An_{80-70}) augite opaques	labradorite microlites and sideromelane or tachylite glass
	7	Gray andesite porphyry flows	plag (An_{85-60}) +/- augite opaques	andesine and clinopyroxene microlites, opaques and and intersertal glass
San Jacinco	6*	Brown or orange-brown altered basalt lapilli-stone and tuff	Plag Augite olivine	reddish-brown to black glass
Santa Clara	5	Gray olivine basalt porphyry flows and tephra	plag (An_{75-70}) opaques olivine (Fo_{50})	labradorite and augite microlites, opaques and minor glass
Cerro de Aguero	4	Gray olivine andesite porphyry flows and tephra	plag (An_{80-70}) opaques olivine (Fo_{75})	labradorite and augite microlites, olivine, opaques and glass
El Najo	3	Gray olivine pyroxene basalt porphyry flows	plag (An_{80-75}) augite olivine	labradorite and clinopyroxene microlites, opaques and intersertal glass
La Ceiba	2	Grey and red pyroxene andesite flows	plag (An_{85-65}) bronzite opaques +/- olivine	plagioclase and clinopyroxenes microlites in glass
Cerro Los Portillos	1	Gray olivine basalt porphyry flows	plag (An_{85-60}) olivine (Fo_{95-85}) +/- augite	labradorite and clinopyroxene microlites, opaques, minor glass

history of Masaya (Williams, 1983). Caldera-forming eruptions have been frequent in Masaya's volcanic history; at least four are known between 2700 and 30 000 years BP (Williams, 1983; van Wyk de Vries, 1991, from Rymer et al., 1998). Stoiber et al. (1986) estimated that approximately 33×10^6 m^3 of basaltic lavas were erupted since the Spanish Conquest (1524). This gives an average rate of 0.07×10^6 m^3 yr^{-1}, which is significantly lower compared to what Williams (1983) calculated for the average prehistoric rate of $1.9\text{-}5.5 \times 10^6$ m^3 yr^{-1}.

One unusual aspect of Masaya is the degassing crises that have occurred since 1852 (Stoiber et al., 1986). Five of these crises have occurred in the past, and one is ongoing since 1993 (Rymer et al., 1998). The gas is coming out of the active Santiago crater. During the episode from 1977 to 1985, Stoiber et al. (1986) measured SO_2 fluxes in the gas plume by COSPEC and estimated an average flux of 1275 metric tonnes/day. This degassing rate implies that 10 km^3 of magma have been degassed over the last century. This indicates a discordance between the gas emission rate and the lava emission rate. The ratio of erupted solid material to the volume of intrusive degassed magma (0.1 km^3 yr^{-1}) is only 0.0007 (Metaxian, 1994). An active lava lake was sometimes visible in Santiago from 1965 to 1979. Cooling of this lava lake formed the platform which is visible today at a depth of 150 m in Santiago. After partial collapse of this platform in 1989, a new lava lake was visible 150 m deeper than the platform (SEAN Bulletin, 1989). This state lasted for 1½ months and was terminated by further collapse of the southern part of the crater (Metaxian, 1994). From 1990 to 1993, activity was restricted to very small gas emissions (less than 25 metric tonnes/day SO_2) (Bulletin of the Global Volcanism Network, 1992). In 1993, the volcano entered a new degassing phase, and a new lava lake was visible (Rymer et al., 1998). This renewal in activity was accompanied by an increase in the permanent tremor amplitude by a factor of 4 as recorded at the volcano (Metaxian, 1994). The source of tremor is located beneath the active crater of Santiago (Metaxian and Lesage, 1997).

Volcanic Activity of Telica

During historic time, two volcanoes in the Telica Complex have been active: Santa Clara and Telica. Historical volcanic activity at Santa Clara was restricted to solfateric activity during the sixteenth century (Lefebure, 1986). Telica has had extended periods of solfateric activity and numerous small explosive eruptions during the last 500 years (Lefebure, 1986). Since the beginning of the twentieth century, the activity has increased, ejecting ash during at least 22 different eruptive periods (Lefebure, 1986). A lava lake was observed in 1971 at the bottom of Telica's deep circular crater. Historic eruptions at Telica have resulted in vertical ejections of basaltic ash and gases over periods of days or weeks with associated seismic activity. During stronger eruptions, lapilli, bombs and blocks were sometimes ejected onto the crater rim and flanks. The eruptions resemble many of the features of Strombolian-type volcanoes (Lefebure, 1986).

References

Bice, D.C., 1985. Quaternary volcanic stratigraphy of Managua, Nicaragua: correlation and source assignment for multiple overlapping plinian deposits. Geol. Soc. Am. Bull., 96: 553-566.

Brown, G.C., Everett, S.P., Rymer, H., McGarvie, D.W., and Foster, I., 1991. New light on caldera evolution – Askja, Iceland. Geology, 19: 352-355.

Bulletin of the Global Volcanism Network, 1994. Masaya volcano. Smithsonian Institution 18: 7, 11.

Carr, M.J., 1984. Symmetrical and segmented variations of physical and geochemical characteristics of the Central American volcanic front. J. Volcanol. Geotherm. Res., 20: 231-252.

Connor, C.B., and Williams, S.N., 1989. Interpretation of gravity anomalies, Masaya caldera complex, Nicaragua. Transactions of the 12th Caribbean Geological Conference.

Eggers, A., Krausse, J., Rush, H., and Ward, J., 1976. Gravity changes accompanying volcanic activity at Pacaya volcano, Guatemala. J. Volcanol. Geotherm. Res., 1: 229-236.

Eggers, A.A., and Chavez, D., 1979. Temporal gravity variations at Pacaya volcano, Guatemala. J. Volcanol. Geotherm. Res., 6: 391-402.

Eggers A.A., 1983. Temporal gravity and elevation changes at Pacaya volcano, Guatemala. J. Volcanol. Geotherm. Res., 19: 223-237.

Kieffer, G., and Creusot-Eon, A., 1992. La caldeira de Masaya (Nicaragua): une dépressiom polyphasée de type « maar ». C.R. Acad. Sci. Paris, 315: 1403-1409.

Lefebure, D.V., 1986. The mina El Limon area and the Telica complex: two examples of Cenozoic volcanism in northwestern Nicaragua, Central America. Unpublished Ph.D. Thesis, Department of Geology, Carleton University, Ottawa, Canada, 269 pp.

Maciejewski, A.J.H., 1995. Evolution and present-day activity of the Masaya volcanic complex. Unpublished manuscript, The Open University, 37 pp.

Malfait, B.T., and Dinkelman, M.G., 1972. Circum-Caribbean tectonic and igneous activity and the evolution of the Caribbean plate. Geol. Soc. Am. Bull., 83: 251-272.

McBirney, A.R., 1956. The Nicaraguan volcano Masaya and its caldera. EOS Trans. AGU, 37: 83-96.

McBirney, A.R., and Williams, H., 1965. Volcanic history of Nicaragua. University of California, Publications in Geological Sciences, 55: 1-73.

McClelland, L., Simkin, T., Summers, M., Nielsen, E., and Stein, T. C. 1989. Global Volcanism 1975-1985. The first decade of reports from the Smithsonian Institution's Scientific Event Alert Network (SEAN). Prentice Hall, Englewood Cliffs, New Jersey, AGU, 655 pp.

Metaxian, J.-P., 1994. Etude sismologique et gravimétrique d'un volcan actif: Dynamisme interne et structure de la Caldeira Masaya, Nicaragua. Unpublished Ph.D. Thesis, Université de Savoie, Savoie, France, 319 pp.

Metaxian, J.-P., and Lesage, P., 1997. Permanent tremor of Masaya volcano, Nicaragua: Wave field analysis and source location. J. Geophys. Res., 102: 22 529-22 545.

Rymer, H., 1989. A contribution to precision microgravity data analysis using Lacoste and Romberg gravity meters. Geophys. J., 97: 311-322.

Rymer, H., 1994. Microgravity change as a precursor to volcanic activity. J. Volcanol. Geotherm. Res., 61: 311-318.

Rymer, H., and Locke, C.A., 1995. Microgravity and ground deformation precursors to eruption: a review. Cahiers du Centre Européen de Géodynamique et de Séismologie, 8: 21-39.

Rymer, H., van Wyk de Vries, B., Stix, J., and Williams-Jones G., 1998. Pit crater structure and processes governing persistent activity at Masaya volcano, Nicaragua. Bull. Volcanol., 59: 345-355.

Stoiber, R.E., and Carr, M.J., 1973. Quaternary volcanic and tectonic segmentation of Central America. Bull. Volcanol., 37: 304-325.

Stoiber, R.E., Williams, S.N., and Huebert, B.J., 1986. Sulfur and halogen gases at Masaya caldera complex, Nicaragua: total flux and variations with time. J. Geophys. Res., 91: 12 215-12 231.

Van Wyk de Vries, B., 1993. Tectonics and magma evolution of Nicaraguan volcanic systems. Unpublished Ph.D. Thesis, Department of Earth Sciences, Open University, Milton Keynes, UK, 328 pp.

Vieira, R., Toro, C., and Araña, V., 1986. Microgravity survey in the caldera of Teide, Tenerife, Canary Islands. Tectonophys., 130: 249-257.

Viramonte, J.G., Navarro Collado, M., and Malavasi Rojas, E., 1997. Nicaragua-Costa Rica Quaternary Volcanic Chain. IAVCEI 1997 General Assembly, Puerto Vallarta, Mexico, Guidebook for Field Trip 17, 59 pp.

Walker, J.A., Williams, S.N., Kalamarides, R.I., and Feigenson, M.D., 1993. Shallow open-system evolution of basaltic magma beneath a sudbuction zone volcano: the Masaya caldera complex, Nicaragua. J. Volcanol. Geotherm. Res., 56: 379-400.

Weyl, R., 1980. Geology of Central America. Gebruder Borntraeger, Berlin, Germany, 371 pp.

Williams, S.N., 1983. Plinian airfall deposits of basaltic composition. Geology, 11: 211-214.

CHAPTER I

The nature and origin of gravity anomalies at Telica volcano, Nicaragua

Alexandre Beaulieu[1], John Stix[1], Hazel Rymer[2], Glyn Wiliams-Jones[2]

[1]Département de Géologie
Université de Montréal
Montréal, Québec, H3C 3J7
Canada

[2]Department of Earth Sciences
Open University
Milton Keynes, MK7 6AA
United Kingdom

Abstract

The Telica complex, Nicaragua, has been very active in historic time and is a potentially dangerous volcano. Telica has undergone extended periods of fumerolic activity and numerous small explosive eruptions. An interpretation of gravity data collected in 1997 and 1998 was made to better delineate the geologic structure of the Telica Complex. During the static gravity survey, a total of 245 stations were occupied in the vinicity of the volcano. Compilation of the gravity data revealed a large anomaly oriented north-south. This body has a positive density contrast of around 400-600 kg m^{-3}. This anomaly of dimensions 2 km × 2 km × 6 km at a depth of about 1 km is probably an intrusion or magma reservoir. It is situated in the middle of the Telica complex and may feed all the volcanoes situated in the complex. The regional structure is concordant with this intrusion, with three north-trending tensional faults and the alignment of the cones being oriented approximately parallel to the gravity anomaly. The ongoing seismic activity may indicate magma replenishment into this reservoir or the occurence of a pressure buildup, since there is practically no visible degassing at the surface of the volcano.

Introduction

Telica is an active volcano in northwestern Nicaragua forming part of the chain of Quaternary volcanoes along the western margin of Central America (Fig. 1.1). Telica and its adjacent volcanoes, including Santa Clara, Cerro Aguero and San Jacinto, are part of the Telica complex situated in the Marrabios Range on the southwestern margin of the Nicaraguan Depression (Fig. 1.2). Telica rises to a

FIGURE 1.1

Map of the Quaternary volcanoes of Central America showing the location of Telica volcano (From Weyl, 1980).

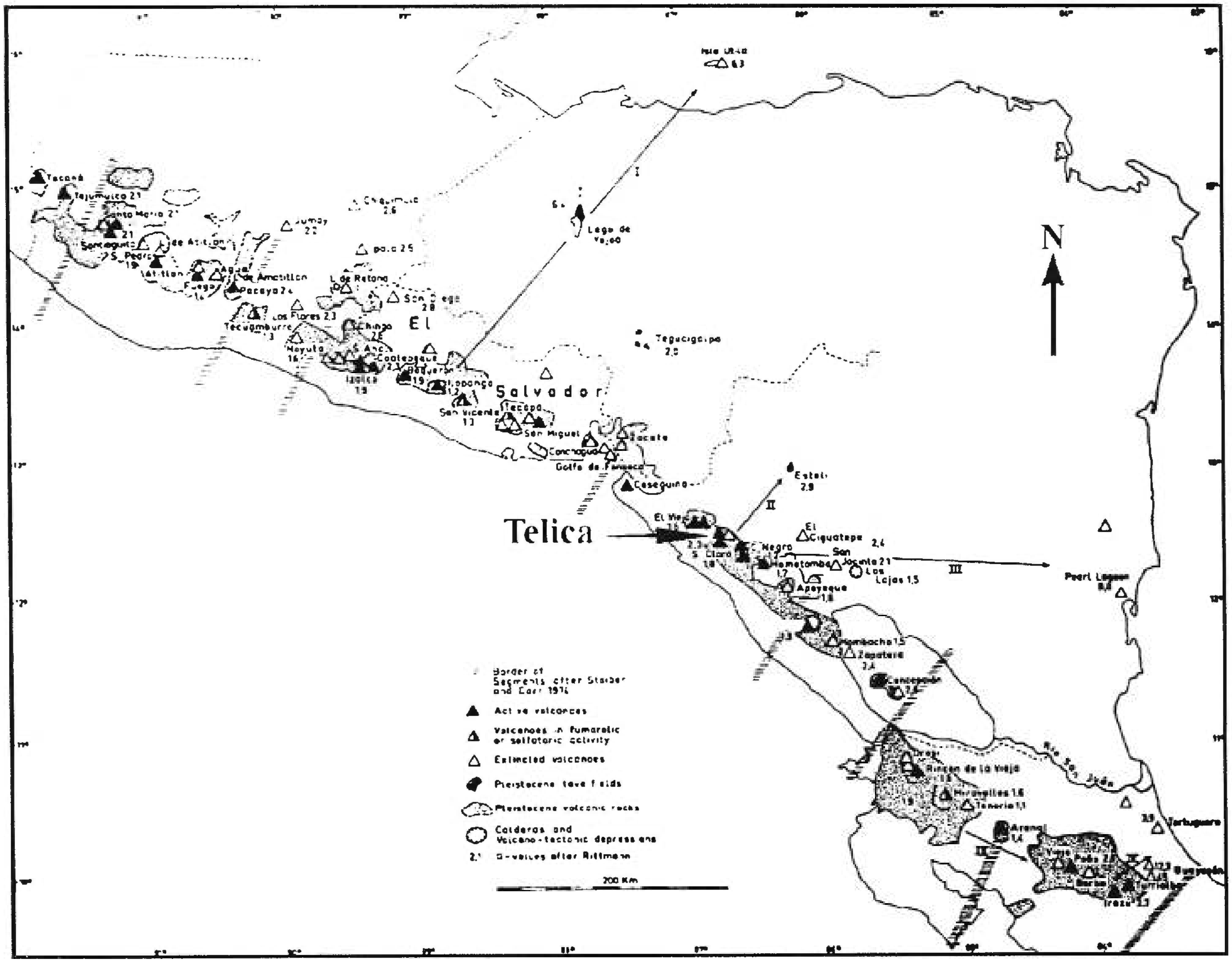

N
Telica
El Salvador
Tegucigalpa
Golfo de Fonseca
Cosegüina
Estelí
Pearl Lagoon
Tortuguero
Arenal
Irazú
Turrialba
Rincon de la Vieja
Miravalles 1,6
Tenorio 1,1
Concepción
Zapatera
Mombacho 1,5
Apoyeque
Momotombo
Cerro Negro
El Ciguatepe
San Jacinto 2,1
Los Lajas 1,5
El Viejo
San Miguel
Conchagua
San Vicente
Tecapa
Ilopango
Izalco
Santa Ana
Coatepeque
Boquerón
Tecuamburro
Pacaya 2,4
Fuego
Agua
Atitlán
Santiaguito
Santa María
Tajumulco 2,1
Tacaná
Lago de Yojoa
Border of Segments after Stoiber and Carr 1974
Active volcanoes
Volcanoes in fumarolic or solfataric activity
Extincted volcanoes
Pleistocene lava fields
Pleistocene volcanic rocks
Calderas and Volcano-tectonic depressions
200 Km

FIGURE 1.2

Geological map of the Marabios Range, Nicaragua (Form Weyl, 1980).

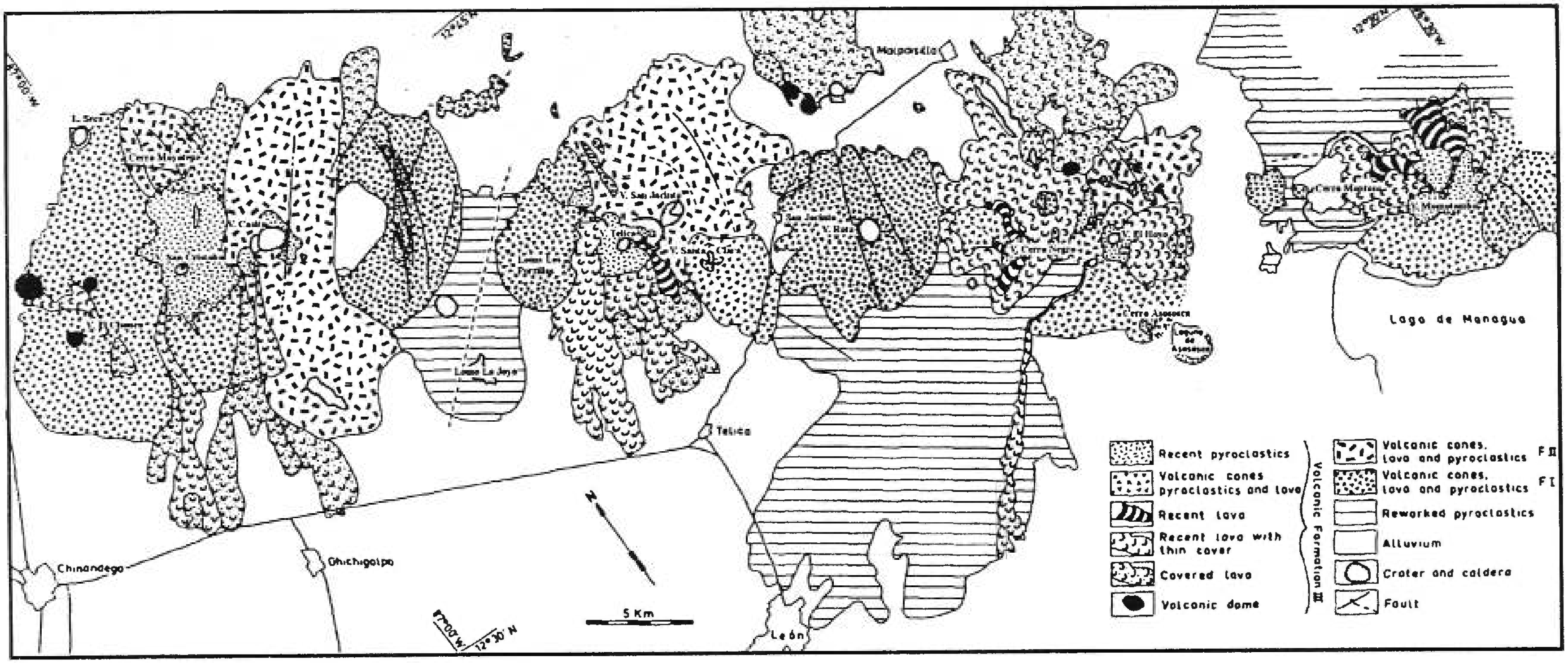
Lago de Managua
Malpaisillo
Telica
León
Chinandego
Chichigalpa
Laguna La Joya
Cerro Asososca
Laguna de Asososca
5 Km
N
87°00' W
12°30' N
Recent pyroclastics
Volcanic cones pyroclastics and lava
Recent lava
Recent lava with thin cover
Covered lava
Volcanic dome
Volcanic Formation III
Volcanic cones, lava and pyroclastics F II
Volcanic cones, lava and pyroclastics F I
Reworked pyroclastics
Alluvium
Crater and caldera
Fault

maximum elevation of 1060 m above sea level; elevation at the base of the volcano is around 100 m. The volcano has a very steep-sided cone with an active crater of 700 m diameter. The Telica Complex consists of overlapping lava flows, tephra, alluvium, lahars and intrusive rocks. One of Nicaragua's most active volcanoes, Telica has erupted intermittently since the time of the Spanish conquest. Historical activity at Telica consists of extended periods of fumerolic emissions and numerous small explosive eruptions (Lefebure, 1986). Eruptions in the sixteenth century have been reported at Santa Clara (Lefebure, 1986), but its eroded and breached crater has been covered by forests throughout historical time. Telica is currently monitored with a telemetered seismic station by INETER (Instituto Nicaragüense de Estudios Territoriales). From December 1996 to June 1997, the number of volcanic/seismic and seismic events increased from ~100/day to ~220/day (GVNB 22:03, 22:05 and 22:06). Solfateric activity is very low at Telica, with the SO_2 flux measured by COSPEC on 17 March 1996 averaging 40 ± 20 t/d and nearly zero in March 1997, based on nine measurements (GVNB 21:04, 22:03). The volcano is also monitored with microgravity; measurements since 1993 have shown no significant changes (H. Rymer, personal communication, 1998).

Knowledge of the internal structure and dynamics of volcanoes improves our means to understand volcanic activity. Knowing the location of a large dike or a shallow intrusion makes it possible to focus monitoring on that particular point. This knowledge also may be used for economic purposes; e.g., geothermal energy which could provide electricity. Investigation of volcanoes by geophysical means enhances our understanding of their internal structure when integrated with geological, petrological and geochemical methods. Gravity surveys are well suited to the study of internal structures of volcanoes because the density contrasts encountered in a volcanic environnement can be substantial. A gravity survey permits the detection of bodies which have a different density than the surrounding rocks, for example, deep or shallow magma chambers, magma dikes or pipes and low-density fragmental material which may fill a caldera or a crater depression. The utility of gravity and microgravity data on volcanoes has been amply demonstrated (Rymer and Brown, 1986; Eggers, 1987; Metaxian, 1994; Rymer, 1994). To better define the subsurface and internal structure and to delineate possible intrusive magma volumes, a gravity survey of Telica volcano and the surrounding area was made in the winters of 1997 and 1998. From this survey, a series of Bouguer anomaly maps were made.

Methodology

A total of 245 stations were occupied in the vinicity of Telica volcano during the months of February and March in 1997 and 1998. Gravity measurements were made with Lacoste and Romberg meter G-513 (see Table A1 in Appendix A). Leica GPS 200 dual-frequency differential receivers provided positioning and elevation control of the stations (see Table A2 in Appendix A). In the course of the first gravity survey in 1997, measurements were made only in the vinicity of the crater with a dense array. In 1998, the gravity grid was extended farther from the volcano to enlarge the gravity anomaly map. Four base stations (Base1, Base2, Base3 and Basefinal) were used to connect all the stations together. The stations are not connected to an absolute gravity station, so the gravity values are calculated relative to Base3. The locations of these base stations are shown in Figure 1.3. Base2, Base3 and Basefinal

FIGURE 1.3

Topographic map of the Telica complex showing location of the base station, the two gravity profiles and a sketch of the intrusion.

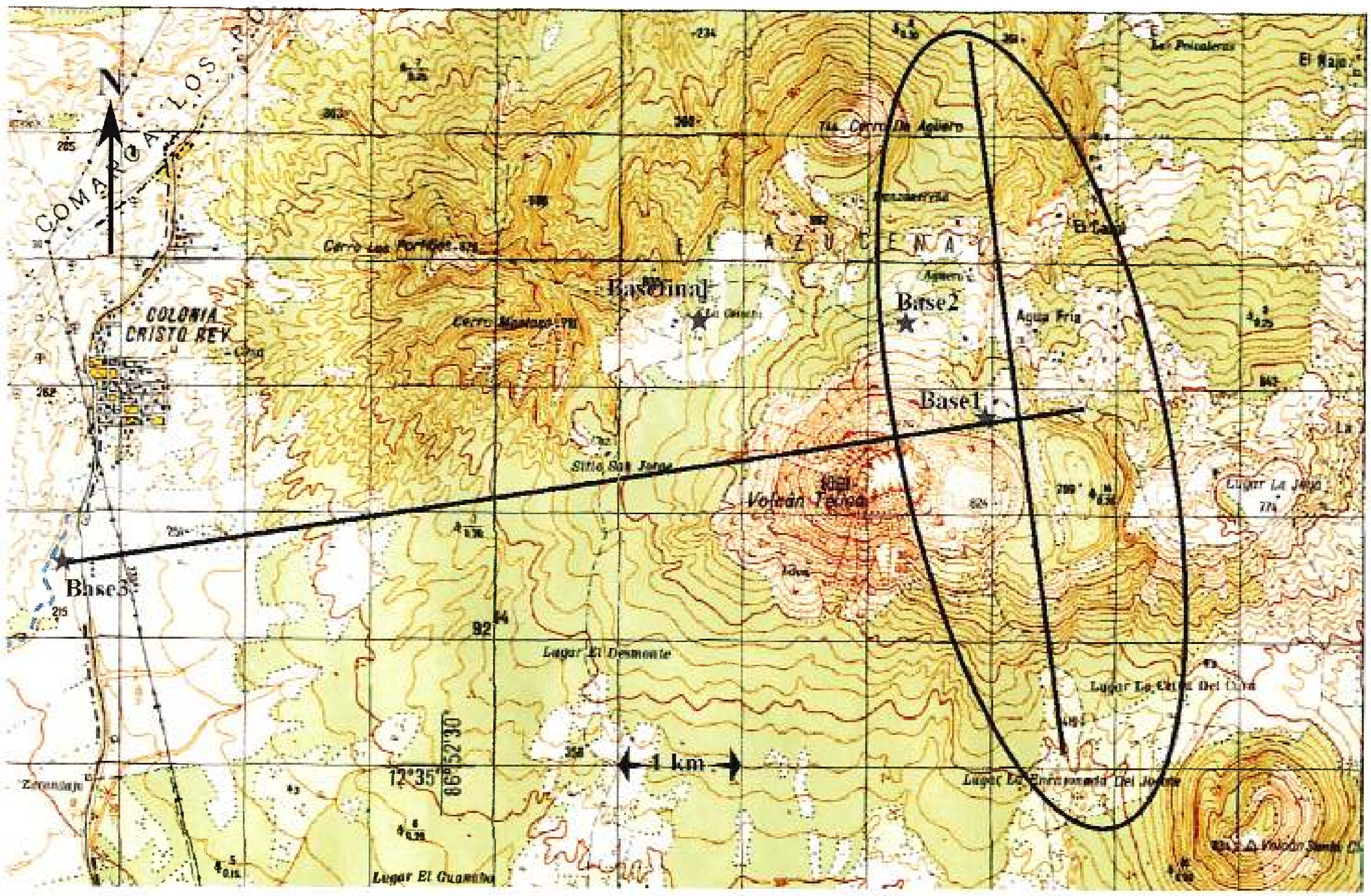
N
COMARCA LOS
COLONIA
CRISTO REY
Base3
Basefinal
Base2
Base1
EL AZUCENA
Agua Fria
Cerro Los Portillos
Cerro Montoso
Cerro Del Agüero
Sitio San Jorge
Volcán Telica
Lugar El Desmonte
Lugar El Guanillo
Lugar La Joya
1 km
12°35'
86°52'30"

are temporary stations located on the road to Telica and are difficult to relocate. Base1 is a good station to use for a new survey or to continue this survey. The station is located about 5 m west of a house (Fig. 1.4) at the foot of the volcano on its northeast side. The latitude and longitude is: 12° 36′ 33.2394″ N, 86° 49′ 56.9752″ W, at an elevation of 734 m. The station is situated on a round dark gray rock 50 cm in diameter and rising up about 15 cm from the soil. Alejandro Acosta, a driver for INETER, is a good contact for more information on the exact location of this station.

All gravity measurements were tide-corrected in the field using GRAVPAC, a solar and lunar tide calculator provided by Lacoste & Romgerg Inc.. Meter drift was not accounted for on a daily basis, since it was generally only of the order of 15-25 μGal (average 17 μGal) after 6-7 hours at the end of the day. Meter drift on a weekly and yearly basis was corrected, since there was an overall drift of 131 μGal between the first and the last day of measurements at Base1 in 1997. The drift of the meter between 20/03/97 and 11/02/98 was 3.690 mGal.

Gravity corrections were made for all stations; a summary of these corrections and measurements is presented in Table A2 in Appendix A. Because of the equatorial bulge and the rotation of the Earth, there is an increase of gravity with latitude (Telford et al., 1990). Correction for latitude ΔG_l is calculated as follows:

$$\Delta G_l = 0.811 \sin 2\phi \Delta s \quad \text{mGal}$$

where Δs is the north-south horizontal distance in kilometers of a station from Base3 and ϕ the latitude in degrees (12.6° N in our case). This correction is positive as we

FIGURE 1.4

Location of station Base1 near the house at the foot of Telica volcano. Photo of the house.

Station Base1

House

move toward the Equator. Because gravity varies inversely with the square of distance, a correction for elevation differences between stations is required. The free-air correction (ΔG_{FA}) is calculated as follows:

$$\Delta G_{fa} = 0.3086 \Delta z \text{ mGal}$$

where Δz is the elevation difference in meters between a station and Base3. Then, a Bouguer correction is made to account for the material between the stations and the reference station that the free-air correction ignores (Base3 in our case). This correction (ΔG_B) is calculated from:

$$\Delta G_B = 0.00004192 \rho \Delta z \text{ mGal}$$

where ρ is the density in kg m^{-3} of the material determined by the Nettleton method (1939) and Δz is the elevation difference in meters between a station and Base3. For accurate corrections (latitude, free-air and Bouguer), the station position and elevation have to be known with accuracy. For an accuracy of 10 μGal, the position of each station has to be known within 10 m and elevation to 3 cm.

Position and elevation of each station were acquired with Leica GPS 200 dual-frequency differential receivers. The precision obtained is about 1 cm horizontally and 1-2 cm vertically. This precision is relative between stations when they are connected to each other. For the absolute position of the gravity network, no benchmarks were available. Thus, during the survey of 1997, the reference GPS was always positioned at the same point and measured several time for 6-7 hours each day. This is not a gravity station but a relative reference for the rover GPS. A single-point computation was made at this point and gave an absolute position to about 10 m of precision. The corresponding error for latitude, Free-air and Bouguer corrections is 3.5×10^{-6} mGal, 6×10^{-3} mGal and 2×10^{-3} mGal, respectively. The error for latitude correction is negligible and will not be considered further.

For the terrain correction, only a topographic map of 1:50 000 scale was available. For terrain corrections « A » through « D » (0-170 m radius), the method of Sandberg (1958) was used. It involves approximating the slope near the station, divided into quadrants. The Sandberg tables were used to calculate the correction (Sandberg, 1958). For terrain corrections « E » through « K » (170-9900 m radius), the Hammer (1939) method was used on the topographic map available. Unfortunately, because of the lack of other maps of larger scale, corrections « M » and « L » (9900-21950 m) were not made. The terrain correction in the tables of Hammer (1939) and Sanberg (1958) are calculated for a density of 2000 kg m^{-3}. A conversion has to be made to account for the average density evaluated with the Nettleton (1939) method. For the terrain correction, the error is comparatively high. It is normally about 10 % of the average terrain corrections (Barrows, 1996), which is equal here to 0.62 mGal (6.2 mGal being the average terrain correction).

The density used in the modelling was evaluated from the Nettleton profile made on the volcano (Fig. 1.5a, b). The Nettleton method is a mean to estimate the near-surface density, using a gravity profile over topography, that is not related to density variations. Field readings are reduced using different densities for the Bouguer and terrain corrections. The profile that least reflects the topography is the profile with the best estimated density. An average density of 2400 kg m^{-3} was chosen from the

FIGURE 1.5

Nettleton correction for a gravity profile on Telica volcano using density variation of 1800 kg m^{-3} to 2900 kg m^{-3}. (a) The gravity profile for the different densities. (b) The corresponding elevation profile on Telica.

A

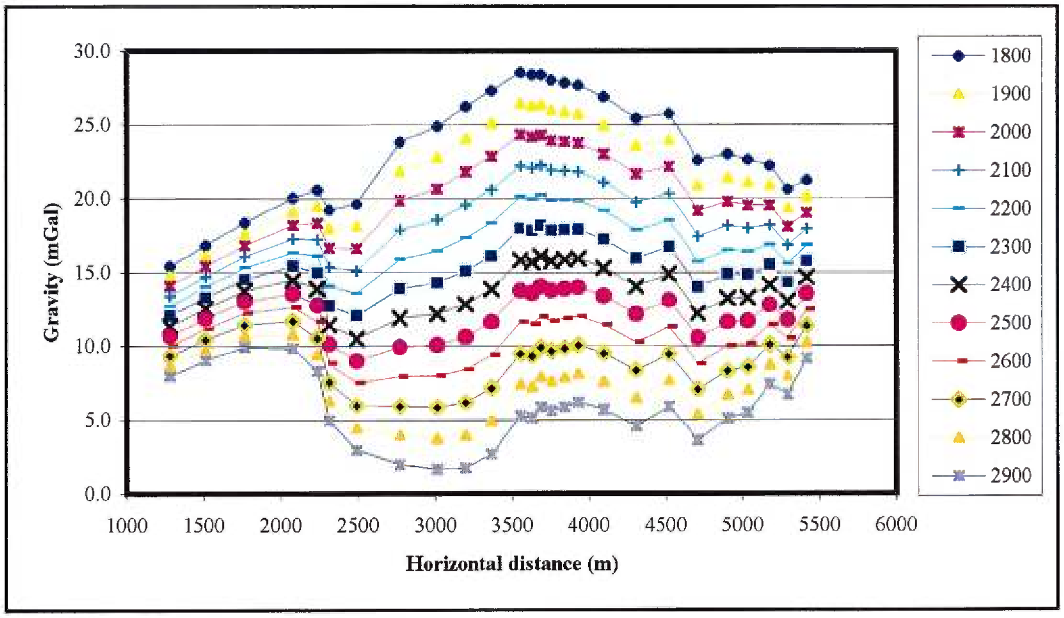
30.0
25.0
20.0
15.0
10.0
5.0
0.0
Gravity (mGal)
1000
1500
2000
2500
3000
3500
4000
4500
5000
5500
6000
Horizontal distance (m)
1800
1900
2000
2100
2200
2300
2400
2500
2600
2700
2800
2900

B

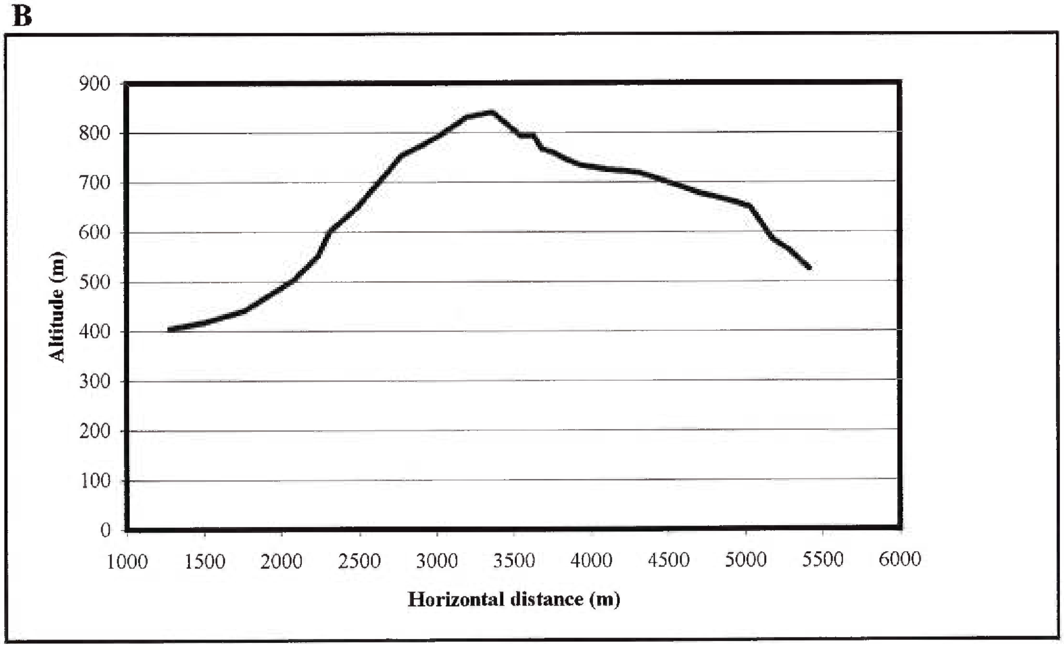
900
800
700
600
500
400
300
200
100
0
Altitude (m)
1000
1500
2000
2500
3000
3500
4000
4500
5000
5500
6000
Horizontal distance (m)

Nettleton correction. For matters of comparison, gravity also was corrected using values of 2300 kg m^{-3} and 2500 kg m^{-3}. Using these densities, three Bouguer anomaly maps were made. The density was used in the Bouguer and terrain corrections. After being corrected, the gravity data were interpolated using a linear method to a 50 m × 50 m grid and contoured using MATLAB.

The error due to gravity measurements is about 0.015 mGal, while the error from elevation control depending on the density estimation (Free-air and Bouguer) should not exceed 0.01 mGal. The estimated error from the terrain correction is 0.62 mGal. Thus, we can say that the error for terrain corrections should not exceed 1.0 mGal. The error on the density estimate, which should not exceed 200 kg/m^3, corresponds to an error of 0.1 mGal. The total error (E) is equal to the following:

$$E = \left[E_G^{\ 2} + E_T^{\ 2} + E_A^{\ 2} + E_\rho^{\ 2}\right]^{\frac{1}{2}}$$

where E_G is the error for the Lacoste and Romberg measurement, E_T is the error from the terrain corrections, E_A the error from elevation control and E_ρ the error from the density evaluation. Thus, the error on the contour map is about 0.63 mGal, mainly due to the terrain correction.

Three Bouguer gravity anomaly maps were made for densities of 2300 kg m^{-3}, 2400 kg m^{-3} and 2500 kg m^{-3}. There are only small differences among the three maps in terms of the anomalies, but the magnitude of the anomalies is different for each map. The gravity anomalies are calculated using Base3 as a zero gravity reference value. The anomaly map for modelling used a density of 2400 kg m^{-3} (Fig. 1.6a), and the two other maps are shown for comparison (Fig 1.6b, c). Two profiles

FIGURE 1.6

Contour map of the gravity anomaly showing the two profiles for density reductions of (a) 2400 kg m^{-3}, (b) 2300 kg m^{-3} and (c) 2500 kg m^{-3}. Contour interval is in mGal. Two profiles are shown which are used for GRAVMAG interpretation.

A

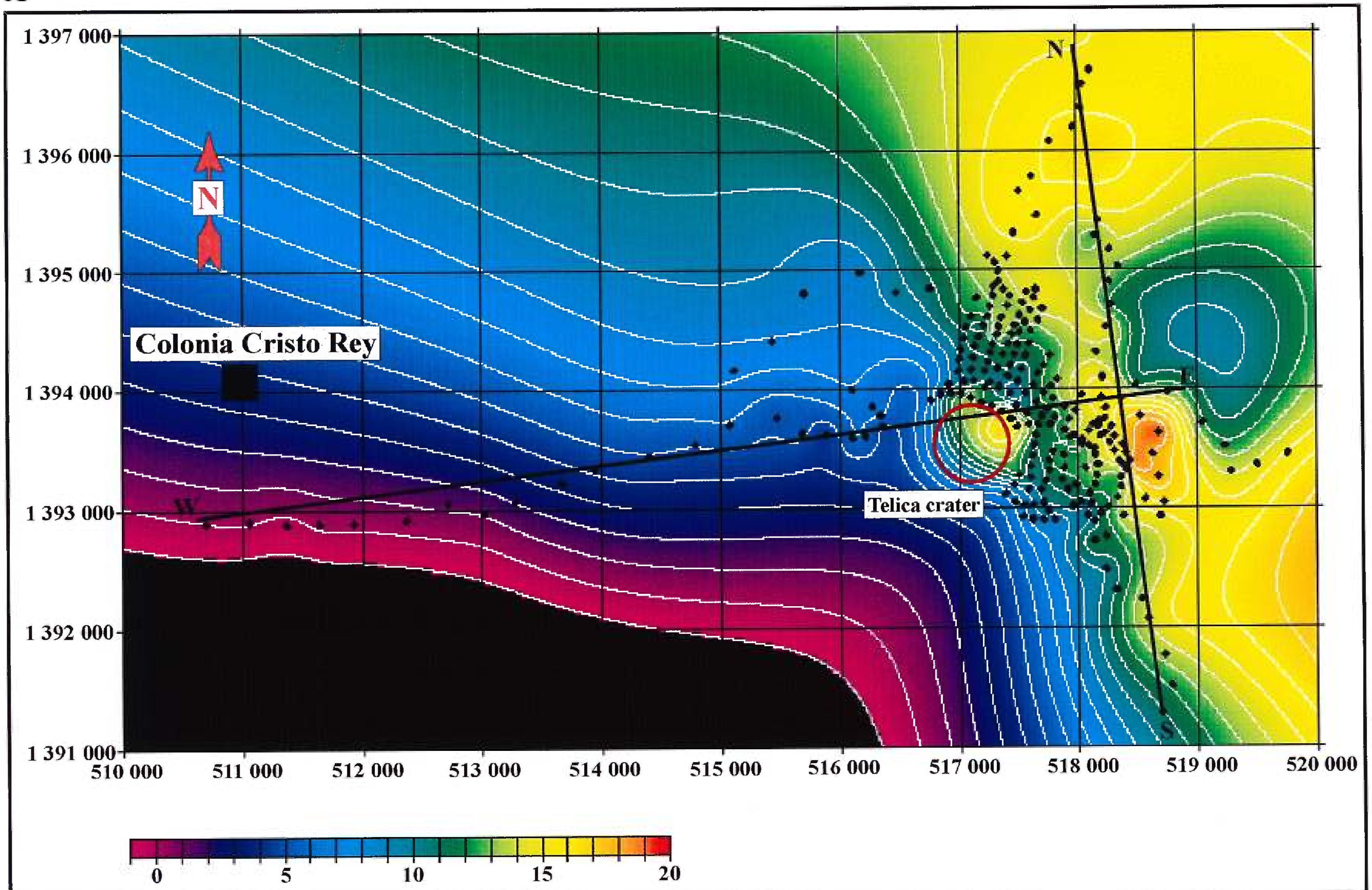

1 397 000
1 396 000
1 395 000
1 394 000
1 393 000
1 392 000
1 391 000
510 000
511 000
512 000
513 000
514 000
515 000
516 000
517 000
518 000
519 000
520 000
N
Colonia Cristo Rey
Telica crater
N
S
W
E
0
5
10
15
20

B

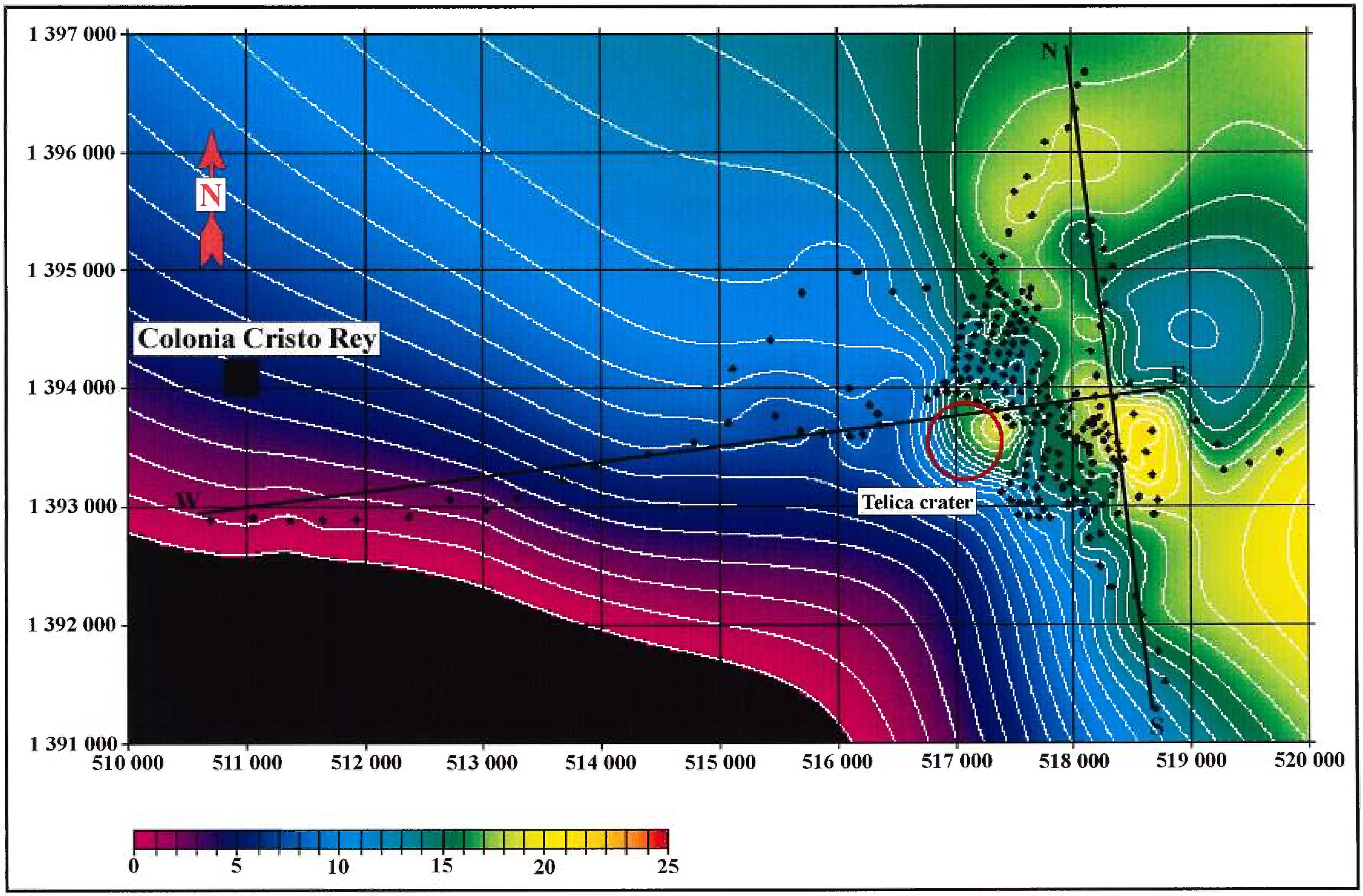
1 397 000
1 396 000
1 395 000
1 394 000
1 393 000
1 392 000
1 391 000
510 000
511 000
512 000
513 000
514 000
515 000
516 000
517 000
518 000
519 000
520 000
N
Colonia Cristo Rey
Telica crater
W
E
N
S
0
5
10
15
20
25

C

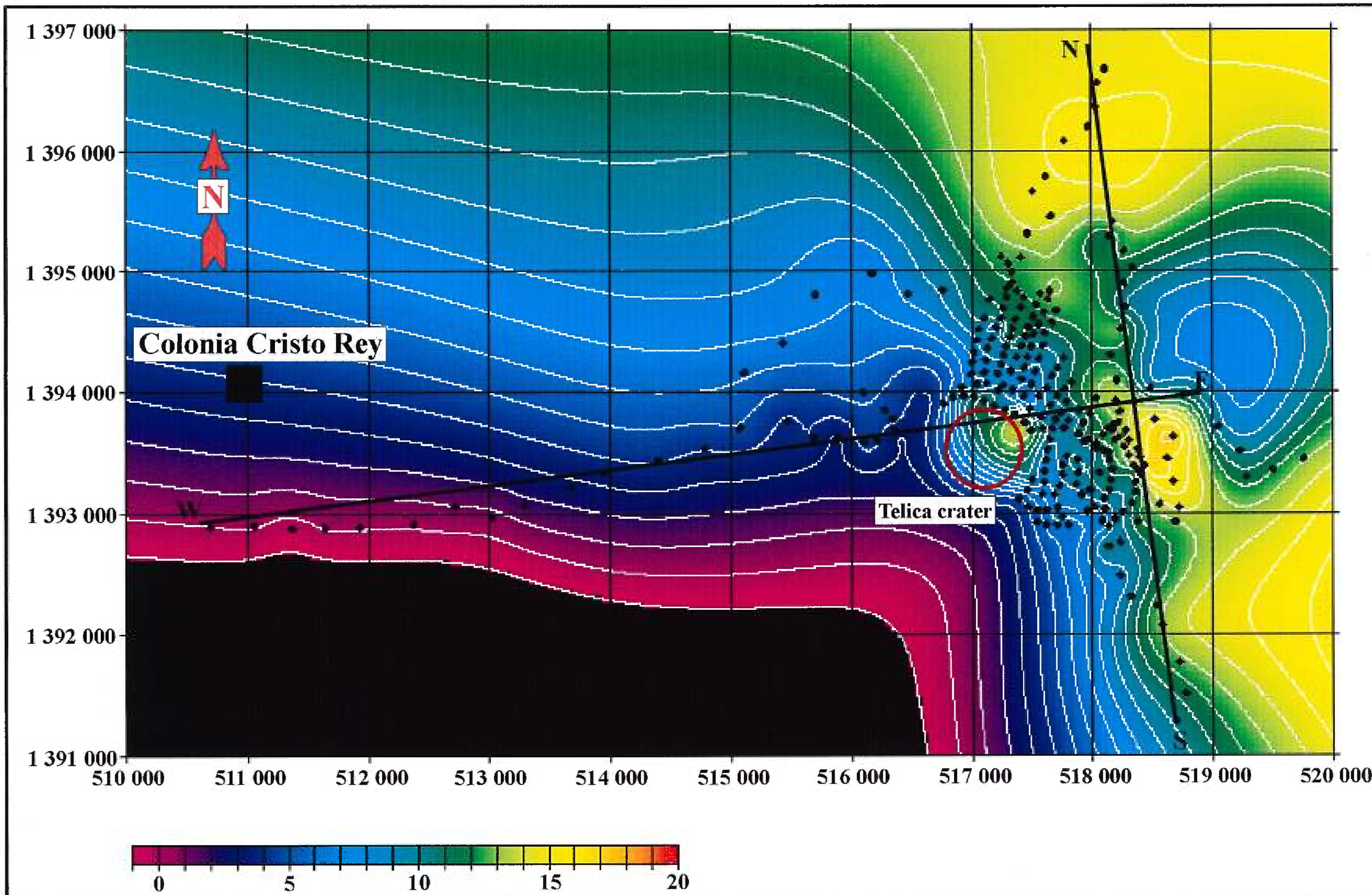

N
Colonia Cristo Rey
Telica crater
N
S
W
E
1 397 000
1 396 000
1 395 000
1 394 000
1 393 000
1 392 000
1 391 000
510 000
511 000
512 000
513 000
514 000
515 000
516 000
517 000
518 000
519 000
520 000
0
5
10
15
20

FIGURE 1.7

Stratigraphic profiles of the Telica complex which correspond approximately to the gravity profile: (a) the north-south profile; (b) the east-west profile.

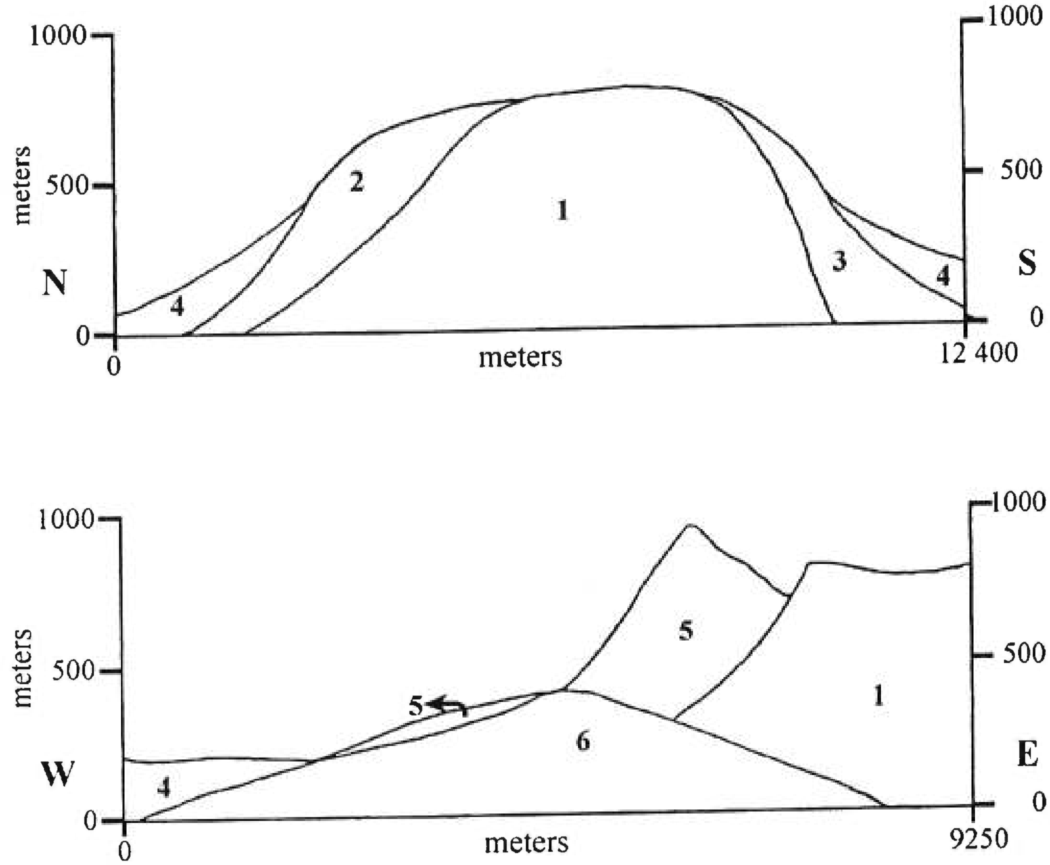

Legend: 1- Andesite flow
2- Andesite and tephra
3- Basalt and tephra
4- Basalt and lapilli-stone and tuff
5- Basalt tephra
6- Basalt flow

were made on the anomaly map, one nearly east-west and the other approximately north-south (Fig.1.6a). The east-west profile has not been place orthogonally to the structural direction but is offset of about 15°. This position was choosen because it better represent the observed anomaly, e.i., it is directly situated on the station array. For the modelling of the anomalies, an interactive 2.5D gravity program, GRAVMAG, was used (Pedley et al., 1993). In conjunction with the modelling, stratigraphic descriptions of the volcano made by Lefebure (1986) were used for the construction of two generalized stratigraphic profiles (Fig. 1.7a, b). Unfortunately, the thicknesses of the various formations are unknown to the author, so the modelling first considers the Lefebure (1986) estimates, and then the thickness of each formation was varied to fit the observed anomalies. For comparison, the east-west profile also was made using reduction densities of 2300 kg m^{-3} and 2500 kg m^{-3} (Fig 1.6b, c).

Results

Examination of the Bouguer anomaly map revealed a general positive anomaly oriented north-northwest-south-southeast (Fig 1.6a). The interval contour are in mGal. Three distinct positive anomalies are visible: (1) at 517 400 and 1 393 700, (2) at 518 000 and 1 396 000 and (3) the highest anomaly at 518 500 and 1 393 500. These positions represent UTM coordinates based on the WGS 84 datum. Other anomalous zones may not be real, since they are extrapolations of the data. Modelling of the profiles was done using a step-by-step analysis. First, simple models and shapes were used to explore the limits of the possible solutions for the anomalies. From these results, the best approximation was used to create a more detailed model. The east-west profile was modelled first. Since the two profiles intersect in the anomalous zone, interpretations made with the east-west profile were then used in the modelling of the north-south profile.

Simple approximations of the anomaly in the crater area (profile east-west in Figure 1.6a) are shown in Figure 1.8a and 1.8b. The modelling demonstrates that the anomaly is created by a relatively small, shallow body rather than a larger, deeper body. A deeper body needs to be very large to match the amplitude of the doubly-peaked positive anomaly; in so doing, the overall anomaly is too large (Fig 1.8b). A smaller and shallower body gives a better fit to anomaly (Fig. 1.8a). The density contrast used for the two bodies is the same (+650 kg m^{-3}), but the half-strike (extension along strike) is 1000 m for the shallow body and 2000 m for the deep body. Modelling using only the volcano stratigraphy along the same profile shows that basalt lava flows (density contrast of +350 kg m^{-3}) are responsible, in part, for the overall anomaly in the eastern part of the profile (Fig. 1.8c). This observation, in conjunction with the two previous models, shows that a shallow body (+600 kg m-3 and half-strike of 1000 m) better fits the high-amplitude doubly-peaked positive anomaly (Fig 1.8d).

Once it was determined that the anomaly is caused by a shallow body of positive density contrast (+600 kg m^{-3}), more detailed modelling was done to match the observed anomaly (Fig. 1.8e). For modelling of the doubly-peaked anomaly, shallow less dense material (-800 kg m^{-3}) was used to fit the trough of the anomaly (Fig. 1.8e, Unit 7). Modifications of the shallow subsurface body alone did not match the anomaly, nor did introduction of two smaller and shallower bodies of positive

FIGURE 1.8

Modelling of the east-west gravity profile using GRAVMAG. (a) An isolated shallow body. (b) A deeper and larger body. (c) The stratigraphic units without an intrusion. (d) The stratigraphic units with a shallow intrusive body. (e) Best fit with a density contrast of 600 kg m^{-3} (intrusion). (f) Best fit with dikes. (g) Best fit with a density contrast of 450 kg m^{-3}.

A

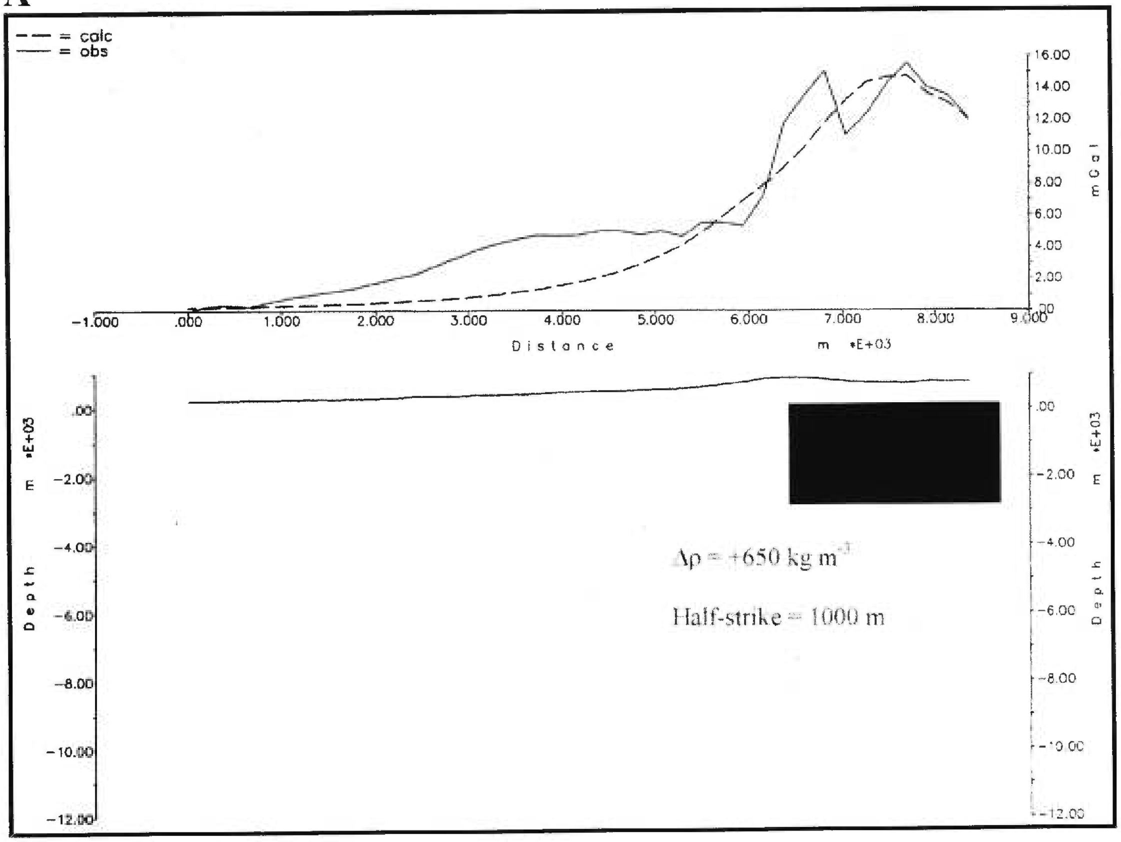

— — = calc
—— = obs
16.00
14.00
12.00
10.00
8.00
6.00
4.00
2.00
.00
mGal
−1.000
.000
1.000
2.000
3.000
4.000
5.000
6.000
7.000
8.000
9.000
Distance
m *E+03
.00
−2.00
−4.00
−6.00
−8.00
−10.00
−12.00
Depth m *E+03
Δρ = +650 kg m-3
Half-strike = 1000 m

B

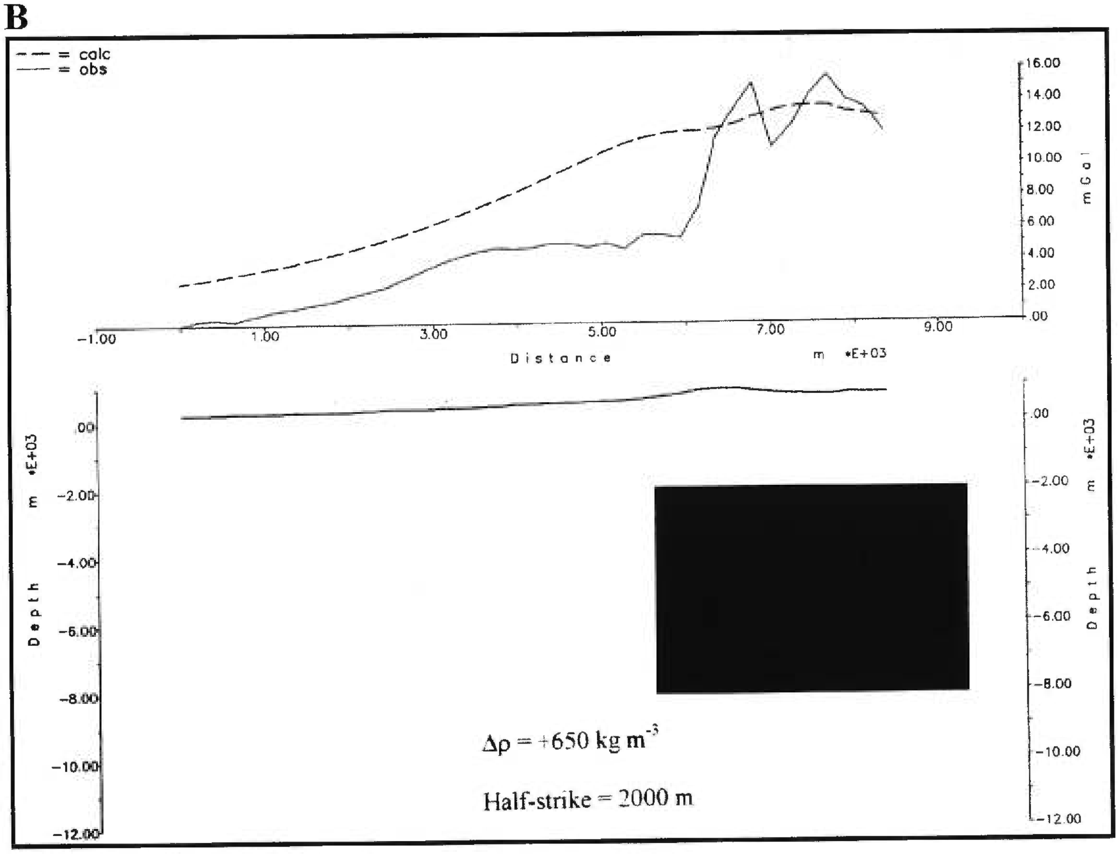

— — = calc
—— = obs
16.00
14.00
12.00
10.00
8.00
6.00
4.00
2.00
.00
mGal
−1.00
1.00
3.00
5.00
7.00
9.00
Distance
m *E+03
.00
−2.00
−4.00
−6.00
−8.00
−10.00
−12.00
Depth m *E+03
Δρ = +650 kg m-3
Half-strike = 2000 m

C

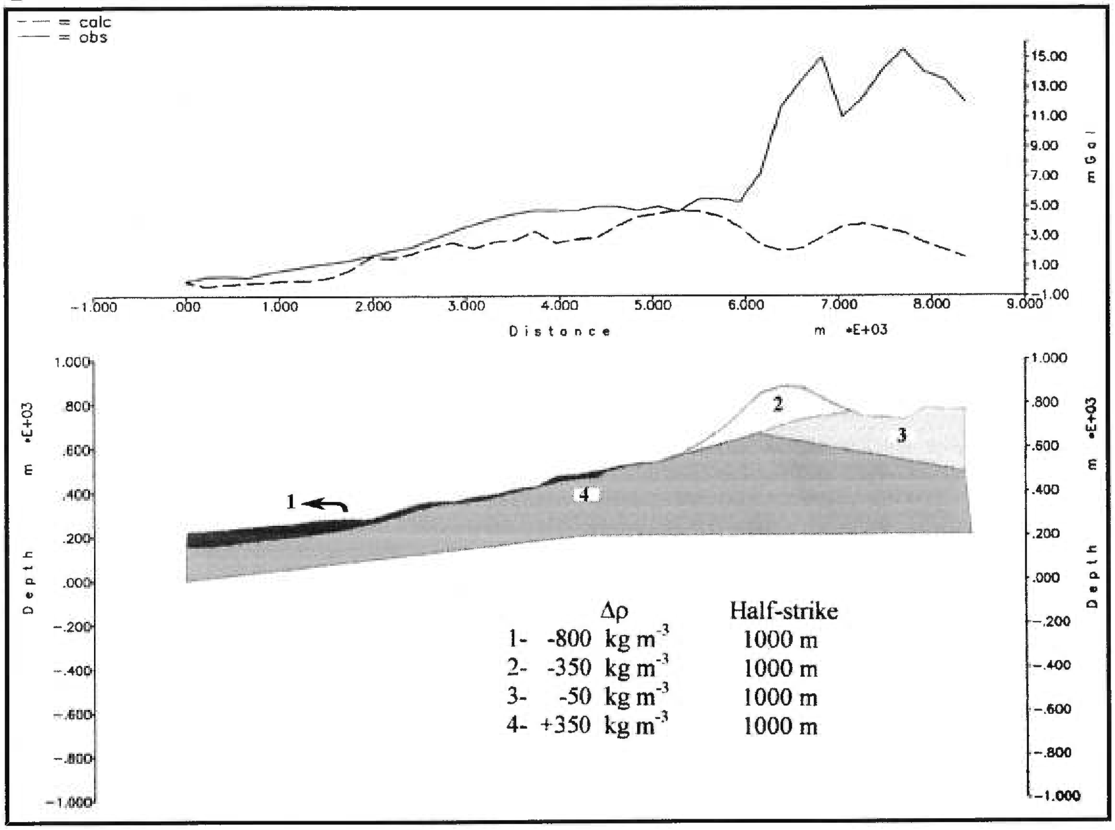

= calc
= obs
mGal
Distance m *E+03
Depth m *E+03
1
2
3
4
Δρ Half-strike
1- -800 kg m-3 1000 m
2- -350 kg m-3 1000 m
3- -50 kg m-3 1000 m
4- +350 kg m-3 1000 m

D

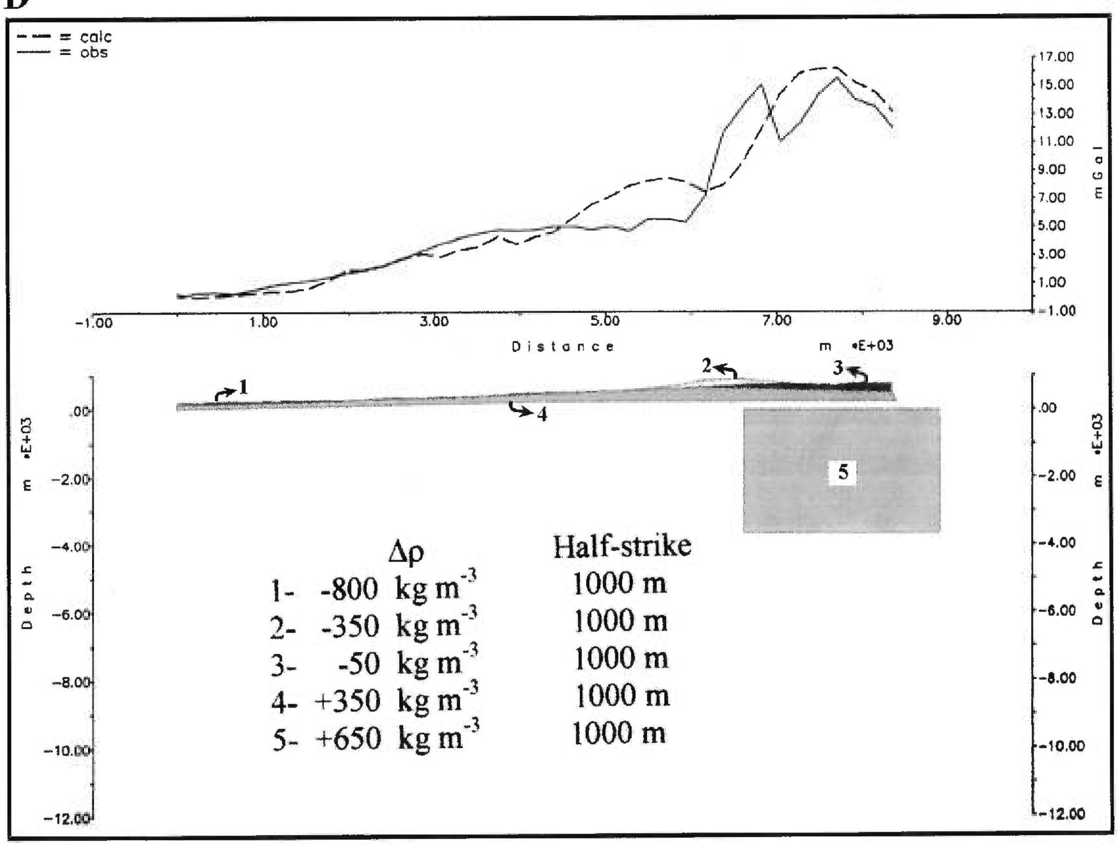

= calc
= obs
mGal
Distance m *E+03
Depth m *E+03
1
2
3
4
5
Δρ Half-strike
1- -800 kg m-3 1000 m
2- -350 kg m-3 1000 m
3- -50 kg m-3 1000 m
4- +350 kg m-3 1000 m
5- +650 kg m-3 1000 m

E

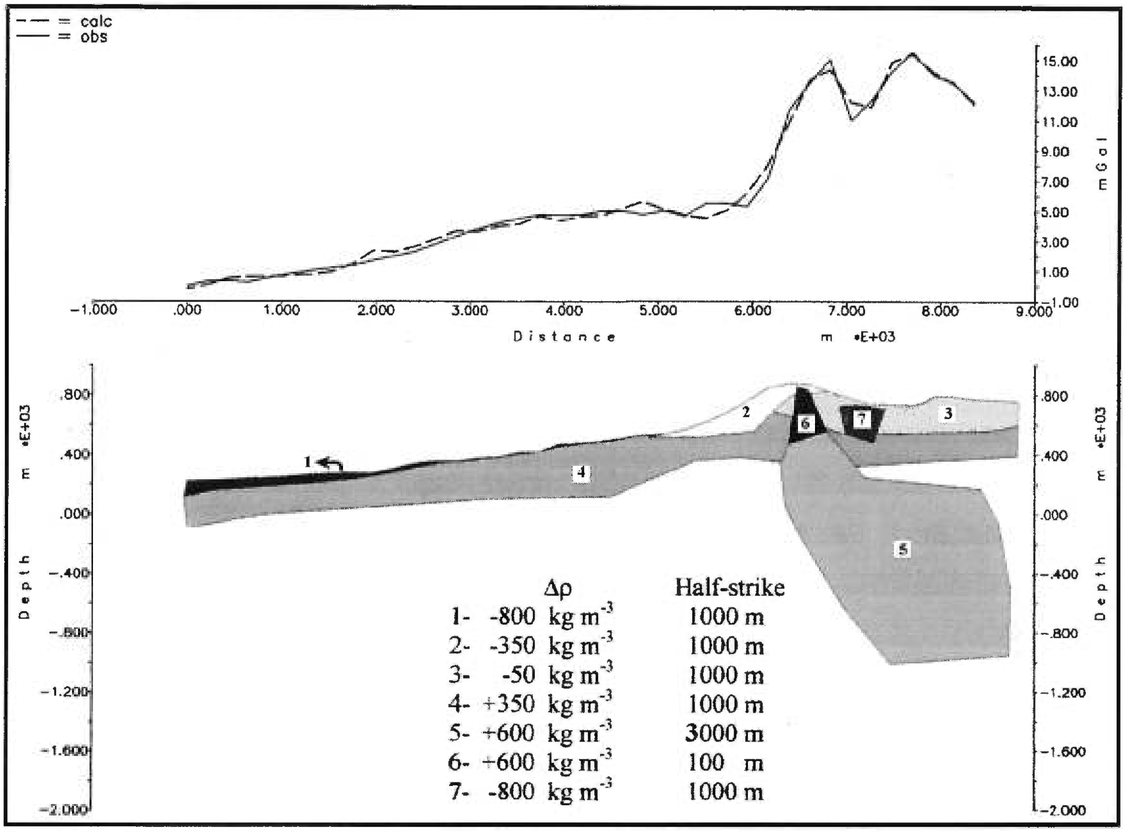

– – – = calc
—— = obs
mGal
Distance m *E+03
Depth m *E+03
1
2
3
4
5
6
7
Δρ Half-strike
1- -800 kg m-3 1000 m
2- -350 kg m-3 1000 m
3- -50 kg m-3 1000 m
4- +350 kg m-3 1000 m
5- +600 kg m-3 3000 m
6- +600 kg m-3 100 m
7- -800 kg m-3 1000 m

F

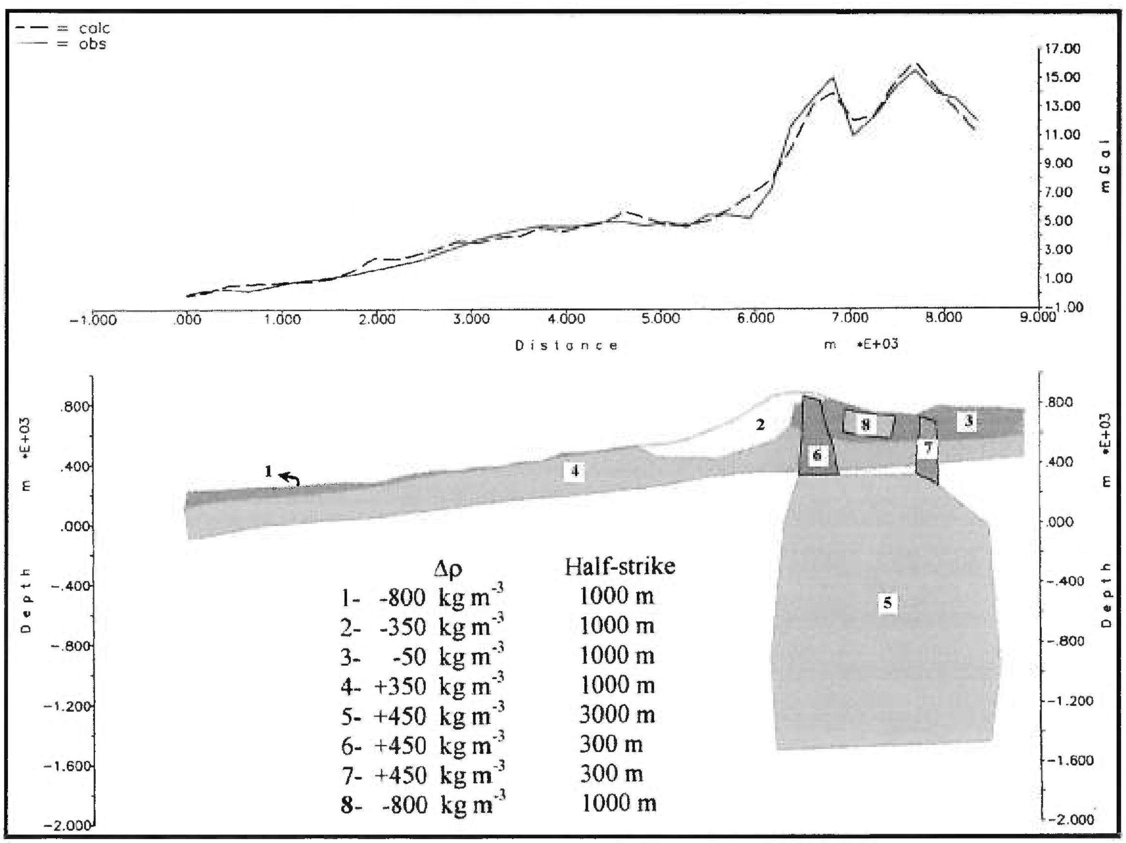

– – – = calc
—— = obs
mGal
Distance m *E+03
Depth m *E+03
1
2
3
4
5
6
7
8
Δρ Half-strike
1- -800 kg m-3 1000 m
2- -350 kg m-3 1000 m
3- -50 kg m-3 1000 m
4- +350 kg m-3 1000 m
5- +450 kg m-3 3000 m
6- +450 kg m-3 300 m
7- +450 kg m-3 300 m
8- -800 kg m-3 1000 m

G

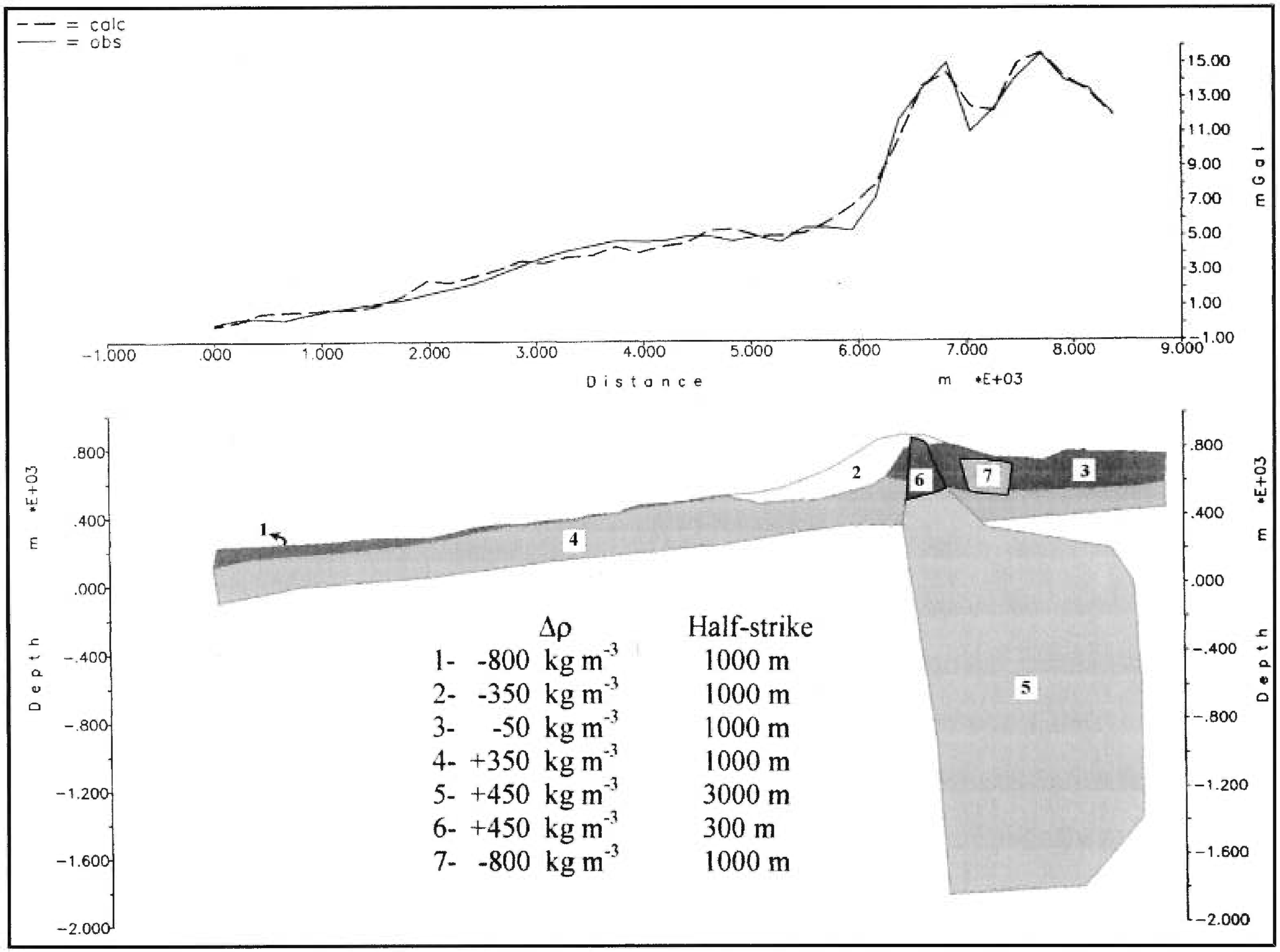

– – = calc
—— = obs
15.00
13.00
11.00
9.00
7.00
5.00
3.00
1.00
-1.00
mGal
-1.000
.000
1.000
2.000
3.000
4.000
5.000
6.000
7.000
8.000
9.000
Distance
m *E+03
.800
.400
.000
-.400
-.800
-1.200
-1.600
-2.000
Depth m *E+03
1
2
3
4
5
6
7
Δρ
Half-strike
1- -800 kg m-3 1000 m
2- -350 kg m-3 1000 m
3- -50 kg m-3 1000 m
4- +350 kg m-3 1000 m
5- +450 kg m-3 3000 m
6- +450 kg m-3 300 m
7- -800 kg m-3 1000 m

density contrast, such as dikes, on each side of the trough (Fig 1.8f). The density contrast of these two dikes needs to be large and the size of the dikes enormous; moreover, low-density material at shallow depth was still needed to fit the anomaly. The density contrast of the large body in Figure 1.8e (Unit 4) is 600 kg m^{-3}, and its half-strike is increased to 3000 m. This increase was made to match the anomaly modelled in the north-south profile (Fig 1.6a, 1.9). Modelling of the two profiles together (east-west and north-south, Fig 1.6a, 1.8e and 1.9) was used to create a realistic scenario. In Figure 1.8g, the body (Unit 4) has a density contrast of 450 kg m^{-3} and a half strike of 3000 m. The thickness and density contrast of the different formations were then modified slightly to fit the anomaly. The half-strike used in the modelling of the north-south profile (Fig.1.6a, 1.9) corresponds to half the width of the body (1000 m) modelled in the east-west profile (Fig. 1.8g), since the bodies in the two profiles intersect each other perpendicularly near the anomaly. The density contrast needed to match the anomaly in the north-south profile is 500 kg m^{-3}, which is 50 kg m^{-3} higher than the body for the east-west profile (Fig 1.9). For this north-south profile, thicknesses of formations again were adjusted to fit the anomalies, but not the densities which are the same as for the east-west profile. A shallow intrusion (Unit 4) had to be introduced into Unit 2 to match the positive peak (Fig. 1.9).

Finally, to compare the anomaly using Bouguer maps made with different densities (2300 kg/m^3, 2400 kg/m^3 and 2500 kg/m^3), a body of similar size and half-strike was modelled in each east-west profile (Fig. 1.10a, b, c). The density contrasts needed to match the anomaly in each profile are: (1) 470 kg m^{-3} for the 2300 kg m^{-3} map, (2) 420 kg m^{-3} for the 2400 kg m^{-3} map and (3) 360 kg m^{-3} for the 2500 kg m^{-3} map.

FIGURE 1.9

Modelling of the north-south gravity profile using GRAVMAG.

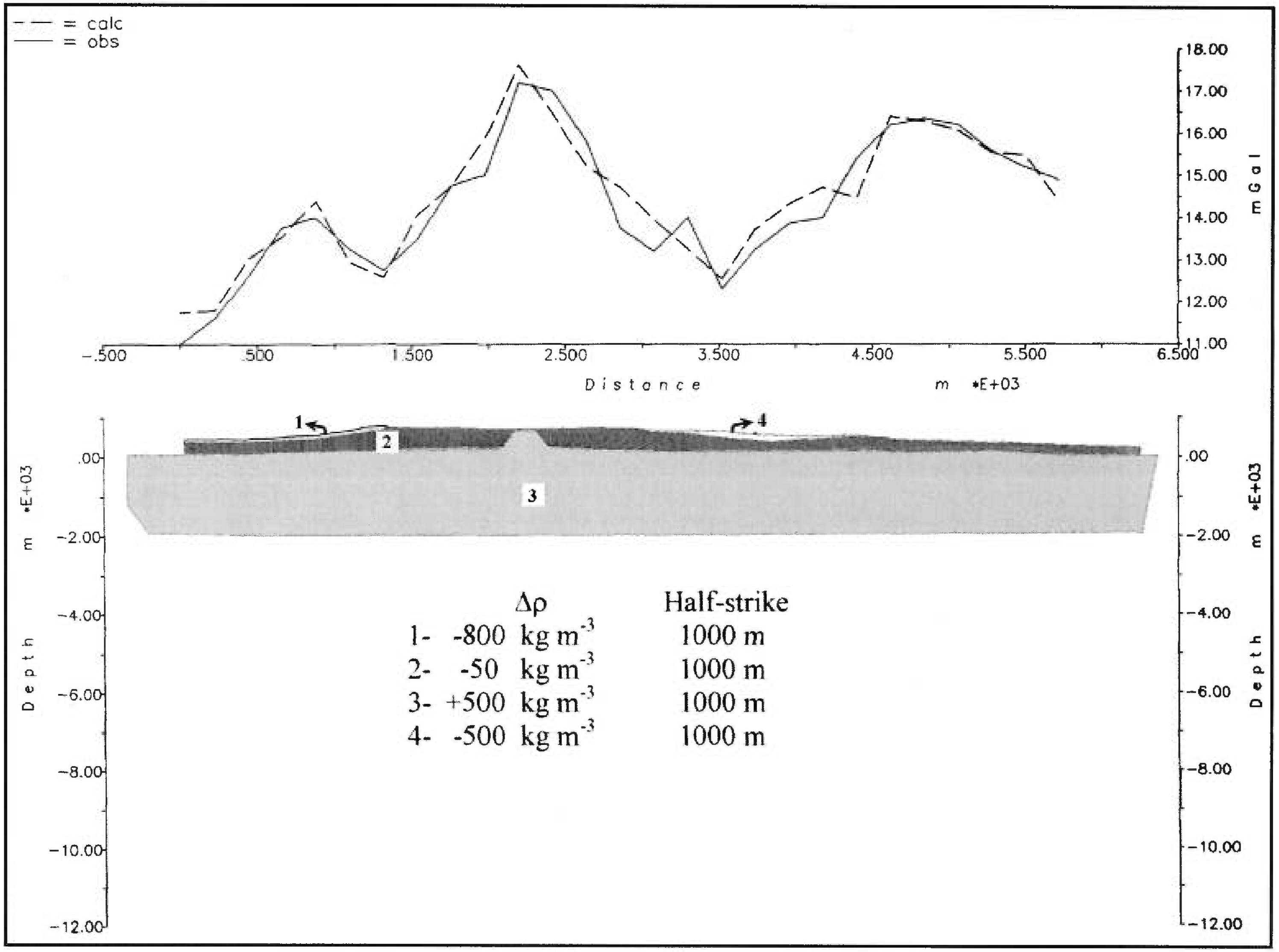

- - = calc
— = obs
mGal
18.00
17.00
16.00
15.00
14.00
13.00
12.00
11.00
-.500
.500
1.500
2.500
3.500
4.500
5.500
6.500
Distance
m *E+03
Depth m *E+03
.00
-2.00
-4.00
-6.00
-8.00
-10.00
-12.00
1
2
3
4
Δρ Half-strike
1- -800 kg m-3 1000 m
2- -50 kg m-3 1000 m
3- +500 kg m-3 1000 m
4- -500 kg m-3 1000 m

FIGURE 1.10

Modelling of the east-west gravity profile with a simple body of 3000 m half-strike for density reductions of (a) 2300 kg m^{-3}, (b) 2400 kg m^{-3} and 2500 kg m^{-3}.

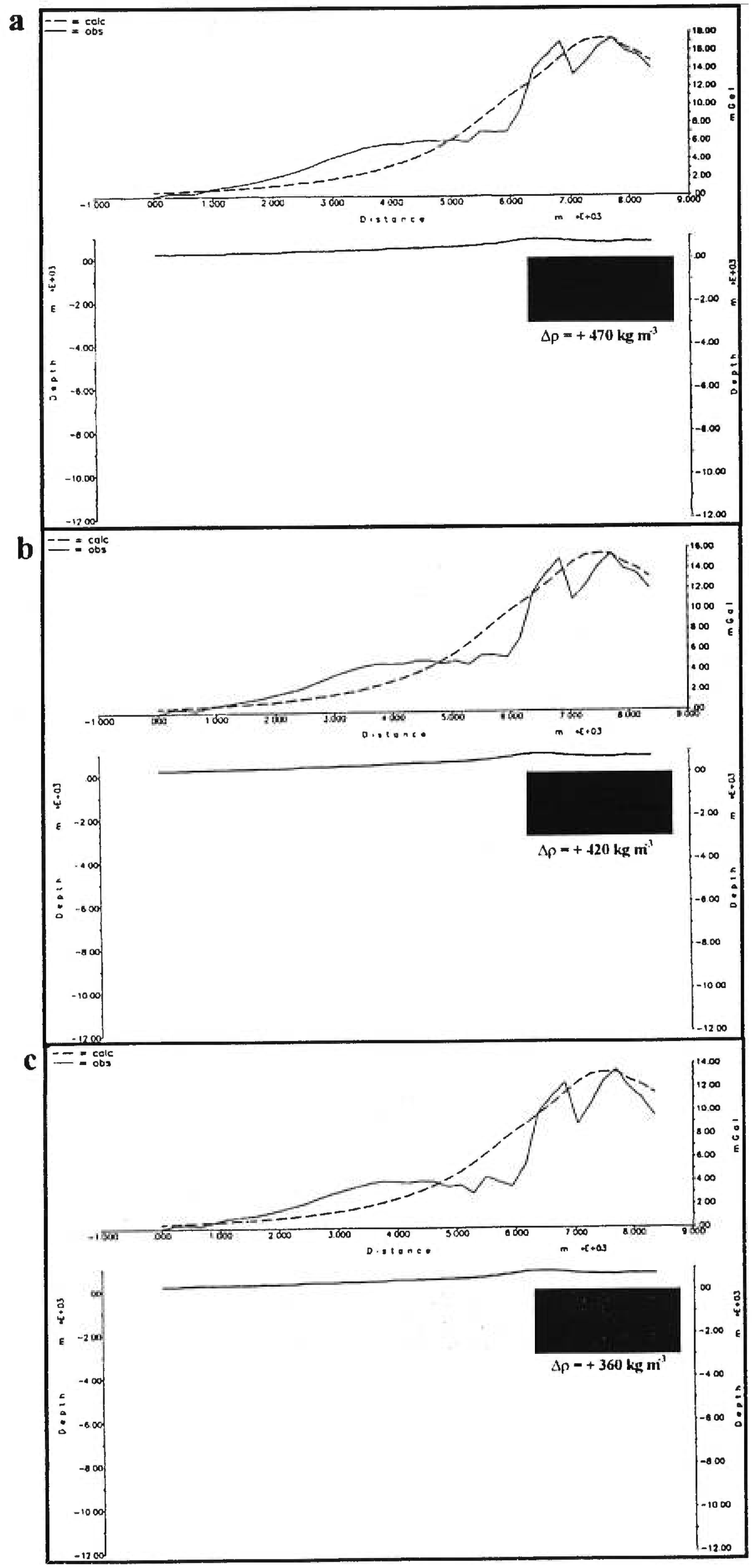
a
b
c
= calc
= obs
Distance
m *E+03
mGal
Depth
m *E+03
Δρ = + 470 kg m⁻³
Δρ = + 420 kg m⁻³
Δρ = + 360 kg m⁻³

Discussion

Modelling of the anomalies defined on the contour maps is not meant to be definitive. The modelling shows possible configurations of structure under a volcano which best fit the observed anomalies and which are geologically plausible. Most importantly, the modelling shows that the anomaly does not seem to be produced by a deep structure but instead by a shallow body with positive density contrast around 400-600 kg m^{-3}. A deeper body gives a broader anomaly than is observed. The best model, made in conjunction with the stratigraphy of the volcano and the two profiles (Fig. 1.8g and 1.9), gives a shallow body 1 km deep with dimensions of 2000 m by 2000 m by 6000 m. This body strikes north-northwest-south-southeast with a density contrast of around 400-600 kg/m^3. The body is probably an intrusion at shallow depth representing some sort of shallow magma chamber or reservoir.

The doubly-peaked anomaly in the east-west profile and the trough in the north-south profile are due to variations in thickness at the surface or very shallow depth low-density material such as tephra. Although the possibility of a dike system is not ruled out, this effect alone could not reproduce the doubly-peaked anomaly observed on the east-west profile. Comparison among the Bouguer maps made with different densities shows that there is not much difference between the density contrast of the bodies. The sum of the density contrasts and the density reduction of the anomaly maps are 2770 kg m^{-3}, 2820 kg m^{-3} and 2860 kg m^{-3}, respectively, for the 2300 kg m^{-3}, 2400 kg m^{-3} and 2500 kg m^{-3} Bouguer maps. Thus, use of 2400 kg m^{-3} density is considered to be justified, since there is not much difference among the other maps. This is confirmed by the anomalies on the three maps (Fig. 1.6a, b, c) which are not very different except for their amplitudes.

A structural study of Central American volcanoes by Carr (1976) shows that north-south-trending faults are tensional. Three north-northwest-south-southeast trending faults have been identified in the Telica complex (Lefebure, 1986). One is situated in the fumarole field of San Jacinto, and the two others to the east (Fig. 1.2). Arcuate or linear scarps, up to 40 m high and 2 km long, are found on the northeastern flanks of the San Jacinto hills and strike in a north-northwest direction. These probably also represent fault traces. Telica erupts predominantly basalts and andesite, with low pressure fractionation and mixing trends (van Wyk de Vries, 1993). Magma intrusion occurs rapidly to high levels due to crustal extension in the area. A central magma chamber located at shallow depth is likely to be formed (van Wyk de Vries, 1993). This idea also is postulated by Lefebure (1986), who suggested that lava flows can erupt laterally from the volcano and tap both the top and sides of a magma reservoir. Effusion of lava at different levels is an indication of the shallow nature of the magma chamber (Lefebure, 1986). Isotope analyses made by Lefebure (1986) showed uniform $^{87}Sr/^{86}Sr$ ratios for the volcanic rocks of the Telica complex, indicating a common parent magma or a relatively uniform source.

This gravity survey of Telica has revealed the presence of a large positive anomaly at shallow depth. This anomaly is probably an intrusion of magma which represents the magma chamber that feeds the volcanoes of the Telica complex. It is oriented north-northwest-south-southeast, similar to the faults in the region. Moreover, Santa Clara, Telica and Cerro Aguerro are nearly aligned (northwest-southeast) with this anomaly. A sketch of the anomaly is presented in Figure 1.3.

Conclusions

A large shallow intrusion of dimensions 2 km × 2 km × 6 km with a depth to top of about 1 km and a density contrast of 400-600 kg m^{-3} is defined in the Telica complex. Telica has been active in its historic past and is currently still very active, showing seismic activity since December 1996 increasing from ~100 events/day to ~220 events/day in June 1997. Practically no visible degassing is occurring, which may reflect a pressure buildup in the system. The seismic activity may also indicate magma movement under the volcano. The intrusion defined with this gravity survey probably represents the magma chamber that fed past eruptions of the volcanoes in the Telica complex. The present seismic activity could indicate that some sort of intrusive or convective activity is occuring presently in this chamber, such as magma replenishment or a buildup of pressure. This gravity survey proved useful in delineating the anomaly, but further investigations are needed to better define the body. Longer profiles should be used to better model the anomaly's depth and size, which was not possible to model with confidence using the available profiles from the contour map.

Acknowledgments

The authors gratefully ackowledge the staff of INETER for their support, especially Martha Navarro, Wilfried Strauch, Alejandro Acosta and Oscar Péres. Thanks also to Isabelle Lépine, Sandy Archibald, Katie St-Amand and Dora Knez for their help in the field. Many thanks to Mark Davies for his help and his living room and to Luis Acosta for driving us in Nicaragua. We are most grateful to the farmers living at the foot of Telica volcano for giving us free access to their fields and for their assistance.

References

Barrows, L., 1996. Microgravity surveying: new developments, new capabilities. The Professional Geologist, November 1996, p. 6-17.

Bulletin of the Volcanism Network, 1996. Telica volcano, 21: 4.

Bulletin of the Volcanism Network, 1997. Telica volcano, 22: 3.

Bulletin of the Volcanism Network, 1997. Telica volcano, 21: 5.

Bulletin of the Volcanism Network, 1997. Telica volcano, 21: 6.

Carr, M. J., 1976. Underthrusting and Quaternary faulting in northern Central America. Geological Society of America Bulletin, 87: 825-829.

Eggers, A.A., 1987. Residual gravity changes and eruption magnitudes, J. Volcanol. Geotherm. Res., 33: 210-216.

Hammer, S., 1939. Terrain corrections for gravity stations. Geophysics, 4: 184-194.

Lefebure, D.V., 1986. The mina El Limon area and the Telica Complex: two examples of Cenozoic volcanism in northwestern Nicaragua, Central America. Unpublished Ph.D. thesis, Department of Geology, Carleton University, Ottawa, Canada, 255 pp.

Metaxian, J.-P., 1994. Etudes sismologique et gravimétrique d'un volcan actif: Dynamisme interne et structure de la caldeira de Masaya, Nicaragua. Unpublished Ph.D. thesis, Université de Savoie, France, 309 pp.

Nettleton, L. C., 1939. Determination of density of reduction of gravimeter observation. Geophysics, 4: 176-183.

Rymer, H., and Brown G.C., 1986. Gravity fields and the interpretation of volcanic structures: geological discrimination and temporal evolution. J. Volcanol. Geotherm. Res., 27: 229-54.

Rymer, H., 1994. Microgravity change as a precursor to volcanic activity. J. Volcanol. Geotherm. Res., 61: 311-328.

Sandberg, C.H., 1958. Terrain correction for an inclined plane in gravity computations. Geophysics, 23, 4: 701-711.

Telford, W. M., Geldart, L. P., Sheriff, R. E., 1990. Applied Geophysics: 2nd edition. Cambridge: Cambridge Univerity Press, 770 pp.

Van Wyk de Vries, B., 1993. Tectonics and magma evolution of Nicaraguan volcanic systems. Unpublished Ph.D. thesis, Department of Earth Sciences, Open University, Milton Keynes, UK, 328 pp.

Weyl, R., 1980. Geology of Central America. Berlin: Gebruder Borntraeger, 371 pp.

CHAPTER II

Temporal variations of microgravity at Masaya volcano, Nicaragua

Alexandre Beaulieu[1], John Stix[1], Hazel Rymer[2], Glyn Wiliams-Jones[2] and Katie St-Amand[1]

[1]Département de Géologie
Université de Montréal
Montréal, Québec, H3C 3J7
Canada

[2]Department of Earth Sciences
Open University
Milton Keynes, MK7 6AA
United Kingdom

Abstract

Temporal variations of microgravity were observed at Masaya caldera, Nicaragua, from 4 March to 17 March 1997, and from 27 January to 14 March 1998. During the survey of 19 days in 1997, conducted with Scintrex and Lacoste & Romberg gravity meters, a decrease of 55-80 μGal was observed near the active crater, Santiago. Some differences between the two instruments were observed during the survey, but in general, they show the same trend of temporal variation, except at a single station (B1A). In 1998, the observed microgravity variations were of the same amplitude (55-63 μGal) but were also seen on a shorter timescale and were increases instead of decreases. A detailed experiment was conducted at one station (A7) during one day in 1997 and during three days in 1998 during which microgravity was measured continuously. Two instruments were used simultaneously for approximately 7 hours in 1997 and one instrument for about 13-14 hours for each day in 1998. COSPEC measurements of SO_2 flux were made to examine degassing trends of the active vent during the days of continuous gravity measurements. In 1998, during the continuous gravity monitoring, pressure and seismicity were monitored at the same time. In 1997, both instruments showed an increase in microgravity, 45 μGal for the Lacoste & Romberg and 20 μGal for the Scintrex. Microgravity variations with amplitudes of 40, 20 and 35 μGal were observed on 25 February, 6 March and 13 March 1998, respectively. A tentative correlation is made between microgravity changes and diurnal tides. No direct correlations were observed with the SO_2 flux in both cases. Gravity variation induced by atmospheric pressure changes is unlikely, since no direct links are observed. The

cause of these gravity variations is linked to density variation in the magma which in turn is an effect of fluctuation in the vesicularity of the magma in the order of 3-5 % that could be related mechanically to the diurnal and fortnightly tidal variations.

Introduction

Masaya Caldera is situated approximately 25 km south-southeast of Managua, the capital of Nicaragua. The caldera is oriented northwest-southeast, parallel to the alignment of the volcanic chain (Fig. 2.1). The length of the longest axis of Masaya caldera is 11.5 km and its width is 6 km. The caldera consists of a lake (Laguna de Masaya) and four pit craters: Masaya, Santiago (presently active), Nindirí and San Pedro (Fig. 2.2). Historical activity at Masaya consists of lava flows in 1670 and 1772, episodic lava lake formation associated with pit crater formation, small strombolian eruptions and periodic degassing crises. There is also geological evidence of pyroclastic and plinian eruptions from Masaya in the more distant geologic past (Williams, 1983). Recurrent lava lake episodes with significant degassing activity have occurred several times in recorded history from Santiago crater. Stoiber et al. (1986) estimated that 10 km^3 of basaltic magma have been degassed in five degassing crises since 1852. This output of gas is devastating to the coffee crop surrounding the affected area; damaged and dead vegetation is most conspicuous on the slopes leading up to the Llano Pacaya rim (Johnson and Parnell, 1986). Significant degassing was occuring from Santiago crater during our microgravity surveys in March 1997 and February-March 1998. In 1997, the SO_2 fluxes observed were between 300-500 t/d. In 1998, the SO_2 fluxes were

FIGURE 2.1

The Central American volcanic chain showing the segments of Carr (1984) and Masaya volcano (From Metaxian, 1994).

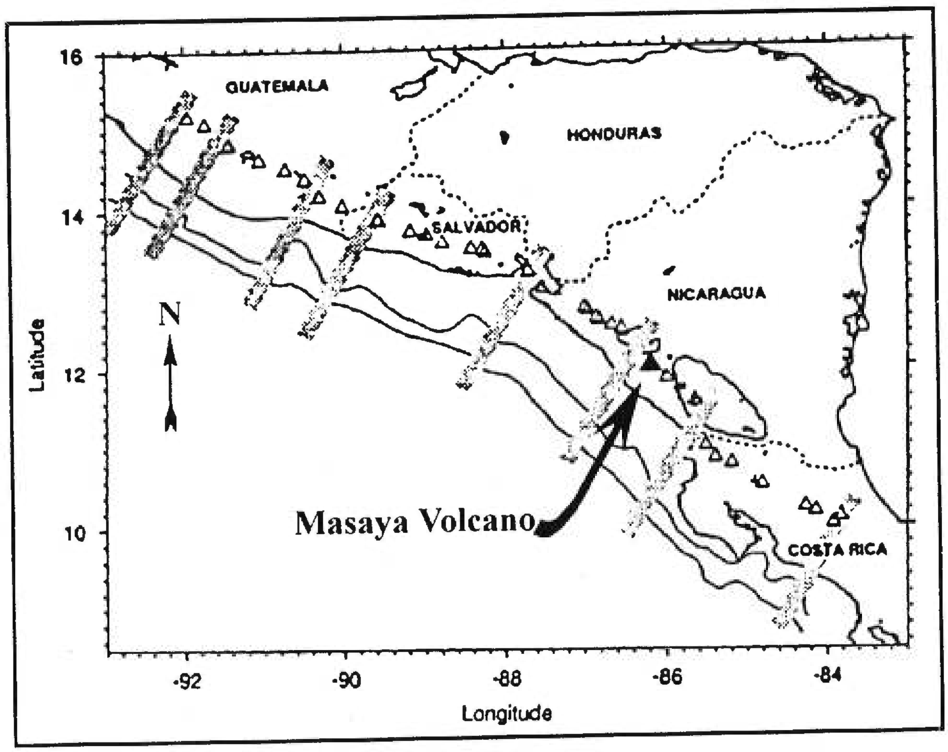

GUATEMALA
HONDURAS
SALVADOR
NICARAGUA
COSTA RICA
Masaya Volcano
N
16
14
12
10
-92
-90
-88
-86
-84
Latitude
Longitude

FIGURE 2.2

Map of Masaya caldera showing the different cones and craters (From Viramonte et al., 1997).

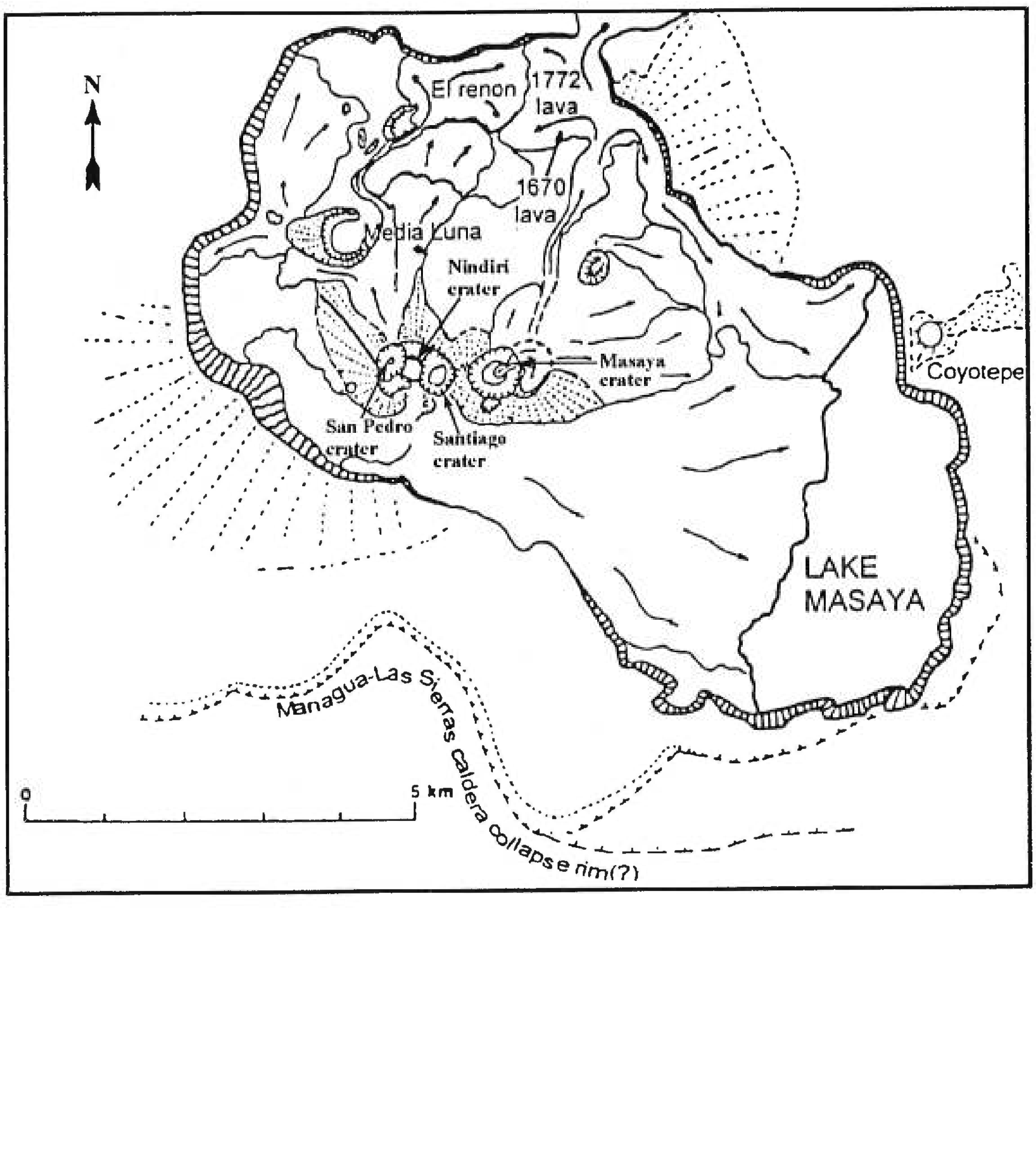
N
El renon
1772 lava
1670 lava
Media Luna
Nindiri crater
Masaya crater
San Pedro crater
Santiago crater
Coyotepe
LAKE MASAYA
Managua-Las Sierras Caldera collapse rim(?)
0
5 km

significantly higher, ranging from 700 to 4000 t/d.

The present study was conducted in two field trips (March-April 1997 and February-March 1998) during which microgravity and GPS measurements were taken at five stations in 1997 and seven stations in 1998. The stations used to monitor the volcano were part of an existing microgravity survey line at Masaya caldera. This line of seventeen stations was established by French researchers (Metaxian, 1994) and continued by Rymer et al. (1998). The microgravity was monitored using two gravimeters, a Scintrex CG-3 #9101184 (loan by Scintrex Ltd) and a Lacoste and Romberg #G-513 (LCR) (loan by Hazel Rymer) in 1997, and in 1998 with only the LCR #G-513. Altitudes were monitored using Leica GPS 200 dual-frequency differential receivers to assess possible changes in altitude on the microgravity results. During the same period, COSPEC measurements of SO_2 flux were made to examine degassing trends of the active vent. Rymer et al. (1998) made microgravity measurements once a year for the past five years (1993-1997) at Masaya; between 1993 and 1994 they observed decreases on the order of 90 μGal at stations near Santiago crater (Fig 2.3). They correlated this decrease to an increase in the gas flux, indicating a change in the shallow plumbing system. Between 1994 and 1997, they recorded gradual increases in gravity of about 56 μGal in conjunction with minor pit crater collapse and a decline in degassing. They related the gravity variations to a convective overturn at shallow depth and not to a major intrusion.

The main goal of the current experiment was to obtain microgravity measurements at some of the stations used by Rymer et al. (1998) in order to obtain measurements over a shorter period of time. This would allow us to observe

FIGURE 2.3

Gravity changes at stations within Masaya caldera; station locations are shown in Figure 2.4 (From Rymer et al., 1998).

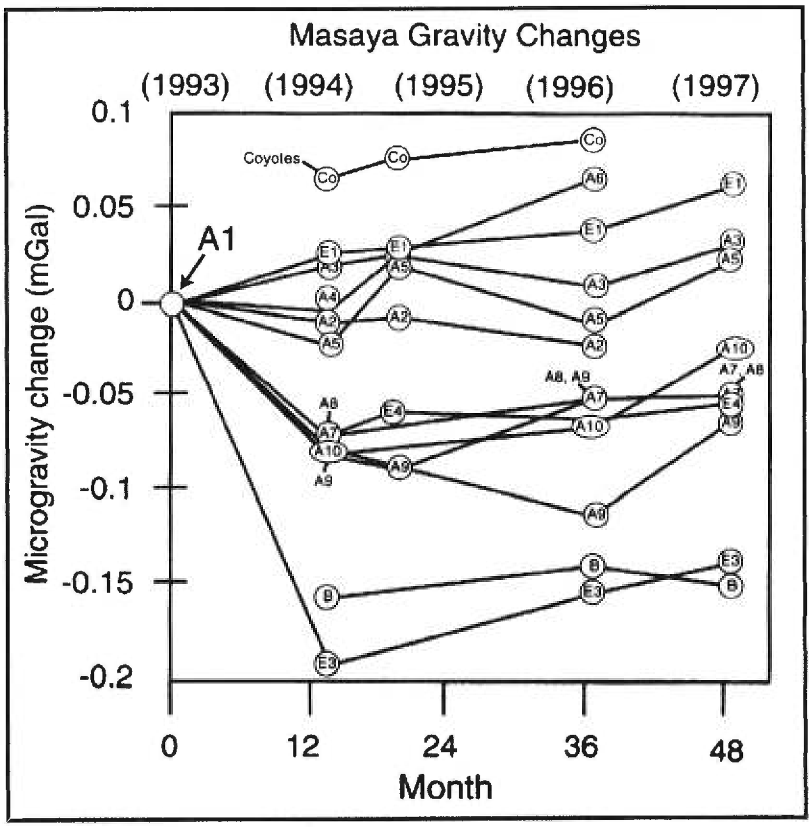

Masaya Gravity Changes
(1993) (1994) (1995) (1996) (1997)
Microgravity change (mGal)
0.1
0.05
0
-0.05
-0.1
-0.15
-0.2
A1
Coyotes
Co
A6
E1
A3
A5
A4
A2
A8, A9
A7, A8
A7
A10
E4
A9
A8
B
E3
0
12
24
36
48
Month

FIGURE 2.4

Location of the gravity stations in Masaya caldera. Stations B1A and B2 are proximal and are represented by B (From Rymer et al., 1998).

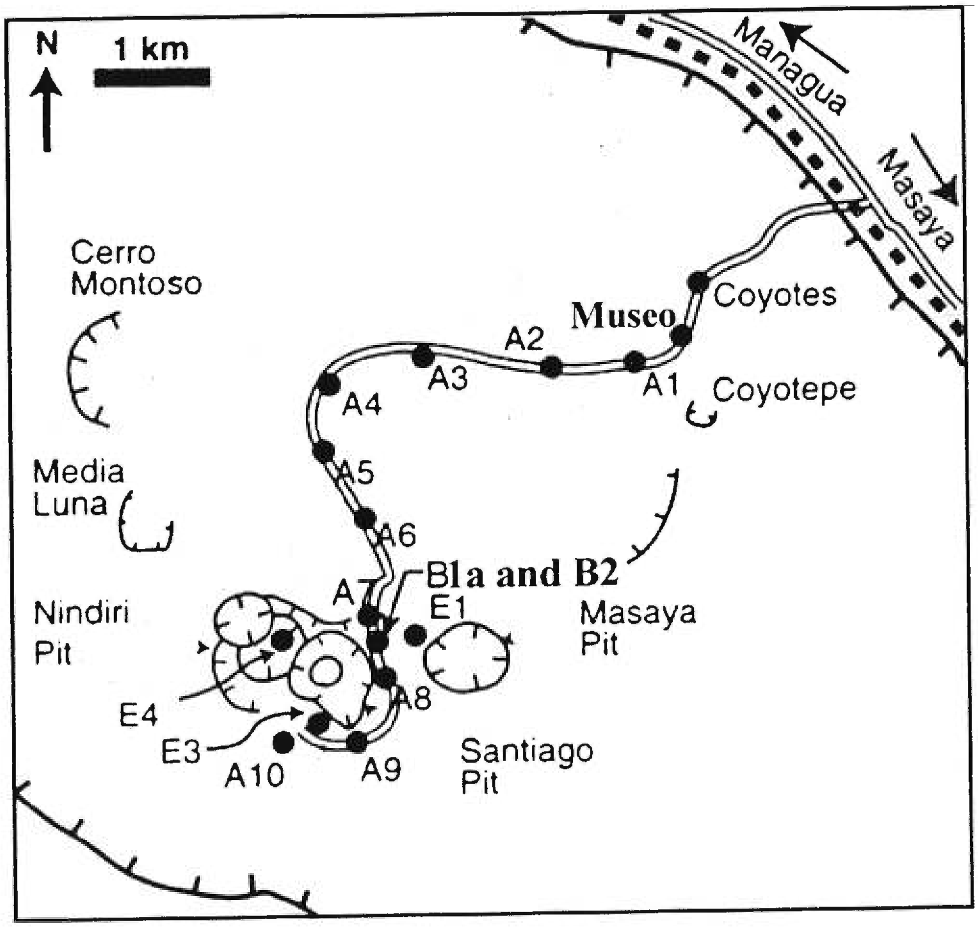

N
1 km
Managua
Masaya
Cerro
Montoso
Museo
Coyotes
A2
A3
A1
A4
Coyotepe
Media
Luna
A5
A6
B1a and B2
A7
E1
Nindiri
Pit
Masaya
Pit
E4
A8
E3
A10
A9
Santiago
Pit

microgravity variations on timescales of years, weeks, and days. During the survey, SO_2 flux, atmospheric pressure and seismicity measurements were also made to better understand the gravity changes. Comparisons with tidal variations was also made.

Methodology

The stations that were used from the existing line are easy to locate and access. The stations are MUSEO, A1, A3, A5, A7, B2 and B1A, A1 being the base station; MUSEO and A5 are the two stations that were added in 1998 (Fig. 2.4). A secondary base station, REGIS, was established in 1998 outside of the caldera, at the Hotel Regis in Masaya City, about 7 kilometers east of Santiago, to examine gravity variations other than in the crater area (station A7, B2 and B1A). Microgravity measurements (tide-corrected) and GPS measurements for the altitude control were taken repeatedly at each station over a period of about three weeks in 1997 and 1998. In order to obtain gravity variations, a microgravity survey line was established, in this case represented by stations MUSEO, A1, A3, A5, A7, B2 and B1A, with A1 as base station. Then a relative difference in microgravity was calculated between the base station and the other stations (Rymer, 1989). The differences obtained were then monitored with time. Changes in excess of 25 μGal are considered significant at the 95% confidence level (H. Rymer, personal communication, 1997). Since the base station (A1) is several kilometers from the active vent in the caldera in a more stable environment, it is considered not to vary during the survey. Measurements taken at REGIS verify this: the standard deviation of the differences between REGIS and MUSEO and REGIS and A1 are 14 μGal and 12 μGal, respectively. Variations of the REGIS station, measured at the beginning and the end of each day, are about 20 μGal and always in the same direction which probably represent a drift. This slight drift of the meter occurred since it was slightly unstable after a power failure on 14 March 1998, which caused a decrease in the meter temperature. The second set of REGIS measurements were usually made late in the day, so there was a long lapse of time when the meter was stored in a car and not used. This may account for the drift.

The same procedure was followed for microgravity measurements at each station to minimize sources of error due to manipulations and readings (Rymer, 1989). Two different ways of taking measurements were used in the surveys of 1997 and 1998. In 1997, a measurement was taken at the base station and then at all the other stations sequentially and finally at the base station again. With a larger number of stations, repeating certain stations along the line is recommended for better precision and to locate possible tares. In the case of the present survey, only the base station was repeated because of the small number of stations (5 in 1997). In 1998 measurements were made in order to obtain three gravity differences between two individual stations. For example, a first measurement was taken at A1, a second at A3, a third at A1 and a fourth at A3. The line was continued in this manner for each pair of stations until the last station was connected to the base station. The differences obtained were then averaged and used as reference values to which the results of subsequent days are compared. The number of measurements is higher in the second technique, but the precision is better and the tares easily located. Both techniques give good results when done with care. Continuous daily-variation measurements were made only at station A7, once in 1997 and three times in 1998. During the daily

FIGURE 2.5

(a) Scintrex and LCR daily gravity changes at Masaya volcano at station A7, March 12 1997. (b) Temporal variation of SO_2 vs temporal variation of microgravity for the LCR meter at Santiago crater, 12 March 1997.

A

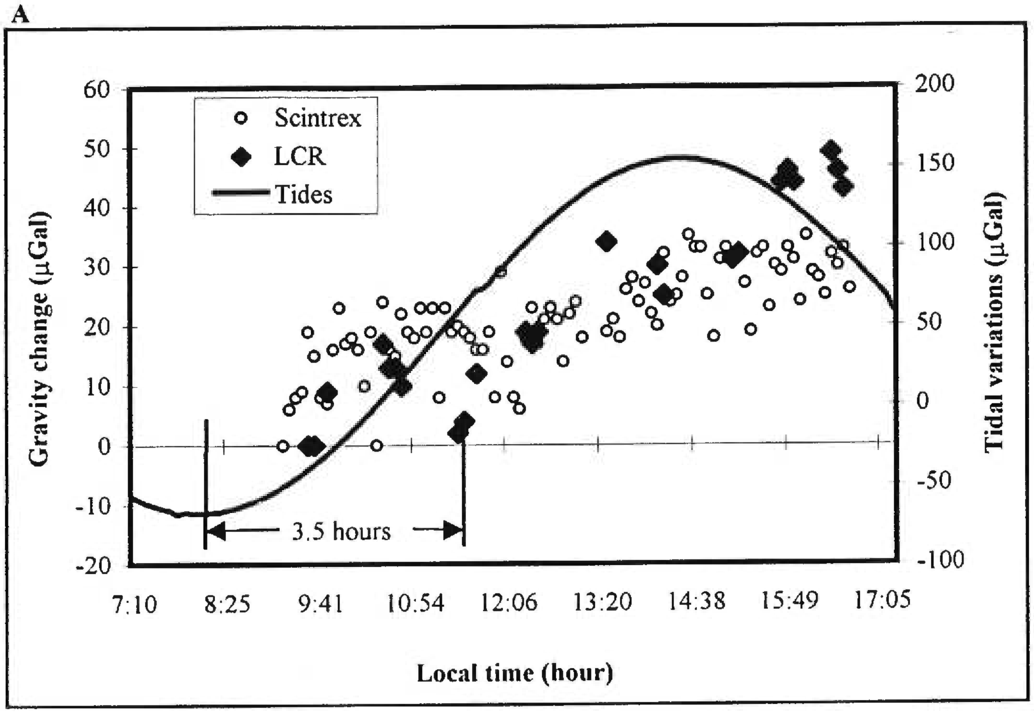

Scintrex
LCR
Tides
Gravity change (μGal)
Tidal variations (μGal)
3.5 hours
60
50
40
30
20
10
0
-10
-20
200
150
100
50
0
-50
-100
7:10
8:25
9:41
10:54
12:06
13:20
14:38
15:49
17:05
Local time (hour)

B

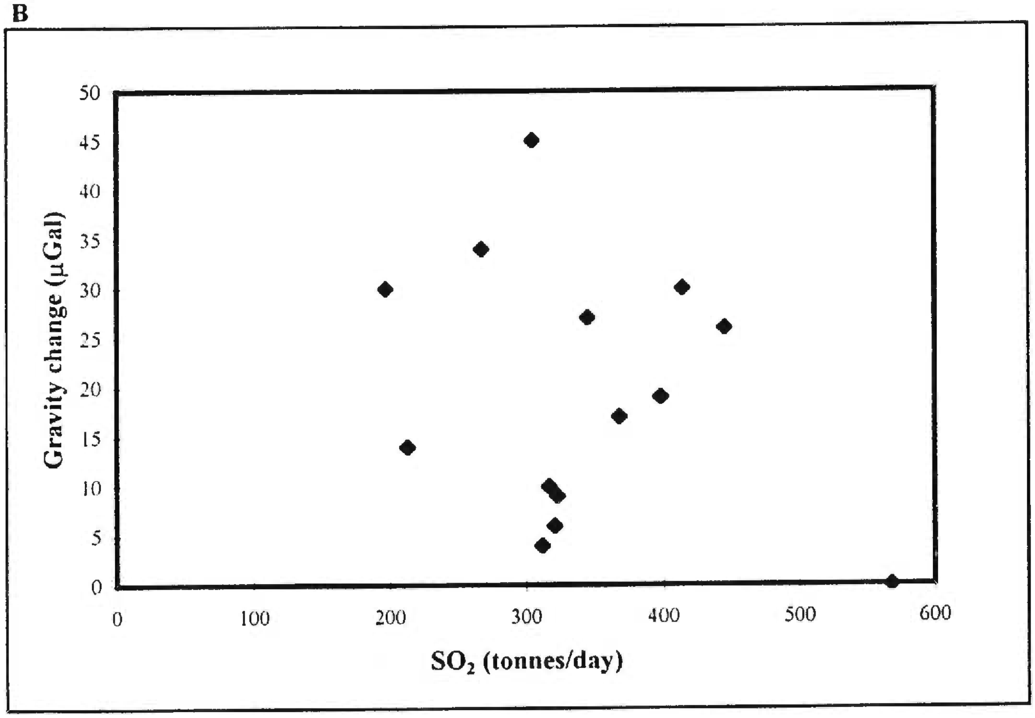

Gravity change (μGal)
50
45
40
35
30
25
20
15
10
5
0
0
100
200
300
400
500
600
SO₂ (tonnes/day)

survey in 1998, the atmospheric pressure was monitored constantly at the Hotel Regis in Masaya City using a Vaisala PTB 100 pressure meter. Pressure measurements were taken every five minutes. Precision of the pressure meter is around 0.03 mbar but because of the analog-to digital converter which digitizes the raw data, precision is of the order of 0.5 mbar. There was also a portable seismometer installed 10 m from station A7 to record the volcanic tremor which is present in the crater area.

Results

Daily Gravity Variations

An initial experiment was conducted in 1997 at a single station near Santiago crater to look for gravity variations during the course of a day. This was conducted at station A7 for half a day on 12 March with the LCR and the Scintrex instruments. The two gravity meters were set at station A7, with 2 m distance between them. The Scintrex was set to measure during 120 seconds with a cycle time of 5 minutes; for the LCR, we took measurements every 30 minutes (Appendix B, Table B1). The LCR shows an increase of about 45 μGal over 7 hours (Fig. 2.5a). Although the Scintrex also shows an increase (Fig. 2.5a), it is of lower amplitude (about 20 μGal). These results were calculated from linear regression of the data. In Figure 2.5a, the earth tide variation is plotted with our observed gravity variations of both meters. In general, the observed gravity changes increase in magnitude sympathetically with the tidal variations. The gravity changes may be shifted with respect to the tides by 3-4 hours, i.e., the observed gravity minimum and maximum may occur later than those for tides. However, this relation is not clear due to a lack of data. During this experiment, a second team monitored the amount of SO_2 degassing from Santiago by use of a COSPEC (Fig. 2.5b), since our microgravity measurements were conducted next to the crater. There does not appear to be a direct correlation between the increase in microgravity and the SO_2 degassing. The difference of 25 μGal between the two instruments is difficult to interpret. Since the Scintrex was in cycling mode, it was not touched during the day except for checking the levelling once. Thus, there should not have been any tare or variation due to movement of the instrument. As for the LCR, it was not moved during the experiment. It was only clamped and unclamped before and after each measurement. Thus, there should not be much tare for this instrument either. There is no error from reading the Scintrex since it is digital. The LCR may have some error due to the reading dial, but it should not exceed 10 μGal if the correct procedure is followed (Rymer, 1989). The measurements for the LCR were done by two readers, with a switch made at 14:06 local time. This may account for an error of about 10 μGal considering the different way to interpret the nulling point on the meter by different readers. Another difference between the two instruments may be the tide corrections. The Scintrex has a tide correction program, and there may be a slight difference between this program and the one used (GRAVPAC) for correcting the tide for the LCR. But it is certainly not of the order of 15 to 20 μGal. There is also the possibility of drift in the case of the Scintrex; even with the correction that is made by the Scintrex, there may be additional drift that may affect the data over an extended period of time. A third possibility is that the Scintrex gives better results in unstable environments than the LCR, which may be affected by vibration and seismicity. To achieve this, the

Scintrex must average a number of measurements and then reject values that are too far from the average. This rejection could induce additional errors. In summary, the difference between the two gravimeters is difficult to explain, and a repeat of this experiment would be necessary to better explain the cause of this difference (Appendix C). But because it is not of large amplitude and is of the same order and in the same direction, it is possible to say that the two instruments' response to the microgravity variation is approximately the same.

The experiment was continued in 1998, measurements being taken continuously every 10-15 minutes with the LCR instrument during the course of three days (25 February, 6 March and 13 March 1998) (Appendix B, Table B2). During two days, atmospheric pressure was monitored (pressure measurements are lacking for the first day because of equipment failure), and seismicity was monitored in the vinicity of station A7 for the three days. COSPEC measurements of SO_2 flux were acquired in the afternoon of 13 March. Compared to 1997 when gravity measurements lasted 7 hours, the time in 1998 was extended to about 13-14 hours each day in order to better characterize the microgravity changes. The first day of measurements (25 February) started at 10:01 local time (16:01 GMT). All the measurements are tide-corrected using tidal values given by the GRAVPAC software. There is an increase in gravity of about 32 μGal at a rate of 6.8 μGal/hour from 10:01 to 15:22, then the gravity decreases about 40 μGal at a rate of –5.8 μGal/hour, and finally, gravity seems to increase again, but there are not sufficient data to define a slope (Fig. 2.6a). On the second day (6 March), results are different. A gravity increase of 22 μGal at a rate of 5.6 μGal/hour is observed in the morning starting at

09:58 and ending at 13:21 (Fig. 2.6b). Subsequently, there are no significant gravity variations. The rate of gravity variation during this period is about –0.7 μGal/hour, which is trivial. During the third day of continuous monitoring (13 March), an increase in gravity is observed in the morning, followed by a decrease (Fig. 2.6c). From 10:50 to about 15:32, gravity increases about 15 μGal at a rate of 2.8 μGal/hour; from 15:32 to 22:55, gravity decrease about 35 μGal at a rate of – 3.8 μGal/hour. Similar to 25 February, the gravity then appears to increase, but there are not sufficient data to confirm this.

A certain correlation is observed between the daily earth tides and the observed gravity variations, particularly on 25 February and 13 March. On these two days, the maxima of the gravity variation seem to be offset by approximately three to four hours after the first maximum of the tidal variation (Fig. 2.6a and 2.6c). The minima of gravity are also offset by approximately four hours after the tidal minimum. Moreover, the observed gravity variation is higher when the amplitude of the tidal variation is larger. The gravity variation on the first day is of the order of 40 μGal, while the amplitude of the tides is 263 μGal from the first maximum to the first minimum. On the second day, the gravity variation, which is not so clearly linked to the tides as for the other two days, is on the order of 20 μGal, while the amplitude of the tides from the first minimum to the maximum is of 135 μGal. For the third day, the gravity variation is about 36 μGal and the tidal amplitude is 233 μGal. Results obtained in 1997 for the continuous measurements are not sufficiently long to obtain such maxima, so they are extrapolated. This extrapolated maximum gravity variation is about 45 μGal and the maximum tidal amplitude is

FIGURE 2.6

Daily gravity variation at station A7 for (a) 25/02/98, (b) 06/03/98 and (c) 13/03/98. (d) Maximum gravity changes vs. maximum tidal amplitude for daily variations in 1997 and 1998. (e) Maximum gravity changes vs. maximum tidal amplitude for daily variations in 1998 only. (f) Fluctuation of SO_2 vs. gravity changes on 13 March 1998 at station A7.

A **25 February 1998**

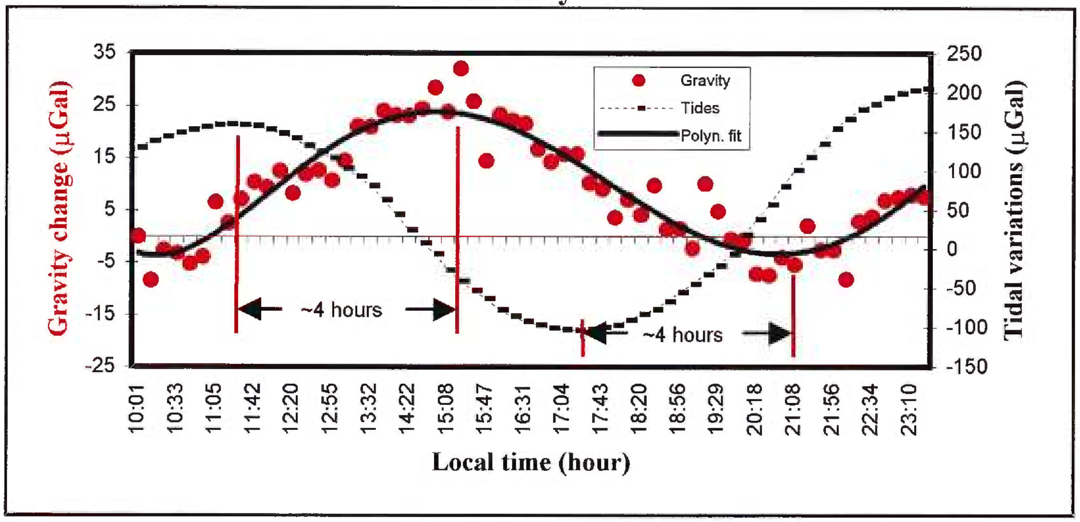

B **6 March 1998**

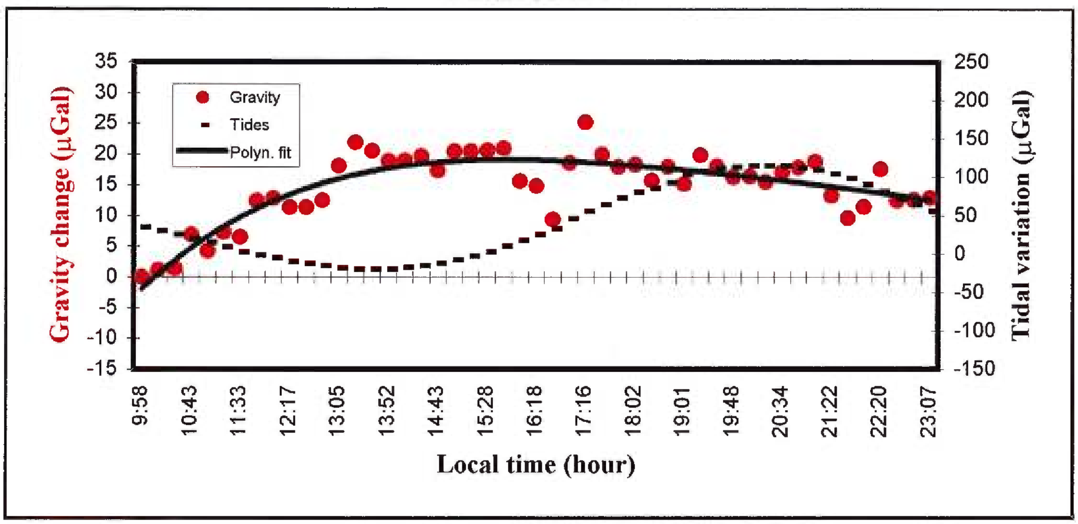

C **13 March 1998**

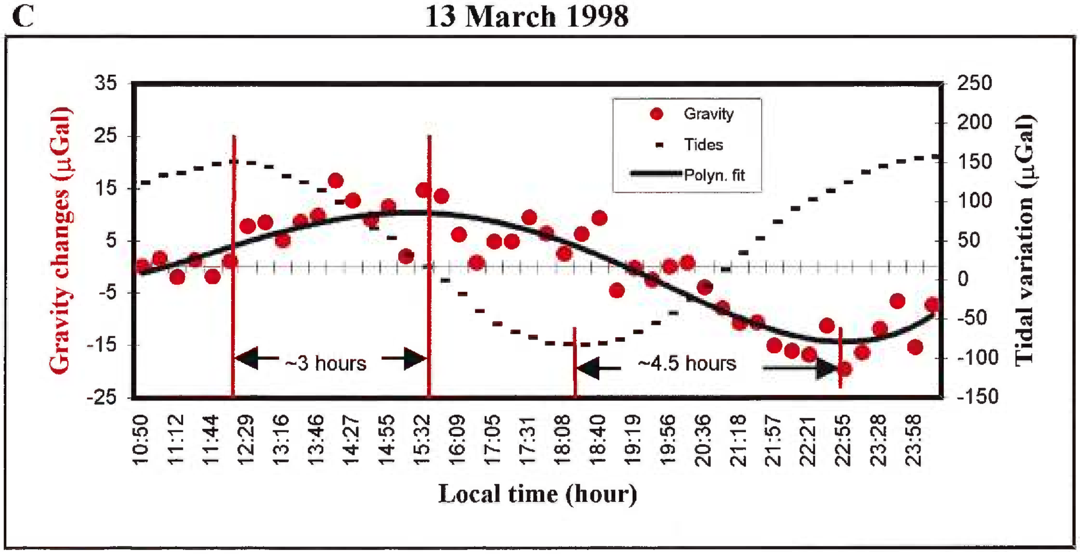

D

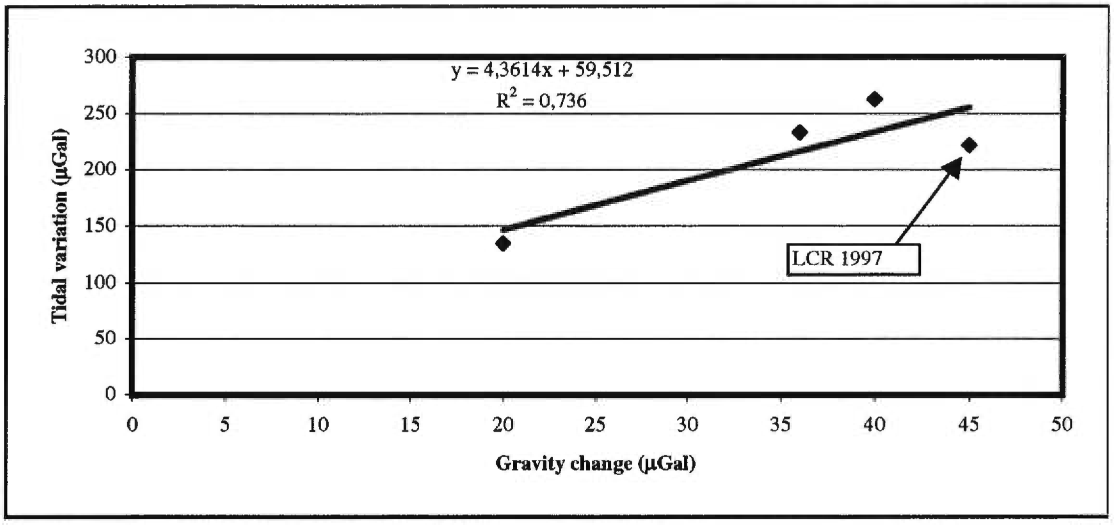

y = 4,3614x + 59,512
R^2 = 0,736
LCR 1997
Tidal variation (µGal)
Gravity change (µGal)
300
250
200
150
100
50
0
0
5
10
15
20
25
30
35
40
45
50

E

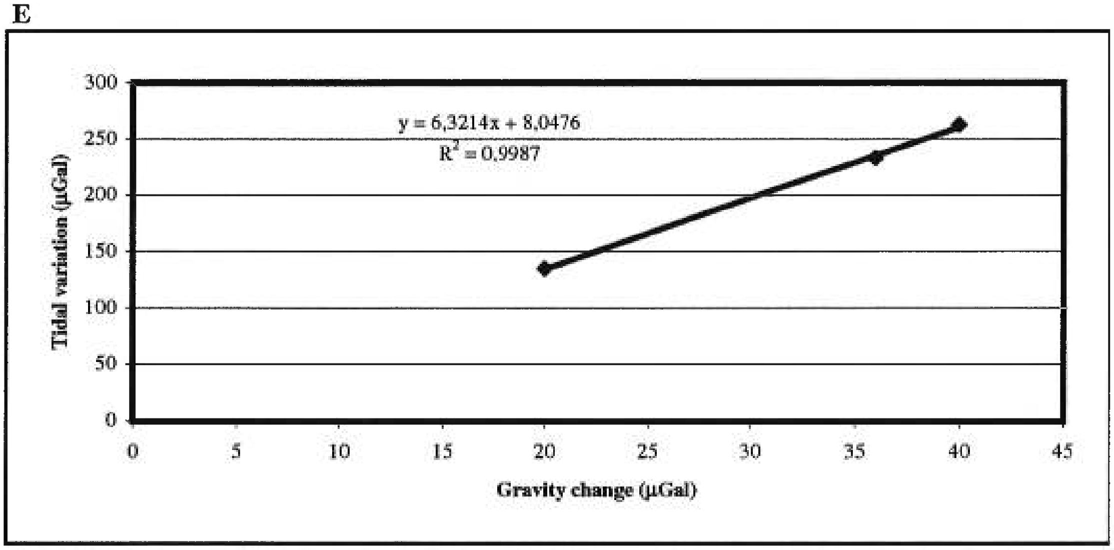

y = 6,3214x + 8,0476
R^2 = 0,9987
Tidal variation (µGal)
Gravity change (µGal)
300
250
200
150
100
50
0
0
5
10
15
20
25
30
35
40
45

F

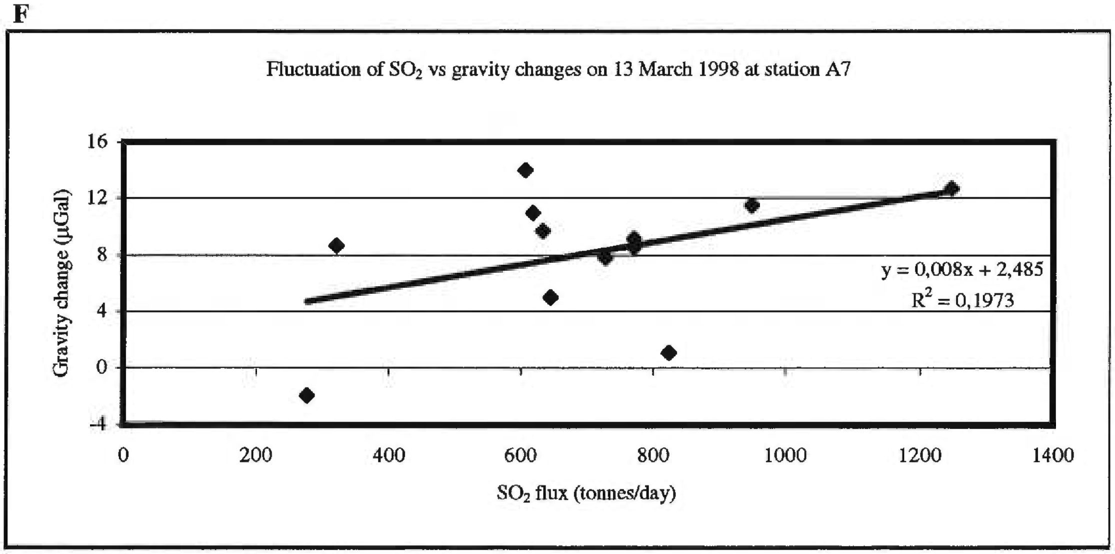

Fluctuation of SO_2 vs gravity changes on 13 March 1998 at station A7
y = 0,008x + 2,485
R^2 = 0,1973
Gravity change (µGal)
SO_2 flux (tonnes/day)
16
12
8
4
0
-4
0
200
400
600
800
1000
1200
1400

222 μGal. When plotted, a clear positive correlation appears between the maximum tidal amplitude and the maximum gravity variation (Fig. 2.6d). The ratios of maximum gravity variations to maximum tidal amplitudes are similar for each day, except for the 1997 data, so a direct correlation of the gravity variations to tidal variations is tempting (Table 2.1). The Scintrex ratio of maximum gravity to maximum tidal amplitude for 1997 do not match with the ratio of 1998 so they are not plotted in Figure 2.6d. Plotted alone, the positive correlation for the 1998 ratios of maximum gravity variations to maximum tidal amplitudes is very good (r^2= 0.999) (Fig 2.6e). More data are necessary to verify this relationship. When comparing the gravity changes to the SO_2 flux variations for the same period of time for the 13 March 1998, a positive correlation is tempting (Fig 2.6f). However, the period of time is not very representative since the SO_2 fluxes were measured only for 2.5 hours beginning at noon.

Atmospheric pressure measurements were taken at the Hotel Regis in Masaya City during the course of the second and the third days of continuous gravity monitoring. A first look at figure 2.7a and 2.7b gives the impression that gravity variations are related inversely to pressure variations. But on closer inspection, the rates of the pressure and gravity variations show that there is no clear relation between pressure and gravity. For 6 March (Fig 2.7a), the gravity increase of 5.6 μGal/hour between 09:58 and 13:32 corresponds to decreasing pressure at a rate of – 0.8 mbar/hour. After 13:32, the gravity does not vary significantly (-0.7μGal/hour), while the pressure increases at a rate of 0.5 mbar/hour. For 13 March, the increase in gravity at rate of 2.8 μGal/hour from 10:50 to 15:32 occurs at a pressure decrease of

Table 2.1: Maximum gravity and tides variation and their ratio in 1997 and 1998

	Max Grav	Max tide	Ratio G/T
LCR-98	40	263	0.1520913
LCR-98	20	135	0.1481481
LCR-98	36	233	0.1545064
LCR-97	45	222	0.2027027
Scintrex	20	222	0.0900901

FIGURE 2.7

Daily gravity changes vs. pressure fluctuations at station A7 for (a) 06/03/98 and (b) 13/03/98. (c) Pressure variation rate vs. gravity variation rate for daily variations in 1998 at station A7.

A

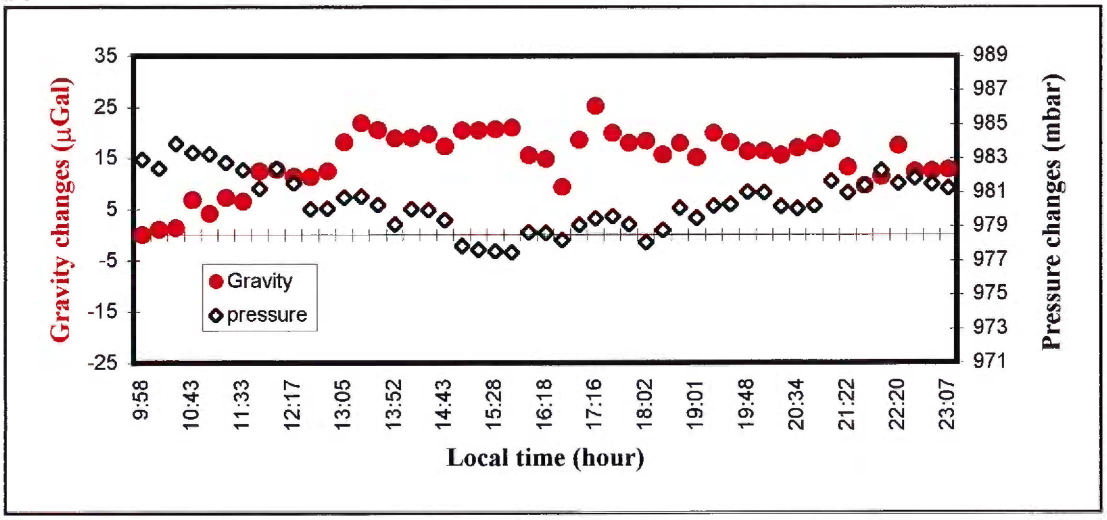
Gravity changes (μGal)
35
25
15
5
-5
-15
-25
Pressure changes (mbar)
989
987
985
983
981
979
977
975
973
971
Gravity
pressure
9:58
10:43
11:33
12:17
13:05
13:52
14:43
15:28
16:18
17:16
18:02
19:01
19:48
20:34
21:22
22:20
23:07
Local time (hour)

B

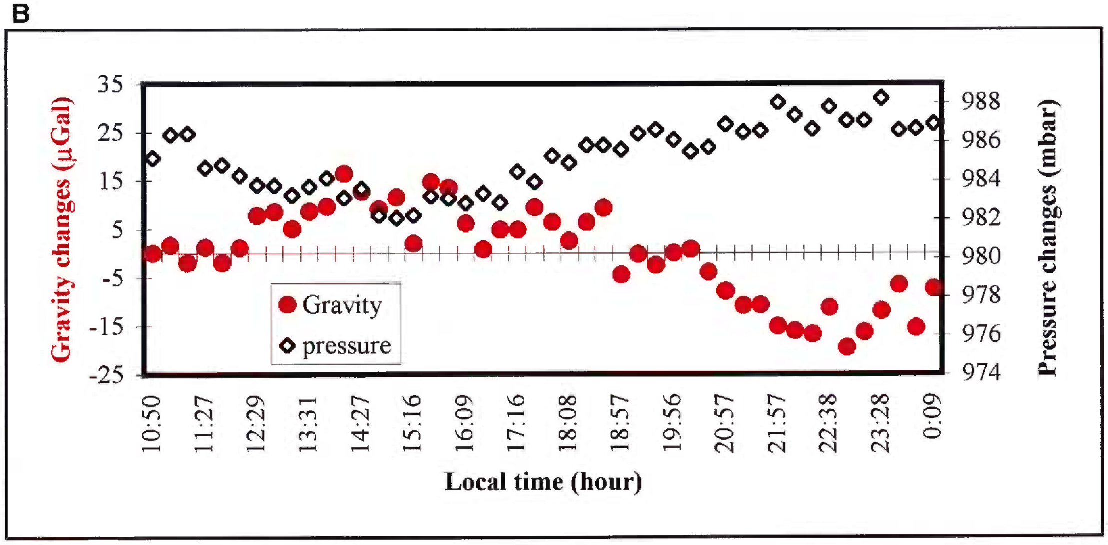
Gravity changes (μGal)
35
25
15
5
-5
-15
-25
Pressure changes (mbar)
988
986
984
982
980
978
976
974
Gravity
pressure
10:50
11:27
12:29
13:31
14:27
15:16
16:09
17:16
18:08
18:57
19:56
20:57
21:57
22:38
23:28
0:09
Local time (hour)

C

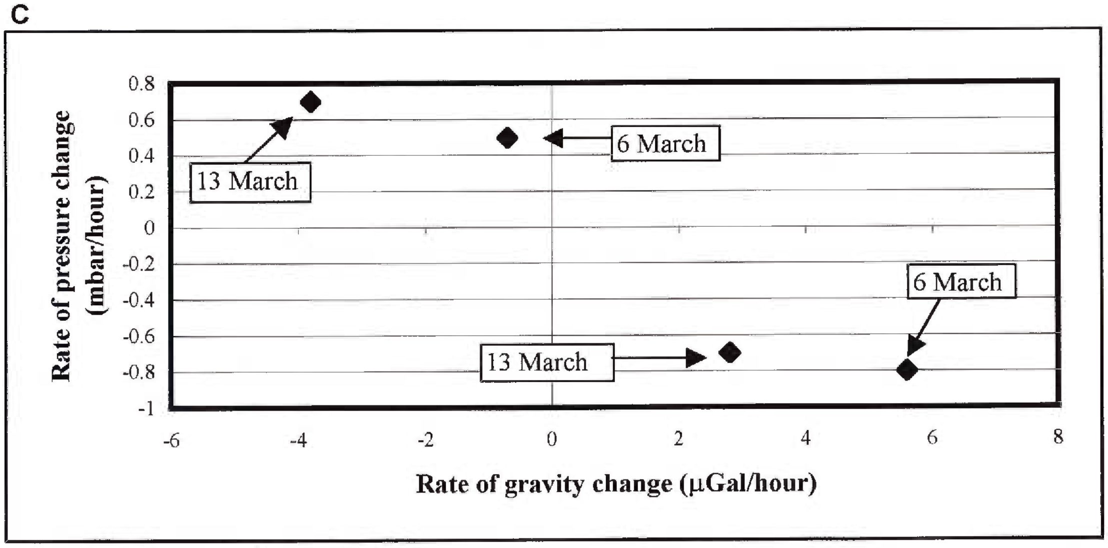
Rate of pressure change (mbar/hour)
0.8
0.6
0.4
0.2
0
-0.2
-0.4
-0.6
-0.8
-1
13 March
6 March
6 March
13 March
-6
-4
-2
0
2
4
6
8
Rate of gravity change (μGal/hour)

–0.7 mbar/hour (Fig. 2.7b). After 15:32, the gravity decrease of –3.8 μGal/hour corresponds to a pressure increase of 0.7 mbar/hour. On a plot of gravity variation rate vs. pressure variation rate, it appears that there could be a relation between the two parameters (Fig. 2.7c). However, a closer look at the plot shows that for pressure variation rates of 0.5 mbar/hour and 0.7 mbar/hour, the corresponding gravity rates are –0.7 μGal/hour and –3.8 μGal/hour, which correspond to ratios of –1.4 μGal/mbar and –5.4 μGal/mbar, respectively. The lack of a linear trend on this diagram and the difference in the ratios strongly imply that the gravity variations are not caused by variations in atmospheric pressure. Even if the gravity variation were affected by a pressure leak in the LCR meter, there is no clear relation between pressure and gravity variations observed at Masaya volcano on a daily basis. For 6 March, the maximum pressure change was on the order of 5 mbar, which corresponds to approximately –2 μGal. For 13 March, the maximum pressure change was about 7 mbar, corresponding to about –3 μGal. These gravity changes are much smaller than those observed on a daily basis, indicating that atmospheric pressure does not play an important role.

The response of the meter to the temperature variation over the durations of the experiements also does not appear to be significant. For the case of 25 February, the ambient temperature first increased, then decreased during the course of the day. It might be possible to correlate these temperature changes with the initial increase and subsequent decrease of gravity for 25 February (Fig. 2.6a). However, gravity begins to increase a second time at about 22:00 local time. This increase cannot be caused by temperature, since the region was cooling during the nightime. Similar observations can be made for 6 March and 13 March 1998.

Continuously occurring volcanic tremors is recorded beneath Santigo (Metaxian and Lesage, 1997). It is possible that variations in the intensity of tremors may reflect changes in the magmatic activity, which in turn may also cause changes in microgravity. During the gravity measurements, seismicity has been monitored constantly. Investigation of the seismic data show that there is a continuous background tremor of 10 digital units of amplitude. No significant variations in amplitude were observed for the maxima and minima of observed gravity on 25 February, 6 March and 13 March 1998. Some isolated seismic events from an unknown source were also detected. No correlation was found between the seismicity and gravity changes.

Weekly Gravity Variations in 1997

Results presented in this section are from the microgravity line consisting of stations A1, A3, A7, B2 and B1A. The relative differences are calculated with A1 as the base (Appendix B, Table B3); they represent variations between 4-17 March 1997. Measurements on 4 March were made by Hazel Rymer. The LCR instrument shows a decrease of approximately 30-40 μGal between 4-10 March for the three stations near the crater (A7 = 36 μGal , B1A and B2 = 31 μGal) (Fig. 2.8a). Between 10-13 March, gravity was mostly stable except for station A7 where there was an increase of 19 μGal. Between 13-17 March, a decrease was observed at every station near the crater. This decrease was of variable amplitude depending on the station (62 μGal for A7, 38 μGal for B2 and 24 μGal for B1A). In general, the temporal

FIGURE 2.8

(a) Weekly gravity changes for the LCR in 1997. (b) Gravity changes vs diurnal tidal variation, 4-17 March 1997 at station A3, A7, B1A and B2.

A

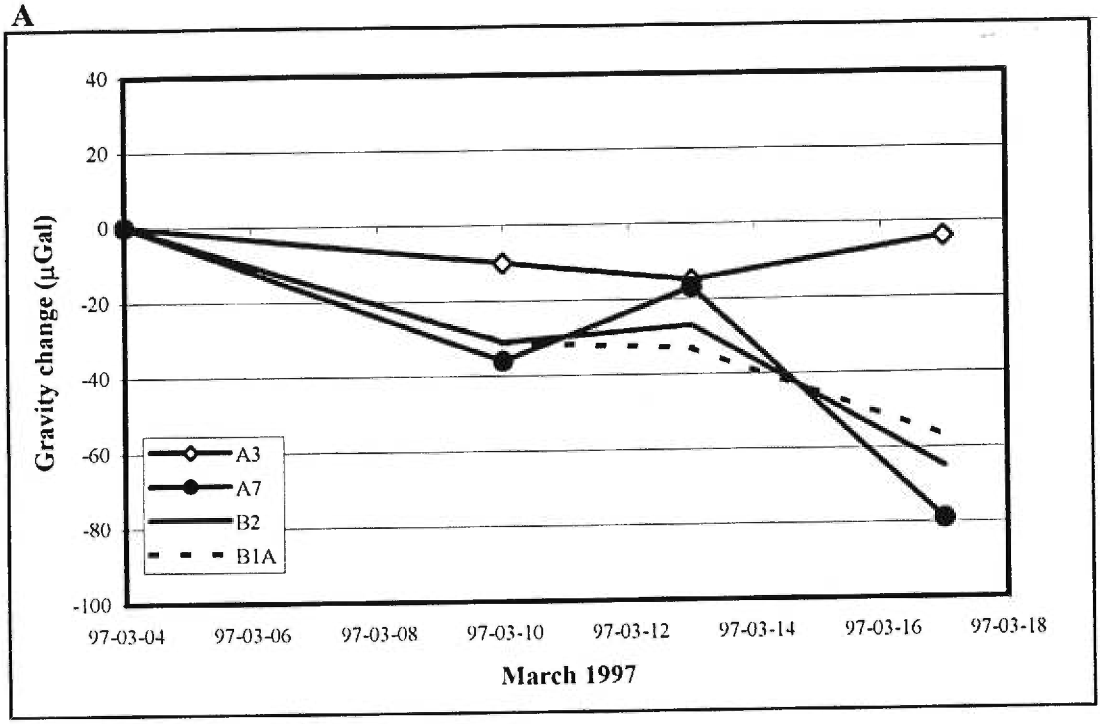

Gravity change (μGal)
40
20
0
-20
-40
-60
-80
-100
A3
A7
B2
B1A
97-03-04
97-03-06
97-03-08
97-03-10
97-03-12
97-03-14
97-03-16
97-03-18
March 1997

B

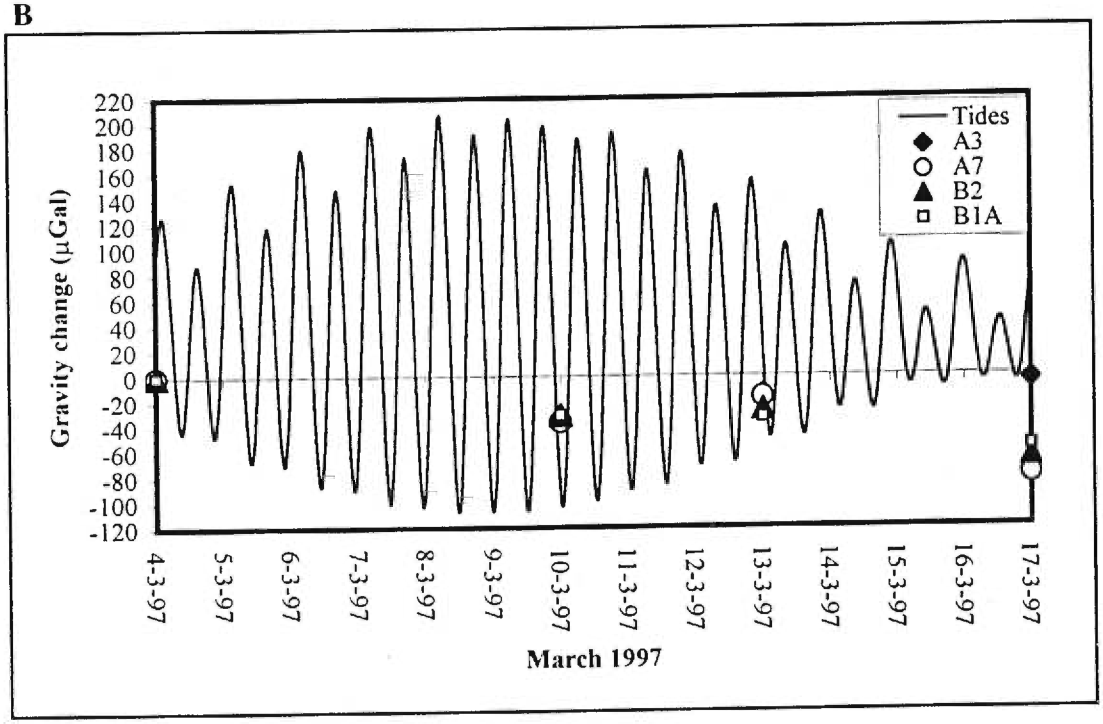

Gravity change (μGal)
220
200
180
160
140
120
100
80
60
40
20
0
-20
-40
-60
-80
-100
-120
Tides
A3
A7
B2
B1A
4-3-97
5-3-97
6-3-97
7-3-97
8-3-97
9-3-97
10-3-97
11-3-97
12-3-97
13-3-97
14-3-97
15-3-97
16-3-97
17-3-97
March 1997

variation of microgravity during this period is similar among the three stations. For station A3, located in the caldera three kilometers north of the active crater (Fig. 2.4), there was no significant variation observed. The gravity changes observed between 4-13 March consist of a decrease of 15 μGal, while between 13-17 March an increase of 11 μGal was observed. However, these variations are not significant at the 95% confidence level, so as stated above, there are no significant variations at A3. Therefore, the gravity changes are confined to the vinicity of the crater area; this conclusion is also made by Rymer et al. (1998).

The microgravity changes occurred at stations near the crater due to its higher level of activity. During the period February 1993 to March 1994, precision levelling within the caldera revealed an uplift of 2-3 cm at the summit relative to a station 5 km east (J.B. Murray personal communication, 1997; Global Volcanism Network Bulletin, 1994). GPS data also indicate that there have been no vertical movements in excess of 2 cm or horizontal movements in excess of 1 cm between 1994 and 1997. This altitude variation corresponds to 6 μGal and is small compared to the microgravity variations observed (Rymer et al. 1998). It is therefore clear that the microgravity variations observed are not due simply to altitude variations. As the tidal amplitude decreased from 9 March to 16 March, so did the gravity during the same period (Fig. 2.8b). However, as the gravity decreased between 4 March to 10 March, the fortnightly tidal amplitude increased, which is in the opposite sense. Thus, no clear relation between the gravity changes observed from 4-17 March and the tidal variations is observed.

Weekly Gravity Variations in 1998

Gravity variations observed in 1998 extend from 27 January to 14 March. In total, 10 days of microgravity measurements were taken over a duration of 47 days, starting on 27 January. Measurements taken on 27 January were made by Hazel Rymer, and those taken on the 18 and 27 Febuary, and 14 March were made by Glyn Williams-Jones. From 27 January to 18 February, there are no consistent gravity variations except for a large decrease of 55 μGal at Museo, which is due to an error from the misplacement of the station between 27 January and 18 February (Fig. 2.9a). For certain days (18 and 27 February and 14 March 1998), variations of less 30 μGal are considered not to be significant (G. Williams-Jones, personal communication, 1998). Because of a problem with the electrical wire connecting the LCR meter to the battery, there was a power failure on 14 February which caused the meter temperature to fall by 3-4 °C. Because of this problem, the meter was unstable for about a week; the associated error is higher than usual, depending on the technique used to acquire data. Between 18-24 March, there is no variation in the crater area (A7, B2 and B1A), but an increase of about 27 μGal is observed at stations A3 and A5. This is surprising, since there are no variations at the summit area and at MUSEO. This variation is near the error limit of 25 μGal, thus not too much weight should be placed on this difference. Between 24 February and 1 March, a peak is observed at all stations except MUSEO. This peak is more prominent for stations A7, B2 and B1A, where there are increases of 62, 63 and 55 μGal, respectively, from 24 to 27 February. From 27 February to 1 March, there are decreases of 53 μGal for A7, 46 μGal for B2 and 41 μGal for B1A. The gravity variation at A5 for the 24

February-1 March peak corresponds to an increase of 29 μGal and a subsequent decrease of 33 μGal. For A3, the peak is represented by an increase of 10 μGal and then a decrease of 12 μGal. It seems that either an event occurred between 24 February and 1 March which increased the magma density in the crater area, or alternatively there is a problem with the data of 27 March. After this peak, gravity variations are generally less than 25 μGal, except for stations B2 and B1A which show increases of 32 μGal and 24 μGal, respectively, between 5-9 March. Interestingly, A7 does not follow this trend, and actually shows a small decrease instead, increasing afterward while B2 and B1A decrease between 5-14 March. In general, except for the peak between 24 February and 1 March, there are no consistent variations, considering the level of precision for most of the variations (25-30 μGal).

If the gravity variations measured by the second data acquisition technique (discussed above) are considered alone (24 February and 1, 2, 3, 5 and 9 March 1998), the results are the same but the precision is higher. The precision with this technique is around 12 μGal (twice the standard deviation), so variations larger than 15 μGal should be considered significant at the 95% confidence level. The only gravity variations observed between 24 February and 1 March are at stations B2 and B1A where there are increases of 33 μGal and 40 μGal, respectively (Fig. 2.9b). All the gravity variations at other stations are generally within the level of error. Again, station A7 does not follow the trend of stations B2 and B1A; it shows no real variation during the entire survey. GPS measurements made in 1998 do not show any vertical variation greater than 1-2 cm (G. Williams-Jones, personal communication,

FIGURE 2.9

(a) Gravity changes at Masaya between 27/01/98 and 14/03/98. (b) Gravity changes at Masaya between 24/02/98 and 09/03/98. (c) Gravity changes vs. diurnal tidal variation from 27 January to 14 March 1998.

A

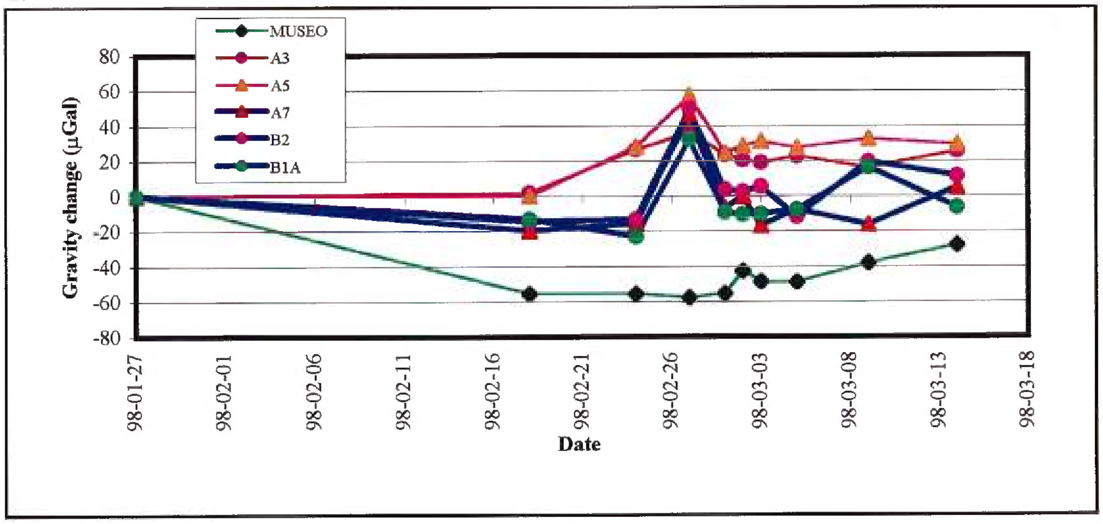
MUSEO
A3
A5
A7
B2
B1A
Gravity change (µGal)
80
60
40
20
0
-20
-40
-60
-80
98-01-27
98-02-01
98-02-06
98-02-11
98-02-16
98-02-21
98-02-26
98-03-03
98-03-08
98-03-13
98-03-18
Date

B

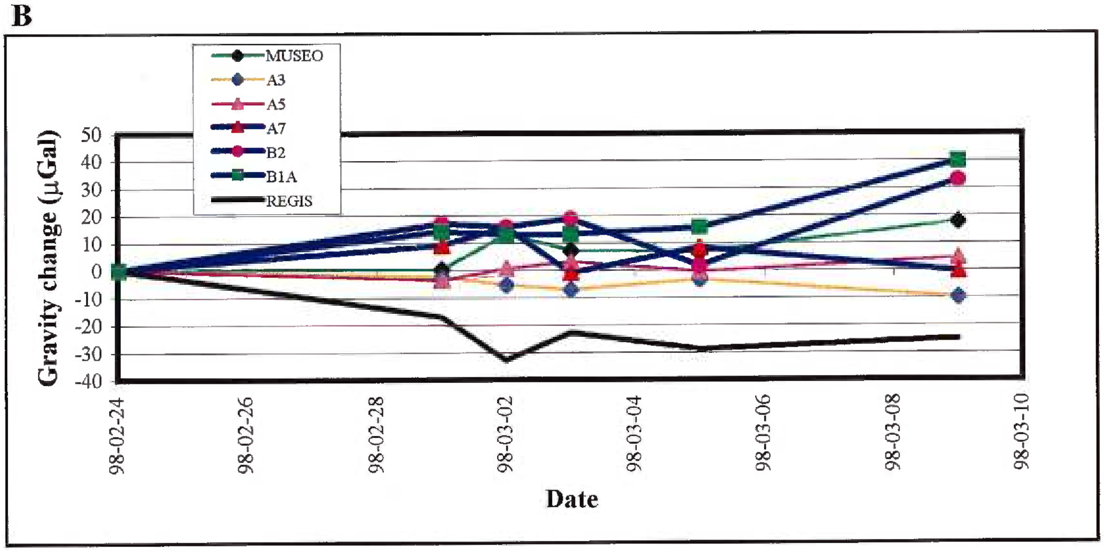
MUSEO
A3
A5
A7
B2
B1A
REGIS
Gravity change (µGal)
50
40
30
20
10
0
-10
-20
-30
-40
98-02-24
98-02-26
98-02-28
98-03-02
98-03-04
98-03-06
98-03-08
98-03-10
Date

C

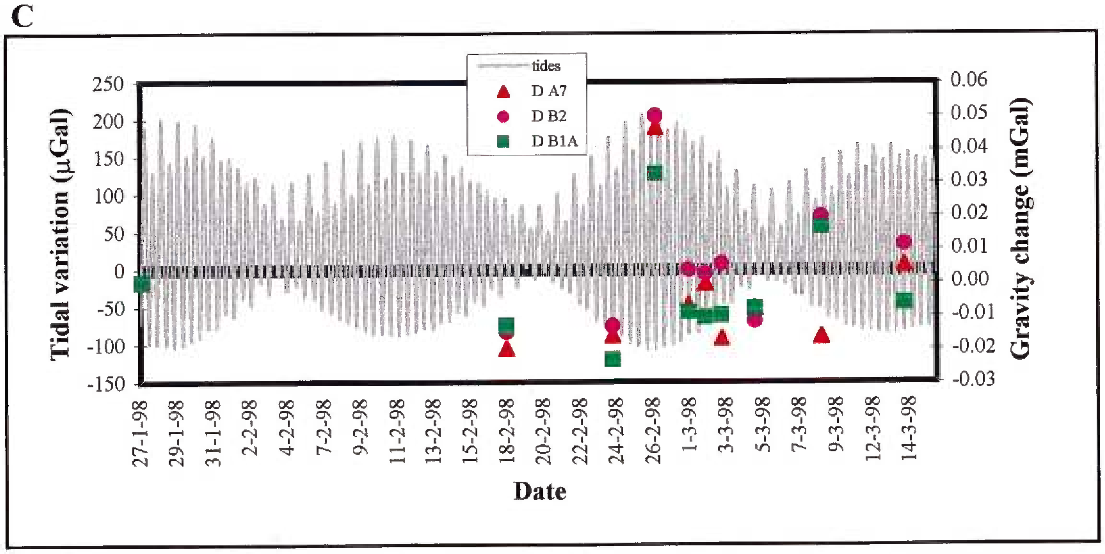
tides
D A7
D B2
D B1A
Tidal variation (µGal)
250
200
150
100
50
0
-50
-100
-150
Gravity change (mGal)
0.06
0.05
0.04
0.03
0.02
0.01
0.00
-0.01
-0.02
-0.03
27-1-98
29-1-98
31-1-98
2-2-98
4-2-98
7-2-98
9-2-98
11-2-98
13-2-98
15-2-98
18-2-98
20-2-98
22-2-98
24-2-98
26-2-98
1-3-98
3-3-98
5-3-98
7-3-98
9-3-98
12-3-98
14-3-98
Date

1998), which corresponds to about 3-6 μGal in gravity. No direct correlation was found with the fortnightly and diurnal tidal variations during this these weekly measurements (Fig. 2.9c).

Annual Gravity Variation, 1997-1998

Variations on a yearly basis are not very significant. If we compare values acquired in 1997 to those of 1998, we see that there are no consistent variations (Fig. 2.3). It is difficult to interpret the gravity on a year-to-year basis, since variations on weekly and even daily basis are sometimes quite large. For example, gravity variations observed at station A7 since 1993 show a clear trend initially because there is only one measurement per year (Fig. 2.10). When one looks at gravity variations in 1997 and 1998, however, the major observation is that gravity varies significantly. If only one measurement was made in 1997 and 1998, the trend of the gravity variation would be variable depending on the day the measurement was taken.

Discussion

Microgravity monitoring of Masaya volcano was initiated by Hazel Rymer in 1993 after the renewal of degassing activity at the active Santiago crater. The goal of the survey was to constrain the shallow structure of the magma system and its geophysical signature in a way to forecast future changes. From 1993 to 1994, Rymer et al. (1998) observed a gravity change at all stations near the active crater and little or no change at stations away from the crater in the caldera (Fig. 2.4). Subsequently, gravity increased slightly each year at stations near the crater. These data indicate that the anomaly causing the gravity changes is centered at the crater

FIGURE 2.10

Annual gravity changes at Masaya for station A7, 1993-1998.

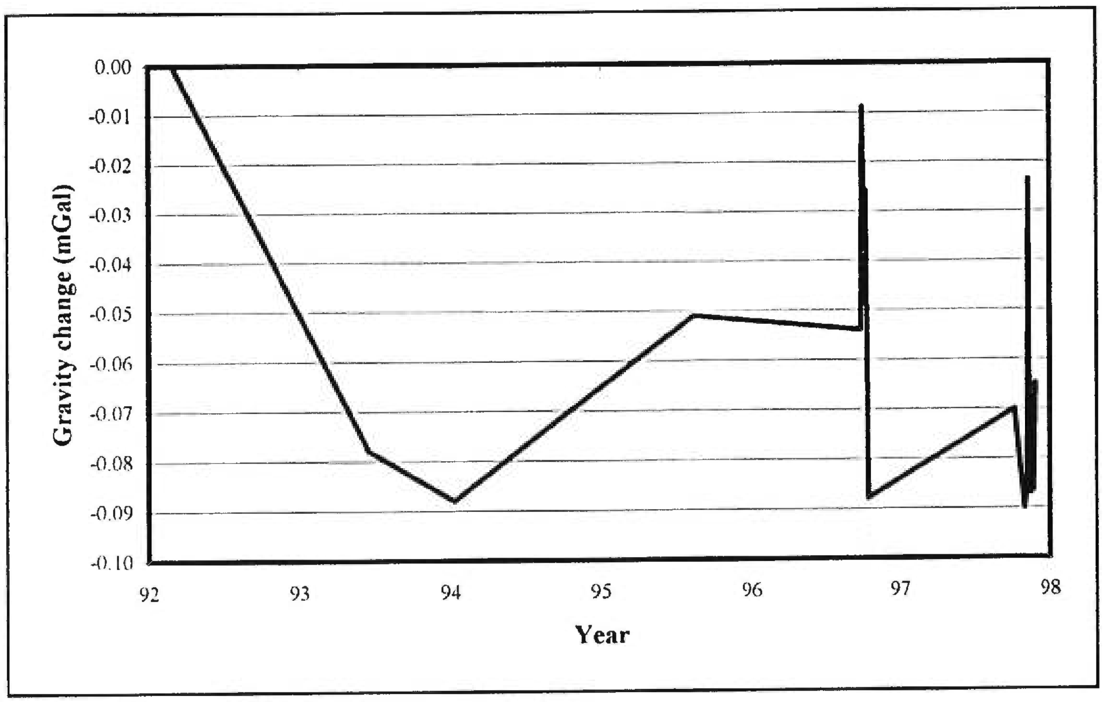

0.00
-0.01
-0.02
-0.03
-0.04
-0.05
-0.06
-0.07
-0.08
-0.09
-0.10
Gravity change (mGal)
92
93
94
95
96
97
98
Year

and at shallow depth. The model that best fits the observed gravity variation is a cylindrical body of reduced density of 440 m diameter and 100 m thick (Rymer et al., 1998). They related this decrease of density by vesiculation of the shallow magma beneath Santiago crater as a result of convective overturn of the magma remaining in the plumbing system from the previous episode of activity in the 1980's.

We now analyze the short-time scale microgravity variation observed at Masaya during 1997-98 and compare it to the above model. Results obtained in 1997 over a period of two weeks showed overall decreases of gravity of about 55-80 μGal at the three stations near the active crater (A7, B2 and B1A) (Fig. 2.8a). In 1998, there were variations of the order of 55-63 μGal over very short periods (3 days) (Fig. 2.9a). One-day experiments in 1997 and 1998 showed gravity changes varying from 20 to 45 μGal at Station A7 near Santiago (Fig. 2.5a, 2.6a,b and c). These variations may be linked to changes in the density of the magma, which in turn probably depend on the bubble content. The dissolved gas content in the magma beneath Santiago does not cause the density to vary much. At low pressure, the variation in the quantity of volatiles dissolved in the magma does not change the magma density significantly. At 50 MPa, a variation of 1 wt% H_2O dissolved in the magma is required to produce a density variation of 30-40 kg/m^3 (Lange and Carmichael, 1990; Lange, 1994). This would not be expected at Masaya considering the amount of volatiles in the magma (about 1 wt %) (K. St-Amand, personal communication, 1998) and the lithostatic pressure of 5 MPa at the base of the magma body at Masaya. The corresponding quantity of H_2O at this pressure for a saturated magma is about 0.95 wt %. Therefore, variation in the dissolved content of H_2O in the magma should not be high enough to produce the density variation needed to account for the gravity changes observed at the surface. An easier way to produce the density variations in a magma is to vary the amount of exsolved volatiles in the magma. At a pressure of 5 MPa, very small fluctuations in the H_2O content (0.01 wt %) can produce density variations of 50-100 kg/m^3. This corresponds to 3-5 % vesicularity.

Short-term variations were observed at Poás volcano in Costa Rica during a period of 43 days where ten sets of gravity measurements were made at different stations around and in the crater area by Rymer and Brown (1987). They concluded that the most probable cause of these gravity fluctuations was changes in the density of the magma. They stated that a variation in the density of the magma of about 30 kg/m^3 was needed to produce the observed gravity variation at the crater station of 120-140 μGal. They also stated that a vesicularity variation of 1 % would be sufficient to produce the inferred change in the density of the magma. At Masaya, the observed gravity variations are of the same order (40-90 μGal). Because of a lack of rain during our field season, the gravity variations observed on a daily basis are clearly not produced by variations in the water table level. Another possible cause to explain the gravity variation observed near the crater is changes in the level of the magma. The problem with this model is that the magma level would have to vary by tens of meters in a very short time to produce the daily gravity changes observed near Santiago at station A7. We can model this using the finite vertical cylinder model to calculate the maximum gravity variation:

$$G_{max}= 2\pi\gamma\rho[L + (z^2 + R^2)^{1/2} - [(z + L)^2 + R^2]^{1/2}]$$

where γ is the universal gravity constant, ρ the density contrast in kg/m^3, L the length of the cylinder in m, z the depth to the roof of the cylinder and R the radius. Using a large body of magma at a depth of 360 m, having a length of 200 m and a radius equal to the Santiago crater radius of 300 m and a depth variation of 10 m for a magma density contrast of 300 kg/m^3, the corresponding gravity variation is 15 μGal. This correspond to the maximum gravity variation that could be observed at the center of the anomaly for a 10 m level variation.

The four continuous sets of measurements made near the crater area during 7-13 hours in 1997 and 1998 showed variations in gravity of the order of 40 μGal. These changes do not seem related to any inherent problems of the meter in response to environmental variations such as atmospheric pressure, temperature and tares, since the meter was not touched for the duration of the experiments. Instrumental drift is not considered for this particular meter (G-513) because it is known to be fairly stable. In fact, the same meter was used to make a Bouguer survey at Telica volcano, and there it proved to be very stable. For example, the average difference between the starting and ending measurements made each day at the reference station during the Bouguer survey was about 17 μGal. This is quite low, considering that fewer precautions were taken for the precision during this survey compared with a microgravity survey. The changes observed with this meter in such a short time period must be the result of changes beneath Santiago crater. As stated above, the most realistic probability over a short time is a fluctuation in the density of the magma, which is more likely in an upper, less dense layer of magma where there are many gas bubbles and degassing activity. Modelling of the anomaly under Santiago showed that the variations observed are caused by a local body of shallow depth and of a size similar to the diameter of Santiago crater. To account for the observed gravity variations, the most plausible body of magma would be about 100-200 kg/m^3 less dense than the surrounding rocks. Density variations of the order of 25-75 kg/m^3 within the magma body would be necessary to produce the observed gravity changes (Fig. 2.11a,b,c and d). These density variations would be more efficient if distributed in a larger body instead of a very thin layer of vesiculated magma like a foam. If the density variations are produced only in a thin layer of about 10-20 meters, they must be very large (300-600 kg/m^3) to produce the observed gravity changes.

A possible response of the magma to diurnal tides was observed for the one-day experiments. there appears to be a time-lag of about 4 hours between the maximum tidal amplitude and the maximum gravity variations, with the maximum gravity variation occuring after the maximum tidal amplitude. The same phenomenon is observed for the tidal and gravity minima. Moreover, the amplitude of the gravity variation appears to be linked to the amplitude of the diurnal tides. It is not yet clear in what way the physical or mechanical effect of the tides modify the magma beneath Santiago. If the daily gravity variations observed at Masaya volcano are considered to be real, then the weekly gravity variations are probably not representative of the processes occuring at Masaya. The same conclusions may apply to the annual variation to a certain extent. Yet one may consider that such short-time fluctuations are residual and should not affect the general trend of the gravity variations on a yearly basis.

The processes causing fluctuations in the density and vesicularity of the magma are not fully understood. Permanent tremor is ongoing at Masaya; its source

FIGURE 2.11

Gravity changes of a body of magma under Santiago crater 120 m thick with an initial density contrast of (a) –120 kg m^{-3} and than increasing to (b) -70 kg m^{-3}, (c) -50 kg m^{-3} and (d) –25 kg m^{-3}.

A

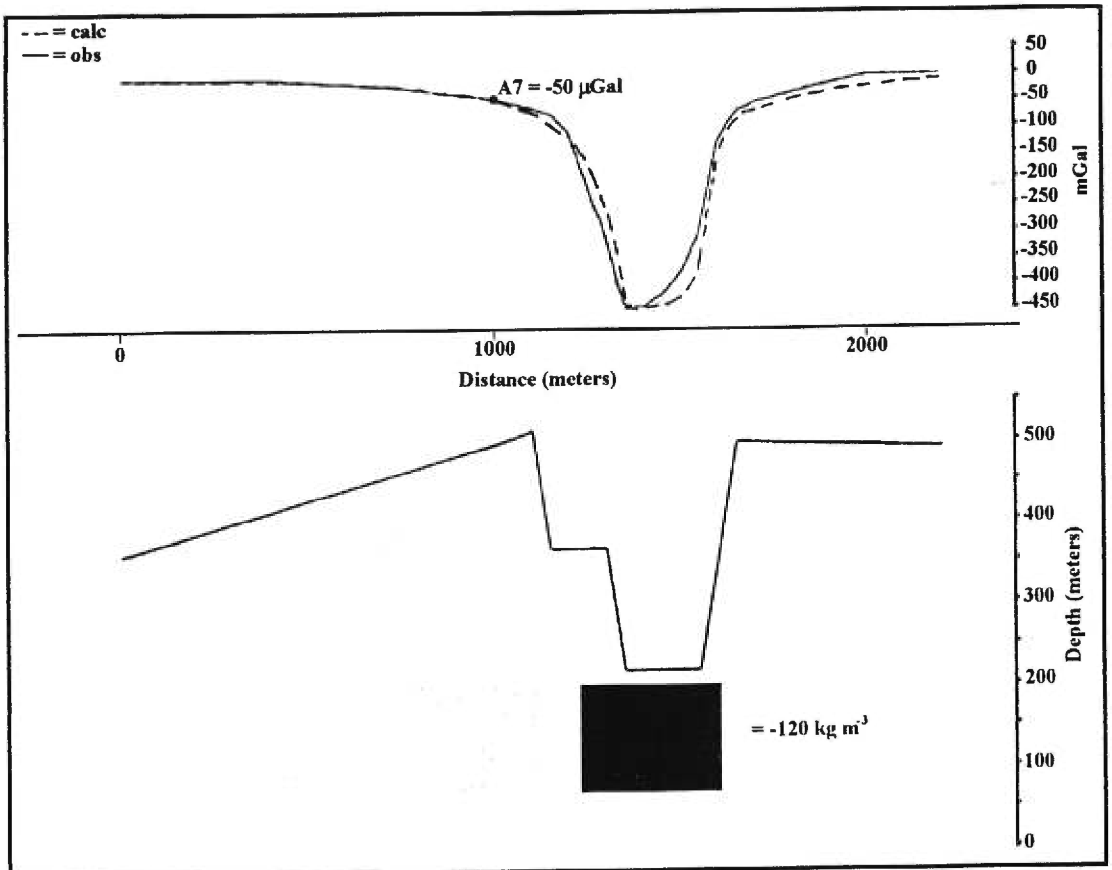

- - = calc
— = obs
A7 = -50 μGal
50
0
-50
-100
-150
-200
-250
-300
-350
-400
-450
mGal
0
1000
2000
Distance (meters)
500
400
300
200
100
0
Depth (meters)
= -120 kg m⁻³

B

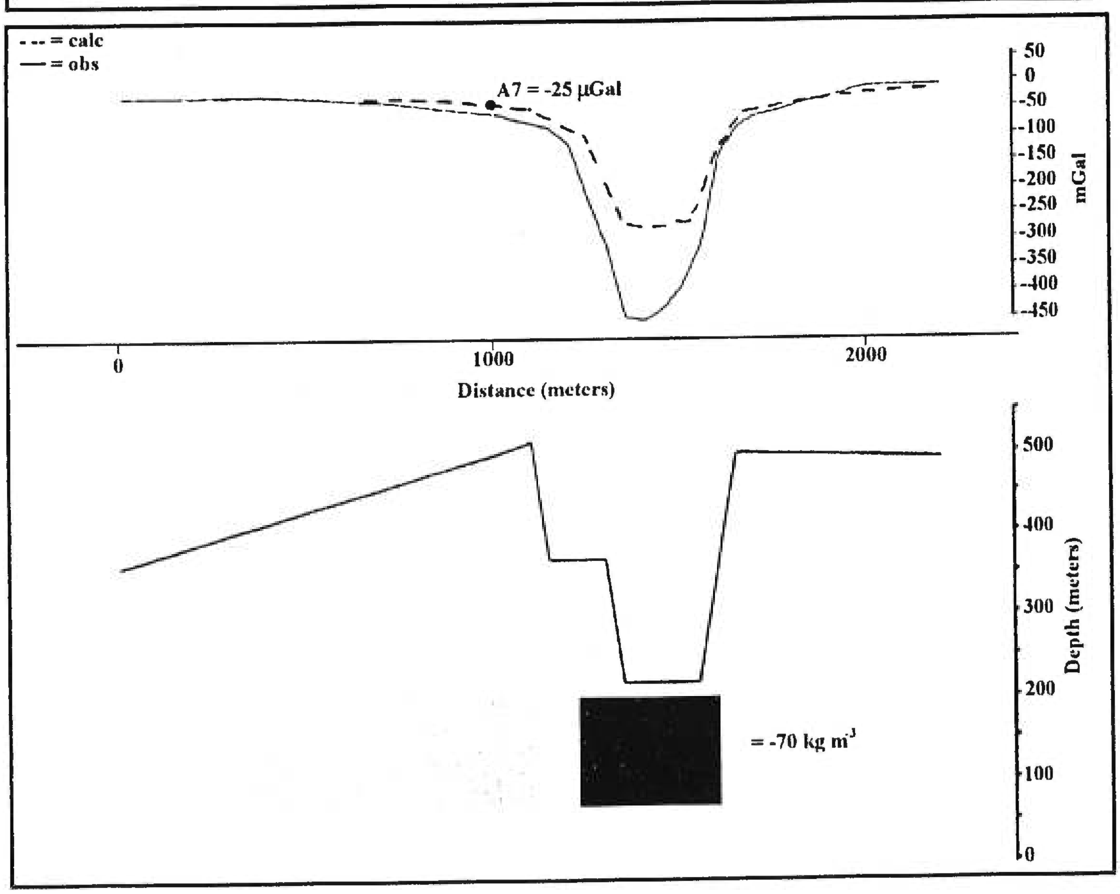

- - = calc
— = obs
A7 = -25 μGal
50
0
-50
-100
-150
-200
-250
-300
-350
-400
-450
mGal
0
1000
2000
Distance (meters)
500
400
300
200
100
0
Depth (meters)
= -70 kg m⁻³

c

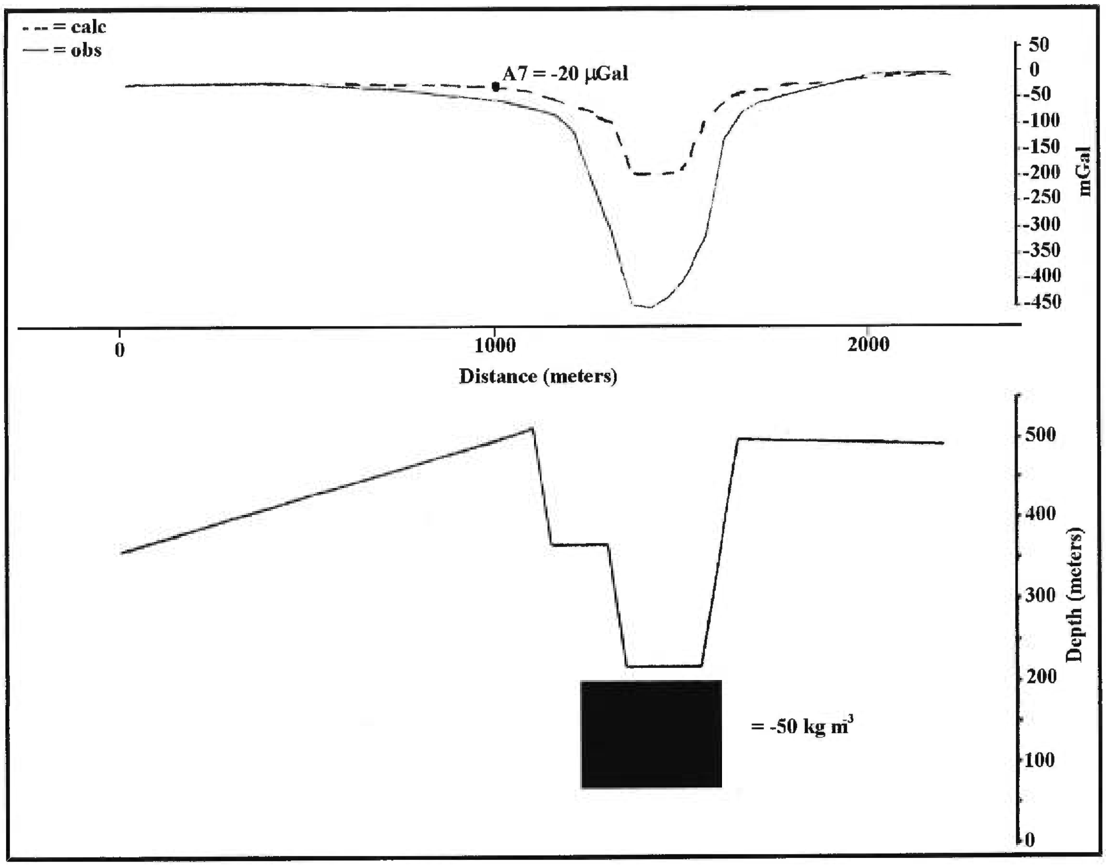

--- = calc
— = obs
A7 = -20 μGal
50
0
-50
-100
-150
-200
-250
-300
-350
-400
-450
mGal
0
1000
2000
Distance (meters)
500
400
300
200
100
0
Depth (meters)
= -50 kg m³

d

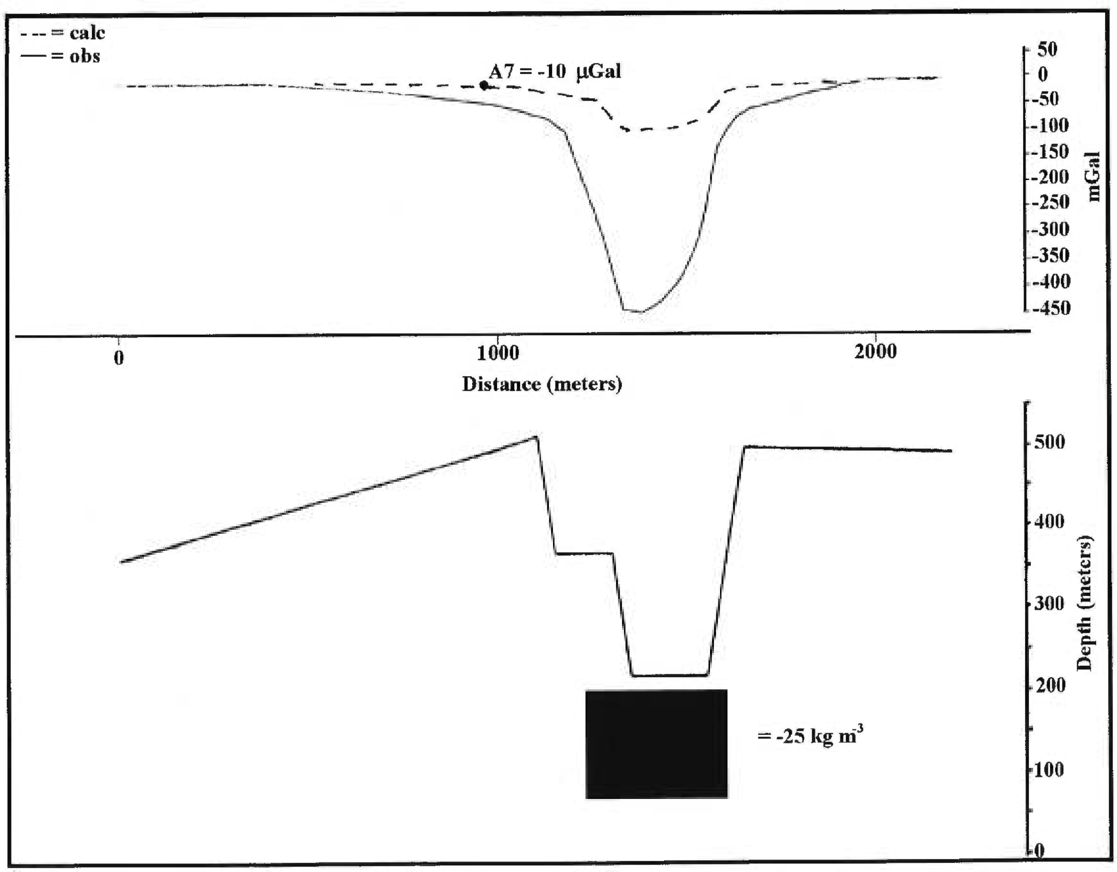

--- = calc
— = obs
A7 = -10 μGal
50
0
-50
-100
-150
-200
-250
-300
-350
-400
-450
mGal
0
1000
2000
Distance (meters)
500
400
300
200
100
0
Depth (meters)
= -25 kg m³

FIGURE 2.12

(a) Fluctuation of SO_2 fluxon March 12 1997. (b) Fluctuation of SO_2 flux on 13 March 1998.

A

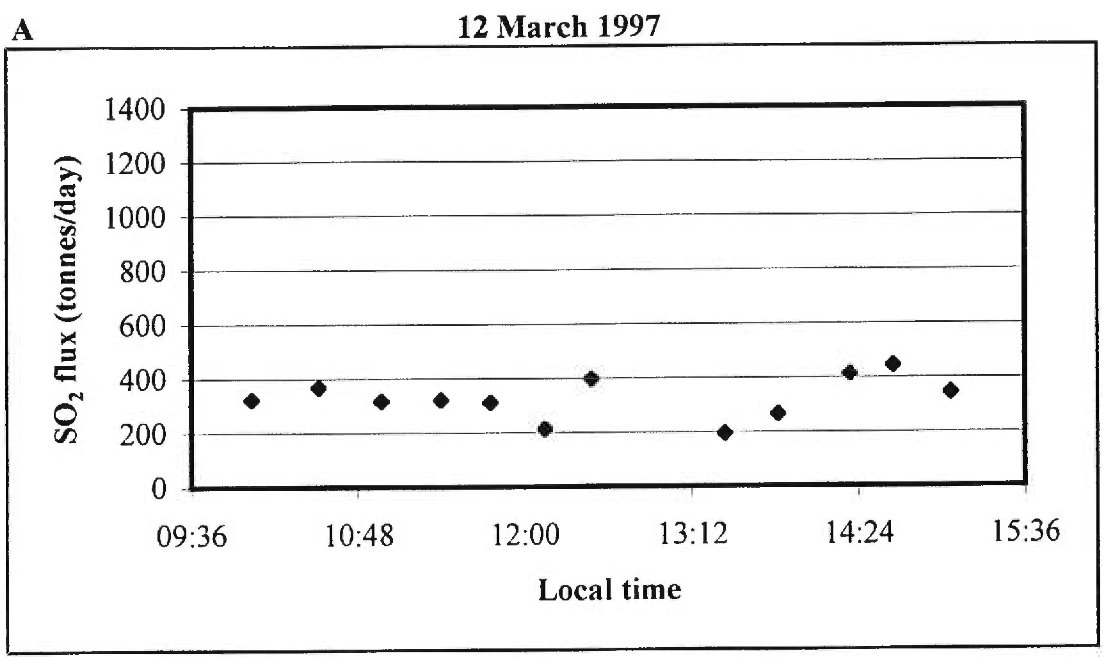

12 March 1997
1400
1200
1000
800
600
400
200
0
SO2 flux (tonnes/day)
09:36
10:48
12:00
13:12
14:24
15:36
Local time

B

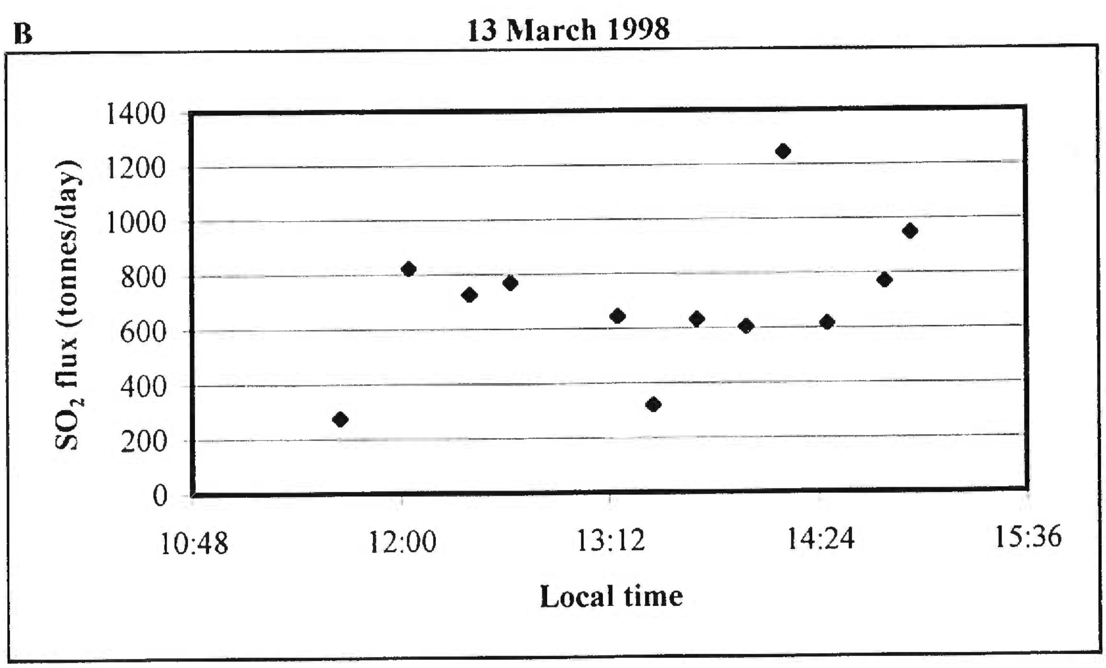

13 March 1998
1400
1200
1000
800
600
400
200
0
SO2 flux (tonnes/day)
10:48
12:00
13:12
14:24
15:36
Local time

is located under the active crater of Santiago. Metaxian and Lesage (1997) observed that the permanent tremor at Santiago is probably generated by the continuous degassing. There may be convective processes in the magma that bring gas-rich magma from deep within the body to shallow levels where it vesiculates to lower the density of the magma. Fluctuations of the SO_2 flux were observed over a period of a day at Masaya (Fig. 2.12a and b). This may indicate that the quantity of gas may vary at the top of the magma over a very short time. Pulses of gas-rich magma from rapid convection could be the cause of these SO_2 fluctuations. These pulses may be driven thermally by convection or by injection of new magma. Another possibility is that batches of gas bubbles could be rising from a deeper part of the magma body under Santiago. Vergniolle (1996) has show that the ascent rate for 1 mm-diameter bubbles is about 1.5×10^{-4} m/s. This corresponds to a rise time of about one month for the 440 meter-thick magma body under Santiago. This timescale is two orders of magnitude higher than that of 4 hours observed between the tidal and gravity variations. Thus, the bubble rise mechanism is not possible for the daily gravity variations which are linked to the diurnal tides. The possibility of a new magma injection into the chamber is unlikely, since it would have left a larger and more widespread gravity signature than the one observed at Masaya by Rymer et al. (1998). Nevertheless, it is clear that the cause of the gravity changes is linked to variations in the density of the magma, which in turn is related to fluctuations in the vesicularity. However, the cyclicity observed in these changes could be driven by several possible mechanisms.

Conclusions

Gravity variations observed at Masaya volcano are linked to fluctuations in vesiculation of the magma beneath Santiago crater. A possible link of earth tides to daily gravity variations was observed at one station (A7) near the active crater. The tides appear to affect the vesiculation of the magma. All the gravity changes observed at different timescales are consider to be the result of the same process, which is changes in density of the magma. These changes are linked to vesiculation fluctuations in the magma. Varying the vesicularity of the magma is an efficient way to produce the gravity variations observed at Santiago. This could occur in many different ways, such as different configurations of bubbles in the magma body; gas pockets heterogeneously distributed in the magma; an upper vesiculated layer; or simply small bubbles scattered uniformly in the magma. No direct links were found between the variation in the SO_2 flux and the gravity changes in 1997, but a possible positive correlation was observed on 13 March 1998. If the cause of the gravity variation is a fluctuation in density due to variation in the vesicularity of the magma, there is probably a direct or indirect link to the SO_2 flux.

Acknowledgments

The authors gratefully acknowledge the staff of INETER for their support, especially Martha Navarro, Wilfried Strauch, Alejandro Acosta and Oscar Péres. For their help on the field, we are grateful to Isabelle Lépine, Mike Burton and Lisa Boardman. Many thanks also to Scintrex Ltd and David Miller who loaned us the Scintrex instrument. Many thanks to Mark Davies for his help and his living room and to Luis Acosta for driving us in Nicaragua. The hospitality of the Gómez de Castillo Family at the Hotel Regis was greatly appreciated. Finally many thanks to the personnel of Masaya National Park for permission to work there and particularly to Señora Guttieres, director of the park.

References

Carr, M.J., 1984. Symmetrical and segmented variations of physical and geochemical characteristics of the Central American volcanic front. J. Volcanol. Geotherm. Res., 20: 231-252.

Johnson, N., and Parnell, R.A., 1986. Composition, distribution and neutralisation of "acid rain" derived from Masaya volcano, Nicaragua. Tellus, 38b, 106-117.

Lange, R. A., and Carmichael, I. S. E., 1990. Thermodynamic properties of silicate liquids with emphasis on density, thermal expansion and compressibility. In: Nicholls, J., and Russell, J. K., eds., Modern Methods of Igneous Petrology: Mineralogical Society of America Reviews in Mineralogy, 24: 44-54.

Lange, R. A., 1994. The effect of H_2O, CO_2 and F on the density and viscosity of silicate melts. In Carroll, M., and Holloway, J. R., eds., Volatiles in Magmas: Mineralogical Society of America Reviews in Mineralogy, 30: 331-369.

Metaxian, J.-P., 1994. Etude sismologique et gravimétrique d'un volcan actif: Dynamisme interne et structure de la Caldeira Masaya, Nicaragua. Unpublished Ph.D. Thesis, , Université de Savoie, Savoie, France, 319 pp.

Metaxian, J.-P., and Lesage, P., 1997. Permanent tremor of Masaya volcano, Nicaragua: Wave field analysis and source location. J. Geophys. Res., 102: 22 529-22 545.

Rymer, H., and Brown, G.C., 1987. Causes of microgravity changes at Poás volcano, Costa Rica: an active but non-eruptive system. Bull. Volcanol., 49: 389-398.

Rymer, H., 1989. A contribution to precision microgravity data analysis using Lacoste and Romberg gravity meters. Geophys. J., 97: 311-322.

Rymer, H., van Wyk de Vries, B., Stix, J., and Williams-Jones G., 1998. Pit crater structure and processes governing persistent activity at Masaya Volcano, Nicaragua. Bull. Volcanol., 59: 345-355.

Stoiber, R.E., Williams, S.N., and Huebert, B.J., 1986. Sulfur and halogen gases at Masaya caldera complex, Nicaragua: total flux and variations with time. J. Geophys. Res., 91: 12 215-12 231.

Vergniolle, S., 1996. Bubble size distribution in magma chambers and dynamics of basaltic eruptions. Earth Planet. Sci. Lett., 140: 269-279.

Viramonte, J.G., Navarro Collado, M., and Malavasi Rojas, E., 1997. Nicaragua-Costa Rica Quaternary Volcanic Chain. IAVCEI 1997 General Assembly, Puerto Vallarta, Mexico, guidebook for Field Trip 17, 59 pp.

Williams, S.N., 1983. Plinian airfall deposits of basaltic composition. Geology, 11: 211-214.

Bulletin of the Global Volcanism Network, 1994. Masaya Volcano,18: 7, 11.

CHAPTER III

Gravity changes induced by variations of the volatile content in magmas

Alexandre Beaulieu[1], John Stix[1],

Hazel Rymer[2]

[1]Département de Géologie
Université de Montréal
Montréal, Québec, H3C 3J7
Canada

[2]Department of Earth Sciences
Open University
Milton Keynes, MK7 6AA
United Kingdom

Abstract

Microgravity surveys have been carried out frequently on volcanoes and calderas to monitor signs of activity, re-activation and potential eruptions. This enables us to better define our concept of the subsurface of volcanoes and the processes occurring magmatic systems. As demonstrated in this study, volatile oversaturation, mainly as a free H_2O phase, is an important factor in triggering eruptions due to overpressure in large silicic magma chambers. It is also possible to monitor an increase in the dissolved volatile content. CO_2 concentrations in magma at the depths modelled in this study (2-8 km) are not sufficiently large to produce significant gravity changes under saturated or undersaturated conditions. Modelling shows that even at depths of 3800 m, it is possible to observe overpressure due to exsolution of gas bubbles induced by crystallisation. These overpressures could produce gravity variations at the surface on the order of 50-100 μGal for a 10 km^3 magma chamber. This is a long process which may take hundreds of years; it is thus difficult to see year-to-year changes for very deep systems. Yet this may prove useful for a long-term survey. For a shallower magma body, the density changes caused by gas exsolution are easier to observe with gravity. The density decrease, they could be as high as 40 kg m^{-3} for an increase of 0.3 wt % H_2O under saturated conditions; such a decrease in density in a 1 km^3 magma body 1900 m deep would produce a gravity change of 50 μGal. In conjunction with other means of monitoring, microgravity can be used to understand subsurface processes in volcanic systems.

Introduction

The importance of volatiles for causing overpressure in a magma chamber and volcanic eruptions is well known. Volatiles such as carbon dioxide, water, and sulfur dioxide can accumulate in a magma chamber under certain conditions. First, a certain amount of H_2O or CO_2 is needed in the magma to produce a free gas phase. Under high-pressure conditions, the magma can accumulate volatile components which remain dissolved in the melt. At some point, however, the magma reaches a solubility limit and becomes saturated in volatiles. After this point, when the solubility of volatiles in the magma has been exceeded, there is free-vapor production and small bubbles forms in the magma. Many factors are involved in the amount of gas that can be exsolved; the solubility of H_2O and CO_2 depends on pressure, temperature, composition of the magma and the presence of other volatiles.

Several processes in a magma chamber can affect the production or the quantity of volatiles. Crystallisation may occur, which would cause the volatile content to increase. There also could be an injection of new magma which is richer in volatiles. Convection could occur to bring magma richer in gas to shallow levels. A trap is also needed for these volatiles to be retained in the magma chamber. In other words, the system needs to be closed; if not, the bubbles in the magma will escape. If the magma chamber is closed, these bubbles can accumulate at the top of the magma chamber or they can be distributed throughout the chamber. This would inevitably cause the magma density to be lowered by a certain amount. If this density variation is large enough, it could eventually lead to an observable gravity variation at the surface. If the system is open, there can still be density variations due to changes in the bubble content in the magma. In shallow environments, such as beneath Masaya volcano, Nicaragua, convection may transport gas-rich magma to shallow levels where it will degas; this process could be repetitive and produce variations in gravity (Rymer et al., 1998; Beaulieu et al., 1998). Any volcanic system where there is a large gas emission could potentially be monitored for gravity variations. Fluctuation in the gas emission is linked to variations in the amount of gas bubbles in the magma, so this could possibly create observable density variations. In a volatile-undersaturated magma, variation in the dissolved volatile content also could lead to a density variation that could be observed by gravity methods. This is a useful tool for a volcanologist to help forecast volcanic eruptions linked to gas accumulations and overpressure in a volcano or lava dome.

The main objective of this study was to show, using a theoretical model, that density changes produced by volatiles in magma are possible to observe at the surface with gravity methods. Calculations of the density of magma were made using different volatile content (H_2O, CO_2, or both) at different depths, e.i., different pressures. Examples demonstrating that gravity changes can be observed at the surface are then modeled using plausible density changes within magma bodiesof various dimensions.

Methodology

Magma chamber shape:

In order to define models that are simple and representative of a magmatic chamber and system, spherical, cubic and cylindrical magma chambers and conduits

FIGURE 3.1

Gravity effect of a sphere, the horizontal axis x/z is the horizontal distance from the center of the sphere, x, and z the depth of the center; the vertical axis is the gravity of a point at a certain horizontal distance from the center of the sphere versus maximum gravity (From Telford et al., 1990).

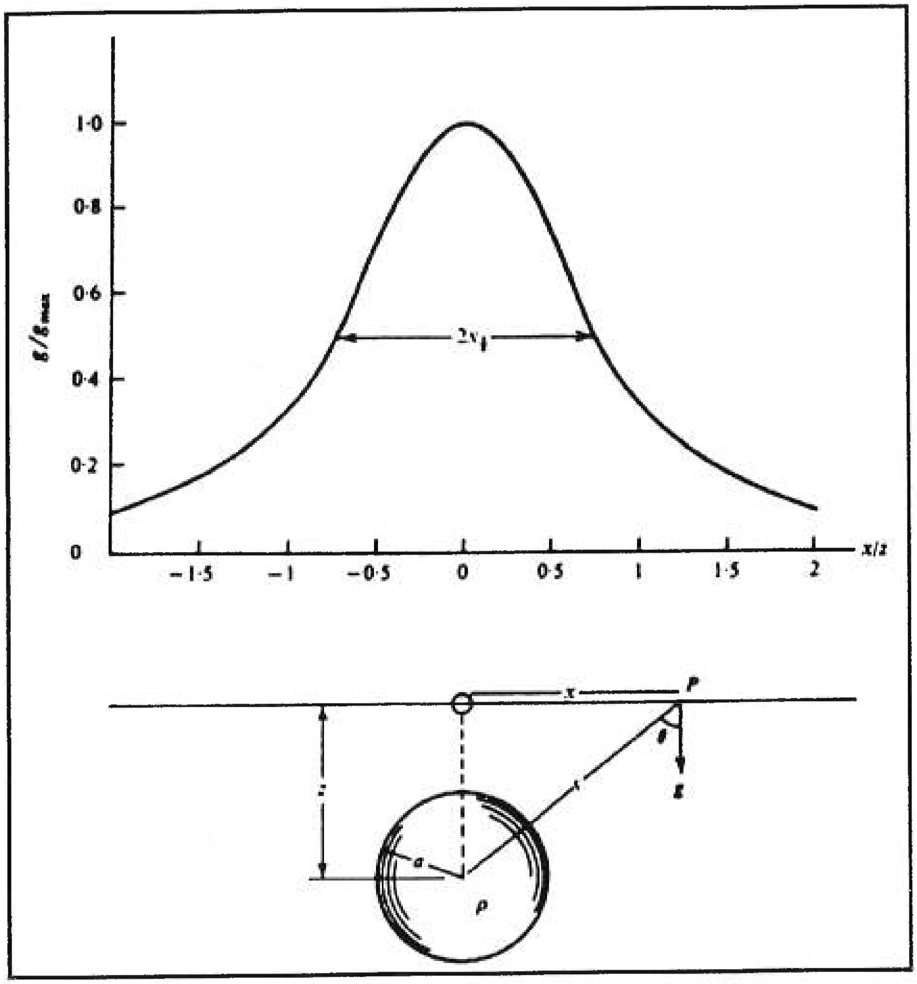

1·0
0·8
0·6
0·4
0·2
0
g/g_{max}
$2x_{\frac{1}{2}}$
−1·5
−1
−0·5
0
0·5
1
1·5
2
x/z
x
P
θ
g
z
r
a
ρ

will be used to model the gravity variation from density fluctuations caused by changes in the dissolved and exsolved volatile content. Different sizes and emplacement depths will also be used. For the spherical model, the magma chamber sizes are 0.1 km^3, 1 km^3 and 10 km^3 at three different depths of 1900 m, 3800 m and 7600 m, each depth representing 50, 100 and 200 MPa, respectively, calculated from:

$$P(z) = \rho g z \tag{1}$$

where P(z) is the lithostatic pressure, z the depth, g the acceleration due to gravity (9.81 m $s^{-2)}$ and ρ the density of the country rocks (2700 kg m^{-3}). In the spherical model, the bubbles in the magma chamber are assumed to be uniformly distributed in a closed system. The gravity effect in this model is calculated from:

$$g_z = 2.79 \times 10^{-2} \Delta\rho z\, r^3/(x^2 + z^2)^{3/2} \tag{2}$$

where g_z is the gravity in mGal, $\Delta\rho$ is the density contrast between the magma chamber and the surrounding rocks, z the depth at the center of the sphere, x the horizontal distance from the center of the sphere, and r the radius of the sphere (Fig. 1) (Telford et al., 1990). The cubic magma chamber is used to define a model where the bubbles are not distributed uniformly in the magma chamber but instead are clustered in a thin foam layer at the top of the chamber or as layers of different thickness in the lower or the middle part of the magma chamber. For the calculation of the gravity effect, GRAVMAG is used; this is a 2.5-dimensional gravity modelling program (Pedley et al., 1993). Finally, to represent variations at smaller scales and closer to the surface, a vertical cylinder will be used to model a magmatic conduit. The maximum gravity effect of a cylinder is calculated as follows:

$$G_{max} = 4.19 \times 10^{-2} \Delta\rho\, [\, L + (z^2 + R^2)^{1/2} - \{(z + L)^2 + R^2\}^{1/2}] \tag{2}$$

where G_{max} is the maximum gravity in mGal, $\Delta\rho$ the density contrast between the magma chamber and the surrounding rocks, z the depth at the top of the cylinder, L the length of the cylinder and R the radius of the cylinder.

Density Variation of Magmas

Volatile Content and Solubility

In order to reach overpressure in a magma chamber or in a volcanic complex, a certain amount of H_2O and/or CO_2 needs to be initially present in the magma. Depending on the solubilities of these components, they will be in the form of free gas or volatiles dissolved in the structure of the magma itself. In the quenched glass inclusions of explosive silicic and andesitic explosions, high water concentrations (4-6 wt%) are commonly found (Stix and Layne, 1996). Infrared spectroscopic measurements of glass inclusions within quartz phenocrysts from a plinian fallout of the Pine Grove, southwestern Utah, USA, show very high concentration of H_2O (6-8 %) (Lowenstern, 1994). For more mafic magma, there is less dissolved water in general. At Kilauea, the parental melt contains approximately 0.30 wt% H_2O and 0.65 wt% CO_2 (Gerlach, 1986). However, high water concentrations are sometimes observed in arc-related basaltic and basaltic andesite magmas; glass inclusions from the 1974 Fuego eruption in Guatemala had values up to 6 wt % H_2O (Harris and Anderson, 1984). Basaltic andesite glass inclusions from Goosenest Volcano, Oregon, contain up to 3.3 wt % H_2O (Sisson and Layne, 1993). At Mt Pinatubo, the initial dacitic melt had concentration of dissolved CO_2 up to 0.4 wt% (Wallace and Gerlach, 1994).

The parameter that will determine the fraction of a volatile component as a free gas phase is the solubility of that component in the magma. For rhyolitic melt, the calculation of the solubility of water is assumed to be proportional to the square root of pressure (Stolper, 1992), with a solubility constant of:

$$S_{H_2O} = 4.186 \times 10^{-6}\, P^{0.5} \tag{4}$$

where P is the pressure in Pascals. For basaltic magma, the solubility law for CO_2 and H_2O used in the modelling is (Stolper and Holloway, 1988):

$$S_{CO_2} = 4.4 \times 10^{-12}\, P^{1.0} \tag{5}$$

and

$$S_{H_2O} = 6.8 \times 10^{-8}\, P^{0.7} \tag{6}$$

Density Calculation of a Crystal- and Volatiles-Bearing Magma

The density of a volatile-bearing magma, ρ, may be defined in terms of the partial volumes occupied by the exsolved volatiles of density ρ_g, the magmatic liquid of density ρ_m, and the crystals of density ρ_c (Bowers and Woods, 1997). If the mass fraction of volatiles in the mixture is n and the mass fraction of crystals is x, then

$$\frac{1}{\rho} = \frac{n}{\rho_g} + \frac{1-n}{\rho_l} \tag{7}$$

$$\rho_l = (1 - x)\,\rho_m + x\rho_c \tag{8}$$

where ρ_l is the density of a cristal-bearing magma and ρ_g is the density of the gas phase assuming that the exsolved volatiles obey the ideal gas law (Tait et al., 1989):

$$\rho_g = \frac{P}{RT} \tag{9}$$

where R is the universal gas constant divided by the molar mass of water or carbon dioxide (R = 461.5 J kg^{-1} K^{-1} for H_2O and 189.0 J kg^{-1} K^{-1} for CO_2) and T is the temperature in Kelvin (1173 K for rhyolite and 1473 for basalt). The density of the magmatic liquids (ρ_m) is calculated with the method of Bottinga et al. (1982). For rhyolitic and basaltic melts at different pressures and H_2O undersaturated conditions, compositions used are from Shaw (1963) (sample DC-1), and from Lange and Carmichael (1990) (Kilauea Tholeiite). Density calculated for the anhydrous magmas with no effect of the pressure is 2333 kg m^{-3} for the rhyolite and 2650 kg m^{-3} for the basalt.

At equilibrium the mass fraction of dissolved volatiles in the melt n_s at pressure P is given by Henry's Law. It is calculated by

$$n_s = S(P) \tag{10}$$

where S is the solubility constant and P the pressure in Pa. If the total initial mass fraction of volatiles in the magma is n_0 and assuming the crystals to be anhydrous (Huppert et al., 1982), the exsolved mass fraction of volatiles n(P) is:

$$n(P) = n_0 - SP^n\,((1\text{-}x)\,\rho_m\,\rho_l) \tag{11}$$

For the compressibility of magma, it is assumed that the volume V of a given mass of liquid magma and crystals changes with pressure P according to the following relation (Blake, 1981; Druitt and Sparks, 1984):

$$\frac{dV}{dP} = -\frac{V}{\beta} \tag{12}$$

where β is the elastic bulk modulus of the liquid mixture. Typical values of β for silicate liquids range from 10 000-40 000 MPa (Tait et al., 1989). The value used in

FIGURE 3.2

Density changes with variation in the water content at different pressures for (a) rhyolitic magma and (b) basaltic magma.

A **Rhyolite**

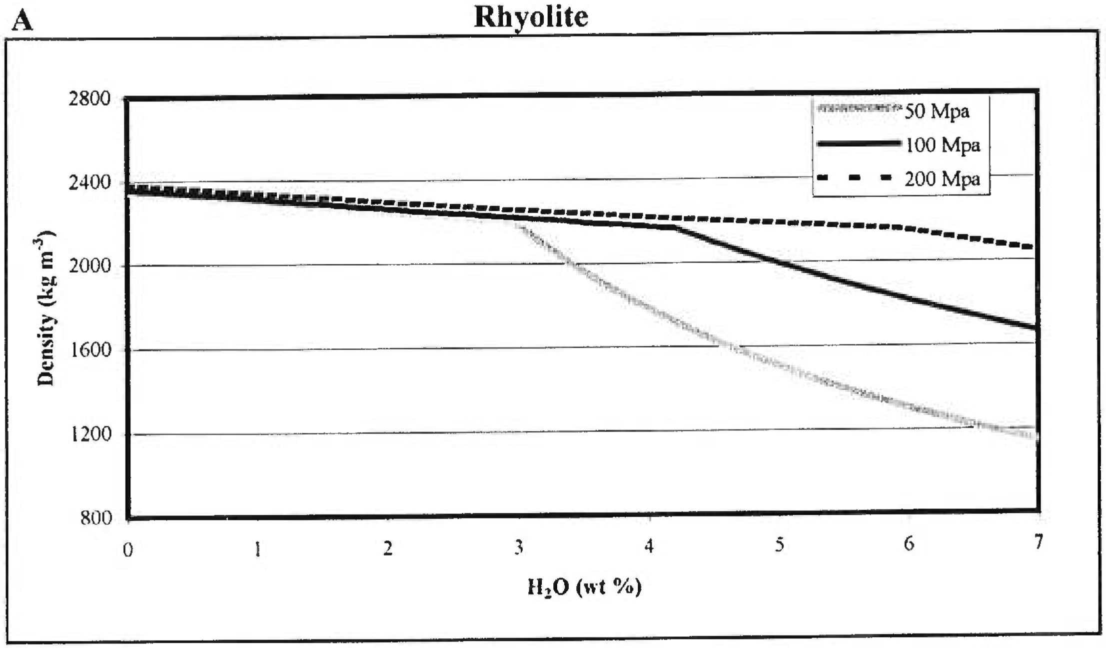

B **Basalt**

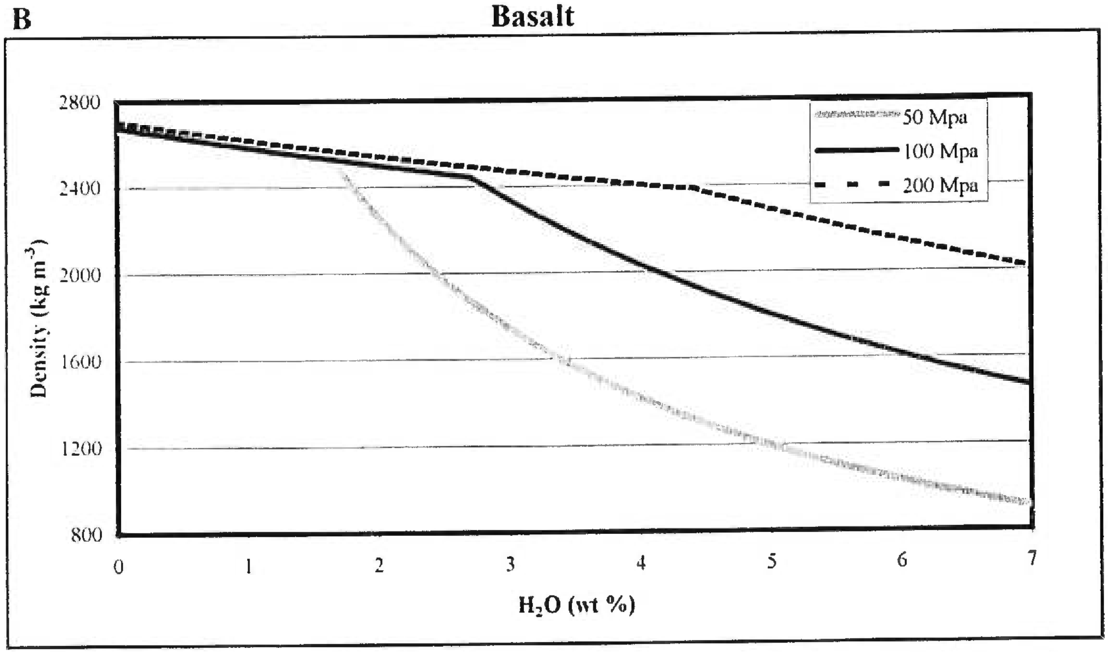

this calculation is 10 000 MPa. Integration of (12) gives an expression for the melt-crystal density ρ_l as a function of pressure:

$$\rho_l(\mathrm{P}) = \rho_{l_0} \exp\left(\frac{\mathrm{P}-\mathrm{P_a}}{\beta}\right) \tag{13}$$

where $\rho_{l0} = \rho_l(\mathrm{P_a})$ is the density of the mixture of melt and crystals at atmospheric pressure $\mathrm{P_a} = 0.1$ MPa (Bowers and Woods, 1997). The density of a magma-volatiles mixture varying with pressure P can be obtained by combining (7) and (13):

$$\frac{1}{\rho} = \frac{n(\mathrm{P})RT}{\mathrm{P}} + \frac{(1-n(\mathrm{P}))}{\rho_{l_0}} \exp\left(-\frac{\mathrm{P}-\mathrm{P}_a}{\beta}\right) \tag{14}$$

Density Modelling of Magma with a Pure H_2O Dissolved-Gas Fraction

In the examples below, modelling was done with a pure H_2O phase varying from 0-7 wt % in a closed system at constant temperature (1173 K for rhyolite and 1473 K for the basalt) for rhyolitic and basaltic magmas. For simplicity, the pressure is assumed to remain constant everywhere in the magma chamber. Figure 2a and 2b shows the density changes for rhyolitic and basaltic magmas with variations in the water content at different pressures (50, 100 and 200 MPa). For both the rhyolite and the basalt, once the exsolution of volatiles begin, the density is lowered drastically at lower pressure (50 MPa and 100 MPa). At 200 MPa, the effect of volatile exsolution is nearly insignificant for rhyolite and low for basalt. In the basaltic magma, the density begins to decrease at lower water content than the rhyolite, indicating that the solubility of water in basalt is lower than in rhyolite. Density is also decreasing faster in the basalt probably because of the greater density contrast between basaltic melt and the H_2O gas phase. For the crystal fraction in the magma (Fig. 3a and 3b), density changes with water content are shown for three different crystal contents. As

FIGURE 3.3

Density changes with variation in the water content at different crystal fractions at 100 MPa for (a) rhyolitic magma and (b) basaltic magma. Density changes with variation in the crystal content at 100 MPa and 4 wt % H_2O for (c) rhyolitic magma and (d) basaltic magma.

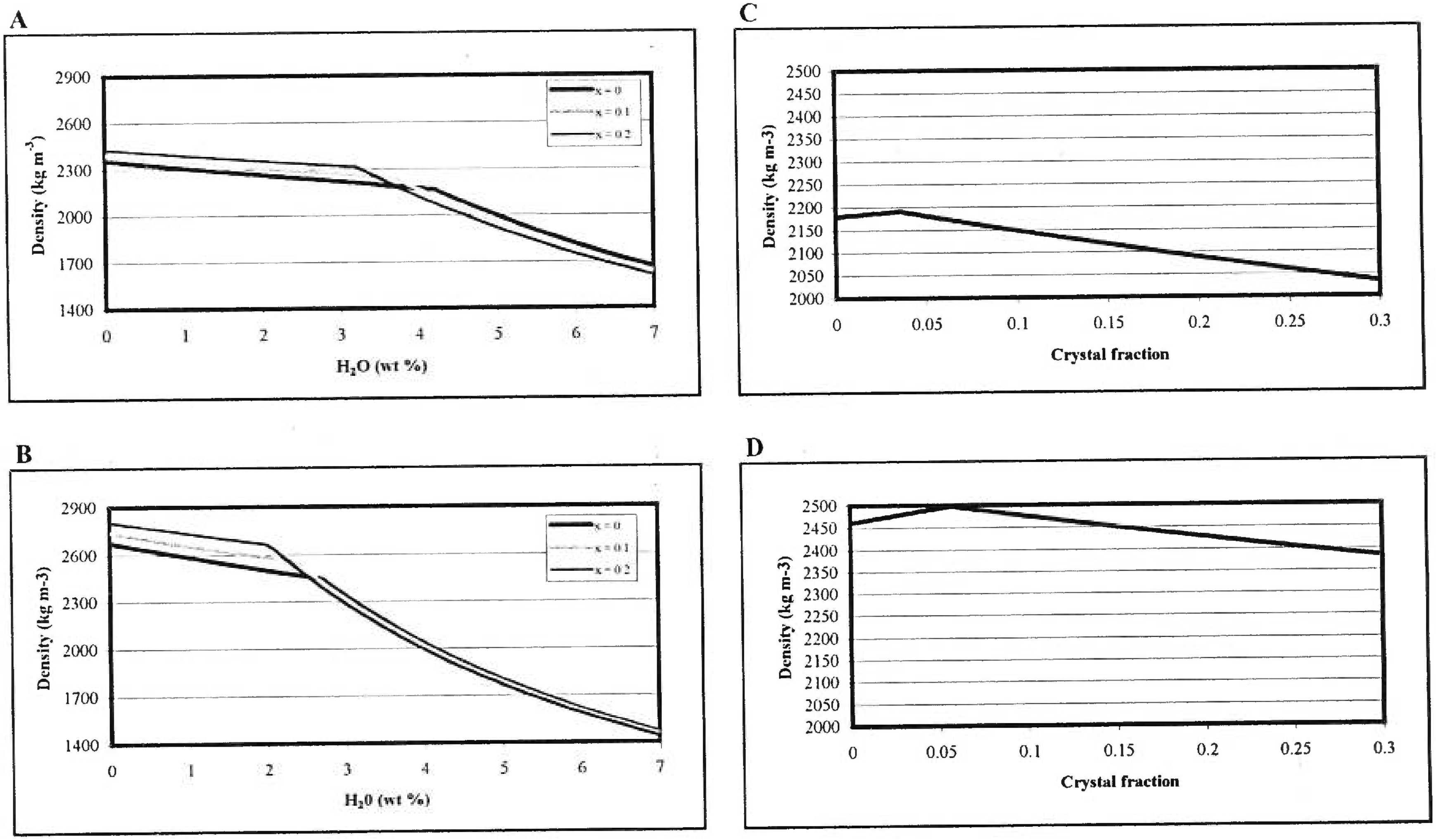
A
2900
2600
2300
2000
1700
1400
Density (kg m-3)
0
1
2
3
4
5
6
7
H2O (wt %)
x = 0
x = 0.1
x = 0.2
B
2900
2600
2300
2000
1700
1400
Density (kg m-3)
0
1
2
3
4
5
6
7
H20 (wt %)
x = 0
x = 0.1
x = 0.2
C
2500
2450
2400
2350
2300
2250
2200
2150
2100
2050
2000
Density (kg m-3)
0
0.05
0.1
0.15
0.2
0.25
0.3
Crystal fraction
D
2500
2450
2400
2350
2300
2250
2200
2150
2100
2050
2000
Density (kg m-3)
0
0.05
0.1
0.15
0.2
0.25
0.3
Crystal fraction

the crystal fraction is increased under volatile-saturated conditions, the density decreases as the crystal fraction is increased. The magnitude of density decrease for the rhyolite (47 kg m^{-3}) is nearly twice that for the basalt (24 kg m^{-3}) when the crystal fraction increases from 0 to 10 %. The relation between density and crystal fraction is demonstrated differently in Figure 3c and 3d, where the density varies with the crystal fraction at a pressure of 100 MPa and initial water contents of 2.5 wt % and 4 wt % for basalt and rhyolite, respectively. As the crystal fraction increases, the residual melt becomes more enriched in volatiles, and a larger mass of these volatiles are exsolved as vapor for a given pressure. First, the density increases and then decreases as exsolution of volatiles begins. As cited above, the density decrease is larger for the basalt because of the larger density contrast between basaltic melt and the H_2O gas phase. The crystal densities used in the modelling are 2700 kg m^{-3} (plagioclase) in the rhyolite and 3300 kg m^{-3} (olivine) for the basalt.

Density Modelling of Basaltic Magma with a Pure CO_2 Dissolved-Gas Fraction

In the following examples, the effect of CO_2 gas exsolution on the density of a basaltic magma is shown; calculation of density for CO_2 undersaturated magma is not included in modelling. Because of the very low solubility of CO_2 in the magma (Holloway and Blank, 1994; Dixon and Stolper, 1995; Papale, 1997), the onset of exsolution of magma starts at a very low CO_2 content compared to H_2O, even at high pressure (Fig. 3.4a). The density change is of much lower amplitude than for H_2O because of the low CO_2 content in the magma. Similar to H_2O, however, the density decrease is proportionately larger at low CO_2 contents and low pressures (Fig. 3.4a). For density variations with crystal content, the density increases instead of decreasing (Fig. 3.4b and 3.4c). In this example, the density of the crystals used is 3300 kg m^{-3}

FIGURE 3.4

(a) Density changes of a basaltic magma at the onset of gas exsolution with variation in the CO_2 content at different pressures. (b) Density variation of a basaltic magma with variation in the CO_2 content with different crystal fractions at 100 MPa. (c) Density variation of a basaltic magma with variation in the crystal content at 100 MPa and at different CO_2 contents.

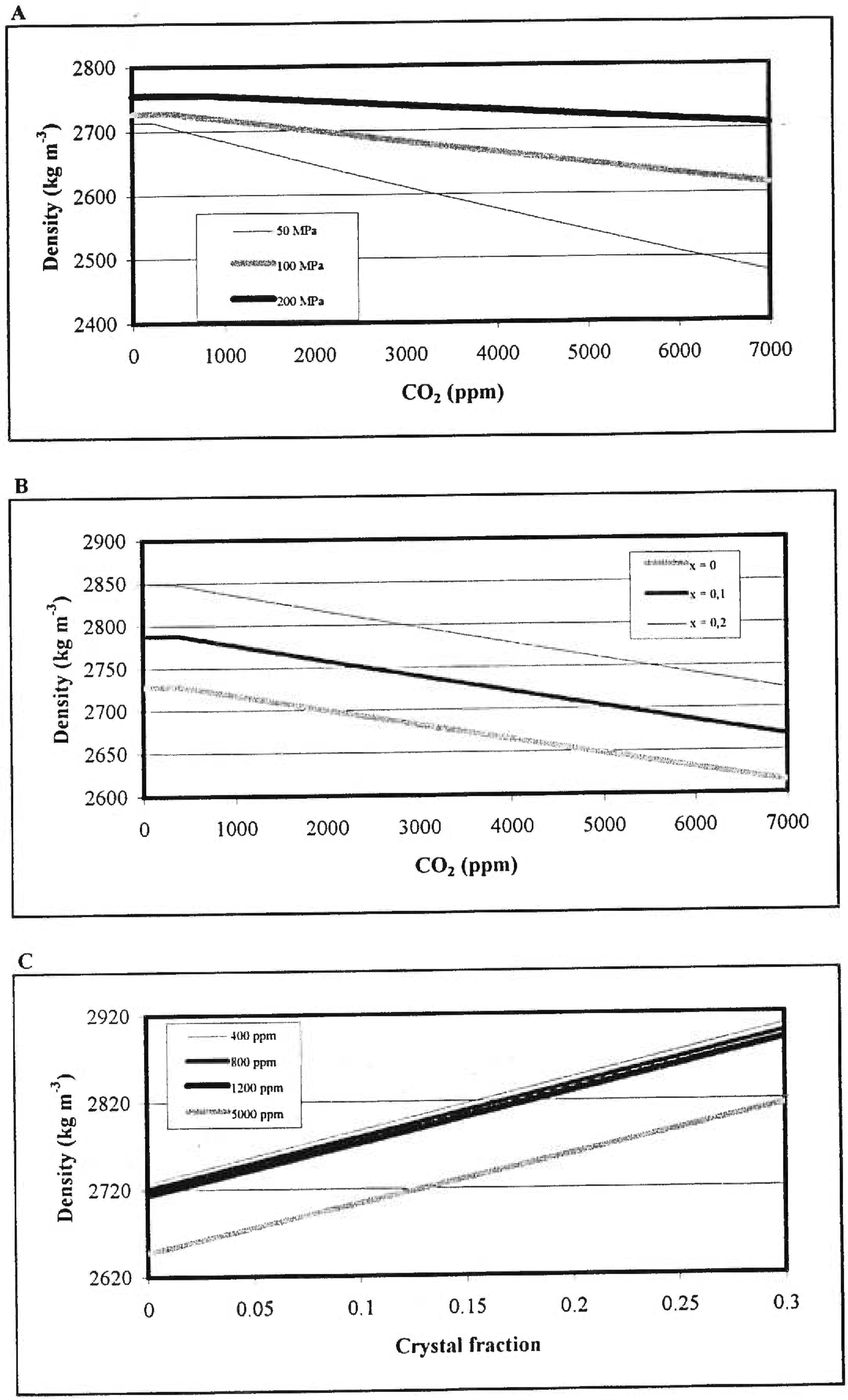
A
2800
2700
2600
2500
2400
Density (kg m-3)
50 MPa
100 MPa
200 MPa
0
1000
2000
3000
4000
5000
6000
7000
CO2 (ppm)
B
2900
2850
2800
2750
2700
2650
2600
Density (kg m-3)
x = 0
x = 0,1
x = 0,2
0
1000
2000
3000
4000
5000
6000
7000
CO2 (ppm)
C
2920
2820
2720
2620
Density (kg m-3)
400 ppm
800 ppm
1200 ppm
5000 ppm
0
0.05
0.1
0.15
0.2
0.25
0.3
Crystal fraction

(olivine); the effect of the increasing crystal fraction is larger than the effect of CO_2 bubbles on the density of the magma.

Density Modelling of Magmas with a Mixed CO_2-H_2O Dissolved-Gas Fraction

The effect of combined volatiles on their solubility is well demonstrated by Dixon and Stolper (1995). They show that for different ratios of CO_2:H_2O, the solubilities of CO_2 and H_2O decrease correspondingly. For a melt containing 1.0 wt % H_2O and 46 ppm CO_2, the saturation pressure is 20 MPa with a vapor phase having a water fraction of 0.5 (Fig 3.5a). If there was only H_2O present at this pressure, the amount necessary to saturate the melt would be 1.4 wt %. Similarly, for a melt with CO_2 as the only volatile, the amount for saturation at this pressure would be 95 ppm. This effect is very important since natural magmas often contain multiple volatile species. The density of a basaltic magma in a closed system with 2.5 wt % H_2O and no CO_2 at 1473 K and 50 MPa is about 2315 kg m^{-3}, and the solubility of water at this pressure is about 2.24 wt % (Fig. 3.5a). For the same magma, if 100 ppm CO_2 is added, the solubility of water is lowered to 1.9 wt %. Since the lowered H_2O solubility means that more water is exsolved, the density decreases a further 220 kg m^{-3}; the density for this magma is thus decreased to 2095 kg m^{-3}. The same kind of relation is demonstrated in Figure 3.5b for a rhyolite at 1173 K. Thus, the effect of CO_2 on the solubility of H_2O and on the density of magma is considerable.

Density Changes as a Function of Volatile Content for Unsaturated Magma

Variation in the volatile content of an unsaturated magma also causes the magma density to change. A good example is shown by Kazahaya et al. (1994). They demonstrated the density changes of basalt for ascending non-degassed magma and descending degassed magma as a function of depth (Fig. 3.6). The effect of the

FIGURE 3.5

Solubility of H_20 + CO_2 as a function of pressure and fluid composition for (a) tholeiitic basalt at 1200 °C and (b) rhyolite at 850 °C (From Holloway and Blank, 1994).

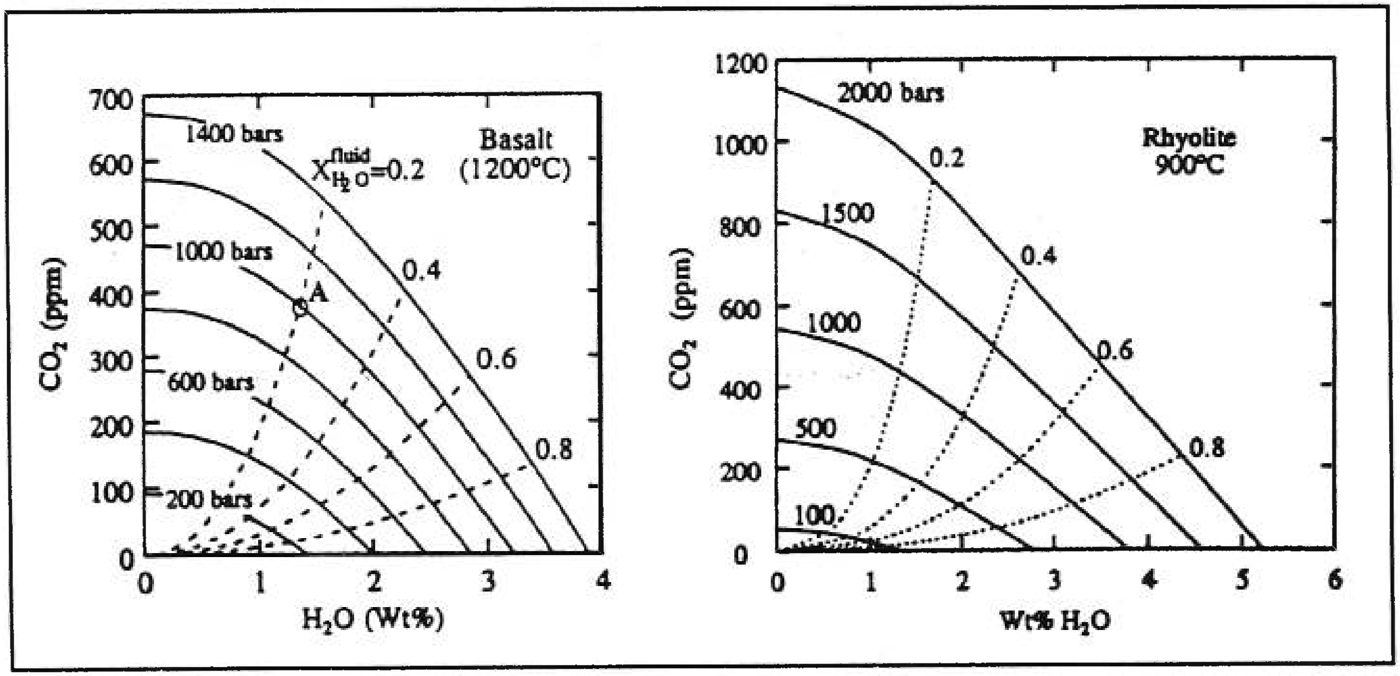

CO2 (ppm)
700
600
500
400
300
200
100
0
1400 bars
1000 bars
600 bars
200 bars
X fluid H2O=0.2
0.4
0.6
0.8
A
Basalt
(1200°C)
0
1
2
3
4
H2O (Wt%)
CO2 (ppm)
1200
1000
800
600
400
200
0
2000 bars
1500
1000
500
100
0.2
0.4
0.6
0.8
Rhyolite
900°C
0
1
2
3
4
5
6
Wt% H2O

FIGURE 3.6

Density changes of ascending non-degassed magma and descending degassed magma as function of depth. Arrows schematically show a path for convective transport of magma caused by density changes. Numbers show water content in wt. % (From Kazahaya et al., 1994).

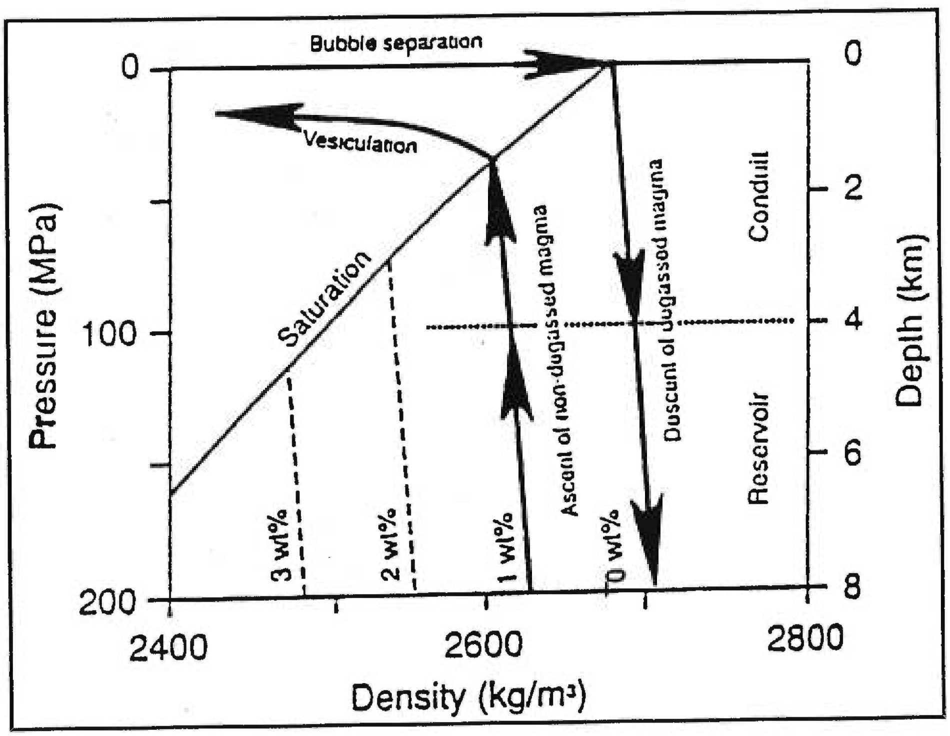

Bubble separation
Vesiculation
Saturation
Ascent of non-degassed magma
Descent of degassed magma
Conduit
Reservoir
3 wt%
2 wt%
1 wt%
0 wt%
0
100
200
2400
2600
2800
0
2
4
6
8
Pressure (MPa)
Depth (km)
Density (kg/m³)

dissolved volatiles, mainly H_2O at low pressure is to lower the melt density as modelled in Figure 3.2a and 3.2b. In both models (Kazahaya et al., 1994 and this work), the effect of pressure variation on H_2O undersaturated magma is not very important. For a variation of 150 MPa (from 200 MPa to 50 MPa), the corresponding density decreases of a volatile-undersaturated basaltic melt is 50 kg m^{-3} according to Kazahaya et al. (1994) and 60 kg m^{-3} for the present modelling.

The effect of CO_2 is not considered since the amount of CO_2 dissolved in the melt at the pressures used in this model (50 MPa, 100 MPa and 200 MPa) is less than 900 ppm (corresponding to 0.09 wt %). Moreover, Lange (1994) demonstrated that for an amount of 3 wt % CO_2 in an alkali olivine basalt, the density decrease by 3.3 %, and that for the same amount of H_2O, the corresponding density decrease is 4.8 %. The effect of CO_2 on the density is thus lower than that of H_2O; this is due to the difference in the molar volume between H_2O and CO_2. Thus, only the effect of H_2O on the melt density is considered in the modelling.

Modelling of Gravity as a Function of Density Variation

Spherical Model

Modelling here represents the changing density of magma on gravity observed at the surface for different sizes and depths of magma chambers of spherical shape. The density variations used for the modelling range from 0-100 kg m^{-3} and represent possible density changes in a magma body due to various mechanisms such as crystallisation producing increases in the volatile content or convection in the magma chamber bringing deep, gas-rich magma to lower lithostatic pressures where exsolutions begins, thereby decreasing the density of the magma.

In the following models, the residual gravity changes from density variation of 0-100 kg m^{-3} in a spherical magma chamber are presented as 20 000 m-wide horizontal profiles. The maximum gravity changes are produced above the center of the sphere, and they decrease rapidly as the horizontal distance increases. This effect is stronger for shallower magma bodies. The gravity effect of a 0.1 km^3 sphere at 1900 m, 3800 m and 7600 m is shown in Figure 3.7. For the magma body at a depth of 1900 m, a large density variation is required (> 100 kg m^{-3}) to observe a gravity variation at the surface. A density change of 100 kg m^{-3} produces a maximum gravity change of 18 μGal (Fig. 3.7a). At depths of 3800 m and 7600 m, very large density variations would be needed to produce observable gravity changes (Fig. 3.7b, c). For example, a density variation of 100 kg/m^3 at a depth of 3800 m produces a gravity change of the same amplitude as that produced at 1900 m for a 25 kg m^{-3} density variation (4.6 μGal). At 7600 m depth, there is no significant gravity variations observed for a density change of 100 kg m^{-3} (1.1 μGal); at this depth, even large density variations up to 500 kg m^{-3} are insufficient to obtain an observable gravity change at the surface (> 20-30 μGal). For larger magma bodies, the gravity effect is accentuated. Thus, the maximum gravity effect for a 1 km^3 chamber at a depth of 1900 m is of the order of 45 μGal for a density change of 25 kg m^{-3} (Fig. 3.8a). The density variation needed to obtain an observable gravity variation is less for a large magma body than for a smaller body; this is true only if the density variation occurs throughout the magma body. For a deeper magma body of the same size (1 km^3), a

FIGURE 3.7

Gravity effect of density variation of a 0.1 km^3 spherical magma chamber at depths of (a) 1900 m, (b) 3800 m and (c) 7600 m.

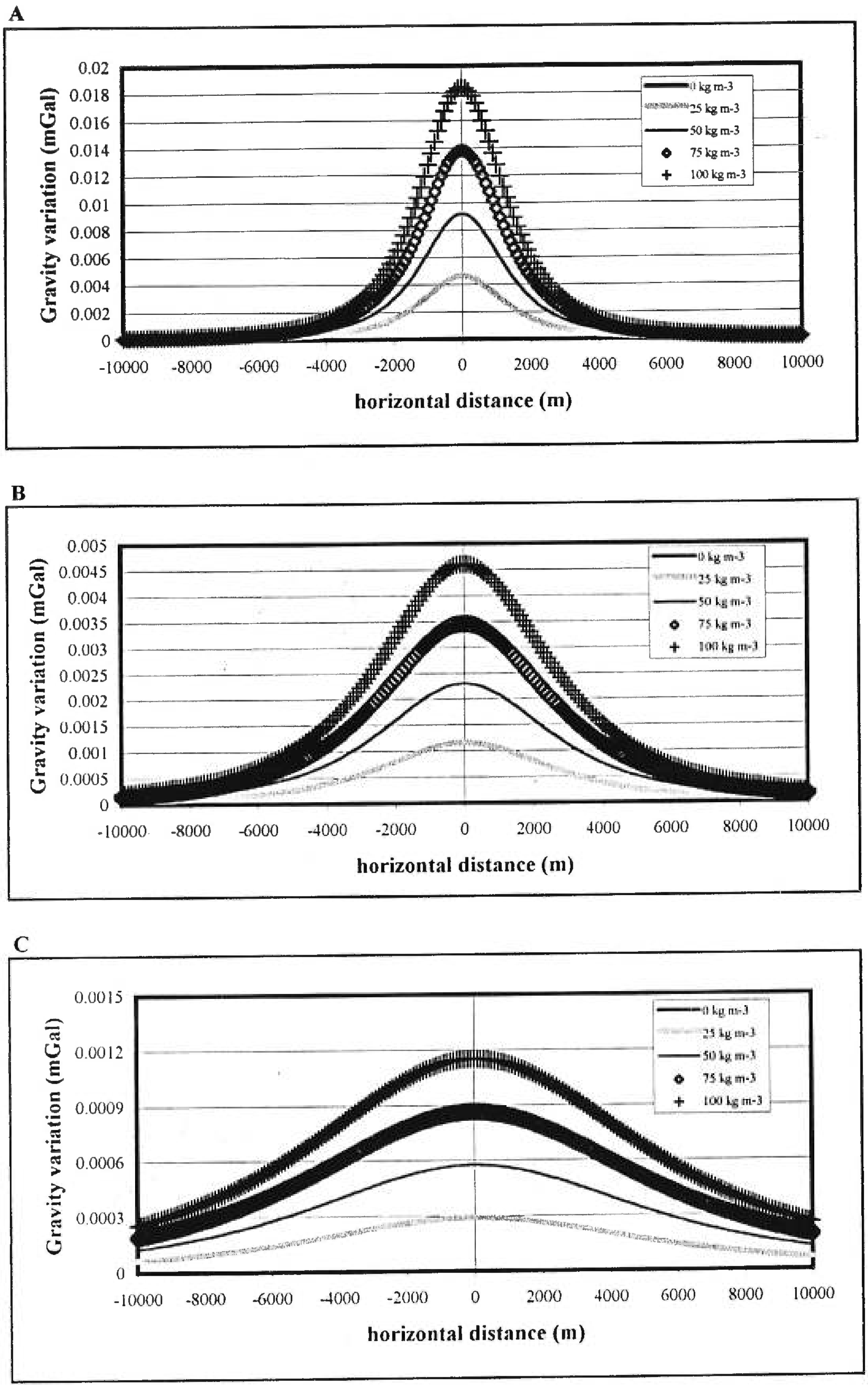
A
Gravity variation (mGal)
0.02
0.018
0.016
0.014
0.012
0.01
0.008
0.006
0.004
0.002
0
-10000
-8000
-6000
-4000
-2000
0
2000
4000
6000
8000
10000
horizontal distance (m)
0 kg m-3
25 kg m-3
50 kg m-3
75 kg m-3
100 kg m-3
B
Gravity variation (mGal)
0.005
0.0045
0.004
0.0035
0.003
0.0025
0.002
0.0015
0.001
0.0005
0
-10000
-8000
-6000
-4000
-2000
0
2000
4000
6000
8000
10000
horizontal distance (m)
0 kg m-3
25 kg m-3
50 kg m-3
75 kg m-3
100 kg m-3
C
Gravity variation (mGal)
0.0015
0.0012
0.0009
0.0006
0.0003
0
-10000
-8000
-6000
-4000
-2000
0
2000
4000
6000
8000
10000
horizontal distance (m)
0 kg m-3
25 kg m-3
50 kg m-3
75 kg m-3
100 kg m-3

Figure 3.8

FIGURE 3.8

Gravity effect of density variation of a 1 km^3 spherical magma chamber at depths of (a) 1900 m, (b) 3800 m and (c) 7600 m.

A

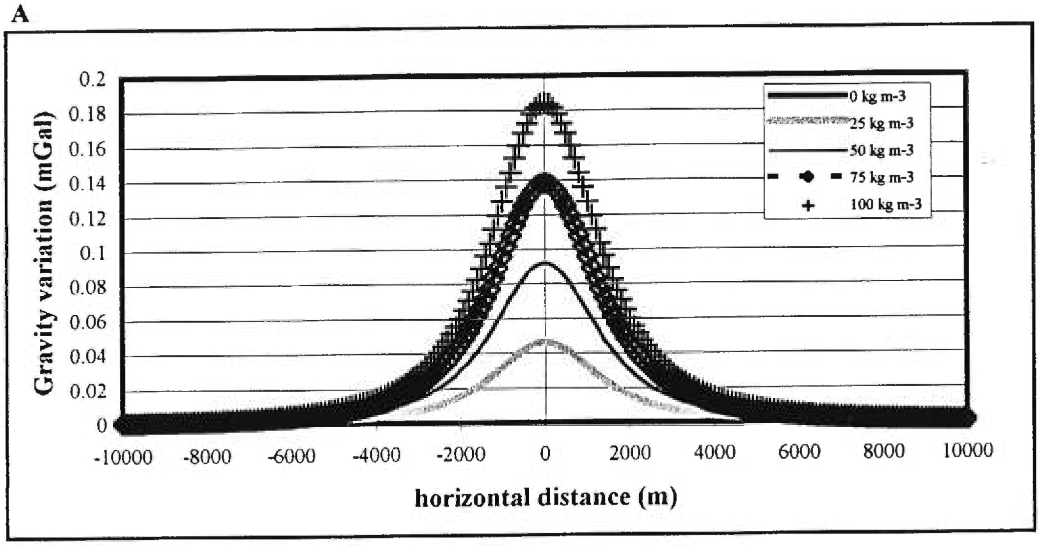
0.2
0.18
0.16
0.14
0.12
0.1
0.08
0.06
0.04
0.02
0
Gravity variation (mGal)
-10000
-8000
-6000
-4000
-2000
0
2000
4000
6000
8000
10000
horizontal distance (m)
0 kg m-3
25 kg m-3
50 kg m-3
75 kg m-3
100 kg m-3

B

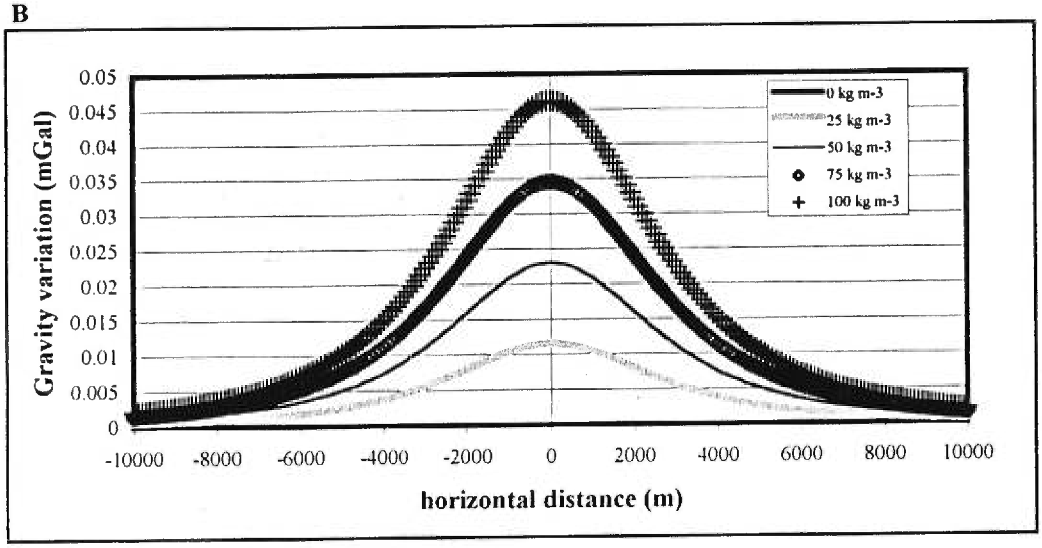
0.05
0.045
0.04
0.035
0.03
0.025
0.02
0.015
0.01
0.005
0
Gravity variation (mGal)
-10000
-8000
-6000
-4000
-2000
0
2000
4000
6000
8000
10000
horizontal distance (m)
0 kg m-3
25 kg m-3
50 kg m-3
75 kg m-3
100 kg m-3

C

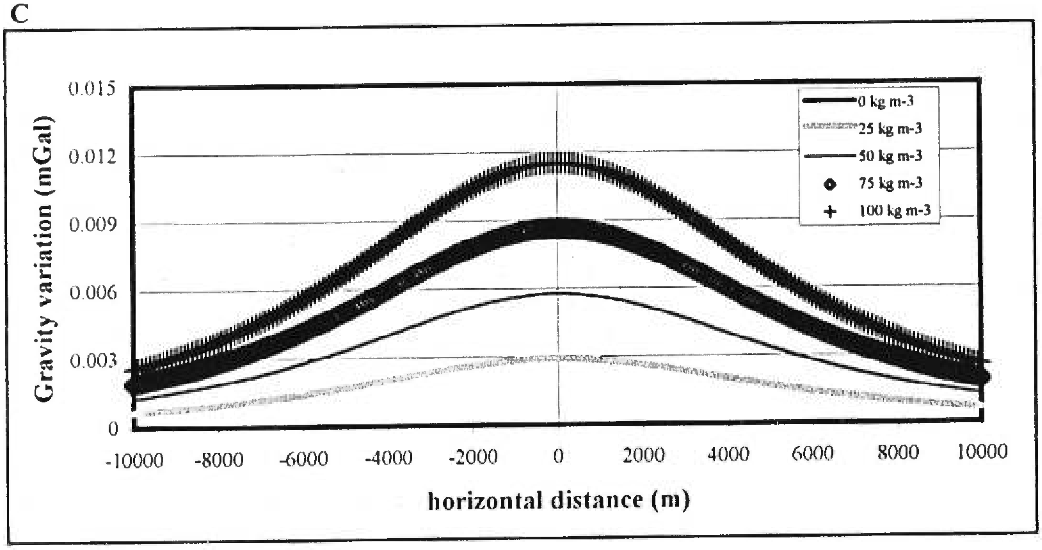
0.015
0.012
0.009
0.006
0.003
0
Gravity variation (mGal)
-10000
-8000
-6000
-4000
-2000
0
2000
4000
6000
8000
10000
horizontal distance (m)
0 kg m-3
25 kg m-3
50 kg m-3
75 kg m-3
100 kg m-3

FIGURE 3.9

Gravity effect of density variation of a 10 km^3 spherical magma chamber at depths of (a) 1900 m, (b) 3800 m and (c) 7600 m.

A

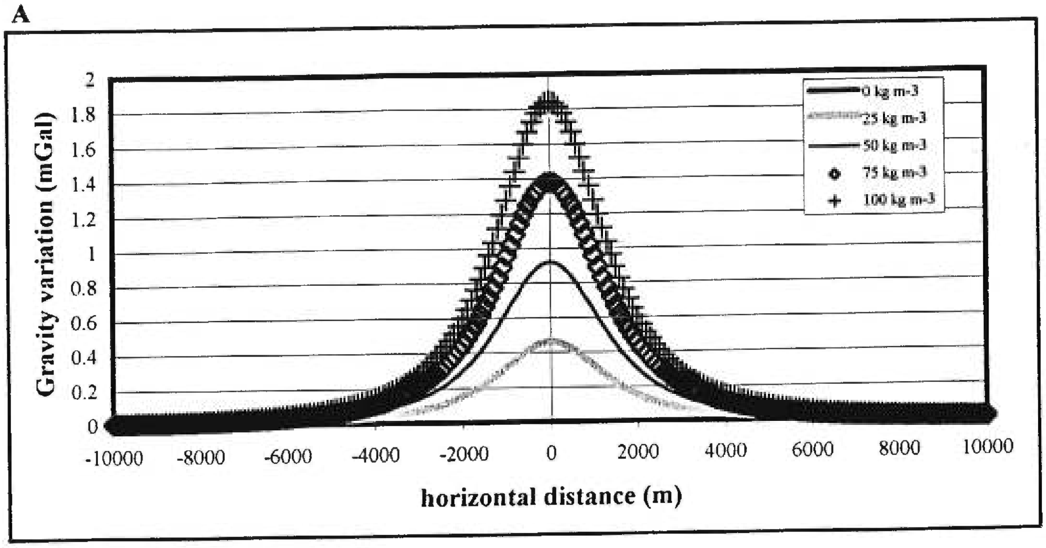
Gravity variation (mGal)
horizontal distance (m)
0 kg m-3
25 kg m-3
50 kg m-3
75 kg m-3
100 kg m-3
0
0.2
0.4
0.6
0.8
1
1.2
1.4
1.6
1.8
2
-10000
-8000
-6000
-4000
-2000
0
2000
4000
6000
8000
10000

B

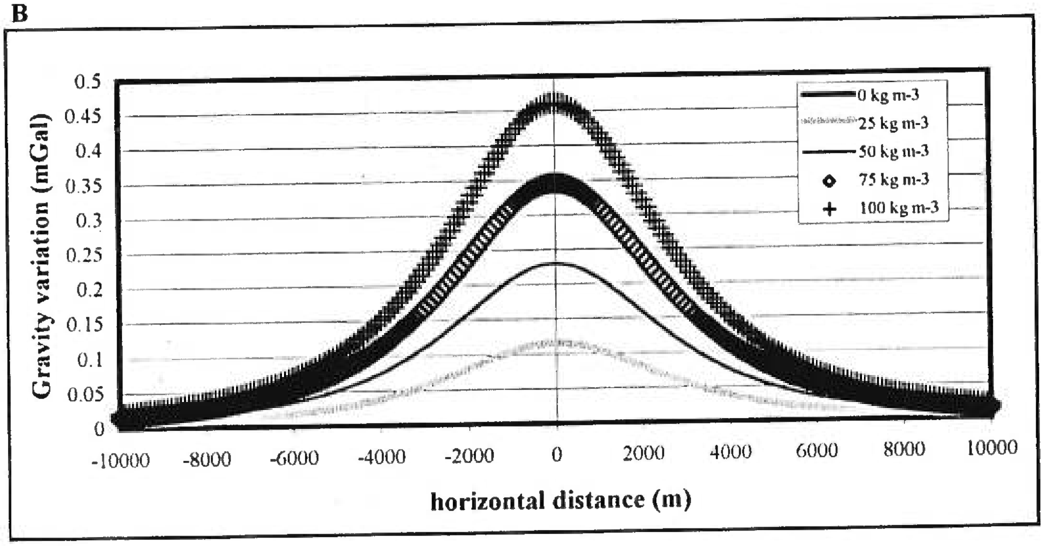
Gravity variation (mGal)
horizontal distance (m)
0 kg m-3
25 kg m-3
50 kg m-3
75 kg m-3
100 kg m-3
0
0.05
0.1
0.15
0.2
0.25
0.3
0.35
0.4
0.45
0.5
-10000
-8000
-6000
-4000
-2000
0
2000
4000
6000
8000
10000

C

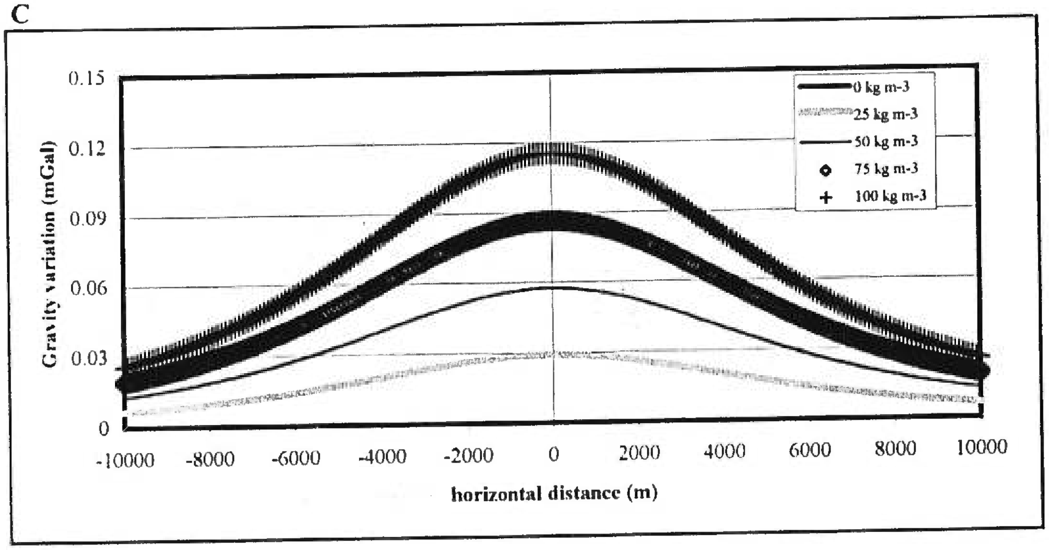
Gravity variation (mGal)
horizontal distance (m)
0 kg m-3
25 kg m-3
50 kg m-3
75 kg m-3
100 kg m-3
0
0.03
0.06
0.09
0.12
0.15
-10000
-8000
-6000
-4000
-2000
0
2000
4000
6000
8000
10000

density variation of 25 kg m^{-3} is still visible, altough very small, in the surface gravity (12 μGal) for a 3800 m deep body but is invisible for a 7600 m deep body (3 μGal) (Fig. 3.8b, c). For a density variation of 25 kg m^{-3} in a 10 km^3 magma body, the maximum corresponding gravity changes at 1900 m, 3800 m and 7600 m are 460 μGal, 115 μGal and 30 μGal (Fig 3.9a, b ,c). Thus, it is clear that for a larger magma body, changes in the density can be readily observed at the surface.

Vertical Cylinder Model

The vertical cylinder model presented here is used to represent either a magma pipe or a large body of magma at shallow depth. For simplicity, pressure, temperature and density are consider to be constant throughout the cylinder. Many variations are possible in a magma pipe or large cylindrical body; there can be variations in the level of magma, in the radius of the pipe or body, in the density, or any combination of these parameters. Depending on the gravity anomaly observed at the surface, certain of these processes better reproduce the anomaly. For example, Rymer and Brown (1984, 1987) modelled gravity variations at Poás volcano, Costa Rica, and concluded that the best model was a density variation of magma in a pipe. They were also able to model gravity variations they observed at the crater stations by variation in the level of magma. However, this model did not fit the observed gravity variations on the flanks of the volcano. They also examined variations in the radius of the pipe but encounted the same problem. There are several possible ways to model gravity variation close to the surface, but the most efficient way is by varying the density. Gravity variations can be large and rapid as seen at Masaya volcano, Nicaragua (Chapter 2).

Figure 3.10a shows gravity changes produced by variation of magma level in a cylinder of 50 m radius, 100 m initial depth and 100 long with a density contrast of 300 kg m^{-3}. At this depth, the gravity changes are small even for large changes in the level (a 10 m change produces a gravity variation of less than 10 μGal). For a deeper body of the same size, only very large variations in the level of magma would produce gravity changes. It is clear that for smaller bodies such as a thin magma pipe of less than 10 m radius, gravity changes would be difficult if not impossible to detect. For the same size of cylinder, variations in density are also not easy to observe since a density variation of 50 kg m^{-3} produces only a 13 μGal gravity change (Fig. 3.10b). Modelling of the Masaya volcano system with the cylinder model gives interesting results (Fig 3.10c, d). The values used for the model of size, emplacement and density contrast are from Rymer et al. (1998). Gravity changes caused by magma level variations can be observed at the surface if they are large (more than 20 m) (Fig. 3.10c). Gravity changes at Masaya occur through the course of one day (Chapter II) and changes in the level of magma would have to be rapid and large to produce the observed temporal gravity anomaly. Seismic monitoring during the daily gravity surveys at Masaya did not show any changes in the seismicity and only rare isolated events (Chapter II). On the other hand, density variation can better explain the gravity variation observed at Masaya (Fig. 3.10d). Rymer et al. (1998) demonstrated that for a density change of 100 kg m^{-3}, only a 5 % increase in the degree of vesiculation would be necessary.

FIGURE 3.10

(a) Gravity change caused by lowering of the level of magma in a vertical cylinder of 50 m radius and 100 m length at a depth of 100 m with a density contrast of 300 kg m^{-3}. (b) Gravity change of a vertical cylinder of 50 m radius, 100 m deep and 100 m long caused by variation in density of the magma. (c) Gravity change caused by lowering the level of magma for a vertical cylinder of 220 m radius and 100 m length at a depth of 300 m with a density contrast of 300 kg m^{-3}. (d) Gravity change of a vertical cylinder of 220 m radius, 300 m deep and 100 m length caused by variation in density of the magma.

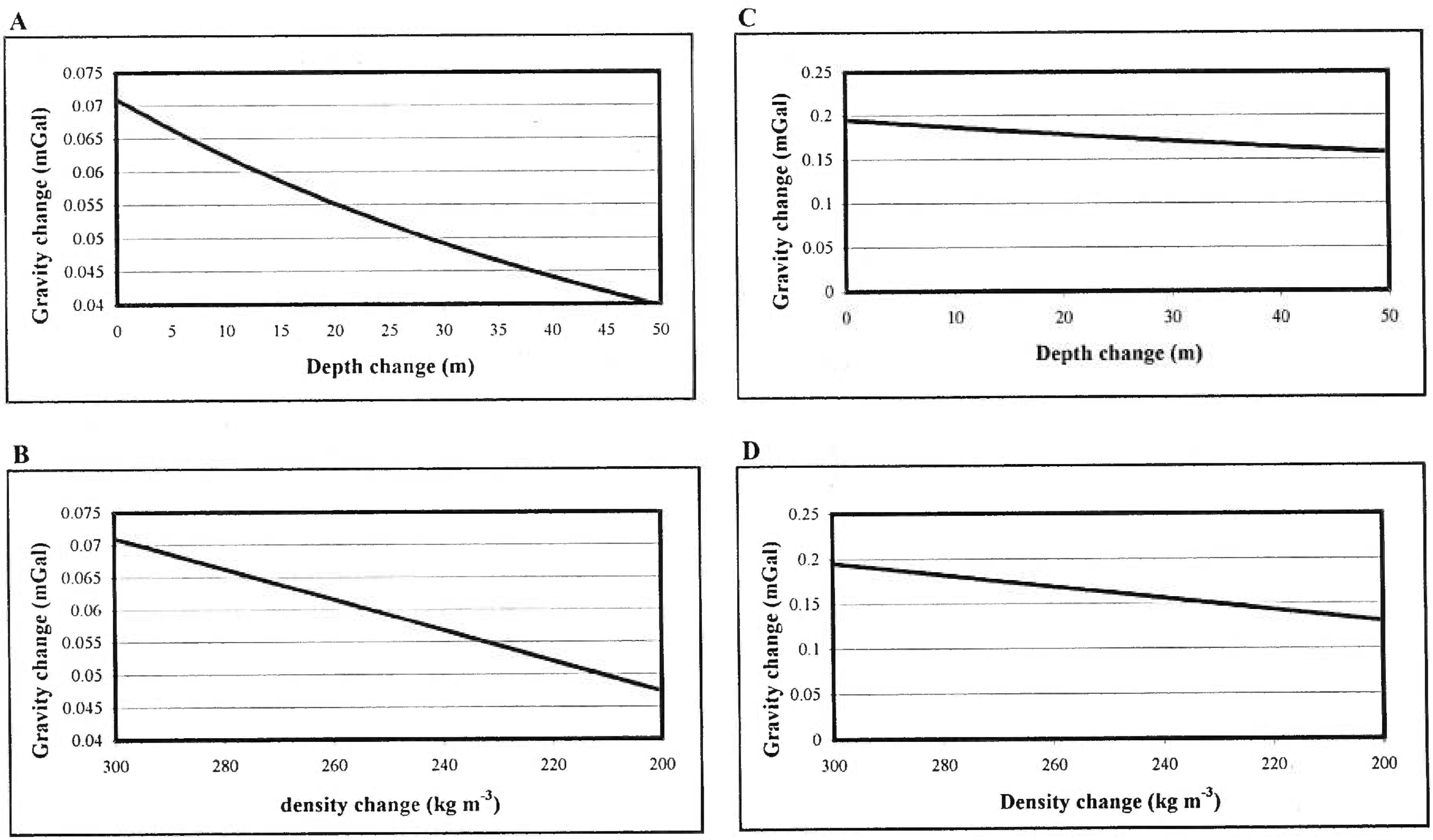
A
Gravity change (mGal)
0.075
0.07
0.065
0.06
0.055
0.05
0.045
0.04
0 5 10 15 20 25 30 35 40 45 50
Depth change (m)
C
Gravity change (mGal)
0.25
0.2
0.15
0.1
0.05
0
0 10 20 30 40 50
Depth change (m)
B
Gravity change (mGal)
0.075
0.07
0.065
0.06
0.055
0.05
0.045
0.04
300 280 260 240 220 200
density change (kg m-3)
D
Gravity change (mGal)
0.25
0.2
0.15
0.1
0.05
0
300 280 260 240 220 200
Density change (kg m-3)

Cubic Shape Chamber

This model is used to show variations of gravity caused by fractionation in a magma chamber where there is creation of a thin low-density layer (10-100 m thick) at the top of the magma chamber or to show accumulation of gas bubbles at the top of a magma chamber such as at Kilauea (Verginolle and Jaupart, 1990). In the case of gravity changes from crystallization in a magma chamber, the model of Blake (1984) is used. Two examples are presented based on his model. First, a magma chamber 4 km thick and 4 km wide at a depth of 2 km is shown (Fig. 3.11a). A thin layer of about 100 m, which represent 2.5 % of the thickness of the chamber, is formed by accumulation of gas at the top of the magma chamber. If the initial H_2O content is 3 wt %, which is near saturation at the top of the magma chamber, a maximum gravity decrease of 105 μGal would be observed after only 6 % crystallisation. For a larger amount of crystallisation (i.e., 12 %), the maximum corresponding gravity change would be about 210 μGal (Fig. 3.11b). These gravity changes result from density changes of 70 kg m^{-3} and 140 kg m^{-3}, corresponding to overpressure of 5 MPa and 10 MPa, respectively. The crystallization required for the overpressure were inferred from Tait et al. (1989). The modelling was also done for a deeper magma chamber (depth of 6 km). At this depth, less crystallization is required to produce the 5-10 MPa overpressure. Thus the density changes are smaller because less gas is produced, and it is more dense at higher pressure (~200 MPa). At this depth (6000 m), the gravity variations are very small and probably cannot be detected at the surface since crystallization can be a long process. Examples of density decreases of 30 kg m^{-3} and 55 kg m^{-3} are shown in Figure 3.12a and 3.12b; the gravity changes

FIGURE 3.11

Gravity change produced in the top layer (100 m thick) of a magma chamber at a depth of 2000 m by a density decrease of (a) 70 kg m^{-3} and (b) 140 kg m^{-3}.

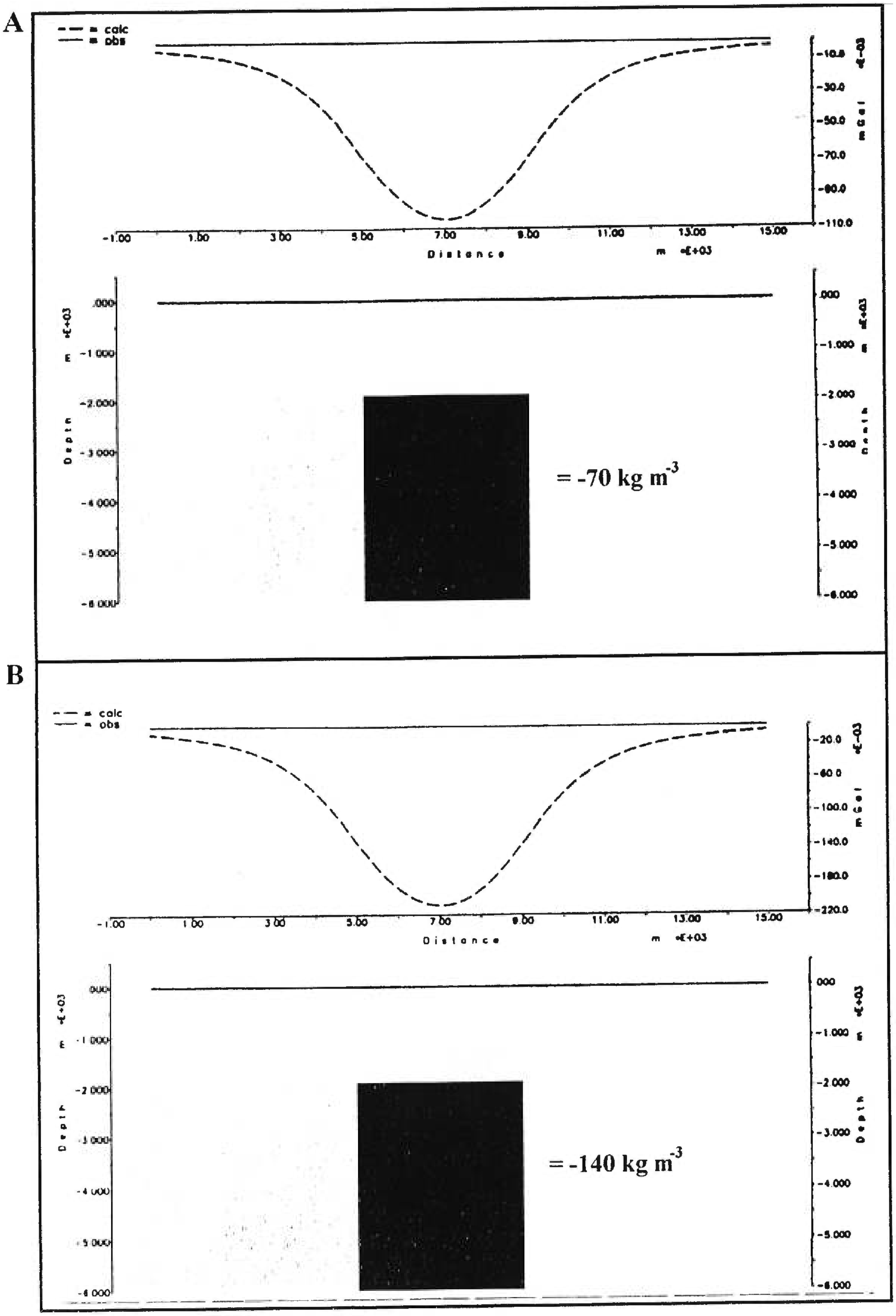
A
= calc
= obs
-10.0
-30.0
-50.0
-70.0
-90.0
-110.0
mGal
-1.00
1.00
3.00
5.00
7.00
9.00
11.00
13.00
15.00
Distance
m ×E+03
Depth
.000
-1.000
-2.000
-3.000
-4.000
-5.000
-6.000
= -70 kg m-3
B
= calc
= obs
-20.0
-60.0
-100.0
-140.0
-180.0
-220.0
mGal
Distance
m ×E+03
Depth
= -140 kg m-3

FIGURE 3.12

Gravity change produced in the top layer (100 m thick) of a magma chamber at a depth of 6000 m by a density decrease of (a) 30 kg m^{-3} and (b) 55 kg m^{-3}.

A

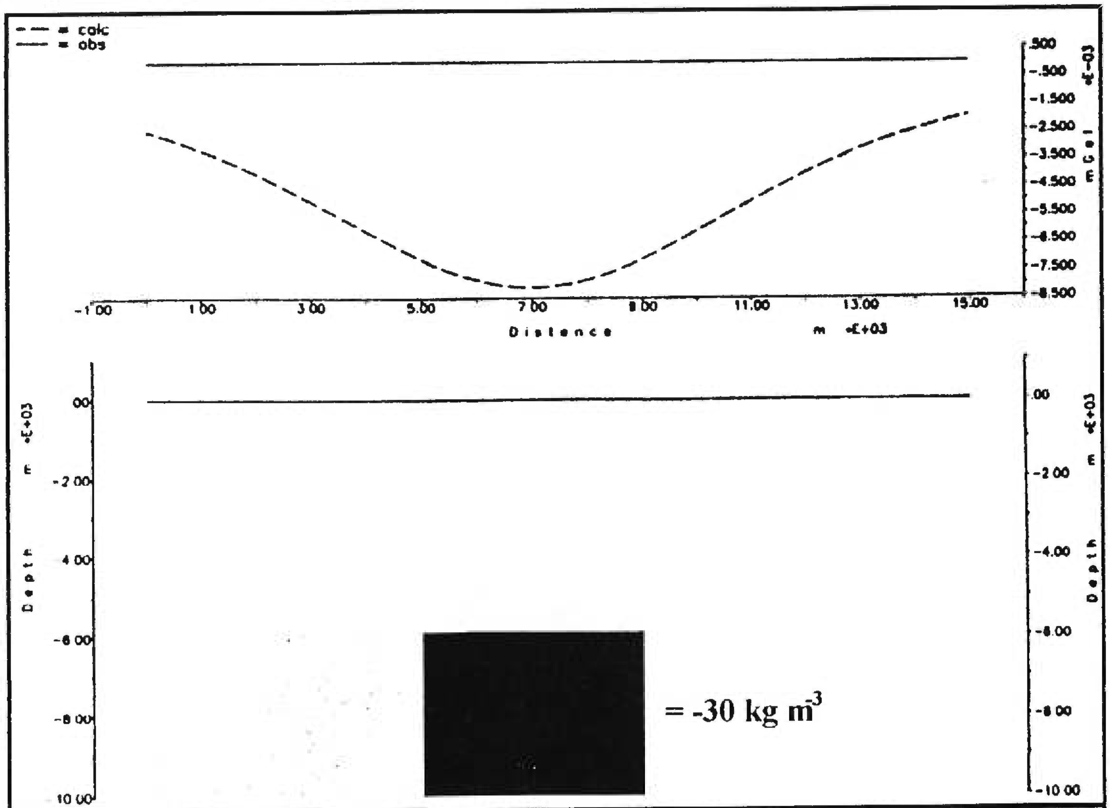

— — = calc
—— = obs
Distance
m *E+03
Depth
m *E+03
mGal
*E−03
= -30 kg m-3

B

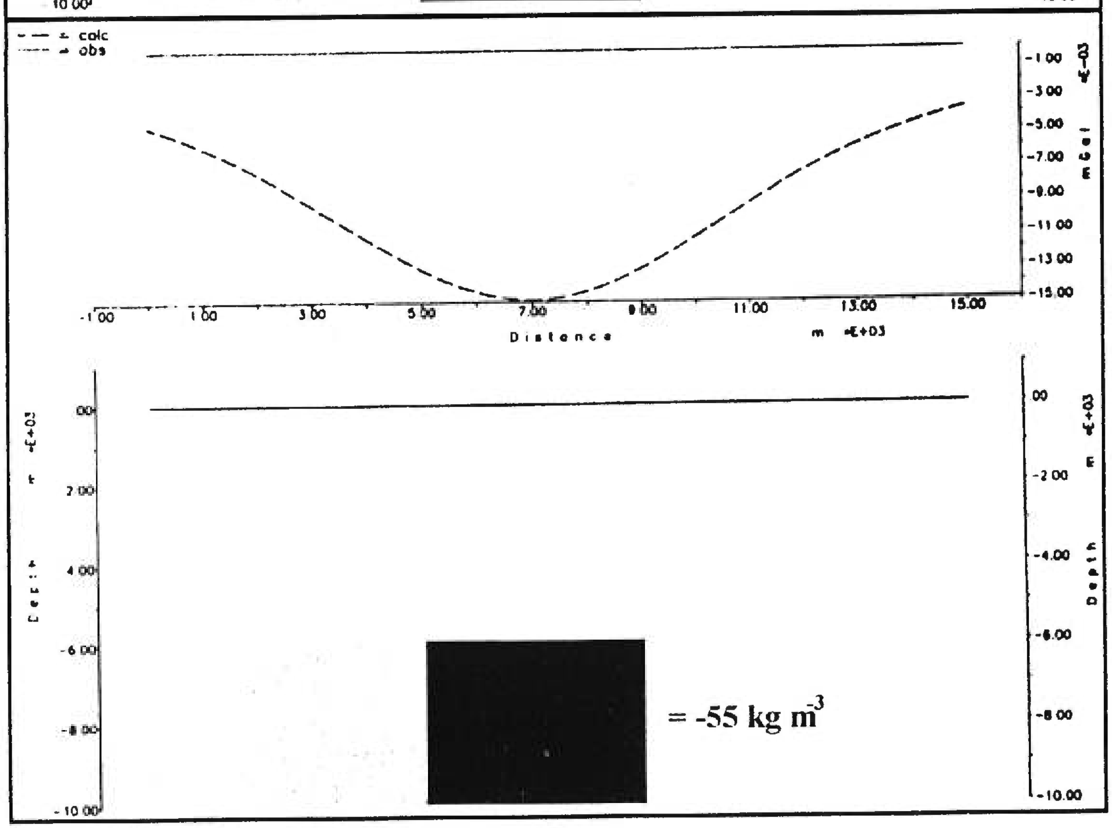

— — = calc
—— = obs
Distance
m *E+03
Depth
m *E+03
mGal
*E−03
= -55 kg m-3

caused by these density changes are 8 and 15 μGal, respectively. The density changes at this depth correspond to crystallization of 17.5 and 31 % for a near H_2O saturated rhyolitic magma, which are much higher than that needed to attain overpressure suggested by Tait et al. (1989) (around 3-6%). For the third example, modelling by Vergniolle and Jaupart (1990) and Vergniolle (1996) on foam accumulations at Kilauea is used. The effect of accumulation of a 1 m thick foam with 70 % bubbles at the top of the subchamber of Kilauea is shown in Figure 3.13. The gravity variation produced by this thin slab of density contrast equal to about –1800 kg m^{-3} is around 17 μGal.

These examples show that gravity variation induced by gas in a magma chamber can be observed at the surface under certain conditions. By comparison, microgravity surveys were conducted in the Kuparuk River oil field (Alaska, United States) to observe gravity changes caused by gas movement and gas displacing oil. At a depth of 1848 m, a horizontal slab of 15.2 m thick, with horizontal dimensions of 4900 m by 4900 m, created a negative anomaly of 26 μGal, and inferred density variations were on the order of 47 kg m^{-3} (Brady et al, 1996).

Discussion

The modelling examples presented above do not fully reproduce real systems, but they can be used to study a particular aspect of dynamic volcanic systems. The simplicity of the models permit manipulations of different models and situations. The first goal was to model gravity variation caused by accumulation of gas in a magma chamber. Swelling of volcanic edifices is often observed, which is evidence for

FIGURE 3.13

Gravity change produced by a foam accumulation at the top of a 2000 m deep basaltic magma chamber.

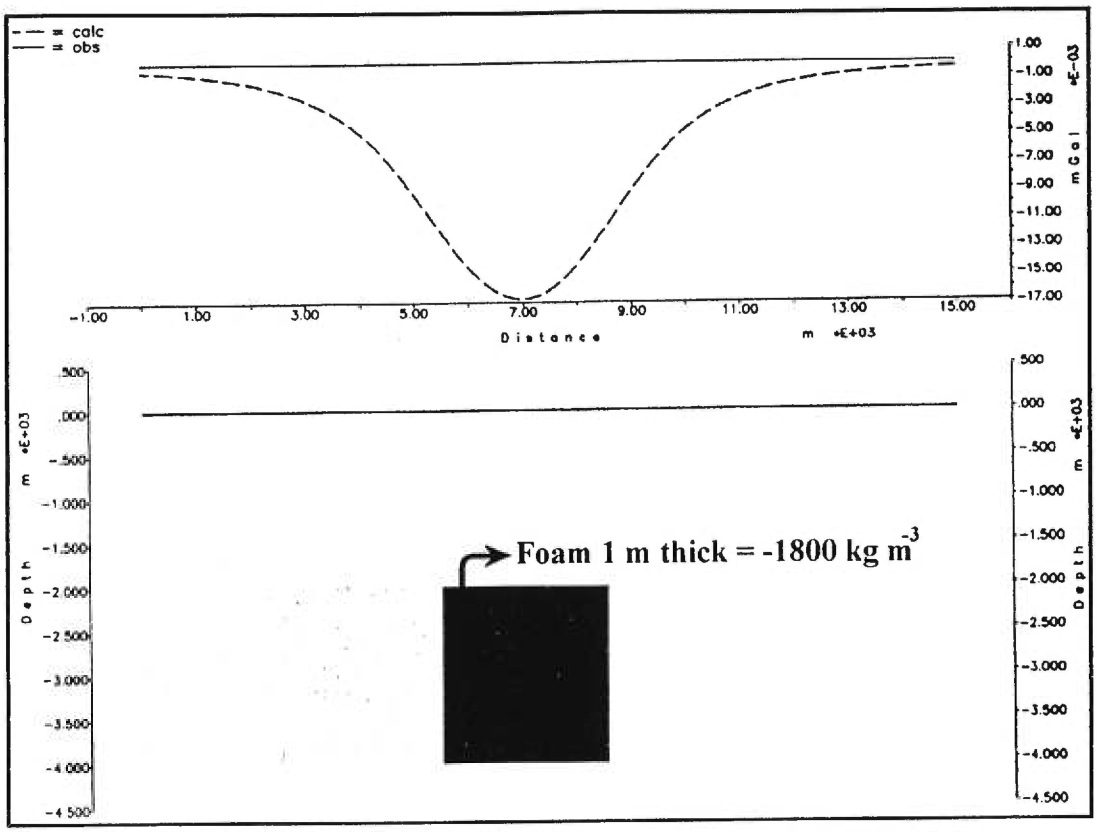

- - - = calc
—— = obs
mGal *E-03
Distance m *E+03
Depth m *E+03
Foam 1 m thick = -1800 kg m-3

overpressure in a magmatic system or upward movement of magma. The gravity change produced by a fractional volume change of 0.001 is less than 10 μGal for a 10 km^3 magma chamber at a depth of 1900 m. In comparison, to account for this volume change, an overpressure of 5-10 MPa is necessary, which corresponds crystallization of 5-10 %. The gravity change produced over the same magma chamber would be 1200 μGal. The overpressure is generated by the presence of free volatiles at the top of the magma chamber (Blake, 1984; Druitt and Sparks, 1984; Tait et al, 1989; Bower and Woods, 1997). This eventually lead to a decrease in the density of the magma at the top. However, there is a certain point beyond which the gas cannot accumulate, since the overpressure exceeds the fracture criterion (Tait et al, 1989). Thus, the density of the gas-melt mixture at the top of the chamber reaches a certain limit depending on the depth of the chamber. Rymer (1994) has demonstrated the possibility of monitoring rhyolitic volcanoes and calderas in order to anticipate a major buildup of pressure. The examples above prove that it is possible to observe gravity variations for shallow to relatively deep systems (2-4 km). For the Kilauea example, the small gravity variations (17 μGal) are more difficult to monitor because other processes are also occurring, such as fracture opening and magma chamber replenishment. Unless frequent or even continuous measurements are made, it is difficult to recognise eruption precursors using microgravity (Rymer, 1989; Rymer, 1994).

For gravity variations above a magma chamber, crystallization is one process that could produce an overall increase in the dissolved volatile content in the magma. Density changes produced in volatile undersaturated conditions could possibly lead to gravity changes large enough to be observed at the surface. On the other hand, it is unlikely for deep systems because the density contrasts are not large enough to produce any appreciable gravity changes. As examples, an overall increase of 0.5 wt % H_2O in a rhyolitic magma chamber of 10 km^3 at a depth of 7600 m would cause a gravity decrease of 90 μGal, and an increase of 0.2 wt % H_2O in a rhyolitic magma chamber of 1 km^3 at a depth of 1900 m would produce a 19 μGal gravity decrease. It is clear that for very large magma chambers (10-100 km^3), variation in the dissolved volatile content can be observed at the surface. Thus, the quantity of dissolved volatiles needed to produce a large gravity variation is reduced. Increase in dissolve coponents can occur by crystallization, convection or an input of new magma. It is not clear, however, how long it would take for such a dissolved volatile variation to occur. Tait et al. (1989) calculated that the rates of respose times, hence typical times for fractional crystallization, for dacitic to rhyolitic melt are around 400-850 years.

Many possible mechanisms may serve to change the exsolved volatile content in a magmatic system. New magma injected into a chamber may be rich in gas than the existing magma. Convection in a magma system can move saturated magma upward to depthswhere it becomes oversaturated. This is what appears to have happened at Masaya between 1993 and 1994 (Rymer et al., 1998). Rapid crystallization and volatile saturation and exsolution could occur within a magma layer (Pyle and Pyle, 1995). At shallow levels in open-systems, gravity variations also could be produced in magma pipes where there is constant degassing and variation in the bubble content in the magma, such as at Masaya.

Conclusions

Gravity variations induced by a variation in the volume fraction of free gas in magma are observable at the surface for a shallow magma chamber, for a subchamber or even in large magma pipes of volcanic edifices. In many cases, volatiles are responsible for overpressure and eruptions. Although density variations produced by exsolution of volatiles are most important, even variations in the dissolved volatile content can be observe at the surface. Although many volatiles are present in magma, H_2O is the most important for varying the density and hence, the gravity. The possibility of monitoring the exsolution of volatiles in a magma chamber, beneath a dome or in the conduit under a volcanic edifice, could enhance our means of forecasting eruptions. Volatiles are not the only cause of gravity variations in volcanic systems; there also could be intrusion of new magma, hydrothermal activity, gas loss and fracture opening and closing. Yet, volatiles are an important aspect of volcano instability, and it is important to understand and monitor their evolution. Microgravity techniques have improved significantly in the past few years. Changes in gravity linked to vesiculation in the magma have already been observed by Rymer and Brown (1984) at Poás volcano and by Beaulieu et al. (1997, 1998) at Masaya volcano. Microgravity monitoring is also being used at oil fields to observe the movement of gas pockets at depths of 1500-3000 m (Brady et al., 1996).

Acknowledgments

The authors are grateful to Claude Dalpé who provided the program for density calculations of magma. Also thanks to Walter Trzcienski and Gilles Gauthier for their advice on computational matters.

References

Beaulieu, A., Stix, J., St-Amand, K., Rymer, H., Gaonac'h, H., and Lovejoy, S., 1997. Gravity studies at Telica and Masaya volcanoes, Nicaragua. AGU Fall Meeting, San Francisco, p. 797.

Beaulieu, A., Williams-Jones, G., St-Amand, K., Stix, J., and Rymer, H, 1998. Gravity studies at Telica and Masaya volcanoes, Nicaragua. AGU Fall Meeting, San Francisco, in press.

Blake, S., 1981. Volcanism and the dynamics of open magma chambers. Nature, 289: 783-785.

Blake, S., 1984. Volatile oversaturation during the evolution of silicic magma chamber as an eruption trigger. J. Geophys. Res., 89: 8237-8244.

Bottinga, Y., Weill, D., and Richet, P., 1982. Density calculations for silicate liquids. I. Revised method for aluminosilicate compositions. Geochim. Cosmochim. Acta, 46: 909-919.

Bower, S. M. and Woods, A. W., 1997. Control of magma volatile content and chamber depth on the mass erupted during explosive volcanic eruptions. J. Geophys. Res., 102: 10273-10290.

Brady, J. L., Wolcott, D. S., and Aiken, C. L. V., 1996. Gravity methods: useful techniques for reservoir surveillance. The Log Analyst July-August 1996: 45-56.

Dixon, J. E., Stolper, E. M., and Holloway, J. R., 1995. An experimental study of water and carbon dioxide solubilities in Mid-Ocean Ridge basaltic liquids. J. Petrol. 36: 1607-1631.

Dixon, J. E., and Stolper, E. M., 1995. An experimental study of water and carbon dioxide solubilities in Mid-Ocean Ridge basaltic liquids. Part II: application to degassing. J. Petrol. 36: 1633-1646.

Druitt, T. H., and Sparks, R. S. J., 1984. On the formation of calderas during ignimbrite eruptions. Nature, 310: 679-681.

Gerlach, T. M., 1986. Exsolution of H_2O, CO_2, and S during eruptive episodes at Kilauea volcano, Hawaii. J. Geophys. Res., 91: 12177-12185.

Harris, D. M., and Anderson, A. T., 1984. Volatiles H_2O, CO_2, Cl in a subduction related basalt. Contrib. Mineral. Petrol., 87: 120-128.

Holloway, J. R., and Blank, J. G., 1994. Application of experimental results to C-O-H species in natural melts. In Carroll, M., and Holloway, J. R., eds., Volatiles in Magmas: Mineralogical Society of America Reviews in Mineralogy, 30: 187-230.

Kazahaya, K., Shinohara, H., and Saito, G., 1994. Excessive degassing of Izu-Oshima volcano: magma convection in a conduit. Bull. Volcanol., 56: 207-216.

Lange, R. A., and Carmichael, I. S. E., 1990. Thermodynamic properties of silicate liquids with emphasis on density, thermal expansion and compressibility. In: Nicholls, J., and Russell, J. K., eds., Modern Methods of Igneous Petrology: Mineralogical Society of America Reviews in Mineralogy, 24: 44-54.

Lange, R. A., 1994. The effect of H_2O, CO_2 and F on the density and viscosity of silicate melts. In Carroll, M., and Holloway, J. R., eds., Volatiles in Magmas: Mineralogical Society of America Reviews in Mineralogy, 30: 331-369.

Lowenstern, J. B., 1994. Dissolved volatile concentrations in an ore-forming magma. Geology, 22: 893-896.

Papale, P., 1997. Modeling of the solubility of a one-component H_2O or CO_2 fluid in silicate liquids. Contrib. Mineral. Petrol., 126: 237-251.

Pedley, R. C., Busdy, J. P., and Dabek, Z. K., 1993. GRAVMAG user manual: Interactive 2.5D gravity and magnetic modelling. British Geological Survey, Natural Environment Research Council, Technical Report WK/93/26/R, 73 pp.

Pyle, D. M., and Pyle, D. L., 1995. Bubble migration and the initiation of volcanic eruptions. J. Volcanol. Geotherm. Res., 67: 227-232.

Rymer H., and Brown, G. C., 1984. Periodic gravity changes at Poás volcano, Costa Rica. Nature, 311: 243-245.

Rymer H., and Brown, G. C., 1987. Causes of microgravity changes at Poás volcano, Costa Rica: an active but non-eruptive system. Nature, 311: 243-245.

Rymer, H., 1994. Microgravity changes as a precursor to volcanic activity. J. Volcanol. Geotherm. Res., 61: 311-328.

Rymer, H., 1989. A contribution to precision microgravity data analysis using Lacoste and Romberg gravity meters. Geophys. J., 97: 311-322.

Rymer, H., van Wyk de Vries, B., Stix, J., and Williams-Jones, G., 1998. Pit crater structure and processes governing persistent activity at Masaya volcano, Nicaragua. Bull. Volcanol., 59: 345-355.

Shaw, H. R., 1963. Obsidian-H_2O viscosities at 1000 and 2000 bars in the temperature range 700 to 900 °C. J. Geophys. Res., 68: 6337-6343.

Sisson, T. W., and Layne, G. D., 1993. H_2O in basalt and basaltic andesite glass inclusions from four subduction-related volcanoes. Earth Planet. Sci. Lett., 117: 619-635.

Stix, J., and Layne, G. D., 1996. Gas saturation and evolution of volatile and light lithophile elements in the Bandelier magma chamber between two caldera-forming eruptions. J. Geophys. Res., 101: 25 181-25 196.

Stolper, E., 1992. Water in silicate glasses: an infrared spectroscopic study. Contrib. Mineral. Petrol., 81: 1-17.

Stolper, E., and Holloway, J. R., 1988. Experimental determination of the solubility of carbon dioxide in molten basalt at low pressure. Earth Planet. Sci. Lett., 87: 397-408.

Tait, S., Jaupart, C., and Vergniolle, S., 1989. Pressure, gas content and eruption periodicity of a shallow, crystallising magma chamber. Earth Planet. Sci. Lett., 92: 107-123.

Telford, W. M., Geldart, L. P., Sheriff, R. E., 1990. Applied Geophysics: Second edition. Cambridge, Cambridge Univerity Press. 770 pp.

Vergniolle, S., and Jaupart, C., 1990. Dynamic degassing at Kilauea volcano, Hawaii. J. Geophys. Res., 95: 2793-2809.

Vergniolle, S., 1996. Bubble size distribution in magma chambers and dynamics of basaltic eruptions. Earth Planet. Sci. Lett., 140: 269-279.

Wallace, P. J., and Gerlach, M., 1994. Magmatic vapor source for sulfur dioxide released during volcanic eruptions: evidence from Mount Pinatubo. Science, 265: 497-499.

Conclusions

General conclusions

Gravity is a useful tool to better define and understand the internal structure of volcanoes and to monitor their activity. Noteworthy conclusions of this work are the following:

1. The gravity survey at Telica volcano revealed the presence of a large shallow intrusion of dimensions 2 km × 2 km × 6 km at a depth of about 1 km, with a density contrast of 400-600 kg m^{-3} and trending nearly north-south.
2. Regional structures and the geomorphology of Telica, such as the north-northwest-south-southeast trending faults and the north-west crater alignment, are parallele to the shallow intrusion.
3. Gravity variations observed at Masaya volcano are linked to fluctuations in the quantity of bubbles in the magma beneath Santiago crater.
4. A possible link of earth tides to short-time gravity variations was observed at one station (A7) near the active crater at Masaya ; tides appear to affect the ability of the magma to release gas by vesiculation.
5. If gravity varies with density due to fluctuation in the vesicularity of the magma, there is probably a direct or indirect link with SO_2 flux at Masaya. This effect was not observed in 1997, but a possible positive correlation was observed on 13 March 1998.
6. Rymer et al.'s (1998) model of convective overturn of magma driven by density changes for renewal of degassing activity at Masaya is confirmed by this work.

7. Theoretical modelling shows that gravity chamges induced by a variation in the volume fraction of free gas in magma are observable at the surface for a shallow magma chamber.
8. Density variations produced by exsolution of volatiles from a magma are larger than density changes due to variations in the quantity of dissolved volatiles in a magma chamber. Nevertheless, changes in the amounts of dissolved species are also able to be seen gravimetrically on the surface if the changes are sufficiently shallow.
9. Although many volatiles are present in the magma, H_2O is the most important for causing variations in the density and hence the gravity.

Recommendations for Future Work

For Telica volcano, the gravity maps produced by this study do not cover a sufficiently large area to define the anomaly with confidence. A longer profile (50 km) would be useful to verify the depth and size of the anomaly. Some stations should be added where there is a lack of points, such as in the southwestern, northeastern and northwestern parts of the volcano. The southeastern part of the volcano was not covered much because of the steepness of the cone and the presence of vegetation. With knowledge of the location of a shallow intrusion at Telica, microgravity stations could be better situated to monitor temporal changes.

At Masaya volcano, the daily gravity monitoring should be done for longer periods of time to better define the relation between the tides and the changes in density in the magma chamber. If this relation holds, monitoring on longer timescales (e.g., years) would be difficult to interpret. The continuous gravity monitoring should be done at other stations in the caldera and beyond. Monitoring of SO_2 flux and gravity should be done simultaneously to better define a correlation, if one exists.

For the modelling of the magma density with dissolved and exsolved volatiles, a better way to calculate the density of the melt under undersaturated condition should be used, such as the MELTS program. The solubility laws for CO_2 and H_2O in rhyolite and basalt should be verified, since new experimental data are being produced on a fairly regular basis.

Appendix A

Telica gravity and GPS data

Table A1

1997 and 1998 raw gravity data at Telica volcano

Station	G_{raw}*	Hour (GMT)	date
1997 data			
base1	1700.094	16:29	20-03-97
tel01	1693.636	17:59	20-03-97
tel02	1658.969	18:30	20-03-97
tel03	1664.052	19:25	20-03-97
tel04	1664.122	20:20	20-03-97
tel05	1661.416	20:42	20-03-97
tel06	1654.692	21:09	20-03-97
base1(fin)	1700.308	22:00	20-03-97
base1	1700.078	15:37	21-03-97
tel07	1697.412	16:02	21-03-97
tel08	1693.700	16:16	21-03-97
tel09	1688.324	16:35	21-03-97
tel10	1680.789	16:58	21-03-97
tel11	1672.407	17:26	21-03-97
tel12	1662.583	18:30	21-03-97
tel13	1666.138	18:51	21-03-97
tel14	1669.735	19:14	21-03-97
tel15	1671.756	19:41	21-03-97
tel16	1672.109	20:06	21-03-97
tel17	1673.509	20:25	21-03-97
tel18	1673.137	20:47	21-03-97
tel19	1672.285	21:08	21-03-97
tel20	1671.368	21:30	21-03-97
base1(fin)	1700.288	22:17	21-03-97
base1	1700.042	16:44	22-03-97
tel21	1692.442	17:00	22-03-97
tel22	1693.522	17:23	22-03-97
tel23	1696.877	17:47	22-03-97
tel24	1696.742	18:33	22-03-97
tel25	1697.269	18:56	22-03-97
tel26	1690.455	19:27	22-03-97
tel27	1688.690	20:01	22-03-97
tel28	1687.531	20:17	22-03-97

tel29	1685.885	20:32	22-03-97
tel30	1685.207	20:52	22-03-97
tel31	1683.101	21:06	22-03-97
tel32	1679.529	21:17	22-03-97
base1(fin)	1700.251	22:04	22-03-97
base1	1700.127	15:46	01-04-97
tel47	1656.755	17:03	01-04-97
tel48	1658.137	17:23	01-04-97
tel49	1660.449	17:42	01-04-97
tel50	1660.299	18:10	01-04-97
tel51	1662.304	18:28	01-04-97
tel52	1663.577	18:46	01-04-97
tel53	1664.708	19:08	01-04-97
tel54	1665.748	19:26	01-04-97
tel55	1665.096	19:44	01-04-97
tel56	1667.845	20:08	01-04-97
tel57	1668.277	20:33	01-04-97
tel58	1669.270	20:49	01-04-97
tel59	1666.050	21:08	01-04-97
base1(fin)	1700.131	22:07	01-04-97
base1	1700.082	15:29	02-04-97
tel60	1667.917	16:14	02-04-97
tel61	1669.587	16:33	02-04-97
tel62	1669.128	16:55	02-04-97
tel63	1668.224	17:13	02-04-97
tel64	1666.003	17:35	02-04-97
tel65	1665.764	17:53	02-04-97
tel66	1668.088	18:28	02-04-97
tel67	1668.429	18:44	02-04-97
tel68	1672.821	19:18	02-04-97
tel69	1672.242	19:27	02-04-97
tel70	1673.639	19:43	02-04-97
tel71	1673.866	20:03	02-04-97
tel72	1673.609	20:24	02-04-97
tel73	1671.361	20:39	02-04-97
tel74	1671.196	20:55	02-04-97
tel75	1674.510	21:15	02-04-97
tel76	1675.439	21:35	02-04-97
base1(fin)	1700.169	22:15	02-04-97
base1	1699.967	15:29	05-04-97

tel110	1696.105	16:05	05-04-97	
tel111	1692.218	16:20	05-04-97	
tel112	1688.316	16:35	05-04-97	
tel113	1682.795	16:52	05-04-97	
tel114	1669.909	17:15	05-04-97	
tel115	1670.037	17:37	05-04-97	
tel116	1669.687	18:16	05-04-97	
tel117	1670.869	18:30	05-04-97	
tel118	1684.221	18:51	05-04-97	
tel119	1683.147	19:07	05-04-97	
tel120	1678.173	19:26	05-04-97	
tel121	1689.142	19:45	05-04-97	
tel122	1697.574	20:14	05-04-97	
base1(fin)	1700.167	21:13	05-04-97	
base1	1699.973	15:29	06-04-97	
tel123	1660.680	16:42	06-04-97	
tel124	1661.779	16:59	06-04-97	
tel125	1662.928	17:20	06-04-97	**tare**
tel125	1662.881	17:45	06-04-97	
tel126	1662.906	18:14	06-04-97	
tel127	1663.783	18:28	06-04-97	
tel128	1665.388	18:47	06-04-97	
tel129	1668.675	19:06	06-04-97	
tel130	1671.925	19:28	06-04-97	
tel131	1674.792	19:47	06-04-97	
tel132	1672.632	20:08	06-04-97	
tel133	1670.800	20:26	06-04-97	
tel134	1671.243	20:39	06-04-97	
base1(fin)	1700.140	22:06	06-04-97	
base1	1700.024	15:46	08-04-97	
tel151	1676.958	17:05	08-04-97	
tel152	1680.138	17:15	08-04-97	
tel153	1682.481	17:33	08-04-97	
tel154	1681.667	17:48	08-04-97	
tel155	1681.667	17:48	08-04-97	
tel156	1681.844	18:00	08-04-97	
tel157	1682.380	18:33	08-04-97	
tel158	1675.879	18:48	08-04-97	
tel159	1678.578	19:06	08-04-97	
tel160	1670.312	19:55	08-04-97	
tel161	1673.510	20:11	08-04-97	

tel162	1674.018	20:25	08-04-97
base1(fin)	1700.009	21:35	08-04-97
BASE2			
station			
base2	1716.159	19:43	23-03-97
tel34	1718.594	19:58	23-03-97
tel35	1720.559	20:21	23-03-97
tel36	1722.902	20:39	23-03-97
tel37	1724.786	21:01	23-03-97
tel38	1726.533	21:25	23-03-97
base2(fin)	1716.341	21:57	23-03-97
base2	1716.252	15:35	27-03-97
tel39	1713.842	15:48	27-03-97
tel40	1710.191	16:06	27-03-97
tel41	1706.452	16:25	27-03-97
tel42	1702.976	16:42	27-03-97
tel43	1696.187	17:23	27-03-97
tel44	1692.820	17:49	27-03-97
tel45	1688.274	18:07	27-03-97
tel46	1681.271	18:26	27-03-97
base2(fin)	1716.091	18:59	27-03-97
base2	1716.096	15:10	03-04-97
tel77	1715.914	15:37	03-04-97
tel78	1714.403	15:55	03-04-97
tel79	1711.448	16:11	03-04-97
tel80	1708.363	16:30	03-04-97
tel81	1705.131	16:51	03-04-97
tel82	1700.659	17:07	03-04-97
tel83	1694.353	17:24	03-04-97
tel84	1685.111	17:42	03-04-97
tel85	1682.338	18:17	03-04-97
tel86	1690.102	18:35	03-04-97
tel87	1695.727	18:55	03-04-97
tel88	1701.455	19:10	03-04-97
tel89	1706.767	19:32	03-04-97
tel90	1710.032	19:49	03-04-97
tel91	1713.308	20:10	03-04-97
tel92	1715.729	20:25	03-04-97
tel93	1718.518	20:40	03-04-97

base2(fin)	1716.280	21:00	03-04-97	
base2	1716.060	15:13	04-04-97	
tel94	1714.117	15:40	04-04-97	
tel95	1712.004	15:59	04-04-97	
tel96	1706.902	16:16	04-04-97	
tel97	1702.417	16:47	04-04-97	
tel98	1696.730	17:06	04-04-97	
tel99	1689.649	17:26	04-04-97	
tel100	1682.663	17:46	04-04-97	
tel101	1673.097	18:36	04-04-97	
tel102	1671.659	18:53	04-04-97	
tel103	1672.836	19:14	04-04-97	
tel104	1669.733	19:41	04-04-97	
tel105	1681.371	20:04	04-04-97	
tel106	1688.202	20:22	04-04-97	
tel107	1692.689	20:39	04-04-97	
tel108	1696.652	21:02	04-04-97	
tel109	1700.724	21:20	04-04-97	
base2(fin)	1716.277	21:51	04-04-97	
base2	1716.052	15:13	07-04-97	
tel135	1719.764	15:35	07-04-97	
tel136	1717.574	15:50	07-04-97	
tel137	1713.165	16:03	07-04-97	
tel138	1709.058	16:22	07-04-97	
tel139	1705.036	16:39	07-04-97	
tel140	1700.439	16:58	07-04-97	
tel141	1695.518	17:12	07-04-97	
tel142	1688.738	17:25	07-04-97	
tel143	1679.268	17:45	07-04-97	
tel144	1678.489	18:17	07-04-97	
tel145	1688.682	18:33	07-04-97	
tel146	1695.051	18:49	07-04-97	
tel147	1701.040	19:07	07-04-97	
tel148	1706.634	19:25	07-04-97	
tel149	1709.993	19:43	07-04-97	
tel150	1718.535	20:12	07-04-97	
base2(fin)	1716.070	20:35	07-04-97	
basefinal	1739.562	15:17	10-04-97	**closure**
base1	1700.015	16:25	10-04-97	
base2	1716.032	17:17	10-04-97	

basefinal	1739.427	18:19	10-04-97
1998 data			
base1	1696.234	16:45	02-02-98
tel175	1697.632	17:26	02-02-98
tel176	1697.874	17:47	02-02-98
tel177	1703.121	18:08	02-02-98
base1	1696.175	18:48	02-02-98
base1	1696.226	15:02	03-02-98
tel178	1708.796	15:39	03-02-98
tel179	1712.193	15:58	03-02-98
tel180	1714.848	16:25	03-02-98
tel181	1730.580	16:50	03-02-98
tel182	1734.869	17:15	03-02-98
tel183	1743.189	17:40	03-02-98
base1	1696.138	22:35	03-02-98
base3	1790.854	14:05	04-02-98
tel191	1789.234	14:27	04-02-98
tel192	1786.615	14:45	04-02-98
tel193	1785.628	15:05	04-02-98
tel194	1783.536	15:25	04-02-98
tel195	1780.116	15:42	04-02-98
tel196	1775.516	16:07	04-02-98
tel197	1770.582	16:25	04-02-98
tel198	1768.676	16:43	04-02-98
tel199	1763.323	17:05	04-02-98
tel200	1758.571	17:31	04-02-98
tel201	1749.420	18:22	04-02-98
tel202	1742.476	18:42	04-02-98
tel203	1739.040	19:02	04-02-98
tel204	1740.312	19:22	04-02-98
tel205	1739.106	19:47	04-02-98
tel206	1732.659	20:26	04-02-98
tel207	1725.054	20:43	04-02-98
tel208	1720.396	21:01	04-02-98
base2	1712.332	21:35	04-02-98
bafinal	1735.727	21:58	04-02-98
base3	1790.828	22:35	04-02-98
base1	1696.274	15:03	05-02-98

tel209	1697.476	15:46	05-02-98
tel210	1702.905	16:07	05-02-98
tel211	1705.256	16:32	05-02-98
tel212	1704.810	16:55	05-02-98
tel213	1704.203	17:15	05-02-98
tel214	1702.480	17:35	05-02-98
tel215	1699.727	18:35	05-02-98
tel216	1692.611	19:24	05-02-98
tel217	1687.701	19:46	05-02-98
tel218	1687.254	20:10	05-02-98
tel219	1691.294	20:35	05-02-98
base1	1696.325	21:50	05-02-98
base2	1712.381	15:06	06-02-98
tel220	1720.468	15:33	06-02-98
tel221	1725.569	15:56	06-02-98
tel222	1726.158	16:27	06-02-98
tel223	1742.789	16:54	06-02-98
tel224	1750.223	17:23	06-02-98
tel225	1762.819	17:55	06-02-98
tel226	1763.116	18:43	06-02-98
tel227	1764.740	19:07	06-02-98
tel228	1770.301	19:26	06-02-98
tel229	1771.672	19:44	06-02-98
base2	1712.454	21:55	06-02-98
tel216	1692.573	14:57	07-02-98
tel230	1706.187	15:36	07-02-98
tel231	1716.644	16:01	07-02-98
tel232	1729.839	16:24	07-02-98
tel233	1741.050	16:55	07-02-98
tel234	1755.301	17:21	07-02-98
tel235	1759.926	18:40	07-02-98
tel236	1761.907	19:07	07-02-98
tel216	1692.703	21:45	07-02-98
bafinal	1735.946	14:40	10-02-98
tel246	1715.989	16:02	10-02-98
tel247	1699.865	16:33	10-02-98
tel248	1691.321	17:03	10-02-98
tel249	1684.897	18:20	10-02-98
tel250	1700.448	19:00	10-02-98
tel251	1707.243	19:35	10-02-98

tel252	1714.336	20:10	10-02-98
tel253	1724.802	20:35	10-02-98
tel254	1731.585	20:57	10-02-98
bafinal	1736.024	21:35	10-02-98
base1	1696.497	15:12	11-02-98
tel255	1677.139	16:13	11-02-98
tel256	1679.016	16:41	11-02-98
tel257	1659.611	17:27	11-02-98
tel258	1656.562	18:25	11-02-98
tel259	1667.429	18:53	11-02-98
tel260	1669.959	19:23	11-02-98
tel261	1673.672	19:25	11-02-98
base1	1696.509	21:12	11-02-98

* After correction factor of Lacoste & Romberg meter G-513

Table A2

Summary of the gravity corrections and the resulting gravity differences relative to Base3

G_{obs} is the gravity measurements which are tides and drift corrected

ΔG_{obs} is the difference between the gravity measurements at a station and Base3

ΔG_l is the latitude correction

ΔG_{FA} is the altitude correction

ΔG_B is the Bouguer correction

ter (a-d) is the terrain correction for Sanberg sections A through D (0-171 m)

(a-d)*ρ is the terrain correction for Sanberg sections A through D corrected for a chosen density (2.3-2.5 g/cm^3)

ter (e-k) is the terrain correction for Hammer sections E through K (171-9900 m)

(e-k)*ρ is the terrain correction for Hammer sections E through K corrected for a chosen density (2.3-2.5 g/cm^3)

ΔG is the sum of ΔG_{obs} and all the corrections reported to zero relative to Base3

Station	G_{obs}	ΔG_{obs}	ΔG_l	ΔG_{FA}	ΔG_B	ter (a-d)	(a-d)*ρ	ter (e-k)	(e-k)*ρ	ΔG	Coordinates in UTM (WGS 84 datum)		
											North (m)	East (m)	Alt (m)
Base3	1794.821	0	0.000	0.000	0.000	0.005	0.006	0.313	0.375	0.000	1392895	510694	222.9
Basefinal	1739.701	-55.12	-0.660	92.762	-30.242	0.000	0.000	1.902	2.283	8.641	1394807	515700	523.5
Base1	1700.209	-94.612	-0.357	157.740	-51.425	0.074	0.089	3.756	4.507	15.560	1393929	518193	734.0
Base2	1716.273	-78.548	-0.651	132.933	-43.338	0.070	0.084	2.827	3.392	13.490	1394780	517431	653.6
tel01	1658.981	-135.84	-0.247	203.660	-66.396	0.759	0.911	10.114	12.136	13.843	1393610	517965	882.8
tel02	1659.035	-135.786	-0.262	203.423	-66.319	0.434	0.521	9.557	11.469	12.663	1393655	517885	882.1
tel03	1664.077	-130.744	-0.278	198.120	-64.590	0.248	0.298	7.830	9.395	11.820	1393700	517760	864.9
tel04	1664.105	-130.716	-0.279	197.712	-64.457	0.103	0.124	7.742	9.291	11.293	1393703	517666	863.6

tel05	1661.385	-133.436	-0.279	200.018	-65.209	0.134	0.161	10.152	12.182	13.056	1393703	517583	871.0
tel06	1654.646	-140.175	-0.272	206.200	-67.224	1.723	2.068	12.271	14.725	14.940	1393684	517485	891.1
tel07	1697.554	-97.267	-0.326	161.382	-52.613	0.017	0.020	3.892	4.670	15.485	1393839	518228	745.8
tel08	1693.846	-100.975	-0.296	165.927	-54.095	0.167	0.200	4.185	5.023	15.403	1393752	518221	760.6
tel09	1688.473	-106.348	-0.288	172.023	-56.082	0.467	0.560	4.556	5.467	14.950	1393730	518173	780.3
tel10	1680.939	-113.882	-0.280	180.512	-58.849	0.693	0.832	5.455	6.547	14.497	1393705	518129	807.8
tel11	1672.553	-122.268	-0.261	189.926	-61.919	0.440	0.528	7.045	8.454	14.079	1393651	518087	838.3
tel12	1662.698	-132.123	-0.234	200.196	-65.267	0.813	0.976	9.005	10.806	13.972	1393573	518032	871.6
tel13	1666.237	-128.584	-0.217	196.721	-64.134	0.541	0.649	8.085	9.702	13.756	1393525	518084	860.4
tel14	1669.817	-125.004	-0.191	193.009	-62.924	0.486	0.583	7.260	8.712	13.805	1393448	518136	848.3
tel15	1671.814	-123.007	-0.162	190.646	-62.153	0.334	0.401	6.798	8.157	13.500	1393364	518164	840.7
tel16	1672.144	-122.677	-0.132	189.734	-61.856	0.559	0.671	6.481	7.778	13.136	1393276	518153	837.7
tel17	1673.503	-121.318	-0.104	187.762	-61.213	0.299	0.359	6.150	7.380	12.485	1393196	518136	831.3
tel18	1673.137	-121.684	-0.079	187.103	-60.998	0.559	0.671	6.103	7.323	11.955	1393123	518093	829.2
tel19	1672.266	-122.555	-0.055	186.678	-60.860	0.374	0.449	6.048	7.258	10.534	1393053	518023	827.8
tel20	1671.338	-123.483	-0.043	186.692	-60.864	0.582	0.698	6.750	8.100	10.719	1393018	517953	827.9
tel21	1692.612	-102.209	-0.272	167.690	-54.669	0.358	0.430	4.270	5.124	15.712	1393682	518275	766.3
tel22	1693.693	-101.128	-0.244	166.529	-54.291	0.567	0.680	4.166	4.999	16.164	1393601	518304	762.5
tel23	1697.045	-97.776	-0.219	162.742	-53.056	0.570	0.684	3.898	4.678	16.672	1393529	518375	750.2
tel24	1696.768	-98.053	-0.195	163.160	-53.192	0.699	0.839	3.910	4.692	16.868	1393460	518392	751.6
tel25	1697.401	-97.42	-0.172	162.616	-53.015	1.006	1.207	3.895	4.674	17.509	1393392	518429	749.8
tel26	1690.562	-104.259	-0.147	170.775	-55.675	0.331	0.397	4.313	5.176	15.885	1393321	518399	776.3
tel27	1688.766	-106.055	-0.173	172.802	-56.336	0.331	0.397	4.462	5.355	15.609	1393395	518344	782.8
tel28	1687.592	-107.229	-0.201	173.992	-56.724	0.635	0.762	4.570	5.483	15.702	1393477	518303	786.7
tel29	1685.932	-108.889	-0.227	175.670	-57.271	0.693	0.832	4.784	5.741	15.475	1393553	518261	792.1
tel30	1685.234	-109.587	-0.253	176.234	-57.455	0.693	0.832	4.944	5.933	15.322	1393629	518222	794.0
tel31	1683.115	-111.706	-0.274	178.278	-58.121	0.693	0.832	5.173	6.208	14.835	1393688	518162	800.6

tel32	1679.533	-115.288	-0.247	182.471	-59.488	0.693	0.832	5.730	6.876	14.774	1393609	518182	814.2
tel34	1718.695	-76.126	-0.671	129.596	-42.250	0.039	0.047	2.789	3.347	13.561	1394839	517372	642.8
tel35	1720.632	-74.189	-0.695	126.958	-41.390	0.039	0.047	2.725	3.270	13.619	1394909	517337	634.3
tel36	1722.962	-71.859	-0.725	124.088	-40.454	0.010	0.012	2.654	3.185	13.865	1394995	517337	625.0
tel37	1724.824	-69.997	-0.750	121.407	-39.580	0.028	0.034	2.741	3.289	14.020	1395068	517303	616.3
tel38	1726.478	-68.343	-0.770	119.021	-38.802	0.039	0.047	2.652	3.182	13.953	1395126	517244	608.6
tel39	1713.872	-80.949	-0.624	135.444	-44.157	0.027	0.032	2.934	3.520	12.886	1394701	517408	661.8
tel40	1710.238	-84.583	-0.589	140.089	-45.671	0.066	0.079	4.120	4.944	13.887	1394602	517360	676.8
tel41	1706.515	-88.306	-0.564	144.614	-47.146	0.060	0.072	4.331	5.197	13.485	1394529	517333	691.5
tel42	1703.055	-91.766	-0.539	148.587	-48.441	0.078	0.094	5.463	6.555	14.108	1394456	517315	704.4
tel43	1696.302	-98.519	-0.512	156.476	-51.013	0.128	0.154	4.351	5.221	11.425	1394376	517286	729.9
tel44	1692.955	-101.866	-0.486	160.438	-52.305	0.178	0.214	4.737	5.684	11.297	1394303	517262	742.8
tel45	1688.421	-106.4	-0.461	165.618	-53.994	0.426	0.511	4.985	5.982	10.874	1394231	517244	759.6
tel46	1681.429	-113.392	-0.434	173.432	-56.541	0.898	1.078	5.937	7.124	10.885	1394152	517210	784.9
tel47	1656.806	-138.015	-0.295	203.761	-66.429	2.534	3.041	11.238	13.485	15.166	1393750	517437	883.2
tel48	1658.182	-136.639	-0.318	202.832	-66.126	2.223	2.668	10.426	12.511	14.546	1393816	517354	880.2
tel49	1660.488	-134.333	-0.332	200.405	-65.335	0.528	0.634	9.557	11.468	12.125	1393858	517278	872.3
tel50	1660.331	-134.49	-0.342	199.956	-65.188	0.862	1.034	9.431	11.317	11.905	1393886	517189	870.8
tel51	1662.332	-132.489	-0.357	196.756	-64.145	0.599	0.719	11.183	13.420	13.522	1393928	517101	860.5
tel52	1663.604	-131.217	-0.367	194.314	-63.349	0.615	0.738	10.235	12.282	12.019	1393958	517018	852.5
tel53	1664.733	-130.088	-0.369	191.668	-62.487	0.618	0.742	9.953	11.944	11.029	1393964	516926	844.0
tel54	1665.774	-129.047	-0.366	188.925	-61.592	0.879	1.055	9.034	10.841	9.434	1393955	516842	835.1
tel55	1665.124	-129.697	-0.350	188.010	-61.294	1.071	1.285	8.117	9.740	7.313	1393909	516763	832.1
tel56	1667.877	-126.944	-0.397	186.627	-60.843	0.620	0.744	8.514	10.217	9.022	1394045	516912	827.6
tel57	1668.316	-126.505	-0.404	187.611	-61.164	0.593	0.712	8.410	10.092	9.961	1394066	517042	830.8
tel58	1669.315	-125.506	-0.407	186.985	-60.960	0.320	0.384	8.274	9.929	10.043	1394074	517121	828.8
tel59	1666.102	-128.719	-0.388	191.921	-62.569	0.341	0.409	9.579	11.495	11.768	1394018	517215	844.8

tel60	1668.026	-126.795	-0.249	193.657	-63.135	0.223	0.268	6.956	8.347	11.712	1393615	517642	850.4
tel61	1669.687	-125.134	-0.218	191.472	-62.423	0.306	0.367	6.193	7.431	11.114	1393527	517626	843.3
tel62	1669.215	-125.606	-0.187	191.478	-62.425	0.509	0.611	6.194	7.432	10.922	1393438	517613	843.4
tel63	1668.3	-126.521	-0.157	192.129	-62.637	0.327	0.392	6.280	7.536	10.361	1393349	517604	845.5
tel64	1666.065	-128.756	-0.125	194.583	-63.437	0.180	0.216	6.932	8.318	10.417	1393258	517595	853.4
tel65	1665.815	-129.006	-0.091	194.001	-63.247	0.018	0.022	6.848	8.217	9.514	1393159	517583	851.5
tel66	1668.119	-126.702	-0.090	192.191	-62.657	0.034	0.041	6.600	7.920	10.321	1393155	517685	845.7
tel67	1668.452	-126.369	-0.115	192.567	-62.780	0.064	0.077	6.650	7.980	10.979	1393228	517727	846.9
tel68	1672.829	-121.992	-0.146	188.352	-61.405	0.114	0.137	5.761	6.913	11.476	1393319	517750	833.2
tel69	1672.247	-122.574	-0.175	189.516	-61.785	0.110	0.132	5.892	7.070	11.803	1393401	517751	837.0
tel70	1673.64	-121.181	-0.201	188.252	-61.373	0.152	0.182	5.750	6.900	12.198	1393476	517786	832.9
tel71	1673.863	-120.958	-0.188	188.517	-61.459	0.017	0.020	5.700	6.839	12.390	1393441	517873	833.8
tel72	1673.605	-121.216	-0.153	188.400	-61.421	0.054	0.065	5.797	6.957	12.250	1393339	517880	833.4
tel73	1671.357	-123.464	-0.119	190.022	-61.950	0.063	0.076	6.193	7.431	11.614	1393240	517864	838.6
tel74	1671.194	-123.627	-0.089	189.527	-61.789	0.177	0.212	6.129	7.355	11.208	1393154	517909	837.0
tel75	1674.512	-120.309	-0.104	186.345	-60.751	0.112	0.134	5.753	6.904	11.838	1393196	517981	826.7
tel76	1675.468	-119.353	-0.152	186.634	-60.845	0.027	0.032	5.601	6.722	12.657	1393334	518057	827.7
tel77	1716.091	-78.73	-0.663	134.008	-43.688	0.135	0.162	2.985	3.582	14.289	1394816	517566	657.1
tel78	1714.577	-80.244	-0.632	135.720	-44.247	0.029	0.035	2.948	3.537	13.788	1394726	517532	662.7
tel79	1711.617	-83.204	-0.596	138.768	-45.240	0.037	0.044	3.133	3.759	13.150	1394620	517505	672.6
tel80	1708.525	-86.296	-0.567	142.354	-46.409	0.069	0.083	3.377	4.052	12.835	1394537	517471	684.2
tel81	1705.281	-89.54	-0.540	146.147	-47.646	0.087	0.104	3.476	4.171	12.315	1394460	517441	696.5
tel82	1700.799	-94.022	-0.512	151.523	-49.399	0.161	0.193	3.807	4.568	11.971	1394377	517409	713.9
tel83	1694.48	-100.341	-0.481	158.942	-51.817	0.317	0.380	4.580	5.496	11.797	1394289	517371	737.9
tel84	1685.225	-109.596	-0.442	169.718	-55.330	0.355	0.426	5.430	6.516	10.909	1394175	517319	772.8
tel85	1682.422	-112.399	-0.418	173.240	-56.479	0.426	0.511	5.408	6.489	10.563	1394107	517411	784.3
tel86	1690.171	-104.65	-0.450	164.117	-53.504	0.263	0.316	4.773	5.728	11.174	1394200	517434	754.7

tel87	1695.779	-99.042	-0.481	157.432	-51.325	0.224	0.269	4.135	4.962	11.433	1394288	517461	733.0
tel88	1701.495	-93.326	-0.511	150.442	-49.046	0.118	0.142	3.727	4.473	11.791	1394375	517494	710.4
tel89	1706.791	-88.03	-0.548	144.366	-47.065	0.046	0.055	3.389	4.066	12.463	1394482	517511	690.7
tel90	1710.044	-84.777	-0.574	140.636	-45.849	0.027	0.032	3.251	3.901	12.987	1394559	517554	678.6
tel91	1713.307	-81.514	-0.611	137.468	-44.816	0.017	0.020	3.026	3.631	13.796	1394663	517596	668.3
tel92	1715.722	-79.099	-0.646	134.901	-43.980	0.035	0.042	3.037	3.644	14.481	1394765	517633	660.0
tel93	1718.46	-76.361	-0.671	131.395	-42.837	0.046	0.055	2.859	3.431	14.630	1394839	517644	648.7
tel94	1714.339	-80.482	-0.616	136.640	-44.547	0.051	0.061	2.989	3.587	14.262	1394679	517700	665.7
tel95	1712.23	-82.591	-0.581	138.455	-45.138	0.018	0.022	3.073	3.688	13.473	1394577	517664	671.5
tel96	1707.128	-87.693	-0.550	143.971	-46.936	0.070	0.084	3.372	4.046	12.539	1394489	517604	689.4
tel97	1702.635	-92.186	-0.514	149.175	-48.633	0.095	0.114	3.664	4.396	11.970	1394385	517591	706.3
tel98	1696.94	-97.881	-0.479	155.828	-50.802	0.140	0.168	4.022	4.827	11.280	1394281	517555	727.8
tel99	1689.846	-104.975	-0.441	164.417	-53.602	0.263	0.316	4.444	5.333	10.666	1394172	517526	755.7
tel100	1682.846	-111.975	-0.404	172.725	-56.311	0.180	0.216	5.239	6.287	10.156	1394065	517492	782.6
tel101	1673.233	-121.588	-0.369	183.914	-59.959	0.428	0.514	6.084	7.301	9.432	1393963	517425	818.9
tel102	1671.778	-123.043	-0.387	185.579	-60.501	0.724	0.869	7.082	8.498	10.633	1394017	517335	824.2
tel103	1672.932	-121.889	-0.401	183.767	-59.911	0.693	0.832	6.794	8.152	10.169	1394055	517254	818.4
tel104	1669.801	-125.02	-0.335	188.645	-61.501	0.873	1.048	6.771	8.125	10.581	1393866	517481	834.2
tel105	1681.416	-113.405	-0.368	174.963	-57.040	0.295	0.354	5.220	6.264	10.387	1393960	517557	789.8
tel106	1688.23	-106.591	-0.395	167.569	-54.630	0.134	0.161	4.671	5.606	11.338	1394038	517624	765.9
tel107	1692.704	-102.117	-0.427	162.064	-52.835	0.155	0.186	4.297	5.156	11.645	1394133	517659	748.0
tel108	1696.65	-98.171	-0.450	157.494	-51.345	0.072	0.086	3.874	4.649	11.882	1394197	517705	733.2
tel109	1700.713	-94.108	-0.479	152.559	-49.737	0.040	0.048	3.616	4.339	12.241	1394282	517762	717.2
tel110	1696.368	-98.453	-0.410	159.580	-52.025	0.082	0.098	3.862	4.635	13.043	1394083	517820	740.0
tel111	1692.487	-102.334	-0.390	163.956	-53.452	0.110	0.132	4.127	4.952	12.483	1394024	517763	754.2
tel112	1688.588	-106.233	-0.371	168.220	-54.842	0.259	0.311	4.491	5.389	12.093	1393968	517706	768.0
tel113	1683.067	-111.754	-0.344	174.308	-56.827	0.398	0.478	5.141	6.169	11.649	1393890	517649	787.7

tel114	1670.177	-124.644	-0.310	189.307	-61.717	0.635	0.762	6.808	8.169	11.187	1393792	517574	836.3
tel115	1670.299	-124.522	-0.304	189.903	-61.911	0.616	0.739	6.907	8.288	11.812	1393776	517694	838.3
tel116	1669.92	-124.901	-0.300	190.837	-62.216	0.616	0.739	6.623	7.948	11.726	1393765	517804	841.3
tel117	1671.09	-123.731	-0.294	190.131	-61.985	0.856	1.027	6.503	7.804	12.570	1393746	517920	839.0
tel118	1684.42	-110.401	-0.321	175.144	-57.099	0.738	0.886	4.914	5.896	13.723	1393823	517976	790.4
tel119	1683.328	-111.493	-0.329	175.605	-57.250	0.616	0.739	4.964	5.957	12.848	1393848	517882	791.9
tel120	1678.332	-116.489	-0.324	180.646	-58.893	0.487	0.584	5.660	6.792	11.935	1393833	517743	808.3
tel121	1689.277	-105.544	-0.354	168.037	-54.782	0.316	0.379	4.473	5.368	12.722	1393921	517786	767.4
tel122	1697.675	-97.146	-0.364	159.856	-52.115	0.128	0.154	3.951	4.741	14.744	1393948	518028	740.9
tel123	1660.976	-133.845	-0.132	199.071	-64.900	0.797	0.956	9.242	11.091	11.860	1393277	517497	868.0
tel124	1662.081	-132.74	-0.103	196.214	-63.969	0.318	0.382	8.326	9.991	9.393	1393194	517462	858.7
tel125	1663.235	-131.586	-0.078	192.422	-62.732	0.415	0.498	7.591	9.109	7.252	1393121	517389	846.4
tel126	1663.249	-131.572	-0.053	192.174	-62.652	0.484	0.581	7.797	9.356	7.453	1393050	517465	845.6
tel127	1664.148	-130.673	-0.046	192.069	-62.617	0.324	0.389	7.781	9.337	8.077	1393029	517544	845.3
tel128	1665.708	-129.113	-0.046	191.491	-62.429	0.244	0.293	7.696	9.235	9.049	1393029	517620	843.4
tel129	1668.978	-125.843	-0.052	189.257	-61.701	0.411	0.493	6.945	8.334	10.107	1393045	517706	836.2
tel130	1672.206	-122.615	-0.027	184.301	-60.085	0.574	0.689	6.277	7.533	9.415	1392973	517745	820.1
tel131	1675.049	-119.772	-0.003	179.226	-58.430	0.730	0.876	5.744	6.893	8.409	1392904	517799	803.7
tel132	1672.863	-121.958	-0.003	181.045	-59.023	0.517	0.620	7.228	8.674	8.974	1392903	517704	809.6
tel133	1671.008	-123.813	-0.004	181.705	-59.239	1.006	1.207	7.320	8.784	8.259	1392908	517612	811.7
tel134	1671.434	-123.387	-0.011	180.470	-58.836	0.852	1.022	7.151	8.581	7.457	1392928	517533	807.7
tel135	1719.974	-74.847	-0.680	127.511	-41.570	0.083	0.100	2.707	3.249	13.381	1394864	517296	636.1
tel136	1717.841	-76.98	-0.653	130.111	-42.418	0.149	0.179	2.812	3.375	13.232	1394787	517289	644.5
tel137	1713.447	-81.374	-0.620	135.567	-44.197	0.183	0.220	2.996	3.595	12.809	1394692	517258	662.2
tel138	1709.361	-85.46	-0.592	140.712	-45.874	0.165	0.198	3.245	3.895	12.497	1394610	517240	678.9
tel139	1703.84	-90.981	-0.565	145.282	-47.364	0.116	0.139	3.604	4.324	10.455	1394530	517202	693.7
tel140	1700.773	-94.048	-0.535	150.387	-49.028	0.183	0.220	3.945	4.734	11.348	1394443	517163	710.2

tel141	1695.86	-98.961	-0.506	156.007	-50.861	0.285	0.342	4.762	5.714	11.354	1394360	517129	728.4
tel142	1689.087	-105.734	-0.472	163.847	-53.416	0.318	0.382	5.345	6.415	10.639	1394262	517118	753.8
tel143	1679.624	-115.197	-0.437	174.632	-56.933	0.723	0.868	6.908	8.289	10.841	1394161	517099	788.8
tel144	1678.845	-115.976	-0.432	174.400	-56.857	0.850	1.020	6.863	8.236	10.009	1394147	516993	788.0
tel145	1689.035	-105.786	-0.466	162.679	-53.036	0.454	0.545	5.231	6.277	9.832	1394245	517004	750.0
tel146	1695.397	-99.424	-0.496	155.444	-50.677	0.232	0.278	4.701	5.641	10.385	1394332	517018	726.6
tel147	1701.376	-93.445	-0.530	148.494	-48.411	0.107	0.128	4.123	4.948	10.803	1394429	517041	704.1
tel148	1706.957	-87.864	-0.561	141.947	-46.277	0.110	0.132	3.496	4.195	11.191	1394519	517058	682.9
tel149	1710.3	-84.521	-0.593	138.337	-45.100	0.153	0.184	3.291	3.949	11.875	1394613	517100	671.2
tel150	1718.81	-76.011	-0.646	127.999	-41.729	0.097	0.116	2.706	3.248	12.595	1394766	517147	637.7
tel151	1677.216	-117.605	-0.162	185.056	-60.331	0.440	0.528	5.875	7.050	14.154	1393365	518369	822.5
tel152	1677.388	-117.433	-0.125	184.173	-60.043	0.500	0.600	5.614	6.737	13.528	1393257	518360	819.7
tel153	1680.418	-114.403	-0.096	180.163	-58.736	0.301	0.361	5.111	6.133	13.041	1393174	518357	806.7
tel154	1682.775	-112.046	-0.066	176.500	-57.542	0.440	0.528	5.045	6.053	13.046	1393087	518324	794.8
tel155	1681.97	-112.851	-0.040	175.762	-57.301	0.534	0.641	4.994	5.993	11.822	1393012	518250	792.4
tel156	1682.153	-112.668	-0.021	174.164	-56.780	0.693	0.832	5.317	6.381	11.526	1392955	518186	787.3
tel157	1682.697	-112.124	0.001	172.406	-56.207	0.440	0.528	5.189	6.227	10.449	1392893	518130	781.6
tel158	1676.197	-118.624	-0.015	179.719	-58.591	0.371	0.445	5.840	7.007	9.560	1392939	518079	805.3
tel159	1669.697	-125.124	-0.048	188.765	-61.540	0.396	0.475	7.076	8.491	10.637	1393035	518103	834.6
tel160	1670.603	-124.218	-0.241	191.543	-62.446	0.253	0.304	6.596	7.916	12.476	1393593	517929	843.6
tel161	1673.788	-121.033	-0.221	188.308	-61.391	0.339	0.407	5.675	6.810	12.498	1393535	518035	833.1
tel162	1674.284	-120.537	-0.209	188.349	-61.405	0.238	0.286	6.386	7.663	13.765	1393501	518132	833.2
tel175	1701.622	-93.199	-0.415	155.129	-50.574	0.166	0.199	3.471	4.165	14.923	1394097	518204	725.6
tel176	1701.874	-92.947	-0.487	152.988	-49.876	0.105	0.126	3.547	4.257	13.679	1394307	518149	718.6
tel177	1707.133	-87.688	-0.562	146.442	-47.742	0.185	0.222	3.538	4.246	14.536	1394522	518234	697.4
tel178	1708.776	-86.045	-0.626	140.234	-45.718	0.035	0.042	3.641	4.369	11.875	1394708	518281	677.3
tel179	1712.169	-82.652	-0.693	135.650	-44.224	0.060	0.072	4.249	5.098	12.870	1394903	518268	662.5

tel180	1714.817	-80.004	-0.738	131.418	-42.844	0.402	0.482	4.136	4.963	12.896	1395033	518335	648.7
tel181	1730.546	-64.275	-0.788	111.521	-36.357	0.372	0.446	2.997	3.596	13.762	1395176	518265	584.3
tel182	1734.835	-59.986	-0.828	104.147	-33.953	0.100	0.120	2.950	3.540	12.658	1395293	518145	560.4
tel183	1743.161	-51.66	-0.870	93.403	-30.451	0.890	1.068	2.629	3.155	14.264	1395415	518172	525.6
tel191	1793.193	-1.628	-0.004	2.444	-0.797	0.006	0.007	0.412	0.494	0.135	1392908	511052	230.8
tel192	1790.567	-4.254	0.005	5.626	-1.834	0.010	0.012	0.448	0.537	-0.290	1392881	511371	241.1
tel193	1789.572	-5.249	0.001	7.680	-2.504	0.050	0.060	0.496	0.595	0.202	1392891	511639	247.8
tel194	1787.473	-7.348	0.002	10.839	-3.534	0.008	0.010	0.509	0.611	0.198	1392890	511929	258.0
tel195	1783.924	-10.897	-0.009	16.294	-5.312	0.017	0.020	0.613	0.736	0.451	1392922	512370	275.7
tel196	1779.436	-15.385	-0.057	23.846	-7.774	0.030	0.036	0.836	1.003	1.287	1393061	512718	300.2
tel197	1774.495	-20.326	-0.028	31.178	-10.164	0.000	0.000	0.707	0.848	1.126	1392976	513019	323.9
tel198	1772.583	-22.238	-0.062	35.097	-11.442	0.024	0.029	0.952	1.143	2.145	1393075	513281	336.6
tel199	1767.223	-27.598	-0.112	44.726	-14.581	0.022	0.026	1.019	1.223	3.303	1393220	513671	367.8
tel200	1762.464	-32.357	-0.155	52.817	-17.219	0.050	0.060	1.210	1.452	4.217	1393343	513944	394.0
tel201	1753.306	-41.515	-0.188	66.952	-21.827	0.075	0.090	1.514	1.816	4.947	1393439	514395	439.8
tel202	1746.361	-48.46	-0.225	77.977	-25.422	0.011	0.013	1.344	1.612	5.114	1393546	514784	475.6
tel203	1742.926	-51.895	-0.280	84.259	-27.470	0.025	0.030	1.404	1.685	5.948	1393707	515073	495.9
tel204	1744.202	-50.619	-0.439	84.255	-27.468	0.000	0.000	1.651	1.981	7.328	1394166	515110	495.9
tel205	1743.004	-51.817	-0.521	86.914	-28.335	0.027	0.032	1.650	1.980	7.872	1394404	515434	504.5
tel206	1736.566	-58.255	-0.722	96.861	-31.578	0.010	0.012	2.149	2.579	8.515	1394986	516170	536.8
tel207	1728.968	-65.853	-0.663	109.379	-35.659	0.139	0.167	2.206	2.647	9.636	1394815	516475	577.3
tel208	1723.952	-70.869	-0.674	118.033	-38.481	0.040	0.048	2.475	2.970	10.647	1394846	516757	605.4
tel209	1701.399	-93.422	-0.355	156.605	-51.055	0.196	0.235	3.223	3.867	15.493	1393922	518352	730.4
tel210	1706.82	-88.001	-0.304	151.072	-49.252	0.221	0.265	3.261	3.913	17.311	1393776	518518	712.4
tel211	1709.161	-85.66	-0.256	148.870	-48.534	0.005	0.006	4.045	4.854	18.900	1393635	518671	705.3
tel212	1708.704	-86.117	-0.193	149.210	-48.645	0.010	0.012	3.375	4.050	17.936	1393455	518624	706.4
tel213	1708.089	-86.732	-0.128	149.249	-48.657	0.024	0.029	3.527	4.232	17.612	1393265	518670	706.5

tcl214	1706.357	-88.464	-0.053	149.043	-48.590	0.128	0.154	3.731	4.477	16.185	1393049	518717	705.9
tcl215	1703.583	-91.238	-0.013	150.742	-49.144	0.216	0.259	3.822	4.587	14.811	1392933	518686	711.4
tcl216	1696.456	-98.365	-0.062	162.586	-53.005	0.410	0.492	3.740	4.488	15.752	1393074	518560	749.7
tcl217	1691.544	-103.277	-0.013	166.832	-54.390	0.005	0.006	4.127	4.952	13.729	1392934	518376	763.5
tcl218	1691.097	-103.724	0.043	163.163	-53.194	0.027	0.032	4.654	5.585	11.525	1392769	518231	751.6
tcl219	1695.141	-99.68	0.056	156.476	-51.013	0.317	0.380	5.058	6.070	11.907	1392733	518132	729.9
tcl220	1724.358	-70.463	-0.767	122.518	-39.943	0.025	0.030	2.641	3.170	14.164	1395115	517407	619.9
tcl221	1729.455	-65.366	-0.836	115.984	-37.813	0.033	0.040	3.046	3.655	15.283	1395316	517460	598.7
tcl222	1730.035	-64.786	-0.886	113.993	-37.163	0.147	0.176	3.998	4.797	15.750	1395461	517656	592.3
tcl223	1746.658	-48.163	-0.956	91.370	-29.788	0.282	0.338	2.881	3.458	15.877	1395665	517505	519.0
tcl224	1754.08	-40.741	-0.999	81.152	-26.457	0.123	0.148	2.668	3.201	15.922	1395789	517617	485.9
tcl225	1766.66	-28.161	-1.100	63.195	-20.602	0.056	0.067	2.545	3.055	16.071	1396081	517770	427.7
tcl226	1766.931	-27.89	-1.141	63.371	-20.660	0.160	0.192	2.392	2.870	16.361	1396198	517966	428.2
tcl227	1768.544	-26.277	-1.197	59.865	-19.517	0.141	0.169	2.575	3.090	15.752	1396360	518028	416.9
tcl228	1774.096	-20.725	-1.265	51.442	-16.771	0.044	0.053	2.547	3.056	15.409	1396558	518050	389.6
tcl229	1775.46	-19.361	-1.303	48.309	-15.749	0.184	0.221	2.880	3.456	15.190	1396670	518111	379.4
tcl230	1710.079	-84.742	0.140	131.508	-42.874	0.693	0.832	4.723	5.668	10.151	1392489	518227	649.0
tcl231	1720.537	-74.284	0.201	116.634	-38.024	0.873	1.048	4.908	5.890	11.082	1392313	518317	600.8
tcl232	1733.73	-61.091	0.227	101.415	-33.063	0.534	0.641	4.798	5.757	13.505	1392238	518524	551.5
tcl233	1744.937	-49.884	0.282	86.278	-28.128	0.317	0.380	4.622	5.547	14.094	1392078	518580	502.5
tcl234	1759.18	-35.641	0.390	67.369	-21.963	0.018	0.022	2.991	3.589	13.385	1391764	518715	441.2
tcl235	1763.759	-31.062	0.479	60.154	-19.611	0.082	0.098	2.107	2.529	12.206	1391509	518781	417.8
tcl236	1765.721	-29.1	0.557	56.119	-18.296	0.059	0.071	1.692	2.030	11.000	1391282	518698	404.7
tcl246	1719.812	-75.009	-0.381	116.738	-38.058	0.317	0.380	2.996	3.595	6.884	1393998	516100	601.2
tcl247	1703.706	-91.115	-0.332	136.806	-44.601	0.346	0.415	4.501	5.401	6.193	1393856	516277	666.2
tcl248	1695.175	-99.646	-0.305	146.969	-47.914	0.575	0.690	5.569	6.682	6.095	1393779	516343	699.1
tcl249	1688.751	-106.07	-0.274	153.671	-50.099	0.948	1.138	5.877	7.052	5.036	1393690	516360	720.8

tel250	1704.283	-90.538	-0.245	134.592	-43.879	0.436	0.523	4.798	5.758	5.830	1393604	516212	659.0
tel251	1711.056	-83.765	-0.241	126.198	-41.142	0.270	0.324	4.109	4.931	5.923	1393592	516109	631.8
tel252	1718.119	-76.702	-0.250	116.103	-37.851	0.179	0.215	2.656	3.187	4.320	1393620	515882	599.1
tel253	1728.562	-66.259	-0.254	102.677	-33.474	0.157	0.188	2.211	2.653	5.149	1393630	515688	555.6
tel254	1735.326	-59.495	-0.300	93.882	-30.607	0.105	0.126	1.605	1.926	5.150	1393764	515470	527.1
tel255	1680.904	-113.917	-0.392	178.092	-58.060	0.262	0.314	5.184	6.221	11.876	1394030	518483	800.0
tel256	1682.802	-112.019	-0.373	178.171	-58.086	0.158	0.190	4.707	5.648	13.149	1393974	518749	800.2
tel257	1663.419	-131.402	-0.283	200.019	-65.209	0.430	0.516	7.355	8.825	12.085	1393714	519044	871.0
tel258	1660.377	-134.444	-0.216	204.962	-66.820	0.121	0.145	7.503	9.004	12.249	1393519	519227	887.1
tel259	1671.238	-123.583	-0.140	193.336	-63.030	0.028	0.034	6.283	7.540	13.774	1393302	519281	849.4
tel260	1673.755	-121.066	-0.160	191.561	-62.452	0.040	0.048	5.564	6.677	14.227	1393359	519501	843.6
tel261	1677.467	-117.354	-0.192	187.685	-61.188	0.220	0.264	5.255	6.306	15.140	1393450	519757	831.1

Appendix B

Masaya microgravity data

Table B1

Daily gravity variations at station A7 in 1997

97-03-12

Local time	GMT time	Ref. time*	Raw Scintrex (mGal)**	Scintrex (µGal)*	Raw LCR (mGal)***	LCR (µGal)*	Tides (µGal)
7:10							-58
7:15							-59.8
7:20							-61.4
7:25							-62.8
7:30							-64.1
7:35							-65.2
7:40							-66.1
7:45							-68.8
7:50							-67.4
7:55							-67.7
8:00							-67.9
8:05							-67.9
8:10							-67.6
8:15							-67.3
8:20							-66.8
8:25							-66
8:30							-65.1
8:35							-64
8:40							-62.7
8:45							-61.3
8:50							-59.6
8:55							-57.8
9:00							-55.8
9:05							-53.7
9:11	15:11	0:00	2456.692	0			-51.3
9:16	15:16	0:05	2456.698	6			-48.9
9:21	15:21	0:10	2456.700	8			-46.2

9:26	15:26	0:15	2456.701	9			-43.4
9:31	15:31	0:20	2456.711	19	1722.097	0	-40.5
9:36	15:36	0:25	2456.707	15	1722.093	0	-37.4
9:41	15:41	0:30	2456.700	8			-34.2
9:46	15:46	0:35	2456.699	7	1722.098	9	-30.9
9:51	15:51	0:40	2456.708	16			-27.4
9:54	15:54	0:43	2456.715	23			-23.8
9:59	15:59	0:48	2456.709	17			-20.1
10:04	16:04	0:53	2456.710	18			-16.3
10:09	16:09	0:58	2456.708	16			-12.3
10:14	16:14	1:03	2456.702	10			-8.3
10:19	16:19	1:08	2456.711	19			-4.2
10:24	16:24	1:13	2456.692	0			0
10:29	16:29	1:18	2456.716	24	1722.071	17	4.2
10:34	16:34	1:23	2456.708	16	1722.064	13	8.6
10:39	16:39	1:28	2456.707	15	1722.059	13	12.9
10:44	16:44	1:33	2456.714	22	1722.051	10	17.4
10:49	16:49	1:38	2456.711	19			21.9
10:54	16:54	1:43	2456.710	18			26.4
10:59	16:59	1:48	2456.715	23			31
11:04	17:04	1:53	2456.711	19			35.5
11:09	17:09	1:58	2456.715	23			40.1
11:14	17:14	2:03	2456.700	8			44.7
11:19	17:19	2:08	2456.715	23			49.3
11:24	17:24	2:13	2456.711	19			53.9
11:29	17:29	2:18	2456.712	20	1722.001	2	58.5
11:34	17:34	2:23	2456.711	19	1721.999	4	63
11:39	17:39	2:28	2456.710	18			67.5
11:44	17:44	2:33	2456.708	16	1722.005	12	72
11:46	17:46	2:35	2456.708	16			73
11:51	17:51	2:40	2456.711	19			76.4
11:56	17:56	2:45	2456.700	8			80.8
12:01	18:01	2:50	2456.721	29			85.1
12:06	18:06	2:55	2456.706	14			89.3

12:11	18:11	3:00	2456.700	8			93.5
12:16	18:16	3:05	2456.698	6			97.6
12:21	18:21	3:10	2456.710	18	1721.973	19	101.5
12:26	18:26	3:15	2456.715	23	1721.968	17	105.4
12:31	18:31	3:20	2456.709	17	1721.968	19	109.2
12:36	18:36	3:25	2456.713	21			112.8
12:40	18:40	3:29	2456.715	23			116.4
12:45	18:45	3:34	2456.713	21			119.8
12:50	18:50	3:39	2456.706	14			123.1
12:55	18:55	3:44	2456.714	22			126.2
13:00	19:00	3:49	2456.716	24			129.2
13:05	19:05	3:54	2456.710	18			132.1
13:10							134.8
13:15							137.3
13:20							139.7
13:28	19:28	4:17	2456.711	19	1721.948	34	141.9
13:33	19:33	4:22	2456.713	21			144
13:38	19:38	4:27	2456.710	18			145.8
13:43	19:43	4:32	2456.718	26			147.5
13:48	19:48	4:37	2456.720	28			149.1
13:53	19:53	4:42	2456.716	24			150.4
13:58	19:58	4:47	2456.719	27			151.6
14:03	20:03	4:52	2456.714	22			152.6
14:08	20:08	4:57	2456.712	20	1721.933	30	153.3
14:13	20:13	5:02	2456.724	32	1721.927	25	154
14:18	20:18	5:07	2456.716	24			154.4
14:23	20:23	5:12	2456.717	25			154.6
14:28	20:28	5:17	2456.720	28			154.6
14:33	20:33	5:22	2456.727	35			154.5
14:38	20:38	5:27	2456.725	33			154.2
14:43	20:43	5:32	2456.725	33			153.6
14:48	20:48	5:37	2456.717	25			152.9
14:51	20:51	5:40	2456.710	18			152
14:56	20:56	5:45	2456.723	31			151

15:01	21:01	5:50	2456.725	33			149.7
15:06	21:06	5:55	2456.723	31	1721.941	31	148.3
15:11	21:11	6:00	2456.724	32	1721.943	32	146.7
15:16	21:16	6:05	2456.719	27			144.9
15:21	21:21	6:10	2456.711	19			142.9
15:26	21:26	6:15	2456.724	32			140.8
15:29	21:29	6:18	2456.725	33			138.5
15:34	21:34	6:23	2456.715	23			136.1
15:39	21:39	6:28	2456.722	30			133.5
15:44	21:44	6:33	2456.721	29	1721.970	44	130.8
15:49	21:49	6:38	2456.725	33	1721.974	46	128
15:54	21:54	6:43	2456.723	31	1721.973	44	125
15:59	21:59	6:48	2456.716	24			121.8
16:04	22:04	6:53	2456.727	35			118.6
16:09	22:09	6:58	2456.721	29			115.2
16:14	22:14	7:03	2456.720	28			111.7
16:19	22:19	7:08	2456.717	25			108.1
16:24	22:24	7:13	2456.724	32	1722.001	49	104.5
16:29	22:29	7:18	2456.722	30	1722.002	46	100.7
16:34	22:34	7:23	2456.725	33	1722.001	43	96.8
16:39	22:39	7:28	2456.718	26			92.9
16:45							88.9
16:50							84.8
16:55							80.7
17:00							76.5
17:05							72.3
17:10							68.1
17:15							59.5

*** Relative to starting time**
**** Already tides-corrected**
***** Not tides-corrected**

Table B2

Daily gravity variations at station A7 in 1998

98-02-25

Time Local	Time GMT	Ref Time*	Raw LCR** (mGal)	A7 (μGal)*	Tides (μGal)
10:01	16:01	0:00	1718.515	0	129
10:14	16:14	0:13	1718.497	-8	138
10:24	16:24	0:23	1718.497	-3	144
10:33	16:33	0:32	1718.492	-3	149
10:43	16:43	0:42	1718.486	-5	153
10:54	16:54	0:53	1718.484	-4	156
11:05	17:05	1:04	1718.492	7	158
11:18	17:18	1:17	1718.487	3	159
11:30	17:30	1:29	1718.492	7	159
11:42	17:42	1:41	1718.497	10	157
11:56	17:56	1:55	1718.500	9	153
12:08	18:08	2:07	1718.508	12	148
12:20	18:20	2:19	1718.511	8	142
12:35	18:35	2:34	1718.524	12	132
12:45	18:45	2:44	1718.532	13	125
12:55	18:55	2:54	1718.538	11	116
13:10	19:10	3:09	1718.555	14	103
13:20	19:20	3:19	1718.572	21	93
13:32	19:32	3:31	1718.584	21	81
13:48	19:48	3:47	1718.605	24	63
14:05	20:05	4:04	1718.623	23	44
14:22	20:22	4:21	1718.642	23	25
14:35	20:35	4:34	1718.659	24	10
14:45	20:45	4:44	1718.674	28	-2
15:08	21:08	5:07	1718.694	24	-27
15:22	21:22	5:21	1718.717	32	-41
15:34	21:34	5:33	1718.722	26	-52
15:47	21:47	5:46	1718.722	14	-64
16:05	22:05	6:04	1718.744	23	-77
16:18	22:18	6:17	1718.752	22	-86
16:31	22:31	6:30	1718.758	21	-92
16:40	22:40	6:39	1718.757	17	-96
16:55	22:55	6:54	1718.759	14	-101
17:04	23:04	7:03	1718.762	16	-102
17:16	23:16	7:15	1718.763	16	-103
17:28	23:28	7:27	1718.757	10	-103
17:43	23:43	7:42	1718.753	9	-100
17:52	23:52	7:51	1718.744	3	-97
18:07	0:07	8:06	1718.741	7	-91
18:20	0:20	8:19	1718.731	4	-83
18:30	0:30	8:29	1718.730	10	-77
18:43	0:43	8:42	1718.712	1	-67
18:56	0:56	8:55	1718.701	1	-55

19:07	1:07	9:06	1718.686	-2	-45
19:19	1:19	9:18	1718.686	10	-32
19:29	1:29	9:28	1718.670	5	-21
19:42	1:42	9:41	1718.649	-1	-6
20:02	2:02	10:01	1718.625	-1	18
20:18	2:18	10:17	1718.598	-7	38
20:33	2:33	10:32	1718.579	-8	57
20:51	2:51	10:50	1718.560	-4	80
21:08	3:08	11:07	1718.537	-6	101
21:22	3:22	11:21	1718.528	2	118
21:37	3:37	11:36	1718.506	-3	135
21:56	3:56	11:55	1718.487	-3	154
22:09	4:09	12:08	1718.470	-8	166
22:24	4:24	12:23	1718.469	3	178
22:34	4:34	12:33	1718.462	4	185
22:48	4:48	12:47	1718.457	7	193
23:00	5:00	12:59	1718.452	7	199
23:10	5:10	13:09	1718.449	8	203
23:21	5:21	13:20	1718.446	8	205
98-03-06					
9:58	15:58	0:00	1719.097	0	34
10:11	16:11	0:13	1719.102	1	30
10:26	16:26	0:28	1719.107	1	25
10:43	16:43	0:45	1719.118	7	20
10:57	16:57	0:59	1719.121	4	15
11:15	17:15	1:17	1719.130	7	9
11:33	17:33	1:35	1719.135	7	3
11:47	17:47	1:49	1719.145	12	-2
12:00	18:00	2:02	1719.149	13	-5
12:17	18:17	2:19	1719.152	11	-10
12:31	18:31	2:33	1719.155	11	-13
12:47	18:47	2:49	1719.159	12	-16
13:05	19:05	3:07	1719.168	18	-18
13:21	19:21	3:23	1719.173	22	-20
13:32	19:32	3:34	1719.172	20	-20
13:52	19:52	3:54	1719.170	19	-20
14:14	20:14	4:16	1719.168	19	-17
14:25	20:25	4:27	1719.166	20	-16
14:43	20:43	4:45	1719.160	17	-12
14:58	20:58	5:00	1719.159	20	-8
15:13	21:13	5:15	1719.154	20	-3
15:28	21:28	5:30	1719.149	21	3
15:46	21:46	5:48	1719.142	21	10
16:03	22:03	6:05	1719.129	16	18
16:18	22:18	6:20	1719.121	15	25
16:33	22:33	6:35	1719.107	9	33
16:58	22:58	7:00	1719.103	19	47
17:16	23:16	7:18	1719.100	25	56
17:31	23:31	7:33	1719.087	20	64
17:49	23:49	7:51	1719.076	18	74

18:02	0:02	8:04	1719.069	18	80
18:14	0:14	8:16	1719.061	16	86
18:31	0:31	8:33	1719.056	18	93
19:01	1:01	9:03	1719.043	15	103
19:13	1:13	9:15	1719.044	20	107
19:33	1:33	9:35	1719.038	18	111
19:48	1:48	9:50	1719.034	16	114
20:02	2:02	10:04	1719.033	16	115
20:19	2:19	10:21	1719.032	16	115
20:34	2:34	10:36	1719.034	17	115
20:49	2:49	10:51	1719.037	18	112
21:05	3:05	11:07	1719.041	19	109
21:22	3:22	11:24	1719.040	13	105
21:39	3:39	11:41	1719.042	10	99
22:00	4:00	12:02	1719.052	11	91
22:20	4:20	12:22	1719.067	18	81
22:38	4:38	12:40	1719.071	12	72
22:53	4:53	12:55	1719.080	13	64
23:07	5:07	13:09	1719.088	13	56
98-03-13					
10:50	16:50	0:00	1719.063	0	124
11:07	17:07	0:17	1719.055	2	134
11:12	17:12	0:22	1719.049	-2	136
11:27	17:27	0:37	1719.046	1	143
11:44	17:44	0:54	1719.038	-2	148
12:08	18:08	1:18	1719.038	1	151
12:29	18:29	1:39	1719.046	8	149
12:48	18:48	1:58	1719.051	9	145
13:16	19:16	2:26	1719.059	5	133
13:31	19:31	2:41	1719.071	9	124
13:46	19:46	2:56	1719.083	10	114
14:05	20:05	3:15	1719.104	16	100
14:27	20:27	3:37	1719.119	13	80
14:48	20:48	3:58	1719.136	9	61
14:55	20:55	4:05	1719.145	12	54
15:16	21:16	4:26	1719.156	2	33
15:32	21:32	4:42	1719.185	15	17
15:50	21:50	5:00	1719.201	14	-1
16:09	22:09	5:19	1719.211	6	-18
16:35	22:35	5:45	1719.228	1	-40
17:05	23:05	6:15	1719.252	5	-60
17:16	23:16	6:26	1719.258	5	-66
17:31	23:31	6:41	1719.270	9	-73
17:55	23:55	7:05	1719.274	6	-80
18:08	0:08	7:18	1719.272	3	-82
18:23	0:23	7:33	1719.276	6	-82
18:40	0:40	7:50	1719.277	9	-80
18:57	0:57	8:07	1719.258	-5	-76
19:19	1:19	8:29	1719.253	0	-66
19:38	1:38	8:48	1719.240	-3	-55

19:56	1:56	9:06	1719.230	0	-43
20:18	2:18	9:28	1719.212	1	-25
20:36	2:36	9:46	1719.191	-4	-8
20:57	2:57	10:07	1719.166	-8	13
21:18	3:18	10:28	1719.142	-11	34
21:36	3:36	10:46	1719.124	-11	53
21:57	3:57	11:07	1718.998	-15	74
22:15	4:15	11:25	1718.980	-16	92
22:21	4:21	11:31	1718.973	-17	97
22:38	4:38	11:48	1718.964	-11	112
22:55	4:55	12:05	1718.943	-20	125
23:14	5:14	12:24	1718.934	-16	137
23:28	5:28	12:38	1718.930	-12	145
23:43	5:43	12:53	1718.929	-7	151
23:58	5:58	13:08	1718.916	-15	156
0:09	6:09	13:19	1718.922	-7	158

*** Relative to starting time**
**** Not tides-corrected**

Table B3

Result of the microgravity line at Masaya caldera for the LCR

VARIATIONS BETWEEN 04/03/97 AND 17/03/97 (A. Beaulieu and H. Rymer)											
	MUSEO-A1	Δ MUSEO	A3-A1	Δ A3	A5-A1	Δ A5	A7-A1	Δ A7	B2-A1	Δ B2	B1A-A1	Δ B1A
04/03/97			0.869	0.000			-56.291	0.000	-57.805	0.000	-57.382	0.000
10/03/97							-56.327	-0.036	-57.836	-0.031	-57.413	-0.031
13/03/97			0.854	-0.015			-56.308	-0.017	-57.832	-0.027	-57.415	-0.033
17/03/97			0.865	-0.004			-56.370	-0.079	-57.870	-0.065	-57.439	-0.057
VARIATIONS BETWEEN 27/01/98 AND 14/03/98 (A.Beaulieu, H. Rymer and G. Williams-Jones)												
	MUSEO-A1	Δ MUSEO	A3-A1	Δ A3	A5-A1	Δ A5	A7-A1	Δ A7	B2-A1	Δ B2	B1A-A1	Δ B1A
98-01-27	-2.106	0.000	0.831	0.000			-56.352	0.000	-57.858	0.000	-57.433	0.000
98-02-18	-2.161	-0.055	0.833	0.002	-17.314	0.000	-56.372	-0.020	-57.873	-0.015	-57.446	-0.013
98-02-24	-2.162	-0.056	0.857	0.026	-17.286	0.028	-56.368	-0.016	-57.871	-0.013	-57.456	-0.023
98-02-27	-2.164	-0.058	0.867	0.036	-17.257	0.057	-56.306	0.046	-57.808	0.050	-57.401	0.032
98-03-01	-2.161	-0.055	0.855	0.024	-17.289	0.024	-56.359	-0.007	-57.854	0.004	-57.442	-0.009
98-03-02	-2.149	-0.043	0.852	0.021	-17.285	0.029	-56.352	0.000	-57.856	0.002	-57.444	-0.011
98-03-03	-2.154	-0.048	0.850	0.019	-17.282	0.031	-56.369	-0.017	-57.853	0.005	-57.443	-0.010
98-03-05	-2.155	-0.049	0.854	0.023	-17.286	0.027	-56.360	-0.008	-57.870	-0.012	-57.441	-0.008
98-03-09	-2.144	-0.038	0.847	0.016	-17.281	0.033	-56.368	-0.016	-57.838	0.020	-57.417	0.016
98-03-14	-2.134	-0.028	0.857	0.026	-17.284	0.029	-56.347	0.005	-57.847	0.011	-57.439	-0.006
VARIATIONS BETWEEN 24/02/98 AND 09/03/98 (A.Beaulieu)												
	MUSEO-A1	Δ MUSEO	A3-A1	Δ A3	A5-A1	Δ A5	A7-A1	Δ A7	B2-A1	Δ B2	B1A-A1	Δ B1A
98-02-24	-2.162	0.000	0.857	0.000	-17.286	0.000	-56.368	0.000	-57.871	0.000	-57.456	0.000
98-03-01	-2.161	0.000	0.855	-0.003	-17.289	-0.004	-56.359	0.009	-57.854	0.017	-57.442	0.014
98-03-02	-2.149	0.013	0.852	-0.005	-17.285	0.001	-56.352	0.016	-57.856	0.016	-57.444	0.013
98-03-03	-2.154	0.007	0.850	-0.007	-17.282	0.003	-56.369	-0.001	-57.853	0.019	-57.443	0.013
98-03-05	-2.155	0.007	0.854	-0.003	-17.286	-0.001	-56.360	0.008	-57.870	0.002	-57.441	0.015
98-03-09	-2.144	0.018	0.847	-0.010	-17.281	0.005	-56.368	0.000	-57.838	0.033	-57.417	0.040
VARIATIONS BETWEEN 1993 AND 1998 (A.Beaulieu, H. Rymer and G. Williams-Jones)												
	MUSEO-A1	Δ MUSEO	A3-A1	Δ A3	A5-A1	Δ A5	A7-A1	Δ A7	B2-A1	Δ B2	B1A-A1	Δ B1A
93-02-01			0.840	0.000	-17.296	0.000	-56.282	0.000				

94-04-01			0.858	0.018	-17.318	-0.022	-56.360	-0.078	-57.836	0.000		
94-10-01			0.865	0.025	-17.274	0.022	-56.370	-0.088				
96-03-01			0.848	0.008	-17.306	-0.010	-56.333	-0.051	-57.807	0.029	-57.402	0.000
97-03-01			0.870	0.030	-17.272	0.024	-56.336	-0.054	-57.851	-0.015	-57.428	-0.026
04/03/97			0.869	0.029			-56.291	-0.009	-57.805	0.031	-57.382	0.020
10/03/97							-56.327	-0.045	-57.836	0.000	-57.413	-0.011
13/03/97			0.854	0.014			-56.308	-0.026	-57.832	0.004	-57.415	-0.013
17/03/97			0.865	0.025			-56.370	-0.088	-57.870	-0.034	-57.439	-0.037
98-01-27	-2.106	0.000	0.831	-0.009			-56.352	-0.070	-57.858	-0.022	-57.433	-0.031
98-02-18	-2.161	-0.055	0.833	-0.007	-17.314	-0.018	-56.372	-0.090	-57.873	-0.037	-57.446	-0.044
98-02-24	-2.162	-0.056	0.857	0.017	-17.286	0.010	-56.368	-0.086	-57.871	-0.035	-57.456	-0.054
98-02-27	-2.164	-0.058	0.867	0.027	-17.257	0.039	-56.306	-0.024	-57.808	0.028	-57.401	0.001
98-03-01	-2.161	-0.055	0.855	0.015	-17.289	0.007	-56.359	-0.077	-57.854	-0.018	-57.442	-0.040
98-03-02	-2.149	-0.043	0.852	0.012	-17.285	0.011	-56.352	-0.070	-57.856	-0.020	-57.444	-0.042
98-03-03	-2.154	-0.048	0.850	0.010	-17.282	0.014	-56.369	-0.087	-57.853	-0.017	-57.443	-0.041
98-03-05	-2.155	-0.049	0.854	0.014	-17.286	0.010	-56.360	-0.078	-57.870	-0.034	-57.441	-0.039
98-03-09	-2.144	-0.038	0.847	0.007	-17.281	0.015	-56.368	-0.086	-57.838	-0.002	-57.417	-0.015
98-03-14	-2.134	-0.028	0.857	0.017	-17.284	0.012	-56.347	-0.065	-57.847	-0.011	-57.439	-0.037

Appendix C

Scintrex-LCR comparison in 1997

During the 1997 survey, the microgravity stations at Masaya were monitored using two meters, the Scintrex CG-3 #9101184 and the LCR model G-513. Some differences were observed between the results for the two meters. The Scintrex instrument does not show exactly the same trend as the LCR instrument for the three stations next to the Santiago crater (A7, B2, And B1A) (Fig C1). The Scintrex measurements began on 10 March. Between 10-13 March, there is some difference in the variation of microgravity between stations near the crater (A7, B2 and B1A) (Fig. C1 & Table C1a). Station A7 shows an increase of 23 μGal, B2 a decrease of 20 μGal and B1A a decrease of 35 μGal. Between 13-17 March, station A7 decreases by 28 μGal, B2 decreases by 26 μGal and B1A increases by 15 μGal. We now compare the temporal variation trend between the two instruments for each station near the crater. To do this, the values obtained on 10 March for the two instruments are used as a reference. Then the temporal variation for the two instruments may be compared for 10, 13 and 17 March. For station A7, the two meters show the same trend, but they have different values (Fig. C1). This is particularly so for 17 March, where the LCR shows a greater decrease. Again, station B2 shows a similar pattern, but here the main difference is for 10 March, where the Scintrex shows a larger decrease. Between 13 and 17 March, the temporal variation observed by the two instruments is practically the same. For station B1A, the results for the LCR instrument and the Scintrex instrument are different. The LCR shows practically no variations between 10 and 13 March and a decrease of 24 μGal between 13 and 17 March. With the Scintrex, there is a decrease of 35 μGal between 10 and 13 March and an increase of 15 μGal between 13 and 17 March. For the two

FIGURE C1

LCR-Scintrex gravity changes at Santiago crater between 10-17 March 1997.

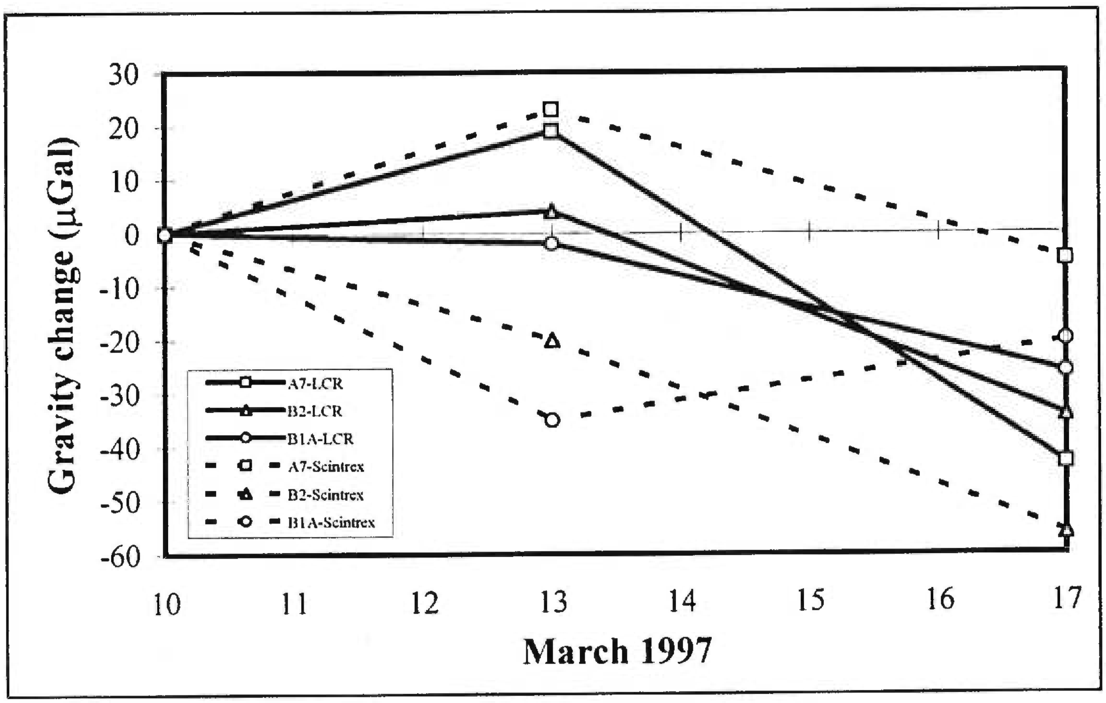

30
20
10
0
-10
-20
-30
-40
-50
-60
Gravity change (μGal)
A7-LCR
B2-LCR
B1A-LCR
A7-Scintrex
B2-Scintrex
B1A-Scintrex
10
11
12
13
14
15
16
17
March 1997

Table C1a: Results of the microgravity line at Masaya for the Scintrex (mGal)

Variation between 10-17 March 1997 for Scintrex and LCR meters							
	A7-A1	Δ A7	B2-A1	Δ B2	B1A-A1	Δ B1A	
10/03/97	-56.372	0	-57.882	0	-57.459	0	LCR
	-56.301	0	-57.789	0	-57.365	0	Scintrex
13/03/97	-56.353	0.019	-57.878	0.004	-57.461	-0.002	LCR
	-56.278	0.023	-57.809	-0.020	-57.400	-0.035	Scintrex
17/03/97	-56.415	-0.043	-57.916	-0.034	-57.485	-0.026	LCR
	-56.306	-0.005	-57.845	-0.056	-57.385	-0.020	Scintrex

Table C1b: Raw data at École Polytechnique and differences between Scintrex and LCR

	Scintrex	LCR
Station	30/04/97	01/04/97
U1	4069.110	4891.296
U2	4069.310	4891.509
U3	4073.321	4895.646
U4	4073.673	4895.994
U1(end)	4069.034	4891.302

	Scintrex	La Coste	
Station	01/04/97	30/04/97	Difference
U4-U1	4.698	4.563	0.135
U3-U1	4.35	4.211	0.139
U2-U1	0.213	0.200	0.013
U4-U3	0.348	0.352	-0.004
U1(fin)-U1	0.006	-0.076	

Table C1c: Differences between A1 and other stations in mGal for the Scintrex and the LCR

Gravimeter	LCR			Scintrex		
Station	10/03/97	13/03/97	17/03/97	10/03/97	13/03/97	17/03/97
A3-A1	nd	0.855	0.866	nd	0.874	0.857
A7-A1	-56.372	-56.353	-56.415	-56.301	-56.278	-56.306
B2-A1	-57.882	-57.878	-57.916	-57.789	-57.809	-57.845
B1A-A1	-57.459	-57.461	-57.485	-57.365	-57.400	-57.385
A1(end)-A1	0.008	0.027	-0.016	-0.052	0.008	-0.009

Difference Scintrex-LCR

Station	10/03/97	13/03/97	17/03/97
A3	nd	19	9
A7	71	75	109
B2	93	69	71
B1A	94	61	100

other stations (A7 and B2), the temporal variation of microgravity is also not the same, but the direction of variation is the same, and the trend for the two lines is similar.

Another experiment was conducted with both instruments at the École Polytechnique in Montreal to again check any differences in the measurement of the two instruments. This was done only one time for each gravimeter in the perimeter of the École Polytechnique building. The Scintrex gave good results since the closure at the end of the survey was 6 μGal. But for the LCR, the closure was 76 μGal (Table C1b). This could be explained by the fact that the Scintrex is more robust in an unstable environment such as the 6^{th} floor of the École Polytechnique, where there is a lot of vibration due to people, the exterior wind and machines. In a stable environment, the LCR model G-513 has proven to be very accurate. For example, during the time of this survey, a Bouguer survey was conducted at another volcano (Telica, Nicaragua) with the LCR, and the average difference at the closure of each gravity line was about 17 μGal. The Telica survey was not conducted as carefully as a microgravity survey. In a microgravity survey, the drift at the end of the day for the LCR model G-513 is generally of the order of 10 μGal if the correct procedure is followed (Rymer, 1989). Thus, this high value of 76 μGal for the LCR at the École Polytechnique Building is not a result of drift. The greater stability of the Scintrex compared to the LCR in noisy environments is due to the rejection system of the Scintrex which eliminates values that are too far from the mean. The LCR cannot do his, and it was difficult to achieve a good measurement since there was a lot of vibration in the mechanism of the gravity meter. The difference between the two instruments was of the order of 140 μGal between station U1&U3 and U1&U4 (Table C1b). The difference is not a matter of calibration, since the largest difference among the stations was less than 5 mGal (discussed below). Another observation is that the difference between the two instruments between U1&U2 and U3&U4 is very small. It is possible that the environment significantly affected our measurements in this case. Because U1 and U2 were measured in a building, they were affected in the same way by the building interference. The same observation could be made for U3 and U4 which were outside the building with less noise. When we compare a station inside and outside the building, however, the response of the two instruments is different. This difference is probably due to the different responses to the vibration for each gravity meter.

In the case of the difference between the measurements for the two gravity meters (Scintrex and LCR) at Masaya, we observe that the LCR always gave larger values (Table C1c). At Masaya, the difference among the stations was of the order of 56-58 mGal. If there is a difference in the calibration of the instruments, this could be the factor of difference. An update in the calibration factor of the LCR reduce the difference between the two gravity meters by a certain amount. The last calibration check was done in 1995 for the LCR (H. Rymer Personal Communication, 1997). There was no correction factor made for the Scintrex at Masaya, but it was done at Scintrex Ltd before it was loaned to us. There also could be some error due to manipulation and tare, but it should not exceed 10-20 μGal. In general, the two instruments are in good agreement.